ISSN 2602-2575 • EISSN 2618-6144

EUROPEAN JOURNAL OF BIOLOGY

OFFICIAL JOURNAL OF ISTANBUL UNIVERSITY'S SCIENCE FACULTY

Volume: 80 • Issue: 2 • December 2021

https://iupress.istanbul.edu.tr/en/journal/ejb/home

ISTANBUL UNIVERSITY PRESS

EUROPEAN
JOURNAL OF
BIOLOGY

Indexing and Abstracting

Zoological Record - Clarivate Analytics

CAB Abstracts - CABI

AgBiotechNet Database

Animal Science Database

VetMed Resource

Environmental Impact Database

Horticultural Science Database

Nutrition and Food Sciences Database

Chemical Abstracts Service (CAS)

TUBITAK-ULAKBIM TR Index

SCOPUS

EUROPEAN JOURNAL OF BIOLOGY

Owner
Prof. Dr. Tansel AK
Istanbul University, Istanbul, Turkey

Responsible Manager
Prof. Dr. Sehnaz BOLKENT
Istanbul University, Istanbul, Turkey
sbolkent@istanbul.edu.tr

Correspondence Address
Istanbul University, Faculty of Science,
Department of Biology,
34134 Vezneciler, Fatih, Istanbul, Turkey
Phone: +90 (212) 455 57 00 (Ext. 15079)
Fax: +90 (212) 528 05 27
E-mail: ejb@istanbul.edu.tr
https://iupress.istanbul.edu.tr/en/journal/ejb/home

Publisher
Istanbul University Press
Istanbul University Central Campus,
34452 Beyazit, Fatih, Istanbul, Turkey
Phone: +90 (212) 440 00 00

Printed by
İlbey Matbaa Kağıt Reklam Org. Müc. San. Tic. Ltd. Şti.
2. Matbaacılar Sitesi 3NB 3 Topkapı / Zeytinburnu,
Istanbul, Turkey
www.ilbeymatbaa.com.tr
Certificate No: 17845

The publication language of the journal is English.

This is a scholarly, international, peer-reviewed and open-access journal published biannually in June and December.

Publication Type: Periodical

EUROPEAN
JOURNAL OF
BIOLOGY

EDITORIAL MANAGEMENT BOARD

EUROPEAN
JOURNAL OF
BIOLOGY

EDITORIAL BOARD

EUROPEAN
JOURNAL OF
BIOLOGY

Aims and Scope

European Journal of Biology (Eur J Biol) is an international, scientific, open access periodical published in accordance with independent, unbiased, and double-blinded peer-review principles. The journal is the official publication of Istanbul University Faculty of Science and it is published biannually on June and December. The publication language of the journal is English. European Journal of Biology has been previously published as IUFS Journal of Biology. It has been published in continuous publication since 1940.

European Journal of Biology aims to contribute to the literature by publishing manuscripts at the highest scientific level on all fields of biology. The journal publishes original research and review articles, and short communications that are prepared in accordance with the ethical guidelines in all fields of biology and life sciences.

The scope of the journal includes but not limited to; animal biology and systematics, plant biology and systematics, hydrobiology, ecology and environmental biology, microbiology, cell and molecular biology, biochemistry, biotechnology and genetics, physiology, toxicology, cancer biology, developmental biology, and stem cell biology.

The target audience of the journal includes specialists and professionals working and interested in all disciplines of biology.

The editorial and publication processes of the journal are shaped in accordance with the guidelines of the International Committee of Medical Journal Editors (ICMJE), World Association of Medical Editors (WAME), Council of Science Editors (CSE), Committee on Publication Ethics (COPE), European Association of Science Editors (EASE), and National Information Standards Organization (NISO). The journal is in conformity with the Principles of Transparency and Best Practice in Scholarly Publishing (doaj.org/bestpractice).

European Journal of Biology is currently indexed by Web of Science Zoological Record, CAB Abstracts (CABI), Chemical Abstracts Service (CAS), TUBITAK-ULAKBIM TR Index and Scopus.

Processing and publication are free of charge with the journal. No fees are requested from the authors at any point throughout the evaluation and publication process. All manuscripts must be submitted via the online submission system, which is available at dergipark.gov.tr/iufsjb. The journal guidelines, technical information, and the required forms are available on the journal's web page.

All expenses of the journal are covered by the Istanbul University.

Statements or opinions expressed in the manuscripts published in the journal reflect the views of the author(s) and not the opinions of the Istanbul University Faculty of Science, editors, editorial board, and/or publisher; the editors, editorial board, and publisher disclaim any responsibility or liability for such materials.

All published content is available online, free of charge at https://dergipark.org.tr/tr/pub/iufsjb. Printed copies of the journal are distributed free of charge.

OPEN ACCESS

Editor in Chief: Prof. Dr. Sehnaz BOLKENT
Address: Istanbul University, Faculty of Science, Department of Biology, 34134 Vezneciler, Fatih, Istanbul, TURKEY
Phone: +90 212 4555700 (Ext. 15079)
Fax: +90 212 5280527
E-mail: sbolkent@istanbul.edu.tr

EUROPEAN
JOURNAL OF
BIOLOGY

Instructions to Authors

European Journal of Biology (Eur J Biol) is an international, scientific, open access periodical published in accordance with independent, unbiased, and double-blinded peer-review principles. The journal is the official publication of Istanbul University Faculty of Science and it is published biannually on June and December. The publication language of the journal is English. European Journal of Biology has been previously published as IUFS Journal of Biology. It has been published in continuous publication since 1940.

European Journal of Biology aims to contribute to the literature by publishing manuscripts at the highest scientific level on all fields of biology. The journal publishes original research and review articles, and short communications that are prepared in accordance with the ethical guidelines in all fields of biology and life sciences.

The scope of the journal includes but not limited to; animal biology and systematics, plant biology and systematics, hydrobiology, ecology and environmental biology, microbiology, cell and molecular biology, biochemistry, biotechnology and genetics, physiology, toxicology, cancer biology, developmental biology, and stem cell biology.

The editorial and publication processes of the journal are shaped in accordance with the guidelines of the International Council of Medical Journal Editors (ICMJE), the World Association of Medical Editors (WAME), the Council of Science Editors (CSE), the Committee on Publication Ethics (COPE), the European Association of Science Editors (EASE), and National Information Standards Organization (NISO). The journal conforms to the Principles of Transparency and Best Practice in Scholarly Publishing (doaj.org/bestpractice).

Originality, high scientific quality, and citation potential are the most important criteria for a manuscript to be accepted for publication. Manuscripts submitted for evaluation should not have been previously presented or already published in an electronic or printed medium. Manuscripts that have been presented in a meeting should be submitted with detailed information on the organization, including the name, date, and location of the organization.

Manuscripts submitted to European Journal of Biology will go through a double-blind peer-review process. Each submission will be reviewed by at least three external, independent peer reviewers who are experts in their fields in order to ensure an unbiased evaluation process. The editorial board will invite an external and independent editor to manage the evaluation processes of manuscripts submitted by editors or by the editorial board members of the journal. The Editor in Chief is the final authority in the decision-making process for all submissions.

An approval of research protocols by the Ethics Committee in accordance with international agreements (World Medical Association Declaration of Helsinki "Ethical Principles for Medical Research Involving Human Subjects," amended in October 2013, www.wma.net) is required for experimental, clinical, and drug studies. If required, ethics committee reports or an equivalent official document will be requested from the authors.

For manuscripts concerning experimental research on humans, a statement should be included that shows the written informed consent of patients and volunteers was obtained following a detailed explanation of the procedures that they may undergo. Information on patient consent, the name of the ethics committee, and the ethics committee approval number should also be stated in the Materials and Methods section of the manuscript. It is the authors' responsibility to carefully protect the patients' anonymity. For photographs that may reveal the identity of the patients, signed releases of the patient or of their legal representative should be enclosed.

European Journal of Biology requires experimental research studies on vertebrates or any regulated invertebrates to comply with relevant institutional, national and/or international guidelines. The journal supports the principles of Basel Declaration (basel-declaration.org) and the guidelines published by International Council for Laboratory Animal Science (ICLAS) (iclas.org). Authors are advised to clearly state their compliance with relevant guidelines.

European Journal of Biology advises authors to comply with IUCN Policy Statement on Research Involving Species at Risk of Extinction and the Convention on the Trade in Endangered Species of Wild IUCN Policy Statement on Research Involving Species at Risk of Extinction and the Convention on the Trade in Endangered Species of Wild Fauna and Flora.

All submissions are screened by a similarity detection software (iThenticate by CrossCheck).

In the event of alleged or suspected research misconduct, e.g., plagiarism, citation manipulation, and data falsification/fabrication, the Editorial Board will follow and act in accordance with COPE guidelines.

Each individual listed as an author should fulfil the authorship criteria recommended by the International Committee of Medical Journal Editors (ICMJE - www.icmje.org). The ICMJE recommends that authorship be based on the following 4 criteria:

1 Substantial contributions to the conception or design of the work; or the acquisition, analysis, or interpretation of data for the work; AND
2 Drafting the work or revising it critically for important intellectual content; AND
3 Final approval of the version to be published; AND
4 Agreement to be accountable for all aspects of the work in ensuring that questions related to the accuracy or integrity of any part of the work are appropriately investigated and resolved.

In addition to being accountable for the parts of the work he/she has done, an author should be able to identify which co-authors are responsible for specific other parts of the work. In addition, authors should have confidence in the integrity of the contributions of their co-authors.

All those designated as authors should meet all four criteria for authorship, and all who meet the four criteria should be identified as authors. Those who do not meet all four criteria should be acknowledged in the title page of the manuscript.

European Journal of Biology requires corresponding authors to submit a signed and scanned version of the authorship contribution form (available for download through the journal's web page) during the initial submission process in order to act appropriately on authorship rights and to prevent ghost or honorary authorship. If the editorial board suspects a case of "gift authorship," the submission will be rejected without further review. As part of the submission of the manuscript, the corresponding author should also send a short statement declaring that he/she accepts to undertake all the responsibility for authorship during the submission and review stages of the manuscript.

European Journal of Biology requires and encourages the authors and the individuals involved in the evaluation process of submitted manuscripts to disclose any existing or potential conflicts of interests, including financial, consultant, and institutional, that might lead to potential bias or a conflict of interest. Any financial grants or other supports received for a submitted study from individuals or institutions should be disclosed to the Editorial Board. To disclose a potential conflict of interest, the ICMJE Potential Conflict of Interest Disclosure Form should be filled and submitted by all contributing authors. Cases of a potential conflict of interest of the editors, authors, or reviewers are resolved by the journal's Editorial Board within the scope of COPE and ICMJE guidelines.

The Editorial Board of the journal handles all appeal and complaint cases within the scope of COPE guidelines. In such cases, authors should get in direct contact with the editorial office regarding their appeals and complaints. When needed, an ombudsperson may be assigned to resolve cases that cannot be resolved internally. The Editor in Chief is the final authority in the decision-making process for all appeals and complaints.

When submitting a manuscript to European Journal of Biology, authors accept to assign the copyright of their manuscript to Istanbul University Faculty of Science. If rejected for publication, the copyright of the manuscript will be assigned back to the authors. European Journal of Biology requires each submission to be accompanied by a Copyright Transfer Form (available for download at the journal's web page). When using previously published content, including figures, tables, or any other material in both print and electronic formats, authors must obtain permission from the copyright holder. Legal, financial and criminal liabilities in this regard belong to the author(s).

Statements or opinions expressed in the manuscripts published in European Journal of Biology reflect the views of the author(s) and not the opinions of the editors, the editorial board, or the publisher; the editors, the editorial board, and the publisher disclaim any responsibility or liability for such materials. The final responsibility in regard to the published content rests with the authors.

MANUSCRIPT SUBMISSION

European Journal of Biology endorses ICMJE-Recommendations for the Conduct, Reporting, Editing, and Publication of Scholarly Work in Medical Journals (updated in December 2015 - http://www.icmje.org/icmje-recommendations.pdf). Authors are required to prepare manuscripts in accordance with the CONSORT guidelines for randomized research studies, STROBE guidelines for observational original research studies, STARD guidelines for studies on diagnostic accuracy, PRISMA guidelines for systematic reviews and meta-analysis, ARRIVE guidelines for experimental animal studies, TREND guidelines for non-randomized public behaviour, and COREQ guidelines for qualitative research.

Manuscripts can only be submitted through the journal's online manuscript submission and evaluation system, available at the journal's web page. Manuscripts submitted via any other medium will not be evaluated.

Manuscripts submitted to the journal will first go through a technical evaluation process where the editorial office staff will ensure that the manuscript has been prepared and submitted in accordance with the journal's guidelines. Submissions that do not conform to the journal's guidelines will be returned to the submitting author with technical correction requests.

During the initial submission, authors are required to submit the following:

- Copyright Agreement Form,
- Author Contributions Form, and

ICMJE Potential Conflict of Interest Disclosure Form (should be filled in by all contributing authors). These forms are available for download at the journal's web page.

Preparation of the Manuscript

Title page: A separate title page should be submitted with all submissions and this page should include:

- The full title of the manuscript as well as a short title (running head) of no more than 50 characters,
- Name(s), affiliations, and highest academic degree(s) of the author(s),
- Grant information and detailed information on the other sources of support,
- Name, address, telephone (including the mobile phone number) and fax numbers, and email address of the corresponding author,
- Acknowledgment of the individuals who contributed to the preparation of the manuscript but who do not fulfil the authorship criteria.

Abstract: Abstract with subheadings should be written as structured abstract in submitted papers except for Review Articles and Letters to the Editor. Please check Table 1 below for word count specifications (250 words).

Keywords: Each submission must be accompanied by a minimum of three to a maximum of six keywords for subject indexing at the end of the abstract. The keywords should be listed in full without abbreviations.

Manuscript Types

Original Articles: This is the most important type of article since it provides new information based on original research. A structured abstract is required with original articles and it should include the following subheadings: Objective, Materials and Methods, Results and Conclusion. The main text of original articles should be structured with Introduction, Materials and Methods, Results, Discussion, and Conclusion subheadings. Please check Table 1 for the limitations of Original Articles.

Statistical analysis to support conclusions is usually necessary. Statistical analyses must be conducted in accordance with international statistical reporting standards. Information on statistical analyses should be provided with a separate subheading under the Materials and Methods section and the statistical software that was used during the process must be specified.

Units should be prepared in accordance with the International System of Units (SI).

Short Communications: Short communication is for a concise, but independent report representing a significant contribution to Biology. Short communication is not intended to publish preliminary results. But if these results are of exceptional interest and are particularly topical and relevant will be considered for publication.

Short Communications should include an abstract and should be structed with the following subheadings: "Introduction", "Materials and Methods", "Results and Discussion".

Editorial Comments: Editorial comments aim to provide a brief critical commentary by reviewers with expertise or with high reputation in the topic of the research article published in the journal. Authors are selected and invited by the journal to provide such comments. Abstract, Keywords, and Tables, Figures, Images, and other media are not included.

Review Articles: Reviews prepared by authors who have extensive knowledge on a particular field and whose scientific background has been translated into a high volume of publications with a high citation potential are welcomed. These authors may even be invited by the journal. Reviews should describe, discuss, and evaluate the current level of knowledge of a topic in clinical practice and should guide future studies. The main text should contain Introduction, Experimental and Clinical Research Consequences, and Conclusion sections. Please check Table 1 for the limitations for Review Articles.

Letters to the Editor: This type of manuscript discusses important parts, overlooked aspects, or lacking parts of a previously published article. Articles on subjects within the scope of the journal that might attract the readers' attention, particularly educative cases, may also be submitted in the form of a "Letter to the Editor." Readers can also present their comments on the published manuscripts in the form of a "Letter to the Editor." Abstract, Keywords, and Tables, Figures, Images, and other media should not be included. The text should be unstructured. The manuscript that is being commented on must be properly cited within this manuscript.

Tables

Tables should be included in the main document, presented after the reference list, and they should be numbered consecutively in the order they are referred to within the main text. A descriptive title must be placed above the tables. Abbreviations used in the tables should be defined below the tables by footnotes (even if they are defined within the main text). Tables should be created using the "insert table" command of the word processing software and they should be arranged clearly to provide easy reading. Data presented in the tables should not be a repetition of the data presented within the main text but should be supporting the main text.

Figures and Figure Legends

Figures, graphics, and photographs should be submitted as separate files (in TIFF or JPEG format with 1200 dpi for graphic and 600 dpi for colour images) through the submission system. The files should not be embedded in a Word document or the main document. When there are figure subunits, the subunits should be labeled merged to form a single image. Each subunit should be submitted separately through the submission system. Images

Table 1. Limitations for each manuscript type

Type of manuscript	Word limit	Abstract word limit	Reference limit	Table limit	Figure limit
Original Article	4500	250 (Structured)	No limit	6	Maximum 10
Short Communication	2500	200	30	3	4
Review Article	5500	250	No limit	5	6
Letter to the Editor	500	No abstract	5	No tables	No media

should be labeled (a, b, c, etc.) to indicate figure subunits. Thick and thin arrows, arrowheads, stars, asterisks, and similar marks can be used on the images to support figure legends. Like the rest of the submission, the figures too should be blind. Any information within the images that may indicate an individual or institution should be blinded. The minimum resolution of each submitted figure should be 300 DPI. To prevent delays in the evaluation process, all submitted figures should be clear in resolution and large in size (minimum dimensions: 100 × 100 mm). Figure legends should be listed at the end of the main document.

All acronyms and abbreviations used in the manuscript should be defined at first use, both in the abstract and in the main text. The abbreviation should be provided in parentheses following the definition.

When a drug, chemical, product, hardware, or software program is mentioned within the main text, product information, including the name of the product, the producer of the product, and city and the country of the company (including the state if in USA), should be provided in parentheses in the following format: "Discovery St PET/CT scanner (General Electric, Milwaukee, WI, USA)".

All references, tables, and figures should be referred to within the main text, and they should be numbered consecutively in the order they are referred to within the main text.

Limitations, drawbacks, and the shortcomings of original articles should be mentioned in the Discussion section before the conclusion paragraph.

References

While citing publications, preference should be given to the latest, most up-to-date publications. If an ahead-of-print publication is cited, the DOI number should be provided. Authors are responsible for the accuracy of references. Journal titles should be abbreviated in accordance with the journal abbreviations in Index Medicus/ MEDLINE/PubMed. When there are six or fewer authors, all authors should be listed. If there are seven or more authors, the first six authors should be listed followed by "et al." In the main text of the manuscript, references should be cited using Arabic numbers in parentheses. The reference styles for different types of publications are presented in the following examples.

Journal Article: Rankovic A, Rancic N, Jovanovic M, Ivanović M, Gajović O, Lazić Z, et al. Impact of imaging diagnostics on the budget – Are we spending too much? Vojnosanit Pregl 2013; 70: 709-11.

Book Section: Suh KN, Keystone JS. Malaria and babesiosis. Gorbach SL, Barlett JG, Blacklow NR, editors. Infectious Diseases. Philadelphia: Lippincott Williams; 2004.p.2290-308.

Books with a Single Author: Sweetman SC. Martindale the Complete Drug Reference. 34th ed. London: Pharmaceutical Press; 2005.

Editor(s) as Author: Huizing EH, de Groot JAM, editors. Functional reconstructive nasal surgery. Stuttgart-New York: Thieme; 2003.

Conference Proceedings: Bengisson S. Sothemin BG. Enforcement of data protection, privacy and security in medical informatics. In: Lun KC, Degoulet P, Piemme TE, Rienhoff O, editors. MEDINFO 92. Proceedings of the 7th World Congress on Medical Informatics; 1992 Sept 6-10; Geneva, Switzerland. Amsterdam: North-Holland; 1992. pp.1561-5.

Scientific or Technical Report: Cusick M, Chew EY, Hoogwerf B, Agrón E, Wu L, Lindley A, et al. Early Treatment Diabetic Retinopathy Study Research Group. Risk factors for renal replacement therapy in the Early Treatment Diabetic Retinopathy Study (ETDRS), Kidney Int: 2004. Report No: 26.

Thesis: Yılmaz B. Ankara Üniversitesindeki Öğrencilerin Beslenme Durumları, Fiziksel Aktiviteleri ve Beden Kitle İndeksleri Kan Lipidleri Arasındaki Ilişkiler. H.Ü. Sağlık Bilimleri Enstitüsü, Doktora Tezi. 2007.

Epub Ahead of Print Articles: Cai L, Yeh BM, Westphalen AC, Roberts JP, Wang ZJ. Adult living donor liver imaging. Diagn Interv Radiol. 2016 Feb 24. doi: 10.5152/dir.2016.15323. [Epub ahead of print].

Manuscripts Published in Electronic Format: Morse SS. Factors in the emergence of infectious diseases. Emerg Infect Dis (serial online) 1995 Jan-Mar (cited 1996 June 5): 1(1): (24 screens). Available from: URL: http:/ www.cdc.gov/ncidodlElD/cid.htm.

REVISIONS

When submitting a revised version of a paper, the author must submit a detailed "Response to the reviewers" that states point by point how each issue raised by the reviewers has been covered and where it can be found (each reviewer's comment, followed by the author's reply and line numbers where the changes have been made) as well as an annotated copy of the main document. Revised manuscripts must be submitted within 30 days from the date of the decision letter. If the revised version of the manuscript is not submitted within the allocated time, the revision option may be cancelled. If the submitting author(s) believe that additional time is required, they should request this extension before the initial 30-day period is over.

Accepted manuscripts are copy-edited for grammar, punctuation, and format. Once the publication process of a manuscript is completed, it is published online on the journal's webpage as an ahead-of-print publication before it is included in its scheduled issue. A PDF proof of the accepted manuscript is sent to the corresponding author and their publication approval is requested within 2 days of their receipt of the proof.

Editor in Chief: Prof. Dr. Sehnaz BOLKENT
Address: Istanbul University, Faculty of Science, Department of Biology, 34134 Vezneciler, Fatih, Istanbul, TURKEY
Phone: +90 212 4555700 (Ext. 15079)
Fax: +90 212 5280527
E-mail: sbolkent@istanbul.edu.tr

EUROPEAN
JOURNAL OF
BIOLOGY

Contents

Research Articles

75 **Histological and Electron Microscopical Observations on the Testis and Male Accessory Glands of *Poecilimon ataturki* Ünal, 1999 (Orthoptera, Tettigoniidae)**

Damla Amutkan Mutlu, Irmak Polat, Zekiye Suludere

82 **Antibiofilm and Anti-Quorum Sensing Activities of Vaginal Origin Probiotics**

Esin Kiray

91 **Oxidative Stress Status in Testis of Type-2 Diabetic Rats Treated with Delta-9-Tetrahydrocannabinol**

Ebrar Tutar, Beti Pesen, Zeynep Mine Coskun Yazici, Sema Bolkent

97 **Biochemical Fingerprints of Some Endemic Plants Growing in Gypsum Soils: Attenuated Total Reflection-Fourier Transform Infrared (ATR-FTIR) Spectroscopic Study**

Aysenur Kayabas, Ertan Yildirim

107 **Investigation of the Effects of Autophagy Signaling on the Transcription of Yeast Retrotransposon Ty2-917**

Sezai Turkel, Ceyda Colakoglu, Tugce Karaduman

119 **Therapeutic Effects of *Momordica charantia* L. Ethanolic Extract on Acetic Acid-Induced Ulcerative Colitis in Rats**

Dilek Ozbeyli, Ali Sen, Asli Aykac, Kerem Terali, Ozlem Tugce Cilingir-Kaya, Ismail Senkardes, Goksel Sener

129 **Antitumoral Properties of a Pincer-Type Isonicotinohydrazone-Hg(II) Complex**

Burcu Saygıdeğer Demir, Aycan Sezan, Ezgi Derinoz, Eylem Nas, Mehmet Ozerten, Ghodrat Mahmoudi, Yasemin Saygideger

138 **The Activation of PI3K/AKT/mTOR Signaling Pathway in Response to Cabazitaxel Treatment in Metastatic Castration-Resistant Prostate Cancer Cells**

Isil Ezgi Eryilmaz, Gamze Guney Eskiler, Ceyda Colakoglu, Unal Egeli, Gulsah Cecener

145 **Proteomic Analysis Revealed Underlying Biological Pathways Associated with Hormetic Response of Hormone-Positive Breast Cancer Cell Line Exposed to Low-Dose Flavonoid Mixture**

Mete Bora Tuzuner, Ayse Begum Ceviz

154 **Antioxidant Activities of *Eremurus spectabilis* M. Bieb. Extracts and Sulfur Compounds**

Bertan Boran Bayrak, Refiye Yanardag

164 **Scape, Rhizome and Root Anatomy of *Polygonatum* Species from Turkey**

Yeter Yesil, Fatma Neriman Ozhatay

173 **Protective Effects of *Petroselinum crispum* (Parsley) Extract Against Methotrexate-Induced Hepatotoxicity**

Busra Ertas, Feyza Berin Turan, Dilek Ozbeyli, Refiye Yanardag, Ozlem Sacan, Goksel Sener

Review Article

179 **Zebrafish Embryo as an Emerging Model Organism in Neurodevelopmental Toxicity Research**

Sukriye Caliskan, Ebru Emekli-Alturfan

ISTANBUL UNIVERSITY PRESS

RESEARCH ARTICLE

Eur J Biol 2021; 80(2): 75-81

Histological and Electron Microscopical Observations on the Testis and Male Accessory Glands of *Poecilimon ataturki* Ünal, 1999 (Orthoptera, Tettigoniidae)

Damla Amutkan Mutlu[1], Irmak Polat[2], Zekiye Suludere[1]

[1]Gazi University, Faculty of Science, Department of Biology, Ankara, Turkey
[2]Çankırı Karatekin University, Faculty of Science, Department of Biology, Çankırı, Turkey

ORCID IDs of the authors: D.A.M. 0000-0002-4780-8520; I.P. 0000-0001-7230-4589; Z.S. 0000-0002-1207-5814

Please cite this article as: Amutkan Mutlu D, Polat I, Suludere Z. Histological and Electron Microscopical Observations on the Testis and Male Accessory Glands of *Poecilimon ataturki* Ünal, 1999 (Orthoptera, Tettigoniidae). Eur J Biol 2021; 80(2): 75-81. DOI: 10.26650/EurJBiol.2021.1001795

ABSTRACT

Objective: The literature has many studies in the world about the morphology and histology of insect tissues, especially structures related to reproductive systems. However, there are no studies about the biology *of Poecilimon ataturki* Ünal, 1999 (Orthoptera, Tettigoniidae). For this reason, we aimed that the morphology and the structure of the testes and the accessory glands in *P. ataturki* are revealed.

Materials and Methods: In the present study, the histology and morphology of organs of the reproductive system in male *P. ataturki*, an endemic species in Turkey was examined by light microscope, scanning electron microscope, transmission electron microscope, and stereomicroscope.

Results: The reproductive system of male *P. ataturki* is composed of two testes, two vas deferens and short and long accessory glands. Each testis includes numerous follicles where the sperm generation occurs in. There are cysts in the follicles, one of which is in a particular sperm development. 3 different development stages are observed in follicles as growth zone, maturation zone and transformation zone. During these developmental stages, first spermatocytes reproduce by mitosis, and then they turn into spermatids by meiosis. Spermatozoa are also formed by the transformation of spermatids. Thus, the stages of spermatogenesis and spermiogenesis are completed. The accessory glands, whose main task is to produce secretion in order to facilitate the feeding of sperm and their transfer to the female, consist of many tubular structures, long and short. It is seen that it consists of single-layered epithelial tissue in cross sections of the accessory gland tubules.

Conclusion: As a consequence of this work, it has been evinced that male reproductive system elements belonging to *P. ataturki* show high similarity with the male reproductive systems of other species in the Tettigoniidae family.

Keywords: Male reproductive system, light microscopy, scanning electron microscopy, transmission electron microscopy, insect

INTRODUCTION

Studying the reproductive systems of the insects is central to bring out their population above threshold levels for endangered species. The male reproductive system has three main functions. These are to produce sperm by the male reproductive cells, to manufacture the protective fluid around the sperm via the glands, and to transfer the sperms that are produced to the female reproductive system (1-5).

Testes in order Orthoptera are made up of approximately 300-350 follicles which are tube or finger-shaped structure (2,4,6). There are cells in different stages of development in a testicular follicle. The germ cells which found at the distal side of follicles are called the sper-

Corresponding Author: Damla Amutkan Mutlu E-mail: damlamutkan@gazi.edu.tr
Submitted: 29.09.2021 • **Revision Requested:** 11.10.2021 • **Last Revision Received:** 11.10.2021 • **Accepted:** 13.10.2021 • **Published Online:** 01.11.2021

matocytes. The spermatocytes are comprised by the mitotic division and their numbers are increased. After that, spermatocytes located at the middle zone of testicular follicles undergo the meiosis and the spermatids occur. In the proximal side of the follicles, the spermatids are finally differentiated to the mature form, spermatozoa. The spermatozoa become mature and after that heads of sperm join together. This structure is named as spermatodesm (4,7,8).

The male accessory glands in insects play an important role for male fertility (9). It is the essential source of the production of proteinaceous secretions, called as accessory gland proteins (5,9,10). The accessory glands proteins are important for the competition between sperm during the mating. This situation is the major factor that affects to the male reproductive success (3,10).

Poecilimon ataturki Ünal, 1999 is an endemic species in Turkey belonging to the Tettigoniidae family (Orthoptera). Previous studies in the literature indicate that the *P. ataturki* is distributed in Bolu, Çankırı, Kastamonu, and Karabük Provinces (11-15). The name of *P. ataturki* is given by Prof. Dr. Mustafa Ünal in honor of Mustafa Kemal Atatürk, the founder of the modern Republic of Turkey in 1923 (11).

There are many literatures are found relevant to the taxonomy, the systematic, and the distribution of this species. However, there are no studies about the biology (such as alimentary system, reproductive organs of male and female individuals) of this species. For this purpose, the morphology and the structure of the testes that produce sperm and the accessory glands that manufacture seminal fluids those mix with sperm in *P. ataturki* are the subject of this paper.

MATERIALS AND METHODS

Supply of the Tissues

Adult individuals of *P. ataturki* were taken using a sweep net in Bolu province, Hamidiye Village in July 2019. Five male were anesthetized via the fumes of ethyl acetate. Some of the testes and male accessory glands were dissected in Na-PBS (pH 7.2) and some in 70% ethanol under stereomicroscope.

Light Microscope (LM) Analysis

Some of the specimens were fixed in formaldehyde (10%), dehydrated and blocked in paraffin. The sections (5-6 µm) were taken and were stained with Mallory's trichrome and routine staining, Hematoxylin-Eosin (H&E). Ultimately, the photos were shot with an Olympus BX51 photomicroscope in Gazi University.

Semi-thin sections taken from araldite blocks prepared in accordance with the procedure given below for transmission electron microscope (TEM) were stained with 1% methylene blue to reveal general histological organization.

Scanning Electron Microscope (SEM) Analysis

For the SEM investigations, the testes and male accessory glands were firstly fixed in 5% glutaraldehyde (pH 7.2) and were dehydrated. In following process, the specimens were dried with critical point dryer (Polaron CPD 7501). Dried specimens were coated with gold (Polaron SC 502). The testes and male accessory glands were finally examined with SEM (JEOL JSM 6060 LV, accelerating voltage 5-10 kV). The observations were done in Prof. Dr. Zekiye Suludere Electron Microscope Center in Gazi University.

Transmission Electron Microscope (TEM) Analysis

For the TEM observations, testis and accessory glands were first fixed twice: in 5% glutaraldehyde and then in 1% osmium tetroxide. After the fixation process, they were dehydrated and were embedded in Araldite blocks. Afterwards, the ultrathin sections were taken from the blocks with using ultramicrotome. Then, they were double stained with lead citrate and uranyl acetate dyes. The examinations with TEM (JEOL JEM 1400, accelerating voltage 80 kV) were done in Prof. Dr. Zekiye Suludere Electron Microscope Center in Gazi University.

RESULTS

The internal reproductive structures of male *P. ataturki* are made up of paired testes which are covered by a peritoneal sheath and aerated by several tracheoles, paired vas deferens, and as well as accessory glands (Figure 1). The testes which lay across the body cavity are elongated ovoid in form (Figure 1). Each testis is coated by an epithelium.

The cells in different stages of development are discriminated in several testicular follicles which are found each testis. The cysts consist of grouping of germ cells in the same growth stage (Figure 2A-B). The cells called spermatogonia are located in the germarium region at the distal end of the follicle. Other developmental stages are growth, maturation and transformation zones. The cells in here are spermatocytes, spermatids and spermatozoa in respectively. Spermatocytes are diploid cells with

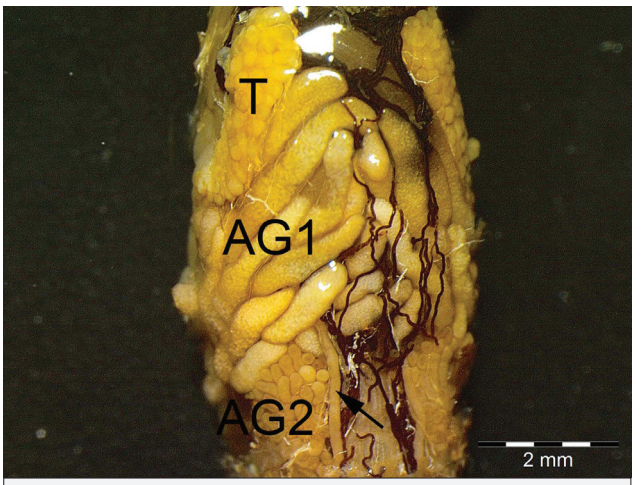

Figure 1. The general stereomicroscopic view of the male reproductive system in *P. ataturki*. T: testis, AG1: long accessory glands, AG2: short accessory glands, arrow: vas deferens, Scale bar=2 mm.

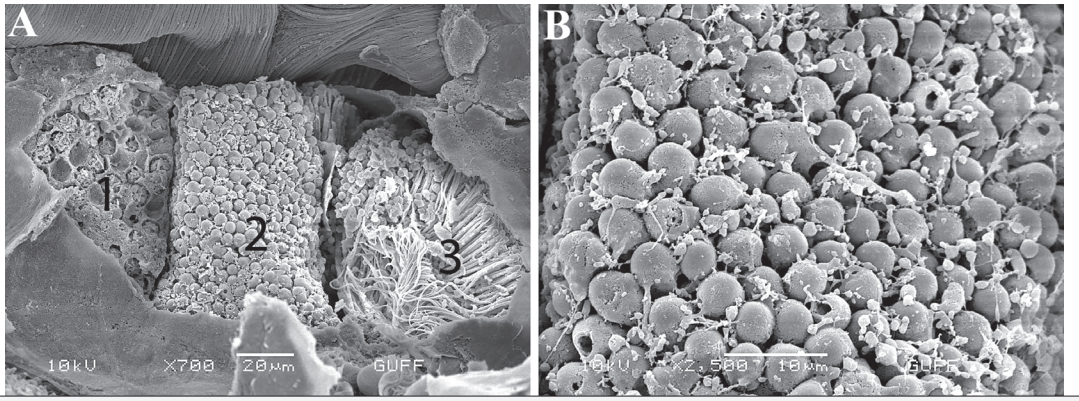

Figure 2. **A.** The SEM image of the cyst with different stages of development in the testicular follicle. 1: spermatocytes before the meiosis 2: early spermatids, 3: spermatozoa, Scale bar=20 µm; **B.** The SEM image of early spermatids with no tail, Scale bar=10 µm.

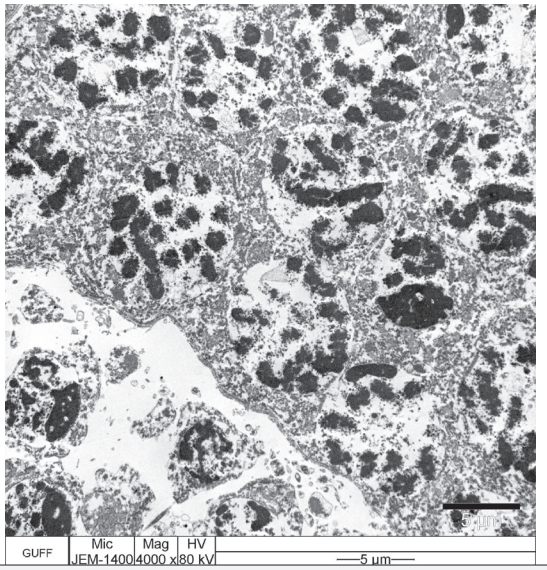

Figure 3. The TEM image of the cyst with spermatocytes, Scale bar=5 µm.

large spherical nuclei without tails that reproduce by mitosis in cysts in the growth zone. Before meiosis, the nucleus of cells looks as if to be fragmented TEM micrograph (Figure 3). When it comes to the maturation zone, spermatocytes form spermatids as a result of meiosis, which are haploid. The transformation of spermatids is characterized by tail formation. The spermatids in the early stage look like cells with elliptical nucleus which is located in the midst of the cell and no tail (Figures 2B, 4A-B). In the late stage of spermatids, the thin tail structure starts to be apparent and cells have a head beginning to elongate and an elongated tail (Figures 4C, 5). When the transformation of the spermatids is finished in the transformation zone, the spermatozoa occur. During the transformation of spermatids into sperm cells or spermatozoa, the head of the sperm completes elongation (Figure 6A-B). The axoneme and two mitochondrial derivates appear along the flagella in the cross sections of the mature sperm cells (Figure 4C).

The acrosome region is seen in the apex of the sperm head. This region is shirt collar in shape and the hole can be observed close to the tip of the acrosome (Figure 6A-B). Sperm heads are

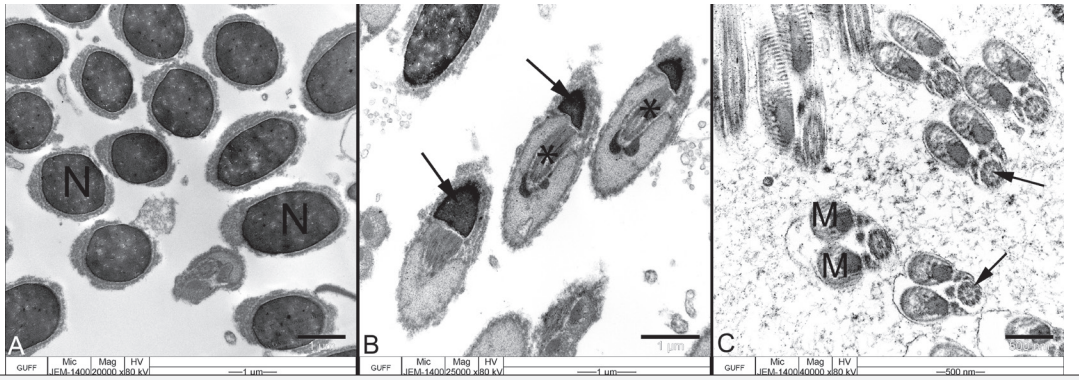

Figure 4. **A.** The TEM image of the beginning of tail formation in spermatids, N: nucleus, Scale bar=1 µm; **B.** The TEM image of the beginning of tail formation in spermatids, arrow: acrosome, asterisk: centriol, Scale bar=1 µm; **C.** The axoneme (arrows) and two mitochondrial derivatives (M) in the TEM image, Scale bar= 500nm.

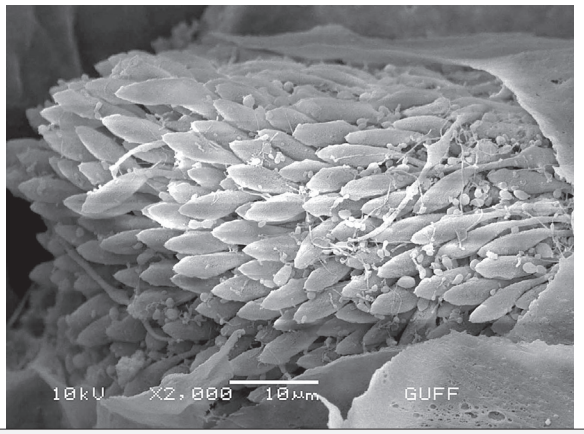

Figure 5. The late stage of spermatids with thin tail and a head beginning to elongate (SEM), Scale bar=10 µm.

19,2±1,7 µm in length. The tail is quite thin and long compared to the head of the sperm. We detected many granules among the spermatozoa (Figure 6A).

The mature spermatozoa are packed together from the head to the holders to form bundles in cysts. This structure is called spermatodesm (Figure 7).

The accessory glands are tubular structures with closed end (Figures 1, 8). The male accessory glands of this species, *P. ataturki* consist of two different types of glandular tubule groups: the first group consisting of short and thin tubules and the second group consisting of long and thick tubules. The long tubes generally arise in front of the hindgut. Its outer surface is quite flat and surrounded by a trachea network. The epithelial layer is seen as a single-layered in cross sections in both groups of tubules. The difference between them is related to tubule lengths and di-

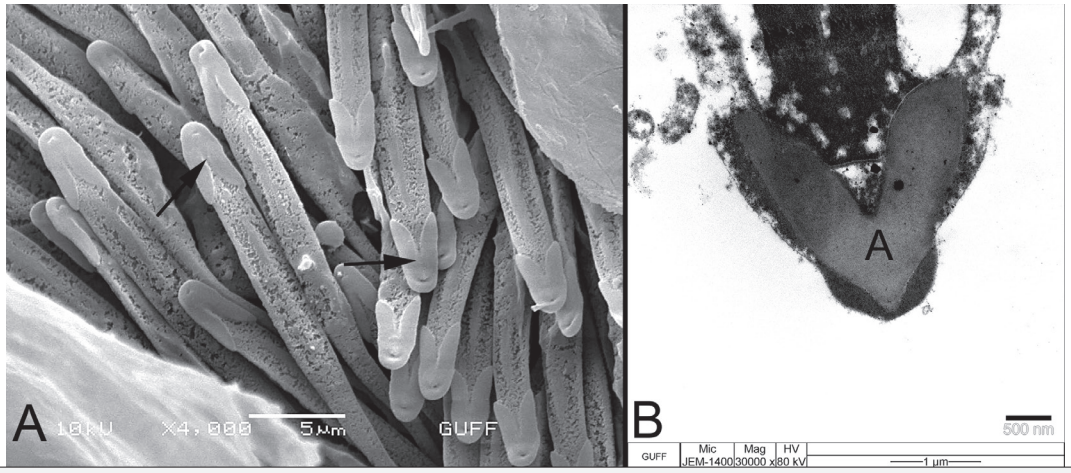

Figure 6. **A.** The SEM image of the mature sperm cell with head which completes elongation and long tail. Arrows: acrosome, Scale bar=5 µm; **B.** The TEM image of the sperm head with acrosome (A), Scale bar= 1 µm.

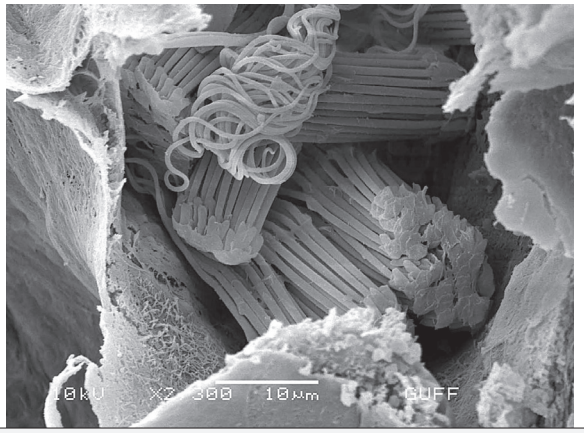

Figure 7. The SEM image of the mature spermatozoa packed together called spermatodesm, Scale bar= 10 µm.

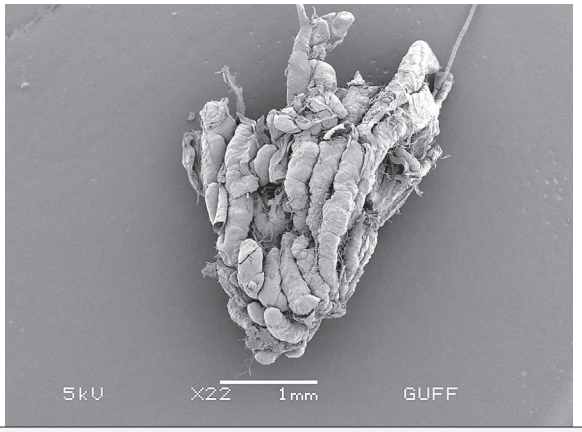

Figure 8. The SEM image of the long accessory glands, Scale bar= 1 mm.

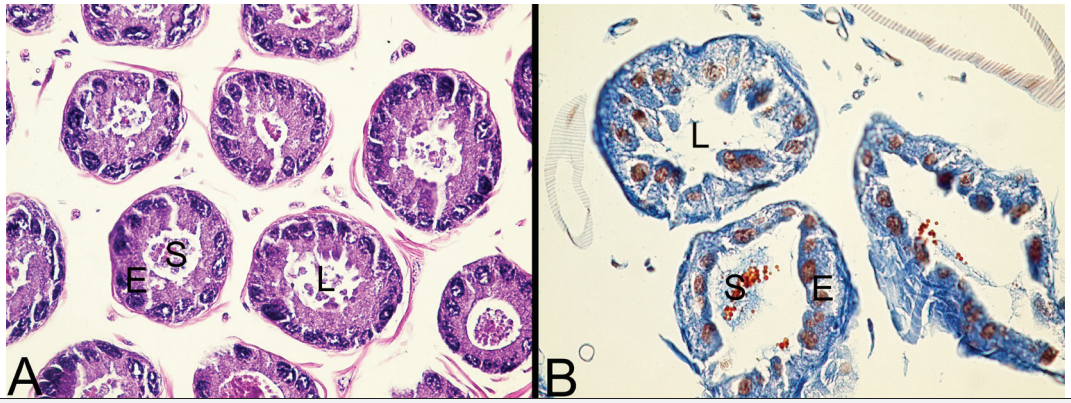

Figure 9. **A.** The light microscopic image of the cross sections of long accessory glands. E: epithelial cell layer, L: lumen, S: secretion of the accessory gland cells, H&E staining, X400; **B.** The light microscopic image of the cross sections of long accessory glands. E: epithelial cell layer, L: lumen, S: secretion of the accessory gland cells, Mallory's trichrome staining, X400.

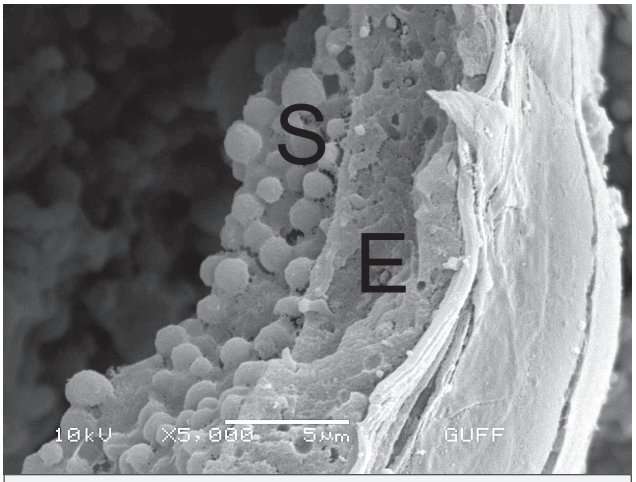

Figure 10. The SEM image of different sizes of secretory granules (S) in the lumen of the accessory glands. E: epithelial cell layer, Scale bar= 5 µm.

ameters. No significant difference was observed ultrastructurally. The shape of the cells in the epithelial layer is cubic or pyramidal (Figure 9A-B). Different sizes of secretory vesicles are observed in the lumen of the accessory gland tubules (Figure 10).

DISCUSSION

Male reproductive organs are generally similar in insect groups. However, some minor or major differences in these structures can be observed between different taxa. Many studies support the idea that many of the differences in these structures can be used as distinctive characters (4,5,16-19).

The elements of the reproductive system are usually testis, vasa deferentia, seminal vesicles, accessory glands, and ejaculatory duct in male insects, despite some differences. In accordance with this rule, two testes, two vas deferens, and ejaculatory duct have been observed in some insect species, such as *Drepanosiphum platanoidis* (Schrank), *Euceraphis betulae* (Koch), *Macrosiphoniella tanacetaria* (Kaltenbach), and *Myzocallis walshii* (Monell) from Aphididae (Homoptera) (20), *Melanoplus sanguinipes* (Fabricius, 1798) (18) and *Pseudochorthippus parallelus parallelus* (Zetterstedt, 1821) from Acrididae (Orthoptera) (4), *Gryllus sigillatus* (Walker, 1869) from Gryllidae (Orthoptera) (21). On the other hand, in addition to these structures, seminal vesicles are also found in some insect species such as *Balclutha brevis* Lindberg, 1954 from Cicadellidae (Hemiptera) (22). In *P. ataturki*, the situation is like the species in the first group, the seminal vesicle is absent.

Insects are the animal group with the most species diversity and high reproductive and survival ability (23, 24). Although insects generally have high reproductive capacity, the number of follicles in each testicle varies between various groups (25). Some species such as *P. ataturki, P. parallelus parallelus* (4), *Poecilimon cervus* Karabağ, 1950 (Orthoptera, Tettigoniidae) (26), and *M. sanguinipes* (18) has a large number of follicles in their testis, while some species has much less follicle number. For example, *Orphullela punctata* (De Geer, 1773) (Orthoptera, Acrididae) (2), larval *Dione juno* (Crameri 1779) (Lepidoptera, Nymphalidae) and larval *Agraulis vanilla* (Linnaeus, 1758) males have four follicles (27), *Martarega betoi* (Heteroptera, Notonectidae) (28) and *Furcatopanorpa longihypovalva* (Hua and Cai, 2009) (Mecoptera, Panorpidae) males have two follicles (29) and *Tuberculatus eggleri* Börner, *E. betulae, D. platanoidis, M. walshii, and M. tanacetaria* (Homoptera, Aphididae) males have three follicles (20) in their testes. One of the most important points we observed in this study we conducted is related to the sperm production capacity of each testis which has a big size. Because, we found a large number of follicles in each testis of *P. ataturki*. Similarly, the number of cysts in the follicles was also quite high. Pitnick and Markow also stated that daily sperm production is generally directly proportional to testicular size (30).

In addition to differences in testicular and follicle structure, sperm structure can also vary greatly between species. This

is due to the fact that the sperm can have a suitable function and structure for successful fertilization of the insect (24,31,32). These differences in sperm structures can be phylogenetically determinant (33).

The size, morphological and histological structure, and the results of histochemical staining of the male reproductive glands in insects may vary greatly (34). For example, there are different subtypes of accessory glands according to the diameter and length of the tubules in various orthopteroid families, such as three or nine in some Acrididae species, six in some Gryllidae species and two in some Tettigoniidae species (21,35,36). The accessory glands of *P. ataturki* include two different types as long and short tubules, as in other Tettigoniidae species, such as *P. cervus*, *Steropleurus elegans* (Fischer), *Bolivarius siculus* (Fischer), *Rhacocleis annulata* Fieber, *Tylopsis liliifolia* Fabricius 1793, and *Platycleis intermedia* (Serville, 1838) (17,26,37). For this reason, the accessory glands of *P. ataturki* also show high similarity morphologically with the accessory glands of other Tettigoniidae species.

CONCLUSION

When all these results are evaluated, it can be said that the male reproductive system of *P. ataturki*, with some minor differences, closely resembles that of other species in the Tettigoniidae family. We hope that this study will serve as a basis for future studies on insect groups, especially species belonging to the order Orthoptera.

Acknowledgments: The authors owe Prof. Dr. Mustafa ÜNAL from Abant İzzet Baysal University a great debt of gratitude for diagnosis of the species studied and Gazi University Academic Writing and Research Center for their help and support in the proofreading of the current study.

Informed Consent: Written consent was obtained from the participants.

Peer Review: Externally peer-reviewed.

Author Contributions: Conception/Design of Study- D.A.P., I.P., Z.S.; Data Acquisition- D.A.P., I.P.; Data Analysis/Interpretation- D.A.P., I.P., Z.S.; Drafting Manuscript- D.A.P., I.P., Z.S.; Critical Revision of Manuscript- D.A.P., I.P., Z.S.; Final Approval and Accountability- D.A.P., I.P., Z.S.

Conflict of Interest: Authors declared no conflict of interest.

Financial Disclosure: Authors declared no financial support.

REFERENCES

1. Gillott C. Male accessory gland secretions: Modulators of female reproductive physiology and behavior. Annu Rev Entomol 2003; 48: 163-84.
2. Silva DSM, Cossolin JFS, Pereira MR, Lino-Neto J, Sperber CF, Serrão JE. Male reproductive tract and spermatozoa ultrastructure in the grasshopper *Orphulella punctata* (De Geer, 1773) (Insecta, Orthoptera, Caelifera). Microsc Res Tech 2018; 81(2): 250-5.
3. Stephens K, Cardullo RA, Thaler CD. *Culex pipiens* sperm motility is initiated by a trypsin-like protease from male accessory glands. Mol Reprod Dev 2018; 85(5): 440-8.
4. Polat I, Amutkan Mutlu D, Ünal M, Suludere Z. Histology and ultrastructure of the testis and vas deferens in *Pseudochorthippus parallelus parallelus* (Orthoptera, Acrididae). Microsc Res Tech 2019; 82(9): 1461-70.
5. Polat I, Amutkan Mutlu D, Suludere Z. Accessory glands of male reproductive system in *Pseudochorthippus parallelus parallelus* (Zetterstedt, 1821) (Orthoptera: Acrididae): A light and electron microscopic study. Microsc Res Tech 2020; 83(3): 232-8.
6. White MJD. Patterns of spermatogenesis in grasshoppers. Aust J Zool 1954; 3: 222-6.
7. Chapman RF. The Insect Structure and Function. 5th ed. UK: Cambridge University Press; 2013.
8. Klowden MJ. Physiological Systems in Insects. 3rd ed. London, UK: Akademic Press; 2013.
9. Sharma V, Pandey AK, Kumar A, Misra S, Gupta HP, Gupta S, et al. Functional male accessory glands and fertility in *Drosophila* require novel ecdysone receptor. PLoS Genet 2017; 13(5): 1-26.
10. Gotoh A, Shigenobu S, Yamaguchi K, Kobayashi S, Ito F, Tsuji K. Transcriptome characterization of male accessory glands in ants to identify molecules involved in their reproductive success. Insect Mol Biol 2018; 27(2): 212-20.
11. Ünal M. Notes on Orthoptera of Western Turkey, with description of a new genus and four new species. J Orthoptera Res 1999; 8: 243-55.
12. Ünal M. Notes on Orthoptera of Western Turkey, with description of a new genus and four new species. J Orthoptera Res 2000; 9: 89-102.
13. Ünal M. *Poecilimon* Fischer (Orthoptera: Tettigoniidae: Phaneropterinae) species of the Batı Karadeniz region of Turkey, NW Anatolia. Trans Am Entomol Soc 2003; 129(3-4): 361-87.
14. Ünal M. Phaneropterinae (Orthoptera: Tettigoniidae) from Turkey and the Middle East. Trans Am Entomol Soc 2005; 131(3-4): 25-448.
15. Ünal M. Phaneropterinae (Orthoptera: Tettigoniidae) from Turkey and the Middle East II. Trans. Am Entomol Soc 2010; 136(1-2): 125-83.
16. Liu X, Zhang J, Ma E, Guo Y. Studies on the phylogenetic relationship of Acridoidea based on the male follicle morphology (Orthoptera: Acridoidea). Orient Insects 2005; 39: 21-32.
17. Marchini D, Brundo MV, Sottile L, Viscuso R. Structure of male accessory glands of *Bolivarus siculus* (Fischer) (Orthoptera, Tettigoniidae) and protein analysis of their secretions. J Morphol 2009; 270: 880-91.
18. Jones N, Taub-Montemayor T, Rankin MA. Fluorescein-dextran sequestration in the reproductive tract of the migratory grasshopper *Melanoplus sanguinipes* (Orthoptera, Acridiidae). Micron 2013; 46: 80-4.
19. Viscuso R, Brundo MV, Marletta A, Vitale DGM. Fine structure of the male genital tracts of some Acrididae and Tettigoniidae (Insect: Orthoptera). Acta Zool 2015; 96(4): 418-27.
20. Vitale DGM, Brundo MV, Viscuso R. Morphological and ultrastructural organization of the male genital apparatus of some Aphididae (Insect, Homoptera). Tissue Cell 2011; 43: 271-82.
21. Nandchahal N. Reproductive organs of *Gryllodes sigillatus* (Walker) (Orthoptera: Gryllidae). J Nat Hist 1972; 6: 125-31.
22. Vitale DGM, Viscuso R, D'Urso V, Gibilras S, Sardella A, Marletta A, et al. Morphostructural analysis of the male reproductive system and DNA barcoding in *Balclutha brevis* Lindberg 1954 (Homoptera, Cicadellidae). Micron 2015; 79: 36-45.
23. O'woma OO, Chigozirim UP, Emmanuel O, Chukwuebuka EM. Reproductive and survival strategies utilized by insect. A review. Am J Zool Res 2016; 4(1): 1-6.

24. Kotze RCM, Muller N, Du Plessis L, Van der Horst G. The importance of the insect sperm: Sperm ultrastructure of *Hermetia illucens* (black soldier fly). Tissue Cell 2019; 59: 44-50.
25. Sturm R. Stereological analysis of the sperm number in the testicular follicles of the Australian field cricket (Insecta: Orthoptera). Linz Biol Beit 2018; 50(1): 865-72.
26. Polat I. *Poecilimon cervus* Karabağ, 1950'un Sindirim, Boşaltım, Dişi ve Erkek Üreme Sisteminin Ültrastrüktürel Özellikleri. G.Ü., Fen Bilimleri Enstitüsü, Doktora Tezi. 2016.
27. Mari IP, Gigliolli AAS, Nanya S, Portela-Castro ALB. Histological and electron microscopy observations on the testis and spermatogenesis of the butterfly *Dione juno* (Cramer, 1779) and *Agraulis vanilla* (Linnaeus, 1758) (Lepidoptera: Nymphalidae). Micron 2018; 109: 11-21.
28. Novais AM, Dias G, Lino-Neto J. Testicular, spermatogenesis and sperm morphology in *Martarega bentoi* Heteroptera: Notonectidae). Arthropod Struct Dev 2017; 46: 635-43.
29. Zhang BB, Lyu QH, Hua BZ. Male reproductive system and sperm ultrastructure of *Furcatopanorpa longihypovalva* (Hua and Cai, 2009) (Mecoptera, Panorpidae) and its phylogenetic implication. Zool Anz 2016; 246: 41-6.
30. Pitnick S, Markow TA. Large-male advantages associated with costs of sperm production in *Drosophila hydei*, a species with giant sperm. Proc Natl Acad Sci 1994; 91(20): 9277-81.
31. Snook RR. Sperm in competiton: not playing by the numbers. Trends Ecol Evol 2005; 20: 46-53.
32. Werner M, Simmons LW. Insect sperm motility. Biol Rev 2008; 83: 191-2.
33. Dallai R, Gottardo M, Beutel RG. Structure and evolution of insect sperm: New interpretations in the age of phylogenomics. Annu Rev Entomol 2016; 61: 1-23.
34. Happ GM. Maturation of the male reproductive systems and its endocrine regulation. Annu Rev Entomol 1992; 37: 303-20.
35. Odhiambo TR. The architecture of the accessory reproductive glands of the male desert locust: III components of the muscular wall. Tissue Cell 1970; 2(2): 233-48.
36. Gallois D, Cassier P. Cytodifferentiation and maturation in the male accessory glands of *Locusta migratoria migratoriodes* (R. and F.) (Orthoptera: Acrididae). Int J Insect Morphol Embryol 1991; 20(3): 141-55.
37. Viscuso R, Narcisi L, Sottile L, Brundo MV. Role of male accessory glands in spermatodesm reorganization in Orthoptera Tettigonioidea. Tisssue Cell 2001; 33(1): 33-9.

ISTANBUL UNIVERSITY PRESS

RESEARCH ARTICLE

Eur J Biol 2021; 80(2): 82-90

Antibiofilm and Anti-Quorum Sensing Activities of Vaginal Origin Probiotics

Esin Kiray[1]

[1]Kirsehir Ahi Evran University, Vocational School of Health Services, Kirsehir, Turkey

ORCID IDs of the author: E.K. 0000-0002-6908-5909

Please cite this article as: Kiray E. Antibiofilm and Anti-Quorum Sensing Activities of Vaginal Origin Probiotics. Eur J Biol 2021; 80(2): 82-90. DOI: 10.26650/EurJBiol.2021.932640

ABSTRACT

Objective: Multidrug-resistant bacteria generally use cell-to-cell communication that leads to biofilm formation as a resistance development mechanism. Some pathogenic bacteria can form biofilms through a mechanism called Quorum sensing (QS). QS inhibition is one of the effective approaches to prevent biofilm formation.

Materials and Methods: 20 Lactic acid bacteria (LAB) previously associated with identification by 16S rRNA sequence analysis were used. Antibiofilm activities of metabolites of strains related to microplate based Antibiofilm method on *Staphylococcus aureus* ATCC 29213, *Escherichia coli* ATCC 25922, *Pseudomonas aeruginosa* ATCC 27853. *Chromobacterium violaceum* ATCC 12472 was used as an indicator in the anti-QS activities of LAB. The study was also performed by ELISA test on the immunomodulatory effect of LAB human peripheral blood mononuclear cells.

Results: All of the metabolites tested showed statistically significant antibiofilm activity on biofilms of pathogenic microorganisms. Although there was a difference between metabolites, *Lactobacullus paracasei* L2 and L20 strains had a high inhibitory effect on *S. aureus* (95.1%) and *P. aeruginosa* by 92.7%, respectively. *L. plantarum* L8 strain had 95.7% antibiofilm activity on *E. coli*. It was also determined that LAB has anti-QS activities in different concentrations. The immunomodulatory effect of LAB was found to produce higher IFN- γ than the controls, whereas IL-10 concentrations were lower.

Conclusion: Bacteria use QS to regulate various sequences of functions, including virulence and biofilm formation. Therefore, using bacteria with strong probiotic properties as QS inhibitory agents seems to be a promising approach to reduce or suppress biofilm formation of pathogenic bacteria.

Keywords: Probiotics, Antibiofilm, Anti-quorum sensing, IFN - γ, IL-10

INTRODUCTION

Today, antibiotic resistance is spreading faster than ever. Resistance to the various antibacterial compounds used by bacteria to treat clinical infections and the spread of these resistant bacteria is a serious problem in society (1). Biofilm formation is one of the uses of bacteria to develop such resistance (2). Biofilms, microorganisms attach to living or non-living surfaces, allowing them to remain after polymeric substances they produce themselves. These structures act as a kind of shield for microorganisms. Microorganisms within the biofilm structure can be protected from effects such as cell response, antimicrobial treatment and adverse environmental conditions (3).

Biofilm-producing bacteria are more resistant to antibiotics, as the biofilm matrix will help prevent penetration of the antibiotic. Therefore, it is necessary to find microorganisms or compounds capable of inhibiting or destroying the biofilm in order to control the attack of the biofilm-forming pathogenic bacteria (3,4).

Quorum sensing (QS) is a mechanism that can detect the population density of microorganisms and control gene expression after this density reaches a certain rate (4).

Corresponding Author: Esin Kiray E-mail: esin.kiray@ahievran.edu.tr

Submitted: 04.05.2021 • **Revision Requested:** 10.08.2021 • **Last Revision Received:** 13.10.2021 • **Accepted:** 14.10.2021 • **Published Online:** 05.11.2021

Some pathogenic bacteria create biofilms using a mechanism called QS. QS is a form of communication between bacteria by various extracellular signaling molecules called autoinductors. Bacteria regulate the expression of virulence factors, production of secondary metabolite products, biofilm formation and communication between the host and other microorganisms through these signal molecules (5). During QS, signal molecules released from bacteria bind to other bacterial receptors and genes that enable communication within and between species are transcribed (6). In addition, virulence factors are also effective in cellular processes such as disinfectant tolerance, spore formation, toxin production, and regulation of mobility (4,7). QS inhibition (QSI) is seen as an effective way of controlling bacterial infections, since pathogenic microorganisms prevent biofilm formation and reduce bacterial virulence (8).

Some recent studies show that the QS mechanism may be associated with bacterial resistance (9). Therefore, inhibition of the QS mechanism is a promising new antibacterial strategy that can not only inhibit the development of bacterial resistance, but also the expression of virulence genes associated with population density (4).

Lactic acid bacteria (LAB) are found in the mouth, vagina and intestines as a normal flora member in humans (5). The metabolites such as lactic acid, acetic acid, hydrogen peroxide and bacteriocin act as a protective agent in these areas thanks to their antagonism effects (10). The number of studies reporting the positive effects of flora member microorganisms such as LAB on the organism has increased and whether they can be used as an alternative in the treatment of diseases (11). It is seen as one of the powerful options (5).

The purpose of this study is to determine the anti-QS activity of LAB with probiotic characters isolated from the vaginal flora using *Chromobacterium violaceum* as an indicator bacteria and to investigate the antibiofilm activity of these bacteria against biofilm-forming bacteria and determine their immunomodulatory effect.

MATERIALS AND METHODS

Bacteria Used in the Experiment

In our study, LAB isolated from vaginal swab samples of healthy women who previously applied to the Kırşehir Ahi Evran University Training and Research Hospital, Department of Obstetrics and Gynecology were used. The strains identified by 16S rRNA sequence analysis were five *Lactobacillus plantarum*, four *Lactobacillus paracasei* and *Lactobacillus rhamnosus*, three *Pediococcus acidilactici* and one *Lactobacillus gasseri*, *Lactobacillus crispatus*, *Lactobacillus acidophilus* and *Lactobacillus acidophilus*. A total of 20 LAB were used (10,12).

Bacterial Culture Conditions

The De Man Rogosa Sharpe (MRS) solid and liquid Broth (Merck, Germany) (pH 6.5) medium was used in the development and activation of LAB. The strains were incubated for 24-48 hours at 37°C in the MRS medium under anaerobic conditions (10). The pathogenic bacteria used in the study were *Staphylococcus aureus* ATCC 29213, *Escherichia coli* ATCC 25922, *Pseudomonas aeruginosa* ATCC 27853, *Enterobacter aerogenes* ATCC 13048, *Bacillus cereus* CU1065, *Enterococcus faecalis* ATCC 29212 and *Bacillus subtilis* (W168*)*. Pathogen bacteria were activated in a Tryptic Soy Broth (TSB) medium under aerobic conditions at 37°C for 18 hours.

Investigation of Anti-Quorum Activities of LAB

The monitor strain *C. violaceum* ATCC 12472.was grown in 50 mL of the TSB medium and then incubated in an orbital shaker (120 rpm) at 28 °C for 48 hours. LAB was streaked on TSA in a straight line and left overnight to develop. Then, 100 µL of the monitor strain (OD 600 = 0.132) were placed in 2 mL of semi-solid agar (0.75% agar) for plating on pre-streaked LABs. After incubation, a positive result was observed with the inhibition of violacein pigmentation (opaque region) around the line of LAB isolates of *C. violaceum* (13).

Extraction of QS Inhibitory Substances

Strains showing anti-QS activity were extracted using the liquid-liquid extraction method (14). Bacterial cultures were grown in 100 mL of the MRS broth medium and then incubated at 28°C for 48 hours in an orbital shaker incubator (120 rpm) (Thermo Scientific MAXQ 4450). After the cultures were centrifuged at 10,000 g for 15 minutes, the supernatants were mixed in equal proportions with ethyl acetate. The solvent layer was allowed to evaporate in the rotary evaporator. An oven vacuum was used to obtain a pure crude extract. The crude extract was stored at -20°C as a 20 mg/mL stock (w/v) (14). The obtained raw extracts were used in other studies to be carried out.

Antibacterial Activity of Extracts

Antibacterial activity of the crude extracts was carried out using the agar well diffusion method. *Staphylococcus aureus* ATCC 29213, *E. coli* ATCC 25922, *P. aeruginosa* ATCC 27853, *E. aerogenes* ATCC 13048, *B. cereus* CU1065, *E. faecalis* ATCC 29212 and *B. subtilis* (W168*)* were used as pathogenic microorganisms in the study. Pathogenic bacteria were developed on Brain Heart Infusion Agar (BHIA) (Merck, Germany). The extracts were then applied to the well with 100 µL of solution at a concentration of 10 and 20 mg/mL. Streptomycin (10 mg/mL) (Merck, Germany) was used as positive control and DMSO as negative control. Plates were incubated at 37°C for 24 hours. The study was repeated three times. Antimicrobial activity was evaluated by measuring the zone diameters in mm around the wells and taking the average of three runs (15).

Detection of Anti-QS Activity

Anti-QS activity of crude extracts against *C. violaceum* was evaluated by agar well diffusion method. After *C. violaceum* was spread on TSA with a sterile drigalski spatula, 6 mm diameter cavities were made on the plates. Then, the extract was applied to the wells at a concentration of 10 and 20 mg/mL (50 µL). In this test, DMSO was used as a negative control and Streptomycin (10 mg/mL) was used as a positive control. The plates were incubated at 28°C for 24 hours. Anti-QS activity was observed

through a turbid halo zone against a background of violacein pigment. The study was repeated three times (13).

Antibiofilm Activity of Extracted QSI

After pathogenic bacteria were developed in BHIA, for antibiofilm testing, equal proportions of crude extract and bacterial cultures (OD 600 = 0.132) were transferred to 96-well microtiter plates (polystyrene) and incubated for 24 hours at 37 °C. Sterile MRS broth (100 µl) was used as negative control. The adhered cells were washed twice, then allowed to air dry. Staining was carried out without being aseptic. Biofilms were stained with 200 µL 0.4% (w/v) crystal violet solution for 30 minutes. After rinsing the wells twice with water, they were allowed to dry with air again. Ethanol was used as solvent. Optical density was measured at 595 nm. BHIB was used as blank and bacterial cultures without extracts were used as controls. Percent biofilm inhibition was calculated by the formula below (3). The study was repeated three times.

$$Percentage\ biofilm\ inhibition\ = \frac{(\text{Control OD595}) - \text{Treated OD595})}{(\text{Control OD595})}\ x\ 100\ \%$$

Quantitative Determination of the Amount of QS

In the quantitative determination of QS production by *C. violaceum* in the presence of LAB, made small changes in the method and was measured by photometrically (16). Briefly, LAB activated in MRS medium was transferred to tubes with 2 ml TSB medium and serial dilutions were made (0.5-0.062 mg/ml). *C. violaceum* was incubated at 28 °C until complete pigmentation was achieved in TSA medium. 100 µl of *C. violaceum* was added to each dilution and incubated for 1 night. The next day, 50 µl of 10% Sodium dodecyl sulfate (SDS) were added onto the cultures transferred to eppendorf tubes (200 µl) and lysed by vortexing for 5 seconds and incubating for 5 minutes at room temperature. Next, 900 µl of butanol were added and centrifuged at 13,000. The absorbance of the supernatant at 585 nm was measured (Spectronic 20D Hewlett Packard, Germany). Percent inhibition results were determined as [(Control OD - processed OD) / control OD] x 100 (16).

Immunomodulatory Effect of LAB

Isolation of human peripheral blood mononuclear cells (hPBMCs) from healthy volunteers and treatment of LAB was performed as previously described. Human PBMCs (2×10^5 cells / well) were seeded in 96-well tissue culture plates and treated with 2×10^6 colony forming LAB (hPBMCs/LAB ratio: 1/10) at 37°C and 5% CO_2 for 48 hours. Use of phytohemagglutinin (2 µg ml^{-1}), *E. coli* lipopolysaccharide (1 µg ml^{-1}) or as medium control experiments only interferon-gamma (IFN- γ) and interleukin-10 (IL-10) concentrations were determined depending on the enzyme according to the manufacturer's instructions (17). The protocol was approved by the Kırıkkale University Faculty of Medicine Ethics Committee.

Statistical Data Analysis

Statistical data analysis was performed using the SPSS program (Ver23, Chicago, IL, USA). All data are given as mean±standard error. Student's t-test method was used for comparison of control and test groups. Differences between groups with a p-value of <0.05 were considered significant.

RESULTS

Anti-QS Activities of LAB

All 20 LAB isolated in previous studies showed different levels of an anti-quorum sensing activity. Inhibition zone diameters of some LAB are given in Figure 1. Especially, L6, L7, L9, L12 and L19 strains were found to have strong anti-quarum sensing activity.

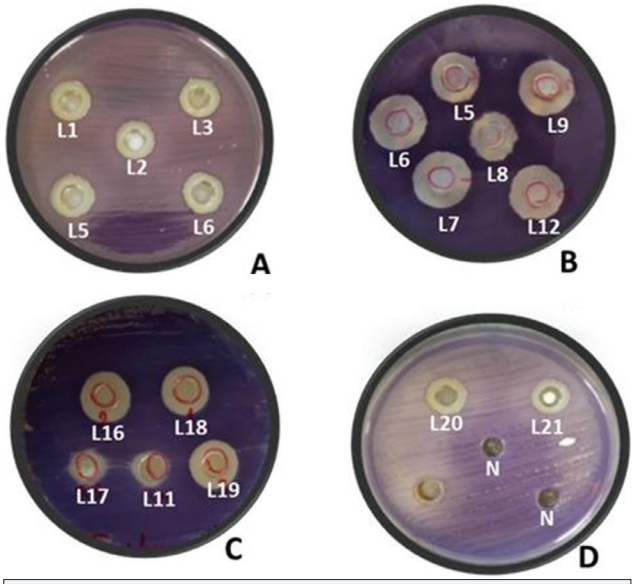

Figure 1. The inhibition zone activity of vaginal LAB bacteria (A,B,C and D) used in the present study.

Antibacterial Activity of Extracts

Antibacterial test was carried out in order to prevent false positive results that may be encountered in antibiofilm test. It has been observed that the crude extracts of 20 LAB produced by using the well diffusion method have a strong antibacterial effect on pathogenic microorganisms. Antibacterial activity was evaluated by measuring the zone diameters in mm around the wells and taking the average of three runs (Table 1). It was found that in addition to the strains with high anti-QS activity, the L5 and L13 strains also showed strong antibacterial activity.

Detection of anti-QS activity

Individual LAB isolates were found to have their own optimal concentrations, but most of them did not show activity at a concentration of 10 mg/mL or showed lower activity, especially better activity at a concentration of 20 mg/mL. It was observed that the *Lactobacillus* L16 strain formed the highest zone diameter at a concentration of 20 mg/mL. The anti-QS activity results of LAB are given in Table 1.

Antibiofilm Activity of Extracted QSI

It has been observed that LAB raw extracts have a different inhibitory activity against all pathogenic microorganisms used in

Table 1. Detection of anti-quarum sensing (QS) activity of crude extracts (mg/mL) and antibacterial activity on pathogenic microorganisms (mm).

Lactic Acid Bacteria	Diameter of pigment inhibition (mg /mL)*		Antibacterial activity on pathogenic bacteria (mm)**						
	10	20	*E. coli* ATCC 25922	*S. aureus* ATCC 29213	*P. aer.* ATCC 27853	*E. aer.* ATCC 13048	*B. cereus* ATCC 6633	*B. subtilis* (W168)	*E. faecalis* ATCC 29212
Lactobacillus paracasei L1	-	14	-	-	14	13	18	10	18
Lactobacillus paracasei L2	-	13	-	-	12	15	18	11	18
Lactobacillus paracasei L3	-	14	-	-	16	12	16	-	16
Lactobacillus crispatus L5	10	15	14	-	13	14	22	12	17
Pediococcus acidilactici L6	9	15	15	14	20	21	20	-	14
Pediococcus acidilacitici L7	10	19	-	-	11	15	18	-	-
Lactobacillus rhamnosus L8	-	15	-	13	10	-	17	11	12
Lactobacillus plantarum L9	10	18	14	-	16	18	16	-	19
Lactobacillus gassei L10	10	13	12	-	-	14	16	-	14
Pediococcus acidilactici L11	-	11	-	-	-	-	16	-	-
Lactobacillus rhamnosus L12	-	19	17	-	-	-	15	12	15
Lactobacillus rhamnosus L13	10	18	20	-	17	18	16	12	19
Lactobacillus acidophilus L14	12	19	17	-	-	-	-	-	12
Lactobacillus rhamnosus L15	11	13	17	14	-	14	14	13	14
Lactobacillus plantarum L16	13	17	23	-	14	16	15	14	-
Lactobacillus spp. L17	-	11	20	-	-	18	17	12	15
Lactobacillus plantarum L18	12	16	14	-	-	-	-	12	18
Lactobacillus plantarum L19	10	16	17	15	-	18	-	19	20
Lactobacillus paracasei L20	9	14	20	-	-	15	-	15	16
Lactobacillus plantarum L21	8	14	-	-	-	17	-	12	14

*It was studied in the antibacterial activity study at concentrations of 10 and 20 mg/mL.
**QS inhibition (radius of pigment inhibition in mm) = Radius of growth and pigment inhibition – radius of bacterial growth inhibition. Not active (–, inhibition zone <3mm); weak active (3–11mm); moderate active (12–15 mm); strong active (>15mm). Abbrevations: CFU: Colony Forming Unit, *P. aer: Pseudomonas aeruginosa*, *E. aer: Enterobacter aerogenes*

the study. As indicated in Figure 2, it was determined that the best biofilm inhibition was in the *S. aureus* ATCC 29213 and *E. coli* ATCC 25922 strains, and the least inhibition activity was on *P. aeruginosa* ATCC 27853.

While the strain showing good inhibitory effect on *S. aureus* was the *Lactobacullus* L2 strain (95.1%), the strain showing the best effect on *E. coli* (95.7%) was the L8 strain. While most of the test strains showed low activity on *P. aeruginosa*, only the L20 strain was found to have a high inhibitory effect of 92.7% (Figure 2).

Quantitative Determination of the Amount of QS

The production of violacein was quantitatively determined by *C. violaceum* in the presence of the LAB extract. The effect of LAB on violet pigment in different concentrations extract (0.5-0.062 mg/ml) is given in Figure 3.

Immunomodulatory Effect of LAB

Culture supernatants of LAB were incubated with hPBMCs isolated from healthy volunteers for 48 hours. Production levels of immunostimulating IFN-γ and immunoregulatory cytokines

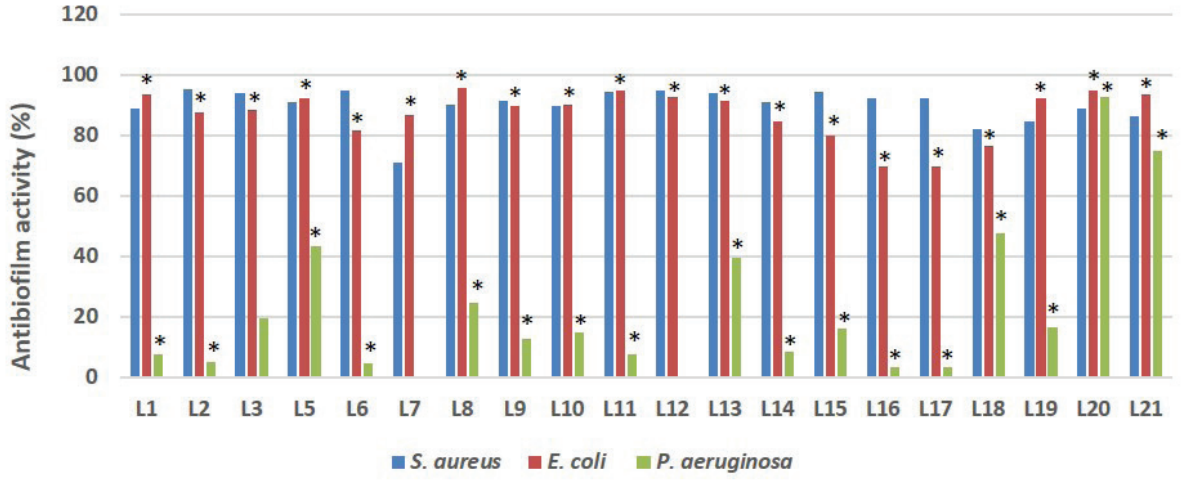

Figure 2. Antibiofilm activity of extracted QSI (20 mg/mL) against pathogenic bacteria. *p<0.05 vs control.

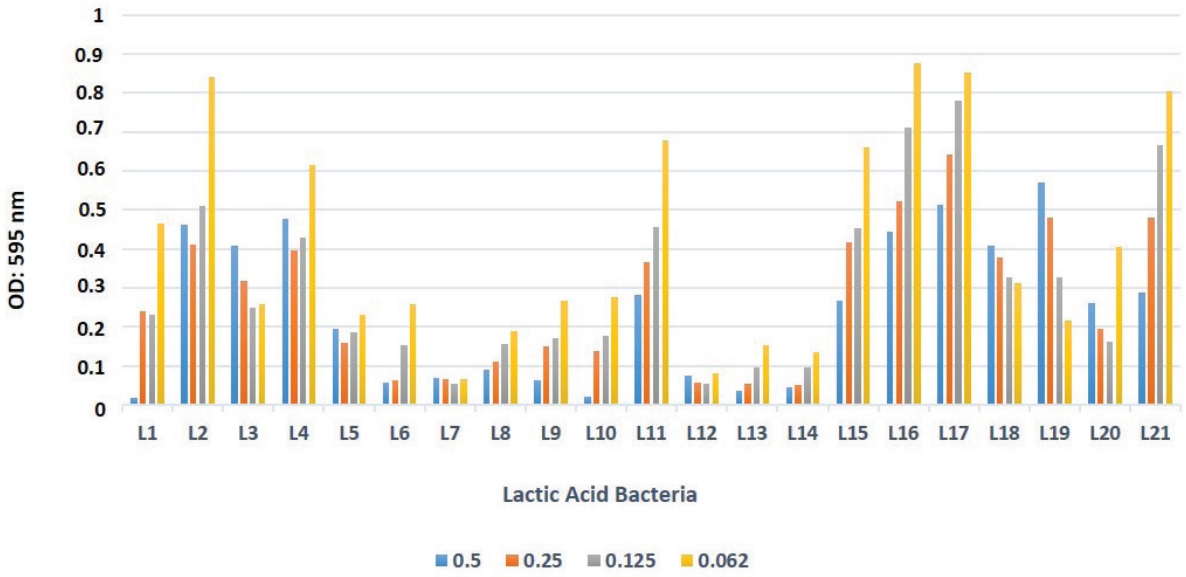

Figure 3. Effect of LAB extracts on violacein production. Different concentration of probiotic extract (0.5-0.062 mg/mL) was used to quantify the inhibition of violacein, an indicator of QS activity.

were measured by ELISA. While all LAB strains were found to produce higher IFN- γ than the controls, the IL-10 concentrations were found to be lower (Table 2). It suggests that LAB has the capacity to support innate responses while suppressing adaptive inflammatory responses (18).

DISCUSSION

Currently, approximately 65% of all bacterial infections have been associated with bacterial biofilms (19). Clinical management of infections is difficult, as biofilms can hardly be detected by routine diagnostic tests. Methicillin-resistant *Staphylococcus aureus* (MRSA), *P. aeruginosa*, *S. epidermidis* and *Gardnerella vaginalis* are the most common biofilm-forming microorganisms in the clinic. Due to the difficulties of these therapeutic agents of high clinical importance, there is a demand for new strategies. Today, antibiotic therapy is insufficient to fight biofilm-related infections; however, understanding the nature of biofilms will help us combat biofilm infections (5).

There is a need for new strategies to combat pathogenic microorganisms that have high clinical importance and cause high morbidity and mortality. Treatment with antibiotics is inadequate with biofilm-associated infections. Therefore, under-

Table 2. Effect of filtered LAB supernatant on interferon-γ (IFN-γ) production and interleukin-10 (IL-10) production in human peripheral blood mononuclear cells using enzyme-linked immunosorbent assay (ELISA)

	Cytokine concentration (pg/ml)*				
Sample	**IFN-γ Mean±SD[a]**	**IL-10 Mean±SD**	**Sample**	**IFN-γ Mean±SD**	**IL-10 Mean±SD**
Control	17±1.0	81±1.0	**Control**	17±1.0	81±1.0
L1	43±0.5	61±0.4	**L12**	56±0.4*	54±0.5
L2	36±0.4	52±0.2	**L13**	28±0.3	45±0.4
L3	56±0.5*	36±0.3*	**L14**	38±0.1	57±0.4
L5	45±0.3	45±0.5	**L15**	46±0.3	62±0.2
L6	21±0.1	41±0.4	**L16**	49±0.2	48±0.1
L7	37±0.5	35±0.1*	**L17**	39±0.2	56±0.4
L8	45±0.4	54±0.2	**L18**	51±0.4	53±0.5
L9	52±0.6	58±0.5	**L19**	47±0.3	38±0.6
L10	38±0.4	46±0.4	**L20**	44±0.6	27±0.3*
L11	46±0.3	51±0.5	**L21**	52±0.1	45±0.4

* It is seen that the supernatants of the L3 and L12 strains indicated with arrows in the table produced higher IFN-γ than the control, and the L3, L7 and L20 strains had higher inhibition rates of IL-10 production compared to the control.
*All results showed significant difference from control ($p<0.05$).
[a]SD: Standard deviation

standing the mechanism of biofilms and preventing the formation of biofilms has the potential to be a savior in combating these bacteria (5).

When bacteria species that communicate through signal molecules reach a certain density, they initiate gene expression that enables the synthesis of virulence factors. Therefore, blocking the communication between bacteria constitutes one of the new targets that can be achieved in antimicrobial therapy (20). Targeting the QS mechanisms, controlling bacterial virulence and the destruction of the infection by the host immune system is a striking strategy. Compounds with QSI effect are also new generation antimicrobial agents (21). Recent studies show that probiotics are one of the strongest options in combating pathogenic biofilms (22,23).

Probiotics are live bacteria that, when administered adequately, have a positive effect on host health. Many in vivo and in vitro studies and genomic analyses such as transcriptomics have proven that probiotics can modify the host's mucosal and systemic immune response and protect the host against pathogenic microorganisms through various mechanisms (10,24). In addition, bacteriocins produced by probiotics, hydrogen peroxide and various organic acids show antimicrobial effects against gastrointestinal pathogens (12). Because of these effects on pathogenic microorganisms, probiotics are thought to have the capacity to inhibit the formation of pathogens and biofilms.

The findings show that probiotics open a new horizon in the fight against biofilms. Probiotics do not exert a strong selective pressure on resistant microorganisms compared to conventional antibiotics used in clinical microbiology. Therefore, since probiotics are less cytotoxic than anti-QS agents and have a natural effect, they can be considered as the ideal choice in combating biofilm forms of pathogens (5).

In our study, using in vitro studies, we determined that various LAB species isolated from vaginal swabs of healthy women showed a strong antibiofilm activity, especially on *S. aureus* and *E. coli* strains, and also had anti-QS activity by using *C. violaceum* as an indicator bacterium.

Studies have shown a biofilm inhibition of 41.7% on *P. aeruginosa* of exopolysaccharide and bacteriocins obtained from various probiotics (11). It showed broad inhibition and antibiofilm effects against *P. aeruginosa* strains of the probiotic the *L. fermentum* strain isolated from local dairy products (25). It has been observed that the bacteriocin produced by *Pediococcus acidilactici* HW01 (HW01 bacteriocin) inhibits the biofilm formation of *P. aeruginosa* at a dose of 2 mg/mL by 66.41% (26).

The mechanism by which probiotics inhibit biofilm formation is not yet clear. Some in vitro studies show that probiotics can affect the expression of genes involved in QS, cell adhesion, virulence factors and biofilm formation (27,28).

Some probiotics have effects that inhibit the physiological behavior of bacteria due to QS. In a study, it was found that the production of lactic acid, short chain N-Acyl homoserine lactones (AHL) produced by probiotics, has an inhibitory effect on QS by suppressing the biofilm formation of *P. aeruginosa* (29). Again, *L. helveticus*, *L. lactis*, and *L. casei* strains showed similar inhibitory effects on *E. coli* O157: H7, *Salmonella typhimurium* and *L. monocytogenes* pathogens (30).

Organic acids synthesized by probiotics can act as QS antagonists, which can inhibit AHL production at the gene expression level and stop biofilm formation (5). In studies conducted in this direction, it was stated that the *L. brevis* strain, which has a strong probiotic property, has the potential to regulate the QS system (31).

Onbas et al. (20) investigated various effects of the probiotic *L. plantarum* F-10 strain isolated from the fecal microbiota of a healthy breastfed baby on *P. aeruginosa* ATCC 27853, methicillin-resistant *S. aureus* ATCC 43300 bacteria. In the study, *L. plantarum* F-10 was found to have antimicrobial, antibiofilm, anti-QS and antioxidant activity (20). Similarly, in our study, it was determined that the strong probiotic LAB isolated from the vaginal swabs of healthy women showed strong antibiofilm properties especially on *S. aureus* ATCC 29213 and *E. coli* ATCC 25922 strains.

Similar to our study, the antibiofilm effect of bio surfactants isolated from *L. casei* on *S. aureus* strains (32), in another study, the biosurfactants isolated from *P. acidilactici* and *L. plantarum* were also tested against *S. aureus*. Its antimicrobial, anti-QS and antibiofilm potential has been proven (33). In another study, it was reported that, *L. reuteri* (ATCC 23272), *L. casei* (ATCC 393), *L. salivarius* (ATCC 11741), and *L. plantarum* (ATCC 14917) strains inhibited biofilm formation and expression of QS-related *Streptococcus mutans* genes. The highest effect on *S. mutans* was detected in the *L. casei* and *L. reuteri* strains (27).

While it was determined that the supernatants of various LAB (*L. lactis, L. rhamnosus* and *L. fermentum*) showed biofilm and anti-QS activity against *P. aeruginosa* (34). The strains used in our study were found to have less antibiofilm and anti-quorum sensing activity on *P. aeruginosa*. Unlike other studies, our study includes various types of LAB together. In our study, it was determined that strains with strong antibiofilm properties showed anti-QS activity. The antibiofilm and anti-QS properties, cytokine profiles and IL-10 production capacities of the strains with proven probiotic importance are presented in comparison.

All the *L. plantarum* strains investigated in our study were found to have anti-QS activity. In a study, it was shown that the *L. plantarum* WCFS1 strain also showed high anti-QS activity similar to our study, and this microorganism also had a peptide-based QS-TCS (two components regulatory system). This has been reported as the reason why this species is more common in the environment and its adaptability is better than other species (35).

Microorganisms with probiotic properties as well as signaling molecules of pathogens low molecular weight have also been reported to produce bioactive compounds. These bioactive components are short-chain fatty acids, bacteriocin-like compounds, organic acids, hydrogen peroxide, nitric oxide and signaling molecules. These molecules toxins created by pathogens, harmful inactivates metabolites and signaling molecules by making or suppressing their production. They have been reported to inhibit the activity of pathogens (36).

In a study conducted in this context, it was shown that the *L. acidophilus* LA-5 strain showed strong anti-QS activity and protein-like molecules produced by this strain reduced enteropathogenic gene transcription, which is effective in the QS mechanism in inhibiting enterohemorrhagic *E. coli* O157:H7 (37). Similar results of a single strain of the *L. acidophilus* L14 strain in our study on *E. coli* ATCC 25922 type strain are given in Table 1 and Figure 2.

IL-10 is a regulatory cytokine that is of great importance in increasing Treg cell function and preventing excessive inflammation by reducing inflammatory cytokine responses. The production of IL-10 by the *Lactobacillus* species is one of the mechanisms that reveal the beneficial effect of probiotic microorganisms on the immune system (18,27).

The number of comparative analyses at species level is low in the studies. For this reason, the immunomodulatory effect of LAB on hPBMC cytokine profiles and proliferative response was compared in our study (Table 2). In our study, supernatants of all LAB strains inhibited IL-10 production, but further research is needed in this area. IFN- γ is the most important macrophage stimulating cytokine. It is critical in natural and acquired immunity. It stimulates the active macrophages to kill the microorganisms that they phagocyte. It induced higher levels of IFN-γ at the site of infection of the tested LAB, which could elicit innate and potentially adaptive immune responses. In other studies, lactic acid produced by vaginal LAB has a suppressive effect on IFN-γ production in human T and natural killer cells, and this production is an important factor that provides protection against bacterial vaginosis (17,38).

CONCLUSION

In the last few decades, a rapid increase in the number of bacteria resistant to antibiotics has been observed. Accordingly, instead of directly killing pathogenic bacteria, treating and controlling bacterial infections by blocking the communication system between them is considered a promising new strategy in the fight against pathogens. The probiotic properties of these strategies, which can be an alternative to antibiotics, have been determined, and it has been proven by studies that they can be mediated by microorganisms that affect the immune system. In our study, it was determined that most of the LABs with previously proven probiotic properties showed strong antibiofilm and anti-QS activity. In the future, the feasibility of anti-QS therapy in the fight against various pathogenic microorganisms is considered. In these treatment methods that can be applied,

the use of probiotic microorganisms is considered appropriate. However, more research, screening programs and testing protocols are needed to establish these treatment modalities. It is also hoped that this practice will not cause the growth of resistant bacteria and will not destroy beneficial bacterial communities in the host, and that QS inhibitors will be used in conjunction with existing antibiotics to increase their effectiveness.

Acknowledgments: We would like to thank the scientific research projects coordinator of Kirsehir Ahi Evran University for their financial contributions.

Informed Consent: Written consent was obtained from the participants.

Peer Review: Externally peer-reviewed.

Ethics Committee Approval: The decision of the ethics committee of the study was taken from Kirikkale University Ethics Committee with the decision no 25/02 on 27.10.2014.

Conflict of Interest: Author declared no conflict of interest.

Financial Disclosure: This research was supported by Kirsehir Ahi Evran University Scientific Research Projects Project No: PYO-FEN.4001.16.012.

REFERENCES

1. Abdula N, Macharia J, Motsoaledi A, Swaminathan S, Vijay Raghavan K. National action for global gains in antimicrobial resistance. Lancet 2016; 387: 3-5.
2. Fuqua C, Greenberg EP. Self-perception in bacteria: quorum sensing with acylated homoserine lactones. Curr Opin Microbiol 1998; 2: 183-9.
3. Theodora NA, Dominika V, Waturangi DE. Screening and quantification of anti-quorum sensing and antibiofilm activities of phyllosphere bacteria against biofilm forming bacteria. BMC Res Notes 2019; 12(1): 732.
4. Zhao X, Yu Z, Ding T. Quorum-sensing regulation of antimicrobial resistance in bacteria. Microorganisms 2020; 8(3): 425.
5. Barzegari A, Kheyrolahzadeh K, Khatibi SMH, Sharifi S, Memar MY, Vahed SZ. The battle of probiotics and their derivatives against biofilms. Infect Drug Resist 2020; 13: 659-72.
6. Krzyżek P. Challenges and limitations of anti-quorum sensing therapies. Front Microbiol 2019; 31(10): 2473.
7. Hawver LA, Jung S A, Ng WL. Specificity and complexity in bacterial quorum-sensing systems. FEMS Microbiol Rev 2016; 40(5): 738-52.
8. Liu L, Wu R, Zhang J, Shang N, Li P. D-Ribose interferes with quorum sensing to inhibit biofilm formation of *Lactobacillus paraplantarum* L-ZS9. Front Microbiol 2017; 8: 1860.
9. Jiang Q, Chen J, Yang C, Yin Y, Yao K. Quorum Sensing: A prospective therapeutic target for bacterial diseases. Biomed Res Int 2019; 2015978.
10. Kiray E, Kariptas E, Dagli SS. Evaluation of vaginal lactobacilli with potential probiotic properties and biotherapeutic effects isolated from healthy Turkish women. Fresenius Environ Bull 2020; 294240-52.
11. Sharma V, Harjai K, Shukla G. Effect of bacteriocin and exopolysaccharides isolated from probiotic on *P. aeruginosa* PAO1 biofilm. Folia Microbiol 2018; 63: 181-90.
12. Kiray E, Kariptas E, Azarkan SA. Evaluation of vaginal lactobacilli with potential probiotic properties and biotherapeutic effects isolated from healthy Turkish women. PSM Micro 2019; 4(3): 56-70.
13. Abudoleh SM, Mahasneh AM. Anti-quorum sensing activity of substances isolated from wild berry associated bacteria. Avicenna J Med Biotechnol 2017; 9(1): 23-30.
14. Younis KM, Usup G, Ahmad A. Secondary metabolites produced by marine streptomyces as antibiofilm and anti-quorum sensing inhibitor of uropathogen *Proteus mirabilis*. Environ Sci Pollut Res 2015; 23(5): 4756-67.
15. Tabbouche SA, Gurgen A, Yildiz S, Kilic AO, Sokmen M. Antimicrobial and antiquorum sensing activity of some wild mushrooms collected from Turkey. MSU J Sci 2017; 5(2): 453-7.
16. Han MSA, Zahin M, Hasan S, Husain FM, Ahmad I. Inhibition of quorum sensing regulated bacterial functionsby plant essential oils with special reference to clove oil. Lett Appl Microbiol 2009; 49(3): 354-60.
17. Vissers YM, Snel J, Zuurendonk PF, Smit BA, Wichers HJ, Savelkoul HFJ. Differential effects of *Lactobacillus acidophilus* and *Lactobacillus plantarum* strains on cytokine induction in human peripheral blood mononuclear cells. FEMS Immunol Med Microbiol 2010; 59(1): 60-70.
18. Forsberg MM, Björkander S, Pang Y, Lundqvist L, Ndi M, Ott M, et al. Extracellular membrane vesicles from lactobacilli dampen IFN-γ responses in a monocyte-dependent Manner Sci Rep 2019; 9: 17109.
19. Jamal M, Ahmad W, Andleeb S, Jalil F, Imran M, Nawaz MA, et al. Bacterial biofilm and associated infections. JCMA 2018; 81(1): 7-11.
20. Onbas T, Osmanagaoglu O, Kiran F. Potential properties of *Lactobacillus plantarum* F-10 as a bio-control strategy for wound infections. Probiotics Antimicro 2019; 11(4): 1110-23.
21. Garcia-Contreras R, Nunez-Lopez L, Jasso-Chavez R. Quorum sensing enhancement of the stress response promotes resistance to quorum quenching and prevents social cheating. ISME J 2015; 9(1): 115-25.
22. Kim NN, Kim WJ, Kang SSJFC. Antibiofilm effect of crude bacteriocin derived from *Lactobacillus brevis* DF01 on *Escherichia coli* and *Salmonella typhimurium*. Food Control 2019; 98: 274-80.
23. Kaur S, Sharma P, Kalia N, Singh J, Kaur S. Antibiofilm properties of the fecal probiotic lactobacilli against vibrio spp. Front Cell Infect Microbiol 2018; 8: 120.
24. Iannitti T, Palmieri B. Therapeutical use of probiotic formulations in clinical practice. Clin Nutr 2010; 29(6): 701-25.
25. Shokri D, Khorasgani MR, Mohkam M, Fatemi SM, Ghasemi Y, Taheri-Kafrani A. The inhibition effect of lactobacilli against growth and biofilm formation of *Pseudomonas aeruginosa*. Probiotics Antimicrobe Proteins 2018; 10(1): 34-42.
26. Lee D, Kim BS, Kang SS. Bacteriocin of *Pediococcus acidilactici* HW01 inhibits biofilm formation and virulence factor production by *Pseudomonas aeruginosa*. Probiotics Antimicro 2020; 12(1): 73-81.
27. Wasfi R, Abd El-Rahman OA, Zafer MM, Ashour HM. Probiotic *Lactobacillus* sp. inhibit growth, biofilm formation and gene expression of caries-inducing *Streptococcus mutans*. J Cell Mol Med 2018; 22(3): 1972-83.
28. James KM, MacDonald KW, Chanyi RM, Cadieux PA, Burton JP. Inhibition of *Candida albicans* biofilm formation and modulation of gene expression by probiotic cells and supernatant. J Med Microbiol 2016; 65(4): 328-36.
29. Kiymaci ME, Altanlar N, Gumustas M, Ozkan SA, Akin A. Quorum sensing signals and related virulence inhibition of *Pseudomonas aeruginosa* by a potential probiotic strain's organic acid. Microb Pathog 2018; 121: 190-7.

30. Gómez NC, Ramiro JM, Quecan BX, de Melo Franco BD. Use of potential probiotic lactic acid bacteria (LAB) biofilms for the control of *Listeria monocytogenes*, *Salmonella typhimurium*, and *Escherichia coli* O157: H7 biofilms formation. Front Microbiol 2016; 7: 863.
31. Qichuang Li, Yonglong Pan, Linxian Ding, Huachang Hong, Shuxia Yan, Binbin Wu, et al. draft genome sequence of *Lactobacillus brevis* Strain 3M004, a probiotic with potential quorum-sensing regulation. Genome Announc 2017; 5(36): e00675-17.
32. Merghni A, Dallel I, Noumi E. Antioxidant and antiproliferative potential of biosurfactants isolated from *Lactobacillus casei* and their antibiofilm effect in oral *Staphylococcus aureus* strains. Microb Pathog 2017; 104: 84-9.
33. Yan X, Gu S, Cui X. Antimicrobial, anti-adhesive and antibiofilm potential of biosurfactants isolated from *Pediococcus acidilactici* and *Lactobacillus plantarum* against *Staphylococcus aureus* CMCC26003. Microb Pathog 2019; 127: 12-20.
34. Rana S, Bhawal S, Kumari A, Kapila S, Kapila R. pH-dependent inhibition of AHL-mediated quorum sensing by cell-free supernatant of lactic acid bacteria in *Pseudomonas aeruginosa* PAO1. Microb Pathog 2020; 28; 142: 104105.
35. Sturme MHJ, Francke C, Siezen RJ, de Vos WM, Kleerebezem M. Making sense of quorum sensing in lactobacilli: a special focus on *Lactobacillus plantarum* WCFS1. Microbiology 2007; 153: 3939-47.
36. Yılmaz-Yıldıran H, Karahan AG, Başyiğit-Kılıç G. Quorum sensing mechanism in lactic acid bacteria. Turk J Hygiene Exper Bio 2015; 72(1): 79-90.
37. Tabasco R, de Palencia PF, Fontecha Peláez C, Requena T. Competition mechanisms of lactic acid bacteria and bifidobacteria: fermentative metabolism and colonization. LWT–Food Sci Technol 2014; 55: 680-4.
38. Aldunate M, Srbinovski D, Hearps AC, Latham CF, Ramsland PA, Gugasyan R, Cone RA, Tachedjian G. Antimicrobial and immune modulatory effects of lactic acid and short chain fatty acids produced by vaginal microbiota associated with eubiosis and bacterial vaginosis. Front Physiol 2015; 6: 164.

ISTANBUL UNIVERSITY PRESS

RESEARCH ARTICLE

Eur J Biol 2021; 80(2): 91-96

Oxidative Stress Status in Testis of Type-2 Diabetic Rats Treated with Delta-9-Tetrahydrocannabinol

Ebrar Tutar[1], Beti Pesen[1], Zeynep Mine Coskun Yazici[1,*], Sema Bolkent[2]

[1]Demiroglu Bilim University, Faculty of Arts and Sciences, Department of Molecular Biology and Genetics, Istanbul, Turkey
[2]Istanbul University-Cerrahpasa, Faculty of Cerrahpasa Medicine, Department of Medical Biology, Istanbul, Turkey

ORCID IDs of the authors: E.T. 0000-0003-2273-7487; B.P. 0000-0003-1449-9749; Z.M.C.Y. 0000-0003-4791-6537; S.B. 0000-0001-8463-5561

Please cite this article as: Tutar E, Pesen B, Coskun Yazici ZM, Bolkent S. Oxidative Stress Status in Testis of Type-2 Diabetic Rats Treated with Delta-9-Tetrahydrocannabinol. Eur J Biol 2021; 80(2): 91-96. DOI: 10.26650/EurJBiol.2021.1001540

ABSTRACT

Objective: Type-2 diabetes (T2D) is a multifactorial disease that occurs as a result of impaired insulin secretion and increased glucose. Researchers emphasize that oxidative stress prevention and improvement strategies are important in the general treatment of T2D. It is reported that delta-9-tetrahydrocannabinol (THC), a component of the cannabis plant, has positive effects against oxidative stress and inflammation. Therefore, this study explored the inhibitory effects of THC on oxidative damage of testis in type-2 diabetic rats.

Materials and Methods: Adult Spraque-Dawley rats were separated into 4 groups. In the control group, physiological saline was given intraperitoneally. In the T2D model group (T2DM), streptozotocin (STZ) + nicotinamide (NAD) was administered intraperitoneally. Three mg/kg/day THC was given to the THC and T2DM+THC groups for 7 days, intraperitoneally. Glutathione (GSH), malondialdehyde (MDA), and protein carbonyl levels (PCO), and superoxide dismutase (SOD) activity were measured spectrophotometrically in testicular tissue. Total oxidant and antioxidant status were determined by ELISA.

Results: Testicular GSH level and SOD activity were significantly decreased in T2D, while MDA and PCO levels increased. In contrast to this effect, the THC treatment increased GSH levels and SOD activity in diabetics, but decreased MDA and PCO levels.

Conclusion: According to the study results, THC may have an oxidative stress inhibitory effect on diabetic rat testis.

Keywords: Diabetes, tetrahydrocannabinol, testis, oxidative stress

INTRODUCTION

Type-2 diabetes (T2D), the most common type, is a chronic disease characterized by high blood sugar. Steroidogenic and spermatogenic dysfunctions are complications of T2D in men. Some researchers suggest that the use of anti-diabetic drugs has a restorative effect on them (1,2). Tian et al. suggested that reactive oxygen species and autophagy act a part in the pathophysiology of diabetes-induced male infertility (3). Consistent with the studies by Tian et al. (3), Ranjan et al. showed that T2D causes testicular dysfunction in mice (4).

The cannabis plant has been used for thousands of years as a medicinal agent and contains approximately 540 natural compounds. One of the most potent bioactive components of cannabis is delta-9-tetrahydrocannabinol (THC) (5). Vella et al. reported that THC could lead to the prevention of cardiovascular dysfunction by reducing blood glucose concentrations and oxidative stress in streptozotocin (STZ)-diabetic Wistar-Kyoto rats given THC (6). In the previous study, THC ameliorated hyperlipidemia and hyperglycemia in type-2 diabetic rats (7). In a study administered THC to multiple low-dose STZ-induced autoimmune diabetic animals, researchers suggested that multiple low dose STZ could

Corresponding Author: Zeynep Mine Coskun Yazici E-mail: zeynepmine.coskun@demiroglu.bilim.edu.tr
Submitted: 06.10.2021 • **Revision Requested:** 18.10.2021 • **Last Revision Received:** 27.10.2021 •
Accepted: 27.10.2021 • **Published Online:** 08.11.2021

cause beta-cell damage, but the administration of THC had the ability to reduce the severity of the autoimmune response (8). Cantele et al. (9) suggested that *Cannabis sativa* L. may be used as a source of natural antioxidant. In addition, an *in vitro* study by Raja et al. (10), showed that THC has a high potential to combat oxidative stress, while no appreciable antioxidant activity of cannabidiol (CBD) was detected. Thus, researchers reported that cannabis extracts exhibited significant antioxidant activity depending on their THC and CBD ratios. Unfortunately, there is no information about the effect of THC on type-2 diabetic rat testis. Therefore, this study examined the effect of THC on oxidative damage in the testis of rats with T2D.

MATERIALS AND METHODS

Experimental Procedures

Experiments were performed on 8-10 week old male Sprague-Dawley rats (n = 24, average weight 214 g). All experimental procedures were performed using approved methods according to the standards of the Istanbul University Animal Research Local Ethics Committee (approval number: 103). All animals were fed and drank water *ad libitum* and were housed at standard status (12 h light-dark cycle). Twenty-four male rats were randomly selected and assigned to one of the four groups: control, T2D model (T2DM), THC, and T2DM+THC. Saline was intraperitoneally injected into the control group. A single dose of 85 mg/kg nicotinamide (NAD; Sigma-Aldrich) and 15 minutes later 65 mg/kg STZ (Sigma-Aldrich) were injected intraperitoneally into the T2DM group (11). Blood glucose levels were determined 72 h after STZ+NAD injections, and animals with a blood glucose concentration ≥ 200 mg/dL were considered type 2 diabetic.

THC (3 mg/kg/day; Lipomed) was administered to the THC group and the T2DM+THC group for 7 days, intraperitoneally. Testicular tissue samples were taken from rats under anesthesia 15 days after THC injection. The tissue samples were fixed with nitrogen (-196°C), and then kept at -86°C.

Biochemical Analysis

Tissue homogenates (10% w/v) were obtained from frozen testicular tissue samples in ice-cold saline. The specimens were centrifuged at 5.000 x g for ten minutes, and supernatants were obtained and used directly to measure biochemical parameters. Glutathione (GSH), malondialdehyde (MDA), and protein carbonyl levels (PCO), and superoxide dismutase (SOD) activity were assessed using the Beutler, Buege and Aust, Reznick and Packer, and Sun et al. methods, respectively (12-15).

The GSH level was detected by following the rate of decline of 5.5'-dithiobis-2-nitrobenzoic acid (DTNB). Shortly, precipitating solution (Na_2EDTA, glacial metaphosphoric acid, NaCl) were added to testis tissue samples and mixed. The reaction mixture was incubated. And then samples were centrifuged. Phosphate and DTNB solutions were added to the supernatant. The difference in absorbance was read at 412 nm. The GSH concentration in samples was calculated from a standard curve. The GSH concentration in testis tissue was expressed in nmol/mg of protein.

MDA levels were analyzed by a thiobarbituric acid reacting substances assay. Two-hundered fifty µL of testis tissue sample was added and then mixed with 1mL of 30% trichloroacetic acid, 0.2mL of 5M HCl, and 1.5mL of 0.75% thiobarbituric acid. The specimens were incubated at 100°C for 20 minutes. Following the incubation period, the specimens were centrifuged for 10 min, and samples read at 532 nm, spectrophotometrically.

PCO reacts with 2, 4-dinitrophenyl-hydrazine (DNPH) to generate chromophoric dinitrophenylhydrazones (1:4, tissue: DNPH). DNPH was dissolved in hydrochloric acid. After the DNPH reaction, proteins were precipitated with an equal volume of 20% (w/v) trichloroacetic acid. Then, obtained pellets were washed with an ethanol/ethyl acetate mixture. Lastly, the PCO precipitates were dissolved in guanidine-HCl solution. The absorbance values were recorded at 360 nm. The PCO concentration was counted using the molar extinction coefficient of DNPH (ε= 22.000M^{-1} cm^{-1}).

The method of SOD enzyme activity involves the inhibition of nitroblue tetrazolium (Sigma-Aldrich) reduction with xanthine/xanthine oxidase (Sigma-Aldrich). The SOD activity was detected by colorimetric evaluation of soluble formazan dye formation at 560 nm. One unit of SOD is described as the amount causing 50% inhibition in the nitroblue tetrazolium reduction rate. The SOD enzyme activity was presented as U/mg protein in the testis.

Total protein levels were detected using the Bradford assay method in which 40 µL of testis tissue specimens was added to 2 mL of Bradford reagent. At the end of the incubation period, the absorbance was read at 595 nm (16). A bovine serum albumin standard was used for calculation, and results were presented as mg protein/mL.

Analysis of Total Antioxidant and Oxidant Statutes

Total antioxidant status and total oxidant status were detected using commercial kits (Rel Assay). Measurements were made according to the kit procedure. The oxidative stress index was checked out according to the following formula.

$$Oxidative\ stress\ index = \frac{\text{Total oxidant status (mmol } H_2O_2 \text{ Eq/L)}}{\text{Total antioxidant status (mmol Trolox Eq/L)}}\ x\ 100$$

Statistics

Data was declared as the mean±standard error of the mean (SEM). The non-parametric Kruskal-Wallis and Mann-Whitney tests were benefited because the data failed to passa normality test. The differences were considered as significant at a *P*-value<0.05 (Prism 5, GraphPad Software).

RESULTS

In this study, there were significant differences in GSH, MDA, and PCO levels, and SOD activity among all groups ($p<0.05$, $p<0.01$, $p<0.01$ and $p<0.05$, respectively) (Figures 1-4). The

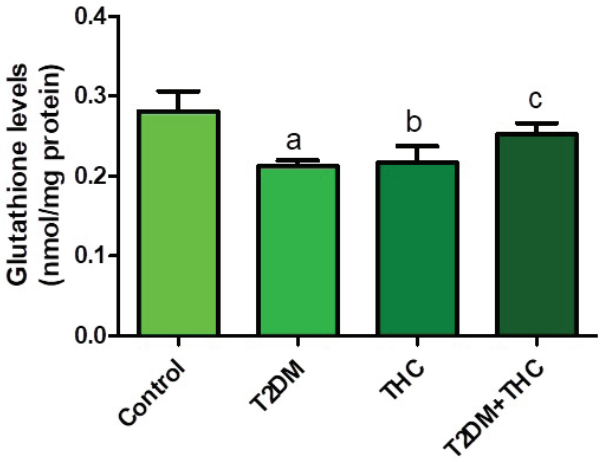

Figure 1. Changes in glutathione levels in testis tissue. T2DM, type-2 diabetes model; THC, delta-9-tetrahydrocannabinol. Values are shown as means±SEM. [a]$p<0.01$ vs Control group, [b]$p<0.05$ vs Control group, [c]$p<0.01$ vs T2DM group.

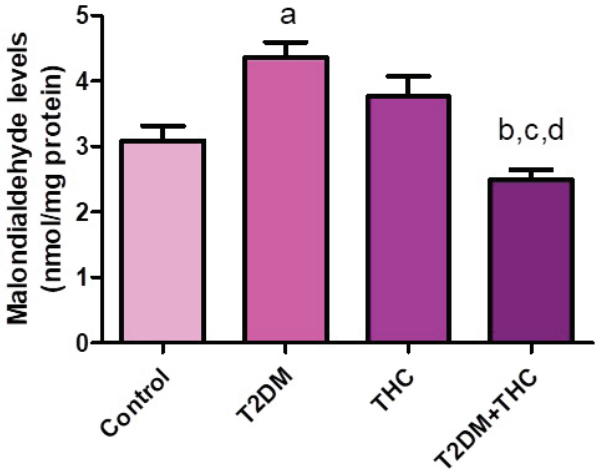

Figure 2. Testicular malondialdehyde levels. T2DM, type-2 diabetes model; THC, delta-9-tetrahydrocannabinol. Values are shown as means±SEM. [a]$p<0.01$ vs Control group, [b]$p<0.05$ vs Control group, [c]$p<0.01$ vs T2DM group, [d]$p<0.01$ vs THC group.

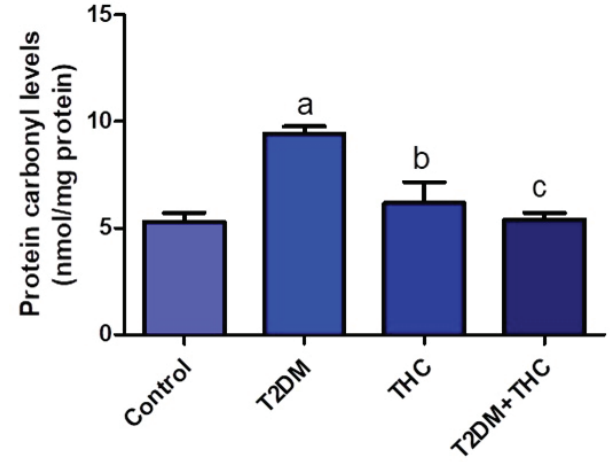

Figure 3. Protein carbonyl levels in testis tissue of rats. T2DM, type-2 diabetes model; THC, delta-9-tetrahydrocannabinol. Values are shown as means±SEM. [a]$p<0.01$ vs Control group, [b]$p<0.05$ vs T2DM group, [c]$p<0.01$ vs T2DM group.

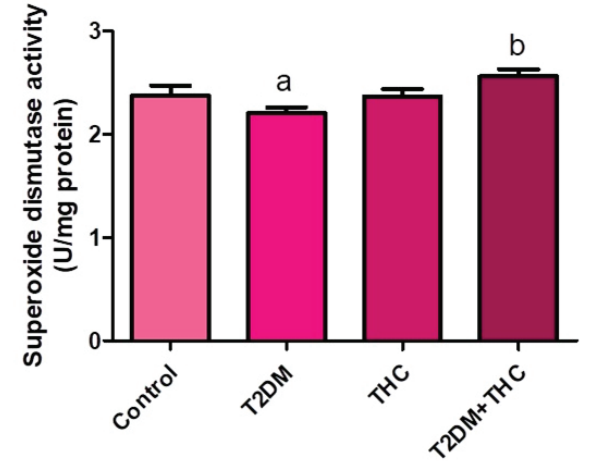

Figure 4. Measurement of superoxide dismutase enzyme activities in testis tissue. T2DM, type-2 diabetes model; THC, delta-9-tetrahydrocannabinol. Values are shown as means±SEM [a]$p<0.05$ vs Control group, [b]$p<0.01$ vs T2DM group.

GSH level in the testis tissue decreased in the T2DM group as compared to the control rats ($p<0.01$). THC administration significantly increased testis GSH level in the T2DM+THC group as compared to the T2DM group ($p<0.01$). MDA, a lipid peroxidation marker, increased in T2DM rats when compared with control animals ($p<0.01$). However, the increase in testis MDA level of the T2DM group decreased significantly with THC treatment ($p<0.01$). Interestingly, when compared to control and THC groups, the lowest MDA level was detected in the T2DM+THC group ($p<0.05$ and $p<0.01$, respectively). Similar to MDA level, type-2 diabetes significantly raised the PCO level when compared to control rats ($p<0.01$). Also, the testis PCO levels showed a significant decrease in the T2DM+THC group as compared to T2DM rats ($p<0.01$). Testis SOD activity decreased in T2DM animals when compared with the control group ($p<0.05$). However, THC treatment significantly increased SOD activity in the T2DM+THC group when compared with the T2DM group ($p<0.01$).

Compared to the control animals, the total antioxidant status value showed an insignificant decrease in the diabetes group, while the total oxidant status value showed an insignificant increase. However, when the THC treatment was applied to the type-2 diabetes group it brought the total antioxidant and ox-

Table 1. Measurements of total antioxidant and oxidant statutes, and oxidative stress index in testis.

	Total Antioxidant Status* (mmol Trolox Equiv. /L)	Total Oxidant Status* (μmol H_20_2 Equiv. / L)	Oxidative Stress Index*
Control	0.40±0.10	14.68±4.18	26388±12090
T2DM	0.11±0.04	28.46±4.52	57909±21913
THC	0.20±0.07	14.69±4.49	16304±5713
T2DM+ THC	0.45±0.12	14.23±5.20	15777±9635
p value	NS	NS	NS

*Data are shown as the mean±SEM. T2DM, type-2 diabetes model; THC, delta-9-tetrahydrocannabinol, NS, non-significant.

idant status values closer to the control group. Similar to the total oxidant status results, the oxidative stress index value was insignificantly increased in T2DM groups as compared with the control group. In addition, the oxidative stress index value was lower in the T2DM+THC group than in the T2DM group (Table 1).

DISCUSSION

This study examined the effects of THC on STZ+NAD-induced diabetic rat testis. The STZ+NAD model of type 2 diabetes was used to create and exhibit symptoms similar to human non-insulin-dependent diabetes mellitus (NIDDM) (11). Numerous studies have shown that the diabetic rat model is useful in studies of different aspects of diabetes (17,18).

Oxidative stress has been recognized as a serious marker for the pathogenesis, and development of type-2 diabetes (19). It has been suggested that hyperglycemia may contribute to increased reactive oxygen species formation and that increased oxidative stress may cause impaired insulin secretion. It has also been emphasized that the inhibition of excessive reactive oxygen species production is very important for delaying the onset of diabetes (20). Studies showed that diabetes causes oxidative damage in rat testis. The oxidative damage in diabetic animals was confirmed by elevations in MDA level and diminishment in GSH level (21-23). Thyagaraju and Muralidhara suggested that PCO levels were higher in diabetic testis and liver tissues than non-diabetics (23). However, testicular SOD activity showed a decrease in diabetic rats (24). A part of a nonenzymatic antioxidant defense system, GSH, protects macromolecules from oxidative damage. In a study by Abdullah et al., it was reported that GSH improves diabetes-induced degraded testicular morphology and sperm quality, thanks to its antioxidant properties (25). Choubey et al. reported that adiponectin reduced oxidative stress and had a protective role against testicular dysfunction in their study in high-fat diet+STZ-induced type-2 diabetic mice (26). In the same research, it stated that the treatment applied to mice decreased the increased lipid peroxidation caused by diabetes and elevated SOD activity. In the current study, T2D decreased GSH levels in testis tissue. MDA, a lipid peroxidation marker, showed an increase in T2DM rats, unlike GSH levels. Similar to MDA level, T2D raised the PCO level in testis tissue of rats. The testis SOD activity decreased in T2DM animals similar to GSH level.

There are other studies which report that THC has antioxidant effects on various tissues (27,28). Also, Vella et al. suggested that the administration of THC may lead to improvements in cardiovascular dysfunction by providing antihyperglycemic and antioxidant effects in diabetic animals (6). It also showed that THC decreased serum MDA levels in diabetic animals. It has been suggested that consumption of white tea prevents testicular oxidative damage by reducing carbonyl groups and lipid peroxidation and increasing the total GSH level in prediabetic rats, thus it was emphasized that sperm quality can be restored (29). Similar to the aforementioned studies, THC administration increased testis GSH level and SOD activity in the diabetic group. The increase in testis MDA and PCO levels of the T2DM group decreased with THC treatment. On the contrary, Mandal and Das (30) reported in their study on healthy mice that THC damaged testicular tissues. It has even been shown that this detrimental effect is more pronounced at low doses than at higher doses. Further, the researchers observed a healing effect and repair in mouse testicles treated with THC treatment at high doses and withdrawal of drug treatments. They suggested that this might be due to the antioxidant defense system. Similarly, this study observed the effects of THC on testis 15 days after THC treatment was terminated. It showed that THC treatment administered to healthy individuals was not as effective as that administered to diabetic rats. It could be because the extra synthesis of the endogenous antioxidant defense system as a protective defense function of THC in reducing the high oxidative stress caused by diabetes.

Researchers investigated the antioxidant mechanisms of THC and CBD and reported that both molecules have antioxidant properties. However, they emphasized that the antioxidant potential of THC is higher than that of CBD (31). While the total antioxidant status value showed a decrease in diabetic rats, the total oxidant status value increased. Although the values were not significant, THC treatment reversed this situation. This may be because THC acts differently in healthy and diabetic individ-

uals. Thus, the total antioxidant and oxidant status, and oxidative stress index values could only approach the values of the control group. THC may be used as supportive therapy for T2D and its symptoms, especially due to its antioxidative features.

CONCLUSION

As mentioned above, T2D leads to an increase in oxidative stress markers in testicular tissue. However, T2D causes a reduction in the molecules involved in an antioxidant defense system. This study concludes that the oxidative stress and antioxidant defense markers in testicular tissue move towards healthier levels by administering THC to rats with T2D.

Ethics Committee Approval: This study was approved by the Istanbul University Animal Research Local Ethics Committee (approval number: 103).

Informed Consent: Written consent was obtained from the participants.

Peer Review: Externally peer-reviewed.

Author Contributions: Conception/Design of Study- Z.M.C.Y., S.B.; Data Acquisition- E.T., B.P., Z.M.C.Y.; Data Analysis/Interpretation- Z.M.C.Y., S.B.; Drafting Manuscript- Z.M.C.Y., S.B.; Critical Revision of Manuscript- Z.M.C.Y., S.B.; Final Approval and Accountability- Z.M.C.Y., S.B., E.T., B.P.

Conflict of Interest: Authors declared no conflict of interest.

Financial Disclosure: Authors declared no financial support.

REFERENCES

1. Derkach KV, Bakhtyukov AA, Bayunova LV, Zorina II, Shpakov AO. Normalization of testicular steroidogenesis and spermatogenesis in male rats with type 2 diabetes mellitus under the conditions of metformin therapy. Dokl Biol Sci 2020;493(1):110-3.
2. Laakso M. Biomarkers for type 2 diabetes. Mol Metab 2019;27(l):139-46.
3. Tian Y, Song W, Xu D, Chen X, Li X, Zhao Y. Autophagy induced by ROS aggravates testis oxidative damage in diabetes via breaking the feedforward loop linking p62 and Nrf2. Oxid Med Cell Longev 2020; 7156579.
4. Ranjan A, Choubey M, Yada T, Krishna A. Nesfatin-1 ameliorates type-2 diabetes-associated reproductive dysfunction in male mice. J Endocrinol Invest 2020;43(4):515-28.
5. Amin MR, Ali DW. Pharmacology of medical cannabis. Adv Exp Med Biol 2019;1162:151-65.
6. Vella RK, Jackson DJ, Fenning AS. Δ^9-Tetrahydrocannabinol prevents cardiovascular dysfunction in STZ-diabetic Wistar-Kyoto rats. Biomed Res Int 2017; 7974149.
7. Coskun ZM, Bolkent S. Biochemical and immunohistochemical changes in delta-9-tetrahydrocannabinol-treated type 2 diabetic rats. Acta Histochem 2014;116(1):112-6.
8. Li X, Kaminski NE, Fischer LJ. Examination of the immunosuppressive effect of delta9-tetrahydrocannabinol in streptozotocin-induced autoimmune diabetes. Int Immunopharmacol 2001;1(4):699-712.
9. Cantele C, Bertolino M, Bakro F, Giordano M, Jędryczka M, Cardenia V. Antioxidant effects of hemp (*Cannabis sativa* L.) inflorescence extract in stripped linseed oil. Antioxidants (Basel) 2020;9(11):1131.
10. Raja A, Ahmadi S, de Costa F, Li N, Kerman K. Attenuation of oxidative stress by cannabinoids and cannabis extracts in differentiated neuronal cells. Pharmaceuticals (Basel) 2020;13(11):328.
11. Masiello P, Broca C, Gross R, Roye M, Manteghetti M, Hillaire-Buys D, et al. Experimental NIDDM: development of a new model in adult rats administered streptozotocin and nicotinamide. Diabetes 1998;47(2):224-9.
12. Beutler E. Glutathione: red cell metabolism. A manual of biochemical methods. Grune and Stratton, New York, 1975:112-4.
13. Buege JA, Aust SD. Microsomal lipid peroxidation. Methods Enzymol 1978; 52:302-10.
14. Reznick AZ, Packer L. Oxidative damage to proteins: spectrophotometric method for carbonyl assay. Methods Enzymol 1994;233:357-63.
15. Sun Y, Oberley LW, Li Y. A simple method for clinical assay of superoxide dismutase. Clin Chem 1988;34:497-500.
16. Bradford MM. A rapid and sensitive method for the quantitation of microgram quantities of protein utilizing the principle of protein-dye binding. Anal Biochem 1976;72:248-54.
17. Macho-González A, Garcimartín A, López-Oliva ME, Ruiz-Roso, B, Martín de la Torre, I, Bastida, S, et al. Can carob-fruit-extract-enriched meat improve the lipoprotein profile, VLDL-oxidation, and LDL receptor levels induced by an atherogenic diet in STZ-NAD-diabetic rats? Nutrients 2019;11(2):332.
18. Rezagholizadeh L, Pourfarjam Y, Nowrouzi A, Nakhjavani M, Meysamie A, Ziamajidi, N, et al. Effect of Cichorium intybus L. on the expression of hepatic NF-κB and IKKβ and serum TNF-A in STZ- and STZ+Niacinamide-induced diabetes in rat. Diabetol Metab Syndr 2016; 8:11.
19. Rehman K, Akash MSH. Mechanism of generation of oxidative stress and pathophysiology of type 2 diabetes mellitus: How are they interlinked? J Cell Biochem 2017;118(11):3577-85.
20. Luc K, Schramm-Luc A, Guzik TJ, Mikolajczyk TP. Oxidative stress and inflammatory markers in prediabetes and diabetes. J Physiol Pharmacol 2019;70(6):809-24.
21. Oyenihi AB, Opperman M, Alabi TD, Mpahleni B, Masola B. Centella asiatica alleviates diabetes-induced changes in fatty acid profile and oxidative damage in rat testis. Andrologia 2020;52(10):e13751.
22. Roy VK, Chenkual L, Gurusubramanian G. Protection of testis through antioxidant action of mallotus roxburghianus in alloxan-induced diabetic rat model. J Ethnopharmacol 2015;176:268-80.
23. Thyagaraju BM, Muralidhara. Ferulic acid supplements abrogate oxidative impairments in liver and testis in the streptozotocin-diabetic rat. Zoolog Sci 2008;25(8):854-60.
24. Al-Megrin WA, El-Khadragy MF, Hussein MH, Mahgoub S, Abdel-Mohsen DM, Taha H, et al. Green *Coffea arabica* extract ameliorates testicular injury in high-fat diet/streptozotocin-induced diabetes in rats. J Diabetes Res 2020;6762709.
25. Abdullah F, Khan Nor-Ashikin MN, Agarwal R, Kamsani YS, Abd Malek M, Bakar NS, et al. Glutathione (GSH) improves sperm quality and testicular morphology in streptozotocin-induced diabetic mice. Asian J Androl 20121;23(3):281-7.
26. Choubey M, Ranjan A, Bora PS, Krishna A. Protective role of adiponectin against testicular impairment in high-fat diet/streptozotocin-induced type 2 diabetic mice. Biochimie 2020;168:41-52.
27. Ismail M, Hasan H, El-Orfali Y, Ismail H, Khawaja G. Anti-inflammatory, antioxidative, and hepatoprotective effects of trans Δ9-tetrahydrocannabinol/sesame oil on adjuvant-induced arthritis in rats. Evid Based Complement Alternat Med 2018;9365464.

28. Vacek J, Vostalova J, Papouskova B, Skarupova D, Kos M, Kabelac M, et al. Antioxidant function of phytocannabinoids: molecular basis of their stability and cytoprotective properties under UV-irradiation. Free Radic Biol Med 2021;164:258-70.
29. Oliveira PF, Tomás GD, Dias TR, Martins AD, Rato L, et al. White tea consumption restores sperm quality in prediabetic rats preventing testicular oxidative damage. Reprod Biomed Online 2015;31(4):544-56.
30. Mandal TK, Das NS. Effect of delta-9-tetrahydrocannabinol on altered antioxidative enzyme defense mechanisms and lipid peroxidation in mice testes. Eur J Pharmacol 2009;607(1-3):178-87.
31. Borges RS, Batista JJr, Viana RB, Baetas AC, Orestes E, Andrade MA, et al. Understanding the molecular aspects of tetrahydrocannabinol and cannabidiol as antioxidants. Molecules 2013;18(10):12663-74.

ISTANBUL UNIVERSITY PRESS

RESEARCH ARTICLE

Eur J Biol 2021; 80(2): 97-106

Biochemical Fingerprints of Some Endemic Plants Growing in Gypsum Soils: Attenuated Total Reflection-Fourier Transform Infrared (ATR-FTIR) Spectroscopic Study

Aysenur Kayabas[1], Ertan Yildirim[2]

[1]Çankırı Karatekin University, Faculty of Science, Department of Biology, Çankırı, Turkey
[2]Gazi University, Faculty of Science, Department of Chemistry, Ankara, Turkey

ORCID IDs of the authors: A.K. 0000-0003-3555-4399; E.Y. 0000-0002-4083-3408

Please cite this article as: Kayabas A, Yildirim E. Biochemical Fingerprints of Some Endemic Plants Growing in Gypsum Soils: Attenuated Total Reflection-Fourier Transform Infrared (ATR-FTIR) Spectroscopic Study. Eur J Biol 2021; 80(2): 97-106. DOI: 10.26650/EurJBiol.2021.1005264

ABSTRACT

Objective: The aim of this study is to reveal the biochemical fingerprints of *Achillea gypsicola* Hub.-Mor., *Alyssum nezaketiae* Aytaç & H.Duman, *Onobrychis germanicopolitana* Hub.-Mor. & Simon, *Paracaryum paphlagonicum* (Bornm.) R.Mill and *Thymus leucostomus* Hausskn. et Velen. grown in extreme gypsum habitats with the Attenuated total reflection-Fourier transform infrared (ATR-FTIR) technique, and to determine the differences and densities of organic and inorganic compounds reflected by extreme environmental conditions.

Materials and Methods: Using ATR-FTIR spectra, the chemical content of endemic plants was elucidated. In addition, band intensities were calculated using the ATR-FTIR spectra. By doing soil analysis, the physical and chemical properties of the regions where the plants grow were tried to be understood.

Results: As a result of the detailed analysis of the ATR-FTIR spectra, it was understood that the chemical substance content was similar, but the amount was different from plant to plant, regardless of soil. These results showed that the same plant species contain different amounts of chemicals.

Conclusion: FTIR spectroscopy is an effective tool that reveals the biochemical fingerprints of plants by contributing to the determination of organic and inorganic compounds in the structures of plants grown on gypsum substrates. Our results provided evidence for the presence of sulfate from organic molecules and the presence of gypsum and calcium oxalate from inorganic compounds. This study, which is the first to determine the biochemical fingerprints of plants growing in gypsum habitats in Turkey, will enrich the generality of future studies and the interpretation of other gypsophytes in the world.

Keywords: ATR-FTIR, band intensities, Çankırı, fingerprints, gypsophyte, soil structure

INTRODUCTION

Gypsum-specific plants, called gypsophiles, have a high affinity for gypsum soils (1). It is still not clear why gypsophiles have a higher affinity for gypsum soils. Parent material, also called substrate, is an important abiotic factor in biodiversity (2). The gypsum and salt-rich outcrops are the best model examples of an edaphic island-like habitat and contain rare and endemic species, many of which are threatened (3). Plant species that grow in gypsum soils with high calcium and sulfur ratios and have high affinity for gypsum are also called edaphic endemics (4). Plants grown in gypsum habitats are named specialist plants called gypsophiles and generalist plants called gypsovags according to their affinity for gypsum (5). These habitats are natural wonders of biogeological heritage that contain rare and endemic species. Considering the distribution of gypsum in the world (6), Turkey is one of the important countries. Gypsum areas cover a large area of the Cen-

Corresponding Author: Aysenur Kayabas E-mail: aysenurkayabas@karatekin.edu.tr
Submitted: 06.10.2021 • **Revision Requested:** 22.10.2021 • **Last Revision Received:** 23.10.2021 • **Accepted:** 26.10.2021 • **Published Online:** 17.11.2021

tral Anatolia region (7), and the diversity of endemic plants in these areas is also quite high.

Gypsum soils present the extreme physical and chemical characteristics of plant species with important adaptations, such as gypsophilic flora (8). Habitats with high gypsum and salt content are in the position of disjunct areas that are described as ecologic islands in regions with arid and semi-arid climatic conditions (3, 9-11). Studies on the determination of ecological strategies based on phytochemical analyzes of plants grown in gypsum soils have attracted a lot of attention recently. However, these studies are based on more floristic diversity and elemental composition analyses. Most of these studies have been carried out by phytochemical analysis of the leaf part of the plant. Phytochemical content analysis in other organs of plants is not sufficient. Since the results in phytochemical analyses are more general, biochemical fingerprinting techniques that allow the identification of functional chemical groups of plants are needed to know whether they are the same as comprehensive analyses of plant biochemistry. Approaches based on the FTIR technique are important in our country, which has a wide range of gypsum habitats, in terms of shedding light on the biochemical and physiological adaptations developed by plants to survive in harsh environments. This study is based on the first biochemical fingerprinting technique to help understand the life of five endemic plants growing on gypsum substrates in harsh environments which have similar affinity to gypsum.

Attenuated Total Reflection-Fourier Transform Infrared (ATR-FTIR) spectroscopy has popular biological applications, from protein content determination to imaging cancer tissues (12-14). FTIR spectroscopy, which performs chemical analysis of biological samples in a practical, cost-effective, and non-destructive way, is a valuable tool in biochemical fingerprinting determination and allows the identification of both organic and inorganic compounds (15-18). Although the use of FTIR spectroscopy is increasing day by day and it is widely used in plants, its application to edaphic endemism studies is very rare in the literature. Palacio et al. reported the similarities and differences of the groups by comparing the FTIR results of the plant groups that developed different ecological strategies grown on gypsum (19). Nikalje et al. elucidated the salt stress responses of the roots and leaves of the halophyte *Sesuvium portulastrum* (L.) L. by determining the FTIR profile (20). Calcium oxalate crystals that occur as intravacuolar deposits (21) are observed in most plants growing in gypsum habitats because of adaptation to extreme conditions (22). Calcium oxalate, calcium carbonate, and amorphous silicas are the most common biominerals (23). FTIR spectroscopy also reveals the biochemical activity of the organism and the presence of biominerals (24) formed because of local accumulation of elements in the extreme environment in which it lives (23).

Approaches based on the FTIR technique are important in our country, which has a wide range of gypsum habitats, in terms of shedding light on the biochemical and physiological adaptations developed by plants to survive in harsh environments. This study is based on the first biochemical fingerprinting technique that will help to understand the life of five endemic plants growing on gypsum substrates in harsh environments.

The aim of this study is to reveal the biochemical fingerprints of *Achillea gypsicola* Hub.-Mor., *Alyssum nezaketiae* Aytaç & H.Duman, *Onobrychis germanicopolitana* Hub.-Mor. & Simon, *Paracaryum paphlagonicum* (Bornm.) R.Mill and *Thymus leucostomus* Hausskn. et Velen. grown in extreme gypsum habitats with the ATR-FTIR technique, and to determine the differences and densities of organic and inorganic compounds reflected by extreme environmental conditions. The biochemical fingerprints of the plants were revealed for the first time by analyzing the root, stem, and leaf parts of five endemic gypsophytes specific to gypsum substrates with the help of ATR-FTIR spectroscopy. In addition, physical and chemical analyses of the soil where the plants were grown were done, and the results of the ATR-FTIR of the plants were correlated with some analysis results of the soil.

MATERIALS AND METHODS

Collection of Plant Species and Study Area

Five gypsophyte plants were selected for analysis: *Achillea gypsicola* Hub.-Mor., *Alyssum nezaketiae* Aytaç & H.Duman, *Onobrychis germanicopolitana* Hub. -Mor. & Simon, *Paracaryum paphlagonicum* (Bornm.) R.Mill and *Thymus leucostomus* Hausskn. et Velen (Figures 1A, 2A, 3A, 4A, 5A). All of them were taken in gypsum soils in May-June 2021.

Plants were taken as whole individuals from gypsum habitats. The plant samples brought to the laboratory were first rinsed with tap water and then purified from dirt and soil. Taxonomic identifications of gypsophytes were done according to the Flora of Turkey and the East Aegean Islands (25, 26). Also, the categories of *A. gypsicola*, *A. nezaketiae*, *O. germanicopolitana*, *P. paphlagonicum*, and *T. leucostomus* were evaluated according to the IUCN Red Data Book (27). The IUCN categories of the studied species are VU, CR, EN, LR (cd), and VU, respectively. All the examined specimens are preserved in Çankırı Karatekin University, Department of Biology as a personal collection.

This study was conducted in gypsum areas between the Aşağıpelitözü and Balıbağı villages (750-900 m a.s.l., 40°30′ N, 33°42′ Çankırı, East of Central Anatolia, Turkey). The study area, which is under the influence of a semi-arid Mediterranean climate, is located within the Irono-Turan phytogeographic region. Vegetation was composed predominantly of shrubs, subshrubs, grasses and steppe plants, like, *Achillea phrygia* Boiss. & Balansa, *Asperula bornmuelleri* Velen, *Asperula cankiriense* B.Şahin & Sağıroğlu, *Bromus tomentellus* Boiss., *Campanula pinnatifida* Hub.-Mor., *Genista albida* Willd., *Gypsophila parva* Barkoudah, *Gypsophila eriocalyx* Boiss., *Helianthemum germanicopolitanum* Bornm., *Paracaryum ancyritanum* Boiss., *Salvia absconditiflora* (Montbret & Aucher ex Benth.) Greuter & Burdet and *Teucrium polium* L.

ATR-FTIR Spectroscopic Analysis

The infrared spectra of dried roots, stems and leaves were obtained by ATR-FTIR spectroscopy, model Thermo Nicolet 6700, supplied by OMNIC and recorded at room temperature in the wavenumber range from 400 to 4000 cm^{-1} at a resolution of 4 cm^{-1} and 32 scans. The intensities of the bands that could be determined and measured in the ATR-FTIR spectra were calculated with the help of the OMNIC software.

Soil Analyses

Soil samples were taken from a depth of 0-20 cm to characterize the substrate on which the gypsophytes were grown. After the soil samples were brought to the laboratory, they were dried at room temperature. Air-dried soil samples are passed through a 2 mm mesh sieve and stone, etc. The materials were removed and made ready for analysis. Soil samples taken from the study area were analyzed according to the following methods. The electrical conductivity (EC) was measured with a glass electrode EC-meter in the soil-water extract prepared at a ratio of 1:1 (28) and the soil reaction (pH) were measured with a pH-meter with a glass electrode in the soil-water extract prepared at a ratio of 1:2.5 (29). Exchangeable cations (Ca, Mg, Na and K) were determined by saturating with 1 M ammonium acetate at pH 7 (30). The percentage of gypsum content in the soil was determined gravimetrically by comparing samples dried at 60°C and 105°C (31).

RESULTS

The results of the ATR-FTIR spectra for the vegetative organs of the *A. gypsicola*, *A. nezaketiae*, *O. germanicopolitana*, *P. paphlagonicum* and *T. leucostomus* are summarized. The frequencies and assignments of the identified main peaks are given in Table 1. The presence of bands belonging to functional groups provided important information about the chemical composition of these specialist plants that can survive in harsh gypsum habitats.

The S-O bending functional group in the gypsum compound was detected at 669 and 600 cm^{-1}, and the O-H stretching functional group was detected broadly at 3000-3500 cm^{-1}. The S-O bending functional group in the sulphates compound was detected at 680-630 cm^{-1} and 900-1180 cm^{-1}. The C-O plane bending functional group in the calcium carbonate compound was detected at 720 and 875 cm^{-1}. The C-O stretching bending functional group, which is also found in the calcium oxalate compound, was detected at 1318 and 1580-1680 cm^{-1}. In addition, another functional group in the calcium oxalate compound, COO^- bending, was determined at 775 cm^{-1}. The functional band of long chain (> C4) alkane structures was seen at 730 cm^{-1}. The band of aromatic CH_2 functional groups of lignin compound is at 830 cm^{-1}, the band of lignin backbone is at 1185-1290 cm^{-1}, the functional band for lignin-phenolic backbone containing aromatic carbons is at 1505-1510 cm^{-1}, lignin and other bands belonging to aromatic double bonds determined to belong to aromatic structures were detected at 1580-1680 cm^{-1}. The broad band determined at approximately 950-1100 cm^{-1} for polysaccharides, silicates, sulphates, and phosphates represents the functional groups found in these species. Bands defining esters were detected at 1185-1290 and 1730-1735 cm^{-1}, respectively. Bands of phenolic (lignin) and aliphatic structures, carboxylate/carboxylic structures were seen at 1380-1480 cm^{-1}. The plane (amide-II) band of N-H in proteinaceous origin was detected at 1555 cm^{-1}. The bands belonging to the carbonyl functional group of the carboxylic acid groups were determined at 1707-1703 cm^{-1}. Bands belonging to aliphatic CH_2 groups in fats, wax and lipids were seen at 2850-2920 cm^{-1}. Hydroxyl bands in cellulosic structures were determined at 3000-3600 cm^{-1}. The presence of bands belonging to functional groups provided important information about the chemical content of gypsum species (Table 1).

The band areas of the bands at 900-1180, 1185-1290, 1380-1480, 1580-1680, 2850-2920 and 3000-3500 cm^{-1}, which can be determined for each plant species and can be measured, were calculated. The band intensities at 900-1180 cm^{-1} for the root, stem, and leaf parts of *A. gypsicola* were calculated as 3125, 2280 and 2900 a.u. (arbitrary units), respectively. It was determined as 125, 10 and 100 a.u. for the bands at 1185-1290 cm^{-1}. Band intensities at 1380-1480 cm^{-1} were measured at 315, 150 and 190 a.u. Intensities in the band range of 1580-1680 cm^{-1} were calculated as 360, 280 and 490 a.u. The areas of the bands at 2850-2920 cm^{-1} were found to be 215, 250 and 680 a.u. The areas of the bands at 3000-3500 cm^{-1} belonging to the hydroxyl band representing the gypsum were calculated as 2750, 2780 and 2300 a.u., respectively (Figures 1B and C).

Different results were obtained when the band intensities of *A. nezaketiae* were compared with those of *A. gypsicola*. In this context, band intensities were calculated as 2400, 2280 and 4000 a.u. for root, stem, and leaf at 900-1180 cm^{-1} in *A. nezaketiae*. The band at 1185-1290 cm^{-1} was observed only in the root with a band with an intensity of 385 a.u., while the intensity of this band could not be detected in the stem and leaves. Band intensities at 1380-1480 cm^{-1} were calculated as 110, 550 and 500 a.u. The intensities of the bands, which are thought to belong to lignin and other aromatics and observed at 1580-1680 cm^{-1}, were found as 360, 160 and 200 a.u. Band intensities at 2850-2920 cm^{-1} were calculated as 520, 400 and 335 a.u. Hydroxyl band intensities were found in this plant species in 1880, 2100 and 1850 a.u. (Figures 2B and C).

In the qualitative analysis of the root, stem, and leaf of *O. germanicopolitana*, band intensities at 90-1180 cm^{-1} were found to be 3400, 245 and 3350 a.u., respectively. Band intensities at 1185-1290 cm^{-1} were calculated as 140, 150 and 180 a.u. The band intensities of the functional groups at 1380-1480 cm^{-1} were determined as 530, 220 and 360 a.u. The band intensities of the aromatic C=C double bonds at 1480-1580 cm^{-1} were found to be 850, 550 and 420 a.u. Band intensities of symmetric and antisymmetric aliphatic functional groups were calculated as 750, 670 and 1280 a.u. The band intensities of the hydroxyl stretch band at 3000-3500 cm^{-1} were found to be 2850, 5025 and 6200 a.u., respectively (Figures 3B and C).

Table 1. Functional groups and band densities in gypsum plants

			Achillea gypsicola			*Alyssum nezaketiae*			*Onobrychis germanicopolitana*			*Paracaryum paphlagonicum*			*Thymus leuscotomus*		
Functional Group	**Compound type**	**Wavenumbers**	**root**	**stem**	**leaf**	**root**	**stem**	**leaf**	**root**	**stem**	**leaf**	**root**	**stem**	**leaf**	**root**	**stem**	**leaf**
S-O bending	Gypsum	(669, 600 cm^{-1})	**	**	**	**	*	*	**	*	*	*	*	*	*	*	*
S-O bending	Sulphates	(630-680 cm^{-1})	**	**	**	*	*	*	**	**	*	*	*	*	*	*	*
C-O plane bending	Calcium carbonate	(720 cm^{-1})	*	*	*	*	**	**	*	*	*	*	*	*	*	*	*
CH_2 wag	Long chain (> C4) alkanes	(730 cm^{-1})	*	*	*	*	*	*	*	*	*	*	*	*	*	*	*
COO^- bending	Calcium oxalate	(775 cm^{-1})	*	**	**	*	**	**	*	**	*	**	**	**	**	**	**
Aromatic CH out of plane	Lignin	(830 cm^{-1})	*	*	**	*	**	**	**	*	*	**	**	*	*	**	**
C-O plane bending	Calcium carbonate	(875 cm^{-1})	**	**	*	*	*	*	**	**	**	**	**	**	**	**	**
Combination of C-O stretching and O-H deformation, Si-O stretching, P-O stretching, S-O stretching	Polysaccharide, Silicate, Phosphate, Sulphate	(900-1180 cm^{-1})	***	***	***	***	***	***	***	***	***	***	***	***	***	***	***
C-O-C stretching, C-N stretching, C-O stretching of phenolic and/or aryl-methyl ethers	Esters, Amide III, Indicative of lignin backbone	(1185-1290 cm^{-1})	***	***	***	***	n.d.	n.d.	***	***	***	***	***	***	***	***	***
C-O stretching	Calcium oxalate	(1318 cm^{-1})	**	**	**	**	*	*	**	**	**	**	**	**	**	**	**
C-H deformations, Symmetric C-O stretch from COO- or stretch and OH deformation, C-O stretching	Phenolic (lignin) and aliphatic structures, Carboxylate/Carboxylic structures (humic acids), Calcium carbonate	(1380-1480 cm^{-1})	***	***	***	***	***	***	***	***	***	***	***	***	***	***	***
Aromatic C = C stretching	Lignin/Phenolic backbone	(1505-1510 cm^{-1})	**	**	**	**	*	*	**	**	**	**	**	**	**	**	**
N-H in plane (amide-II)	Proteinaceous origin	(1555 cm^{-1})	**	**	**	*	*	*	*	*	*	**	**	**	*	*	*
Aromatic C = C stretching and/or asymmetric C-O strech in COO^-, C = O streching, C = O of amide I	Lignin and other aromatics, or aromatic or aliphatic carboxylates, Calcium oxalate, Proteinaceous origin	(1580-1680 cm^{-1})	360	280	490	360	160	200	850	550	420	320	300	250	275	350	530
C = O stretch of COOH	Carboxylic acids	(1707-1703 cm^{-1})	*	*	*	*	*	*	*	*	*	*	*	*	**	*	*
C = O strech of COOR	Esters	(1735-1730 cm^{-1})	**	*	**	**	**	**	**	**	**	**	**	**	**	**	**
Symmetric CH_2 stretching, Antisymmetric CH_2 stretching	Fats, wax, lipids	(2850-2920 cm^{-1})	***	***	***	***	***	***	***	***	***	***	***	***	***	***	***
O-H stretching	Gypsum, Cellulose	(3000-3500 cm^{-1})	***	***	***	***	***	***	***	***	***	***	***	***	***	***	***

*: low density band intensities, **: incalculable band intensities, ***: high density band intensities, **n.d.**: not detected band intensities.

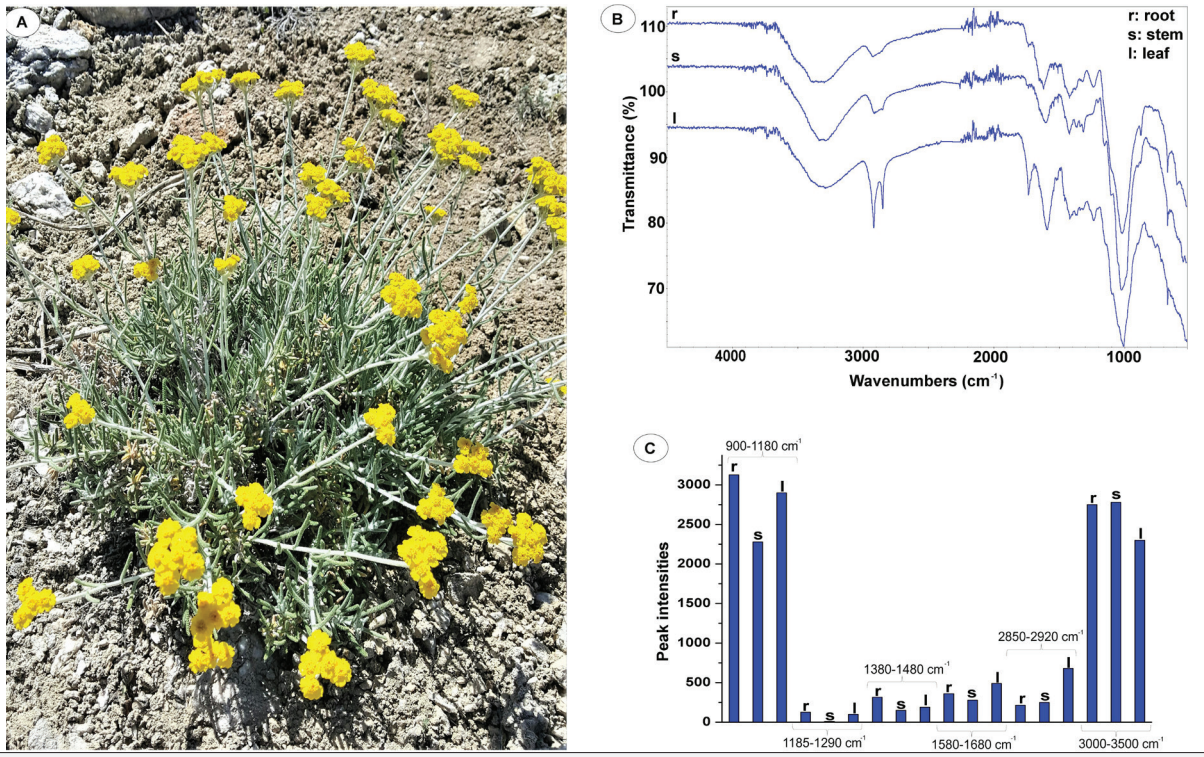

Figure 1. **A.** *Achillea gypsicola* habit (from Çankırı province). **B.** ATR-FTIR spectra of *A. gypsicola*. **C.** Graph of band intensities of *A. gypsicola.*

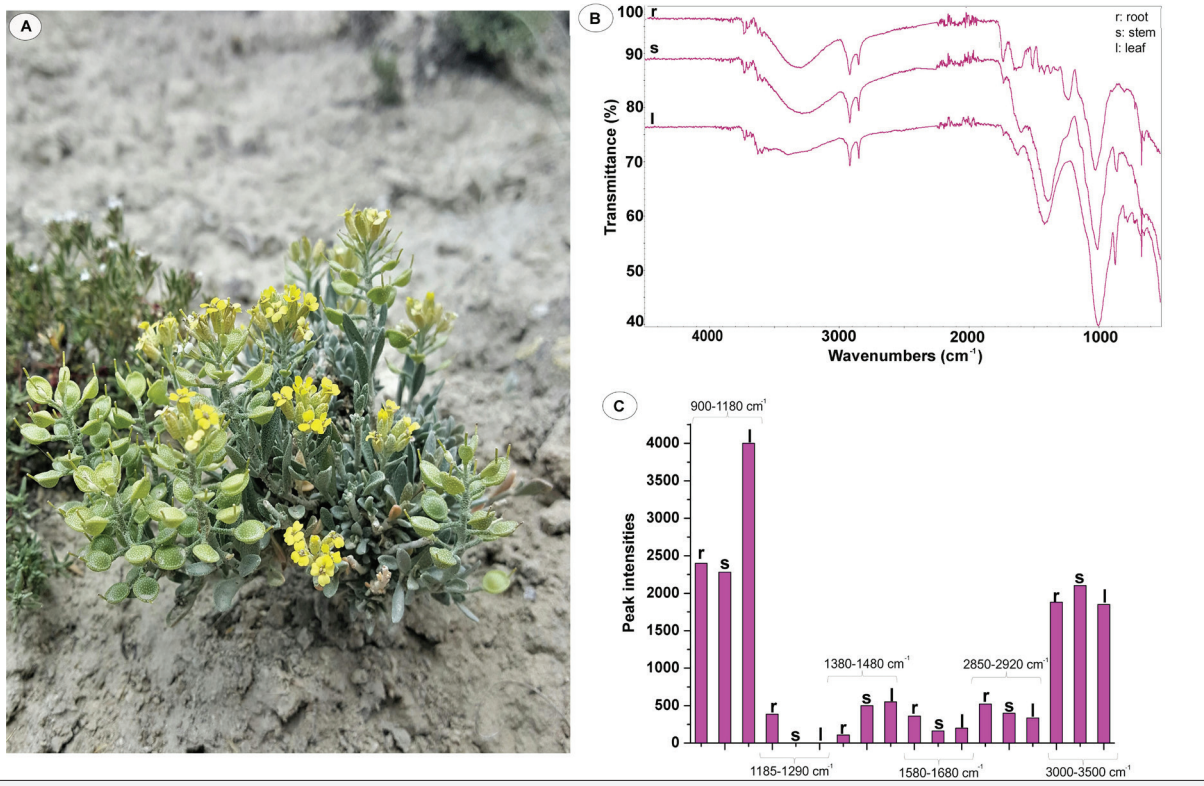

Figure 2. **A.** *Alyssum nezaketiae* habit (from Çankırı province). **B.** ATR-FTIR spectra of *A. nezaketiae*. **C.** Graph of band intensities of *A. nezaketiae.*

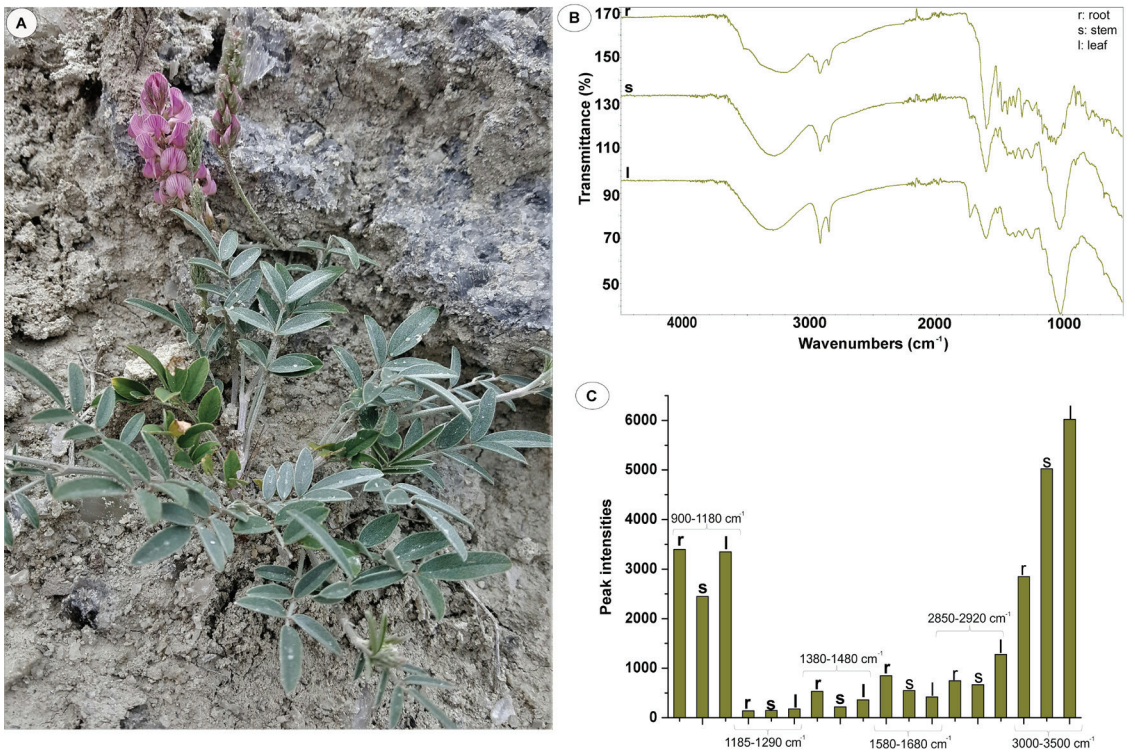

Figure 3. **A.** *Onobrychis germanicopolitana* habit (from Çankırı province). **B.** ATR-FTIR spectra of *O. germanicopolitana*. **C.** Graph of band intensities of *O. germanicopolitana.*

The following data were obtained because of the calculation of the band intensities for the root, stem, and leaf parts of the *P. paphlagonicum*. 3700, 2250 and 2670 a.u. band intensities were determined for the 900-1180 cm^{-1} band range. For the 1185-1290 cm^{-1} range, band intensities were calculated as 275,190 and 110 a.u., respectively. The band intensities of the functional groups at 1380-1480 cm^{-1} were found to be 210, 280 and 56 a.u. The intensities of the bands at 1580-1680 cm^{-1} were calculated as 320, 300 and 250 a.u. Band intensities of 150, 510 and 521 a.u. were calculated for the band range at 2850-2920 cm^{-1}. The band intensities of the hydroxyl groups of gypsum in the plant species at 3000-3500 cm^{-1} were found to be 3350, 2400 and 2910 a.u., respectively (Figures 4B and C).

Finally, the regions and intensities of the bands that can be detected in the ATR-FTIR spectra and whose band intensities can be measured were determined for root, stem, and leaf of *T. leuscotomus*. The band intensities in the broad band at 900-1180 cm^{-1} were found to be 2500, 2620 and 3000 a.u., respectively. The band intensities of the functional groups at 11850-1290 cm^{-1} were calculated as 230, 50 and 85 a.u. While the band intensities at 1380-1480 cm^{-1} were calculated as 480, 120 and 350 a.u., the band intensities at 1585-1680 cm^{-1} were found as 275, 350 and 530 a.u. The intensities of the bands at 2850-2920 cm^{-1}, which are thought to belong to oils, lipids, and waxes, were calculated as 595, 675 and 1250 a.u. The intensities of the broad band at 3000-3500 cm^{-1} were found to be 4850, 2550 and 3600 a.u., respectively (Figures 5B and C).

In summary, at the 900-1180 cm^{-1} band content, the variety of inorganic compounds (silicates, phosphates, and sulphates) is more than organic compounds (polysaccharids). It was determined that the C-O-C stretching, C-N stretching, C-O stretching of phenolic and/or aryl-methyl ethers bending seen at 1185-1290 cm^{-1} were very high in terms of organic compounds including esters, amide, and indicative of lignin backbone. It was determined that the C-H deformations, symmetric C-O stretch from COO^- or stretch and OH deformation, C-O stretching bending seen at 1380-1480 cm^{-1} were very high in terms of organic compounds including phenolic (lignin) and aliphatic structures and carboxylate/carboxylic structures (humic acids). It was determined that the symmetric and antisymmetric CH_2 stretching bending seen at 2850-2950 cm^{-1} were more abundant in terms of organic compounds including fats, wax, and lipids. It is understood from the band intensities that the roots, stems and leaves of the five gypsophytes, the gypsum inorganic compound belonging to the broad O-H stretching bending seen at 3000-3500 cm^{-1}, are in excess in the ATR-FTIR spectra (Table 1, Figures 1C-5C).

The plant species selected in this study were selected from plants grown in gypsum habitats. Knowing the physical and chemical properties of the substrate, that is, the soil, on which these gypsophytes grow, has helped to understand the extreme conditions under which gypsophytes grow. For this purpose, soil properties such as pH, electrical conductivity (EC), exchangeable Ca, Mg, Ca, K, cation exchange capacity (CEC), exchangeable sodium percentage (ESP), gypsum content (%)

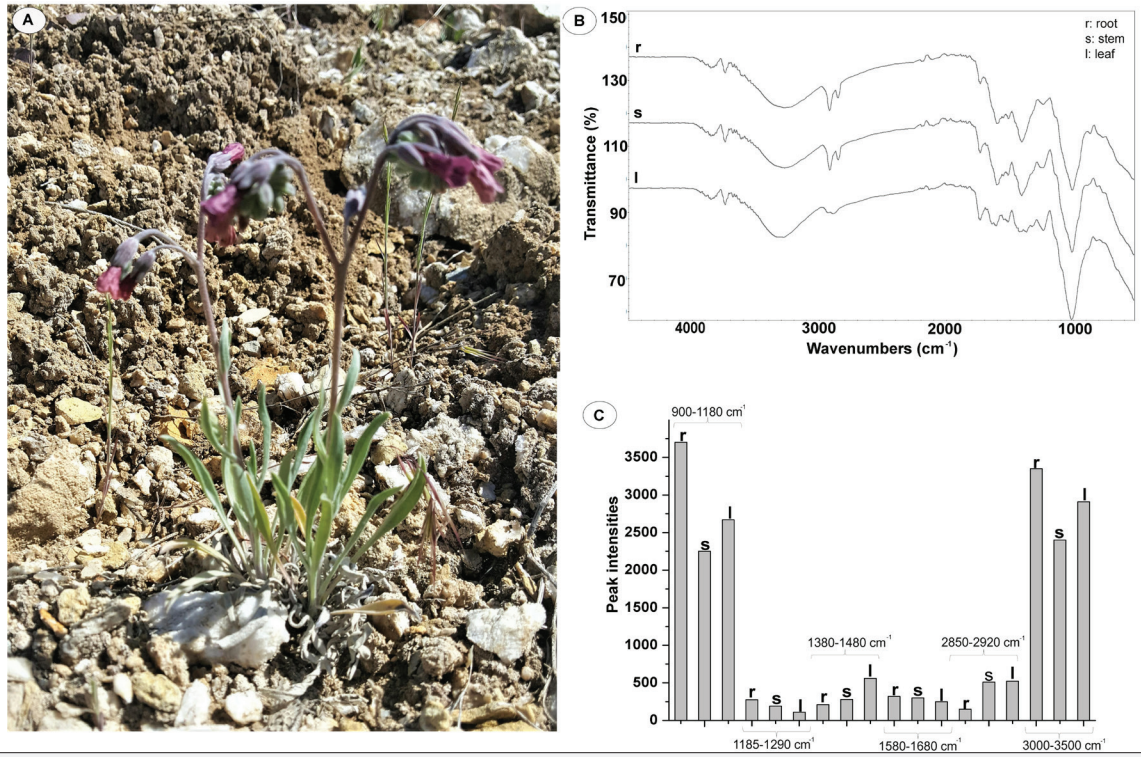

Figure 4. **A.** *Paracaryum paphlagonicum* habit (from Çankırı province). **B.** ATR-FTIR spectra of *P. paphlagonicum*. **C.** Graph of band intensities of *P. paphlagonicum*.

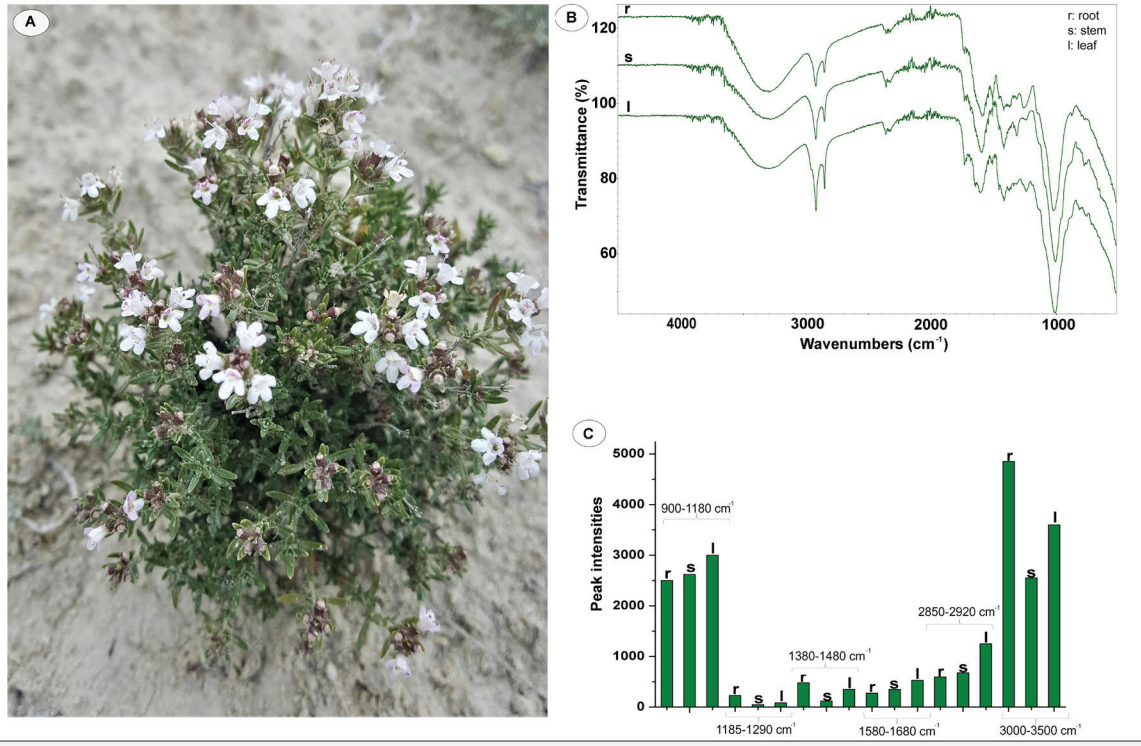

Figure 5. **A.** *Thymus leucostomus* habit (from Çankırı province). **B.** ATR-FTIR spectra of *T. leucostomus*. **C.** Graph of band intensities of *T. leucostomus*.

were also analyzed (Table 2). According to the soil physical analysis, the pH is 7.76 and the EC value is 2.76 dS m^{-1}. Exchangeable Ca, Mg, Ca, K values are 27.04, 4.33, 1.09 and 0.41 meq/L, respectively and CEC is 26.81 meq/100g. The ESP, gypsum values are 7.64 and 68%, respectively.

Table 2. Main soil characteristics (*n*=3)

pH	7.76
EC (dS m^{-1})	2.76 (very saline)
Exchangeable Ca (meq/L)	27.04
Exchangeable Mg (meq/L)	4.33
Exchangeable Na (meq/L)	1.09
Exchangeable K (meq/L)	0.41
CEC (meq/100 g)	26.81
ESP (%)	7.64
Gypsum (%)	68

DISCUSSION

The functional groups and band intensities of the root, stem, and leaf parts of five different gypsophiles were measured by ATR-FTIR. The functional groups of *A. gypsicola, A. nezaketiae*, *O. germanicopolitana*, *P. paphlagonicum*, and *T. leucostomus*, endemic to gypsum soils, were similar. Nedyalkova et al. detected that the S-O bending band at 611 cm^{-1} and showed similar results in this study as it was seen at 605-610 cm^{-1} in gypsum plants (32). Ashfag et al. recorded the wave number of the S-O bending band as 669 cm^{-1} in sulfates, and the related band was observed at 665-670 cm^{-1} in this study (33). Jha et al. determined that the S-O stretching vibrations in sulfates at 1100-1200 cm^{-1} and reported that the band width and density increased with the overlapping of each band in plants (34). In the literature, the band of aromatic CH_2 functional groups of lignin is at ~830 cm^{-1}, the band of lignin backbone is at ~1185-1290 cm^{-1}, the functional band for lignin-phenolic containing aromatic carbons is at ~1505-1510 cm^{-1}, lignin and other bands belonging to aromatic double bonds determined to belong to aromatic structures were detected at ~1580-1680 cm^{-1} (19, 35, 36). Within the scope of this study, results compatible with the literature were obtained for the wavelengths mentioned in the ATR-FTIR spectra. Palacio et al. reported the presence of sulfates, phosphates, silicates, and polysaccharides at 1150-950 cm^{-1} in the ATR-FTIR spectra of gypsum plants (19). In this study, the broad band observed at 1200-950 cm^{-1} was attributed to the functional groups of these species. Since the functional bands of silicate, sulfate, phosphate, and polysaccharides of plant species came to the same spectrum region, the band was seen as very broad at 950-1200 cm^{-1}. In the literature, hydroxyl bands of cellulose containing structures with broad hydroxyl bands have a broad band at 3000-3500 cm^{-1} (37). The broad band of cellulosic groups found in plants is due to dense hydroxyl groups. The presence of bands belonging to functional groups provided important information about the chemical content of gypsum plants.

In this study, the presence of gypsum, one of the inorganic compounds, is observed in the vegetative organs of gypsophytes. Palacio et al. reported the presence of gypsum inorganic compound in the leaves of wide gypsophiles in their FTIR spectroscopic studies with gypsophiles and gypsovags (19). The presence of gypsum compound is compatible with studies (38, 39) specific to Turkey on the phytochemical compositions (as total ash, Ca, and S) of gypsum plants. Duvigneaud and Denaeyer-DeSmet suggested that S accumulates in the form of calcium sulphate (40), but for the first time Palacio et al. reported the presence of the mineral gypsum (19). The presence of mineral gypsum, which is one of the inorganic compounds from gypsophytes, was reported for the first time in Turkey with this study. He et al., suggested that plants that can survive in gypsum soils form oxalate and sulfate crystals to detoxify excess Ca and S (41). The presence of calcium oxalate crystals in the vegetative organs of the plants in this study also supports the results (42). Kayabaş and Kurt reported that *Aethionema turcica* and *A. dumanii*, which are gypsovags grown on gypsum, contain high N (39). Palacio et al. have documented that gypsophite *Lepidium subulatum* has a high N, amino acid, and protein content (43). The presence of protein, peptide, amino acid, and other organic compounds in gypsophytes with high N content may be due to both N and S richness. These results indicate that the phytochemical content of the plant will be in parallel with the results of ATR-FTIR spectroscopy. This study has also documented that the ATR-FTIR technique is a very valuable method for the removal of biochemical fingerprints of plants, since performing these and similar studies with the help of the ATR-FTIR technique provides positive benefits in terms of practicality, time and cost.

When the main soil characteristics summarized in Table 2 are examined, according to the Baize criteria (44), the soil in which the plants grow shows data saline characteristics. About 10% of the earth is affected by soil salinity and/or sodicity (45). The sum of the exchangeable cations (Ca^{2+}, Mg^{2+}, Na^{+}, K^{+}), which significantly affect the physicochemical properties of the soil, is equal to the cation exchange capacity (CEC). The best indicator for calculating this ratio is the calculation of the percent exchangeable sodium (ESP). ESP is the ratio of exchangeable sodium to the CEC of the soil (28). Exchangeable cations significantly affect the physicochemical properties of the soil. The ESP value of the gypsum soil analyzed in this study is 7.64%, and the ESP values are between 0.4-76.5 % when the literature is examined (27, 45-52). Hazelton and Murphy described the soils with 6-14% ESP value as sodium (53). Since the ESP value of the soil analyzed in this study is 7.64%, it also shows high sodium feature. Soils with an ESP value of 6-14% are considered sodium rich (53, 54). High salinity and sodium in the soil negatively affects germination and growth (55). The high percentage of gypsum and sodium content in gypsum soils causes the gypsophytes growing in these habitats to adapt to extreme conditions and thus to spe-

cialize in gypsum. The presence of gypsum crystals may not be relevant to survival strategy in high gypsum-containing soils. There is no gypsum crystal in every plant that grows in soils with high gypsum content and has high S content (42).

As a result, FTIR spectroscopy is an effective tool that reveals the biochemical fingerprints of plants by contributing to the determination of organic and inorganic compounds in the structures of plants grown on gypsum substrates. Our results provided evidence of the presence of sulfate from organic molecules and the presence of gypsum and calcium oxalate from inorganic compounds. This study, which is the first to determine the biochemical fingerprints of plants growing in gypsum habitats in Turkey, will enrich to the generality of future studies and the interpretation of other gypsophytes in the world.

CONCLUSION

Our study investigated the fingerprint properties of endemic gypsophytes which are grown in gypsum habitats by using FTIR techniques. Additionally, the characteristic FTIR spectra of the *A. gypsicola*, *A. nezaketiae*, *O. germanicopolitana*, *P. paphlagonicum* and *T. leucostomus* were obtained. In this study, the ATR-FTIR technique was applied for the first time in Turkey for plants growing in gypsum habitats. By performing the chemical analysis of the ATR-FTIR spectra of the plants and the gypsum soil in which the plants grew, data on the chemical contents of these plants were obtained to understand their adaptation to extreme habitats. ATR-FTIR spectra were taken from vegetative organs of each plant. With the help of functional groups in the ATR-FTIR spectra, the chemical contents of gypsophytes were elucidated. By calculating the band intensities, it was determined that each plant species and part had different chemical contents. For the first time, within the scope of this study, changes in band intensities were calculated by using ATR-FTIR spectra and information about the chemical content and amount of gypsophytes was presented within the scope of this study. This study will shed light on many future studies on the chemical analysis gypsophytes.

Acknowledgements: The authors would like to thank the Soil, Fertilizer and Water Resources Central Research Institute for performing the soil analyses, and the Gazi University Academic Writing and Research Center for their help and valuable support in the proofreading of this study.

Peer-review: Externally peer-reviewed.

Author Contributions: Conception/Design of study: A.K., E.Y.; Data Acquisition: A.K., E.Y.; Data Analysis/Interpretation: A.K., E.Y.; Drafting Manuscript: A.K., E.Y.; Critical Revision of Manuscript: A.K., E.Y.; Final Approval and Accountability: A.K., E.Y.

Conflict of Interest: The authors declare that they have no conflicts of interest to disclose.

Financial Disclosure: There are no funders to report for this submission.

REFERENCES

1. Sánchez-Martín R, Querejeta JI, Voltas J, Ferrio JP, Prieto I, Verdú M, et al. Plant's gypsum affinity shapes responses to specific edaphic constraints without limiting responses to other general constraints. Plant Soil 2021; 462(1): 297-309.
2. Hulshof CM, Spasojevic MJ. The edaphic control of plant diversity. Glob Ecol Biogeogr 2020; 29(10): 1634-50.
3. Bobo-Pinilla J, Salmerón-Sánchez E, Mota JF, Peñas J. Genetic conservation strategies of endemic plants from edaphic habitat islands: The case of *Jacobaea auricula* (Asteraceae). J Nat Conserv 2021;61:126004.
4. Blanco-Sánchez M, Moore MJ, Ramos-Muñoz M, Pías B, García-Fernández A, Prieto M, et al. Phylogeography of a gypsum endemic plant across its entire distribution range in the western Mediterranean. Am J Bot 2021; 108(3): 443-60.
5. Cera A, Duplat E, Montserrat-Martí G, Gómez-Bolea A, Rodríguez-Echeverría S, Palacio S. Seasonal variation in AMF colonisation, soil and plant nutrient content in gypsum specialist and generalist species growing in P-poor soils. Plant Soil 2021; 1-16.
6. Ramon A, Caselle C, Bonetto SMR, Costanzo D, Alonso EE. Effect of microstructure and relative humidity on strength and creep of gypsum. Rock Mech Rock Eng 2021; 54: 4121-45.
7. Ozel S. Identification and assessment of hazard of development in gypsum karst regions: Examples from Turkey. Tiefenbacher JP, editor. Natural Hazards Risk, Exposure, Response, and Resilience. London: Intech Press; 2019. p. 111-24.
8. Denaeyer-De Smet S. Note on the chemical composition of salts secreted by various gypsohalophytic species of Spain. Bulletin de la Societé Royale de Botanique de Belgique 1970; 103: 273-78.
9. Perez-Garcia FJ, Akhani H, Parsons RF, Silcock JL, Kurt L. Ozdeniz E, et al. A first inventory of gypsum flora in the Palearctic and Australia. Mediterr Bot 2018; 39(1): 35-49.
10. Sánchez AM, Alonso-Valiente P, Albert MJ, Escudero A. How might edaphic specialists in gypsum islands respond to climate change? Reciprocal sowing experiment to infer local adaptation and phenotypic plasticity. Ann Bot 2017; 120(1): 135-46.
11. Martín-Rodríguez I, Escudero A, García-Fernández A. Limited effect of a highway barrier on the genetic structure of a gypsum soil specialist. PeerJ 2021; 9:e10533.
12. Cirrincione M, Saladini B, Brighenti V, Salamone S, Mandrioli R, Pollastro F, et al. Discriminating different *Cannabis sativa* L. chemotypes using attenuated total reflectance-infrared (ATR-FTIR) spectroscopy: A proof of concept. J Pharm Biomed Anal 2021; 204: 114270.
13. Götz A, Nikzad-Langerodi R, Staedler Y, Bellaire A, Saukel J. Apparent penetration depth in attenuated total reflection Fourier-transform infrared (ATR-FTIR) spectroscopy of *Allium cepa* L. epidermis and cuticle. Spectrochim Acta A Mol Bio Spectrosc 2020; 224: 117460.
14. Tiernan H, Byrne B, Kazarian SG. ATR-FTIR spectroscopy and spectroscopic imaging for the analysis of biopharmaceuticals. Spectrochim Acta A Mol Bio Spectrosc 2020; 241: 118636.
15. Durak T, Depciuch J. Effect of plant sample preparation and measuring methods on ATR-FTIR spectra results. Environ Exp Bot 2020; 169: 103915.
16. Muhammad S, Wuyts K, Nuyts G, De Wael K, Samson R. Characterization of epicuticular wax structures on leaves of urban plant species and its association with leaf wettability. Urban For Urban Green 2020; 47: 126557.
17. Ordoudi SA, Papapostolou M, Kokkini S, Tsimidou MZ. Diagnostic potential of FTIR fingerprinting in botanical origin evaluation of *Laurus nobilis* L. essential oil is supported by GC-FID-MS data. Molecules 2020; 25(3): 583.

18. Skotti E, Pappas C, Kaiafa M, Lappa IK, Tsitsigiannis DI, Giotis C, et al. Discrimination and quantification of aflatoxins in *Pistachia vera* seeds using FTIR-DRIFT spectroscopy after their treatment by Greek medicinal and aromatic plants extracts. Food Science and Engineering 2020; 1(1): 45-57.
19. Palacio S, Aitkenhead M, Escudero A, Montserrat-Martí G, Maestro M, Robertson AJ. Gypsophile chemistry unveiled: Fourier transform infrared (FTIR) spectroscopy provides new insight into plant adaptations to gypsum soils. PLoS One 2014; 9(9): e107285.
20. Nikalje GC, Kumar J, Nikam TD, Suprasanna P. FT-IR profiling reveals differential response of roots and leaves to salt stress in a halophyte *Sesuvium portulacastrum* (L.) L. Biotechnol Rep 2019; 23: e00352.
21. Paiva EAS. Are calcium oxalate crystals a dynamic calcium store in plants? New Phytol 2019; 223(4): 1707-11.
22. Escudero A, Palacio S, Maestre FT, Luzuriaga AL. Plant life on gypsum: a review of its multiple facets. Biol Rev 2015; 90(1): 1-18.
23. Rosa-Tilapa D, Maceda A, Terrazas T. Characterization of biominerals in Cacteae species by FTIR. Crystals 2020; 10(6): 432.
24. Skinner HCW. Biominerals. Mineral Mag 2005; 69(5): 621-41.
25. Davis PH. Flora of Turkey and the East Aegean Islands Vol. I-IX. Edinburgh: Edinburgh University Press; 1965-1985.
26. Davis PH, Mill RR, Tan K. Flora of Turkey and the East Aegean Islands (Suppl. 1) Vol. X. Edinburgh: Edinburgh University Press; 1988.
27. Ekim T, Koyuncu M, Vural M, Duman H, Aytaç Z, Adıgüzel N. Red data book of Turkish plants (Pteridophyta and Spermatophyta). Turkish Association for the Conservation of Nature & Van Centennial University. Ankara: Barışcan Publishing; 2000.
28. Richards L. Diagnosis and improvement of saline and alkali soils. United States Salinity Laboratory. Agriculture Handbook. Washington: U.S. Department of Agriculture Publishing; 1954.
29. Gee GW, Bauder JW. Partical-size analysis. Klute A, editor. Methods of Soil Analysis. Part 1. Physical and Mineralogical Methods. USA: SSSA Press; 1986. p. 383-411.
30. Bower CA, Reitemeier RF, Fireman M. Exchangeable cation analysis of saline and alkali soils. Soil Sci 1952; 73(4): 251-62.
31. Porta J. Técnicas y Experimentos en Edafologia. Barcelona: Col.legi Oficial d'Enginyers Agrònoms de Catalunya; 2005.
32. Nedyalkova L, Lothenbach B, Renaudin G, Mäder U, Tits J. Effect of redox conditions on the structure and solubility of sulfur-and selenium-AFm phases. Cem Concr Res 2019; 123: 105803.
33. Ashfaq MY, Al-Ghouti MA, Da'na D, Qiblawey, H, Zouari N. Effect of concentration of calcium and sulfate ions on gypsum scaling of reverse osmosis membrane, mechanistic study. J Mater Res Technol 2020; 9(6): 13459-73.
34. Jha MK, Van Nguyen N, Lee JC, Jeong J, Yoo JM. Adsorption of copper from the sulphate solution of low copper contents using the cationic resin Amberlite IR 120. J Hazard Mater 2009; 164(2-3): 948-53.
35. Huang Y, Wang L, Chao Y, Nawawi DS, Akiyama T, Yokoyama T, Matsumoto Y. Analysis of lignin aromatic structure in wood based on the IR spectrum. J Wood Chem Technol 2012; 32(4): 294-303.
36. Boeriu CG, Bravo D, Gosselink RJ, Van Dam JE. Characterisation of structure-dependent functional properties of lignin with infrared spectroscopy. Ind Crops Prod 2004; 20(2): 205-18.
37. Sonker AK, Rathore K, Teotia AK, Kumar A, Verma V. Rapid synthesis of high strength cellulose–poly (vinyl alcohol) (PVA) biocompatible composite films via microwave crosslinking. J Appl Polym Sci 2019; 136(17): 47393.
38. Bolukbasi A, Kurt L, Palacio S. Unravelling the mechanisms for plant survival on gypsum soils: an analysis of the chemical composition of gypsum plants from Turkey. Plant Biol 2016; 18(2): 271-79.
39. Kayabaş A, Kurt A. Is the substrate an important factor in the investigation of gypsophile endemism? Proceedings of the 2nd International Symposium on Biodiversity Research; 2020 November 18-20; Rize, Turkey. pp. 189-207.
40. Duvigneaud P, Denaeyer-De Smet S. Essai de classification chimique (éléments minéraux) des plantes gypsicoles du bassin de l'Ebre. Bulletin de la Société Royale de Botanique de Belgique 1968; 101: 279-91.
41. He H, Bleby TM, Veneklaas EJ, Lambers H, Kuo J. Precipitation of calcium, magnesium, strontium and barium in tissues of four *Acacia species* (Leguminosae: Mimosoideae). PLoS One 2012; 7(7): e41563.
42. Mota JF, Sola AJ, Dana ED, Jiménez-Sánchez ML. Plant succession in abandoned gypsum quarries in SE Spain. Phytocoenologia 2003; 33(1): 13-28.
43. Palacio S, Escudero A, Montserrat-Martí G, Maestro M, Milla R, Albert MJ. Plants living on gypsum: Beyond the specialist model. Ann Bot 2007; 99(2): 333-43.
44. Baize D. Guide des analyses courantes en pédologie. Paris: Inra Press; 1988.
45. Gharaibeh MA, Albalasmeh AA, Pratt C, El Hanandeh A. Estimation of exchangeable sodium percentage from sodium adsorption ratio of salt-affected soils using traditional and dilution extracts, saturation percentage, electrical conductivity, and generalized regression neural networks. Catena 2021; 205: 105466.
46. Paliwal KV, Gandhi AP. Effect of salinity, SAR, Ca: Mg ratio in irrigation water, and soil texture on the predictability of exchangeable sodium percentage. Soil Sci 1976; 122(2): 85-90.
47. Frenkel H, Alperovitch N. The effect of mineral weathering and soil solution concentration on ESR-SAR relationships of arid and semiarid zone soils from Israel. J Soil Sci 1984; 35(3): 367-72.
48. Rengasamy P, Greene RSB, Ford GW, Mehanni AH. Identification of dispersive behaviour and the management of red-brown earths. Soil Res 1984; 22(4): 413-31.
49. Ghafoor A, Muhammed S, Ahmad N, Mian MA. Indices for the estimation of ESP from SAR of soil solution. Pak J Sci 1988; 39:40.
50. Mohamed DM, Ibrahim SI, Elamin EA. Variability and correlation between exchangeable sodium percentage and sodium adsorption ratio in Vertisols of Sudan. Commun Soil Sci Plant Anal 2008; 39(19-20): 2827-38.
51. Seilsepour M, Rashidi M, Khabbaz BG. Prediction of soil exchangeable sodium percentage based on soil sodium adsorption ratio. Am Eurasian J Agric Environ Sci 2009; 5(1): 1-4.
52. Chi CM, Zhao CW, Sun XJ, Wang ZC. Estimating exchangeable sodium percentage from sodium adsorption ratio of salt-affected soil in the Songnen Plain of Northeast China. Pedosphere 2011; 21(2): 271-76.
53. Hazelton P, Murphy B. Soil chemical properties. Interpreting soil test results? What do all the numbers mean? Australia; 2007. p. 106-13.
54. Northcote KH, Skene JKM. Australian soils with saline and sodic properties. Canberra: Csiro Press; 1972.
55. Taşdelen K, Demir Y. Determination of salinity and sodicity conditions of rice growing areas with geographical information systems in Terme Plain. Anadolu Journal of Agricultural Sciences 2020; 35(2): 175-84.

ISTANBUL UNIVERSITY PRESS

RESEARCH ARTICLE

Eur J Biol 2021; 80(2): 107-118

Investigation of the Effects of Autophagy Signaling on the Transcription of Yeast Retrotransposon Ty2-917

Sezai Turkel[1], Ceyda Colakoglu[2], Tugce Karaduman[1]

[1]Bursa Uludag University, Faculty of Arts and Sciences, Department of Molecular Biology and Genetics, Bursa, Turkey
[2]Bursa Uludag University, Faculty of Medicine, Department of Medical Biology Bursa, Turkey

ORCID IDs of the authors: S.T. 0000-0001-7128-6948; C.C. 0000-0002-7471-5071; T.K. 0000-0003-0479-0559

Please cite this article as: Turkel S, Colakoglu C, Karaduman T. Investigation of the Effects of Autophagy Signaling on the Transcription of Yeast Retrotransposon Ty2-917. Eur J Biol 2021; 80(2): 107-118. DOI: 10.26650/EurJBiol.2021.1011143

ABSTRACT

Objective: Ty2-917 is a low copy retrotransposon found in the *Saccharomyces cerevisiae* genome. It has structural similarities to metazoan retroviruses in terms of genome organization and propagation mechanisms in the host cells. The objective of this study is to analyze the effects of autophagy signaling on the transcriptional regulation of Ty2 in yeast cells.

Materials and Methods: Ty2-LacZ gene fusions on the YEp vectors have been used as reporter genes to analyze the effects of amino acid starvation, nitrogen source, and autophagy signals on the transcription of Ty2. These reporter gene fusions have been transformed into the wild type and also isogenic mutant yeast strains that are defective for one of the regulatory factors involved in nutrient sensing and signaling. To activate autophagy signaling, yeast transformants were treated with caffeine or 3-amino 1-2-3 triazole. Transcription levels of Ty2-LacZ gene fusions in treated and untreated yeast cells were analyzed by β-galactosidase assays.

Results: Results of this study show that transcription of Ty2 decreases up to eightfold in response to amino acid starvation. Caffeine treatment of the yeast cells also represses Ty2 transcription, independent of the TOR1 pathway. In addition, our results suggest that Ty2 transcription is also regulated in a nitrogen source-dependent manner through the GATA factors.

Conclusions: Our results suggest that activation of autophagy signal results in significant level repression of Ty2 transcription. We have found that the GATA class of transcription factors is involved in the regulation of Ty2 transcription in response to autophagy signaling.

Keywords: Autophagy, Transcription, Yeast, Retrotransposons, GATA factors

INTRODUCTION

The *Saccharomyces cerevisiae* genome has five different types of mobile genetic elements known as Ty (Transposon Yeast) (1). Ty elements propagate via the RNA intermediate in the yeast genome. They form virus-like particles (Ty-VLP) in the yeast cytoplasm (2). Their genome organization and intracellular propagation mechanisms show a large degree of similarities to metazoan retroviruses (3). They are called retrotransposon due to these similarities. The taxonomic classifications of yeast retrotransposons in the world of viruses have also been assigned. Ty1 and Ty2 are classified in the Pseudovirus genus of the Pseudoviridae family in the Retrovirales order, while Ty3 is included in the Metavirus genus of the Metaviridae family (4).

Ty2-917 (hereafter referred to as Ty2) is one of the retrotransposons found in the yeast genome. It has been discovered as an insertional element within the *HIS4* gene of *S. cerevisiae* (5). Later it was found that it is present as five to ten copies in most of the *S. cerevisiae* laboratory strains (1). Its genome size is 5.9 Kbp and it contains 0.33 Kbp long terminal repeats (LTR) at its 5′and 3′ ends. These LTRs are called delta elements (Figure 1). It has been shown that the intracellular copy numbers

Corresponding Author: Sezai Turkel E-mail: sturkel@uludag.edu.tr
Submitted: 17.10.2021 • **Revision Requested:** 28.10.2021 • **Last Revision Received:** 01.11.2021 • **Accepted:** 03.11.2021 • **Published Online:** 22.11.2021

of Ty retrotransposons are regulated at post-translational levels and do not change drastically in standard laboratory strains of *S. cerevisiae* (6, 7).

Ty genomes are highly expressed. Single types of polyadenylated mRNA are transcribed from the Ty genomes by RNA polymerase II. It is known that Ty mRNAs constitute up to 10% of total mRNA in the yeast cytoplasm (8). Ty mRNAs have two open reading frames, called TYA and TYB. These coding regions functionally show homology to retroviral Gag and Pol polypeptides, respectively (9, 10). TYA peptide forms the capsid part of the Ty-VLP after post-translational processing. TYB polypeptide is proteolytically processed and yields the reverse transcriptase, protease, and integrase enzymes required for the replication cycle of Ty elements. TYB is translated as a fusion protein to TYA by programmed ribosomal frameshift (PRF) (Figure 1) (9, 10).

Promoter regions of Ty2 retrotransposons have multiple overlapping transcription factor binding sites. These regulatory elements are located both upstream and downstream of the transcription initiation site within the 5′ LTR region (11-13). Ty elements do not encode any transcription factors and their transcription is regulated by host-encoded transcription factors. Transcription factors that are involved in the regulation of Ty2 transcription have been identified previously by biochemical and genetic techniques. These factors are; Gcr1, Sgc1, Tec1, Rap1, and chromatin modification complexes such as histone acetyl transferases (14-17). It has previously been reported that

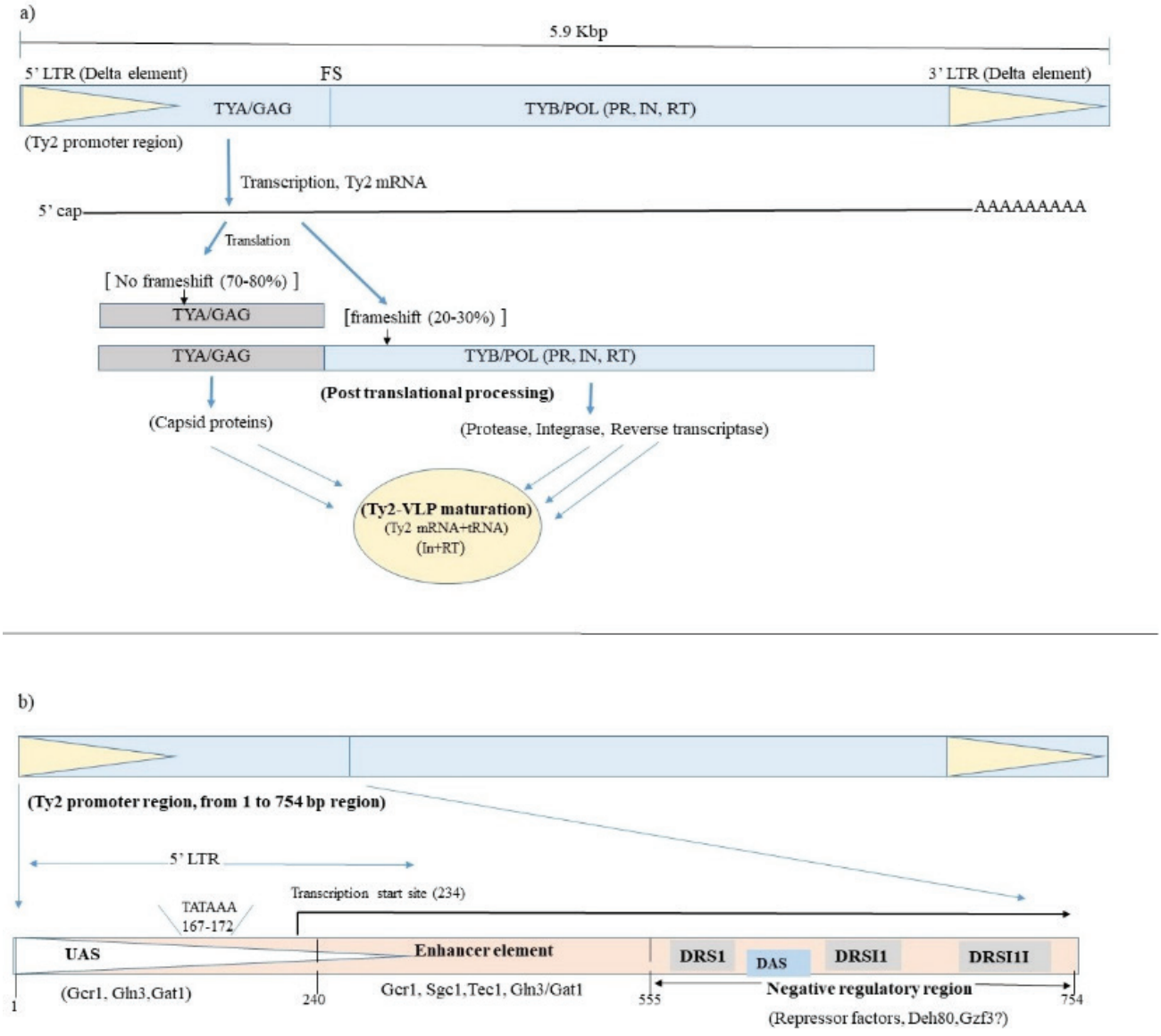

Figure 1. Genome organization and promoter structure of retrotransposon Ty2. a-) Overall genetic structure of Ty2. b-) Organization of functional regulatory region of Ty2 promoter. Abbreviations: FS: Frameshift Site. DRS: Downstream Repression Sites. DAS: Downstream Activation Sites. UAS: Upstream Activation Sequence.

transcription of Ty elements is regulated in response to metabolic signals. Ty2 transcription is controlled by the transcription factor Gcr1 in response to glucose signaling (17). It seems that Gcr1 is the major transcription factor that activates Ty2 transcription since deletion of the *GCR1* gene completely abolishes Ty2 expression (17). Recent evidence indicates that Gcr1 is present as two isoforms. These are $Gcr1^{U}$ and $Gcr1^{S}$. These isoforms show differential stability in the cytoplasm, depending on the growth stage of the yeast cells (18, 19).

It is known that activation of selective autophagy targets Ty1-VLP in yeast and down-regulates Ty1 mediated insertional mutagenesis (20). Moreover, we have recently reported that transcription in Ty1 and Ty2 is differentially regulated by apoptosis-inducing growth conditions (21).

Autophagy has been defined as the lytic cellular process for macromolecule recycling in adverse conditions. It is conserved in all eukaryotes and essential for cellular homeostasis. Molecular components of the autophagy process have been elucidated by Yoshinori Ohsumi using *S. cerevisiae* as the model eukaryotic system (22, 23). Autophagy-related (*ATG*) genes that involve in the initiation and execution of the autophagy process have been identified and functionally analyzed in yeast (23). The target of rapamycin (TOR), AMP-activated protein kinase Snf1, also functions in the initial stages of autophagy signaling. Under nutrient replete growth conditions, TOR1 kinase is active and represses the expression of *ATG* genes (24-28). When TOR1 kinase is inhibited by rapamycin, caffeine treatment, or nutrient-limited growth conditions, the autophagy pathway resumes forming autophagosomes (24-28). Different sets of transcription factors are involved in the regulation of *ATG* genes. Some of these transcription factors are Ume6, Pho23, Rim15, Gcn4, Gln3, Gat1, and Yap1 (25). Moreover, it is known that Gcn4p, Gln3p, Gat1p, and Yap1p are also involved in the transcriptional activation of numerous yeast genes, including Ty elements (29, 30).

Autophagy can be activated by intracellular and extracellular factors. Intracellular events that activate autophagy are misfolded protein accumulations and damaged or dysfunctional cell components. Extracellular factors that activate autophagy are different chemicals and environmental cues such as amino acid starvation and nitrogen limitations (31, 32). Autophagy processes can be classified into different sub-groups depending on reaction mechanisms. These are macro-autophagy, micro-autophagy, and chaperone-mediated autophagy. In all three of these autophagy processes, targeted macromolecules are transported into lysosomes (in vacuole for yeast) for degradation. In macro-autophagy, targeted macromolecules are transported to lysosomes via autophagosomes that are double membraned cytoplasmic structures sequentially formed by Atg factors (32). On the other hand, in micro-autophagy, targeted cytoplasmic structures are directly taken up by lysosomes. In chaperone-mediated autophagy (CMA), targeted macromolecules are first recognized and complexed with chaperon proteins, then taken up by lysosomes via lysosome-associated membrane protein 2A (LAMP-2A) (32). In certain cases, the above-mentioned autophagy processes selectively target specific cellular structures via binding to specific receptors located on targeted cytoplasmic organelles. This type of autophagy is known as selective autophagy and requires specific interactions between one of the components of the autophagy process and a specific receptor on the targeted cytoplasmic structures. Mitophagy, pexophagy, reticulophagy, and ribophagy are well-known examples of selective autophagy (32).

Previously, it was found that the activation autophagy process reduces Ty1 transposition by decreasing the cytoplasmic Ty1-VLP load in *S. cerevisiae* (20). It was shown that Ty1-VLP was selectively transported to the vacuole in Cvt vesicles (Cytoplasm to vacuole) by Atg19-dependent manner in Rapamycin treated yeast cells. Atg19 is a receptor protein that specifically carries targeted structures to Cvt vesicles for degradation at vacuole (33). It was concluded that the selective autophagy process is operated to prevent or to decrease insertional mutagenesis caused by Ty elements within the yeast cells. Autophagy is also involved in the cytoplasmic virus particle destruction in human cells (34, 35). Hence, especially for latent virus particles, autophagy activation has been of interest for potential therapeutic approaches for the eradication of certain human viruses (34, 35). In this study, we have analyzed the effects of autophagy activation on the transcriptional regulation of retrotransposon Ty2. We have shown that activation of the autophagy process downregulates Ty2 transcription at a significant level. Moreover, it appears that TORC1-regulated transcription factors Gln3/Gat1 is involved in the transcriptional regulation of Ty2.

MATERIALS AND METHODS

S. cerevisiae Strains and Ty2 Expression Vectors

The genotypes of *S. cerevisiae* strains used in this study were given in Table 1. The standard laboratory strain of *S.* cerevisiae BY4741 and its deletion mutants were purchased from the EUROSCARF yeast collection. They are isogenic to each other except for the indicated mutations (36). *S. cerevisiae* strains F212 and F113 were used to analyze the effects of amino acid starvation on Ty2 transcription. They are wild type for histidine biosynthesis and commonly used to test the effects of 3-amino triazole-triggered effects of amino acid starvation on yeast genes. *S. cerevisiae* F212 and F113 strains are also isogenic pairs other than *gcn4* mutations (Table 1). *S. cerevisiae* strains YST182 and YST184 were used to test the effects of transcription factors Gln3/Gat1 on Ty2 transcription (37). Yeast strains were grown in YPD (1% Yeast Extract, 2% Pepton, 2% Dextrose) medium for routine cultivations in a 30 C incubator shaker (150 rev/min). To confirm the deletions in mutant strains and the presence of KanMX deletion cassette, mutant strains were streaked and grown on the YPD media containing Geneticin (200 µg/mL) (36).

The characteristics of the yeast expression vectors used in this study were summarized in Table 2. Structures and construction of plasmids pST1, Ty2-555-LacZ, Ty2-754-LacZ, and pST1-Enh-LacZ were described previously (12-14). Expression vector pF-N8X-n is a 2 µ-*URA3*-based plasmid bearing a fusion of the yeast

Table 1. *Saccharomyces cerevisiae* laboratory strains used in this research.

EUROSCARF Accession numbers (relevant mutations)	**Genotypes**
Y00000 (wild type) (BY4741)	MATa, his3Δ1; leu2Δ0; met15Δ0; ura3Δ0.
Y06864(Δ*tor1*)	MATa, his3Δ1; leu2Δ0; met15Δ0; ura3Δ0, YJR066w::kanMX4
Y14311(Δ*snf1*)	MATα, his3Δ1; leu2Δ0; met15Δ0; ura3Δ0, YDR477w::kanMX4
Y07155(Δ*tec1*)	MATα, his3Δ1; leu2Δ0; met15Δ0; ura3Δ0, YBR083w::kanMX4
Y01641(Δ*sgc1*)	MATα, his3Δ1; leu2Δ0; met15Δ0; ura3Δ0, YOR344c::kanMX4
F212* (Δ*gcn4*)	MATα, ura3-52, ino1 gcn4-Δ1 'Kpn1-Mlu1' (wild type for histidine biosynthesis)
F113* (Wild type for *GCN4*)	MATα, ura3-52, ino1 (wild type for histidine biosynthesis) (F212 and F113 strains are also isogenic pairs other than gcn4 mutations)
YST182** (Wild type for GATA factors)	MATα, ade2Δ::hisG, his3Δ200, leu2Δ0, lys2Δ0, met15Δ0, trp1Δ63, ura3Δ0.
YST184 (03167b)(Δ*gln3*/Δ*gat1* double mutant)	MATα, ade2Δ::hisG, his3Δ200, leu2Δ0, lys2Δ0, met15Δ0, trp1Δ63, ura3Δ0, gln3::KanMX4, gat1:: KanMX4

**S. cerevisiae* F212 and F113 strains are from Prof. Dr. Alan Hinnebusch's yeast collection (NIH, Bethesda, Maryland. USA)
***S. cerevisiae* YST182 and YST184 strains are from Prof. Dr. Evelyne Dubois's yeast collection (Université Libre de Bruxelles, Belgium.)

Table 2. Lists of plasmids used in this study.

Plasmids/Gene fusions	**Relevant characteristics**
pST1	His4-LacZ fusions to codon 32 of *HIS4*. The *HIS4* transcriptional activators are replaced by a polylinker containing Xho1, Not1, Kpn1, BamH1 sites. Does not contains any activator binding sites. (YEp, 2μ–*URA3*).
Ty2-555-LacZ	Ty2–917-LacZ fusion at position 555 of Ty2–917, includes entire enhancer element of Ty2-917. (YEp, 2μ–*URA3*).
Ty2-754-LacZ	Ty2–917-LacZ fusion at position 754 of Ty2–917, includes entire enhancer element and downstream negative regulatory region of Ty2-917. (YEp, 2μ–*URA3*).
pST1-Enh-LacZ	His4-LacZ fusions to codon 32 of *HIS4*. The *HIS4* transcriptional activators are replaced by a polylinker into which the Ty2–917 enhancer (240–559) was inserted. (YEp, 2μ–*URA3*).
His4-LacZ (pFN8X-n)	His4-LacZ fusion, includes entire promoter region of *HIS4* gene (YEp2μ–*URA3*).

wild type *HIS4* gene to the *E.coli* lacZ gene (38). Expression of the His4-LacZ fusion on this plasmid is induced in response to amino acid starvation by *GCN4* (39). All plasmids used in this research are the yeast episomal plasmid (YEp)-based expression vectors. YEp plasmids are the shuttle vector that is widely used for the cloning, transformation, and expression of a variety of genes in *S. cerevisiae* (40). It has been previously shown that the copy numbers of these YEp plasmids do not change drastically in the yeast cells grown in the selective growth media (11, 12).

Yeast Transformation

S. cerevisiae strains were cultivated in 25 mL YPD medium at standard growth conditions (30 C in incubator shaker, 150 rev/min) to the logarithmic stage for transformation. The lithium acetate-polyethylene glycol method was used for the transformation of Ty2-LacZ expression vectors to the competent *S. cerevisiae* cells as described (41). Transformants of *S. cerevisiae* strains with BY4741 genetic background were plated onto synthetic complete media (100 μL) without uracil (Sc-Ura, 2% dextrose) and transformation plates were incubated at 30 C incubator for 3-4 days for the growth of transformant yeast colonies. Transformants of *S. cerevisiae* strains F212 and F113 were plated and maintained on the minimal yeast nitrogen base (YNB) medium supplemented with 2% glucose. Transformants of *S. cerevisiae* strains YST182 and YST184 were also plated on YNB medium

supplemented with 2% glucose and auxotrophic requirements (20 mg/L histidine, 30mg/L leucine, 30mg/L lysine, 20 mg/L methionine, and 20 mg/L tryptophan) as described (37). The yeast transformants were stored at 4 C during the experiments. They are used for inoculation of liquid cultures that are used for autophagy experiments as described below.

Activation of Autophagy Signaling

For activation of autophagy conditions in BY4741-derived *S. cerevisiae* strains, yeast transformants first were grown to saturation in 10 mL of liquid Sc-Ura medium supplemented with 2% glucose and then diluted to OD_{600}: 0.1 in 10 mL of fresh Sc-Ura medium supplemented with 2% glucose. Once the cell density reached the mid-logarithmic stage (OD_{600}: 1.0) in these cultures, yeast cultures were divided into two aliquots, 5 mL each. Filter-sterilized caffeine was added to 8 mM final concentration to one aliquot (42). Caffeine-treated and untreated yeast cultures were further incubated for 5 hours at standard growth conditions.

For amino acid starvation experiments, *S. cerevisiae* strains F212 and F113 transformants first were grown to saturation in 5 mL liquid YNB media supplemented with 2% glucose and then diluted to OD_{600}: 0.1 in fresh 10 mL of YNB liquid media. Once the cell density reached OD_{600}: 0.4-0.5, yeast cultures were divided into two aliquots, 5 mL each. Filter-sterilized 3-amino 1,2,4 triazole (3-AT) was added to 10mM final concentration to one portion (29). 3-AT treated and untreated yeast transformants were grown for an additional 10 hours and harvested for β-galactosidase assays.

In order to analyze the effects of GATA factors on the transcriptional regulation of Ty2, *S. cerevisiae* YST182 and YST184 transformants were grown in 5 mL YNB minimal medium supplemented with auxotrophic requirements and different nitrogen sources as described (37). *S. cerevisiae* strains grown to logarithmic stages at standard growth conditions and then harvested for β-Galactosidase assays.

At the end of growth periods, yeast cells were harvested by centrifugation and washed twice with 1 mL of sterile distilled water. After final wash and centrifugation, harvested yeast pellets were resuspended in 200 µL of β-Galactosidase breaking buffer and used for β-Galactosidase assays as described in the next section. Yeast transformants were grown in duplicates and all experiments were repeated at least twice.

β-Galactosidase Enzyme Assay

In order to get yeast cell lysates, 20 µL chloroform and 20 µL 0.1% SDS was added to the yeast suspensions and vortexed vigorously for 1 minute to obtain yeast lysates (27). β-Galactosidase activities of the yeast lysates were determined in triplicates as described previously (11, 43). Protein concentrations in the yeast lysates were determined by the Lowry test (44). β-Galactosidase units are expressed in nano moles of 2-Nitrophenyl β-D-Galactopyranoside (ONPG) cleaved per minute per mg of protein in the permeabilized yeast cell suspensions (nm ONPG/ minute/ mg protein). Standard deviations for β-Galactosidase units were below 10-15% in triplicate assays. Statistical significance (*p*-values) of the results were calculated using a T-test. The expression levels of gene fusions under normal growth versus autophagy induced conditions in the wild type and mutant yeast transformants were compared using a T-test. Transcription levels were found significantly different ($p<0.05$).

***In-Silico* Analysis of the Ty2 and *GCR1* Genes Promoter Regions**

Experimentally proven and putative binding sites for Gcr1 and GATA factors were analyzed using YEASTRACT (www.yeastract.com) and Saccharomyces Genome Database (SGD) (www.yeastgenome.org) search tools. The promoter region of Ty2-917 encompasses the first 800 bp region of the Ty2 sequence and contains all of the known regulatory sites (11, 14-17). *GCR1* gene has an unusually long, alternatively spliced intron region. The first exon of the *GCR1* gene contains only 8 base pairs. The promoter region of the *GCR1* gene (Systematic Name: YPL075W) on chromosome XVI has been re-defined as 1 kbp long DNA region upstream of the first ATG codon of first exon (www.yeastgenome.org). Promoter region sequences of the Ty2 and *GCR1* gene were downloaded from the SGD database. Potential binding sites for Gcr1 and GATA factors were screened using YEASTRACT transcription factor binding site analysis tools.

RESULTS

Effect of Autophagy Activation on Ty2-917 Transcription

We have analyzed the effects of autophagy activation on the transcription of Ty2 retrotransposon and its regulator region, namely the enhancer element. It has previously been reported that autophagy signaling can be generated by caffeine (42). Ty2-754-LacZ gene fusion contains all of the known regulatory regions of Ty2 retrotransposon (Figure 1). Hence we have used this Ty2-754-LacZ gene fusion to test the effects of autophagy activation. Transcription from this Ty2 gene fusion yielded 185 units of activity in the wild type *S. cerevisiae* grown in a normal growth medium. Activation of autophagy signaling by caffeine treatment resulted in a threefold decrease in the transcription of Ty2 in this yeast strain (Table 3). After showing that the caffeine treatment represses the Ty2 transcription, we wanted to determine the molecular components of the caffeine-dependent repression of Ty2 transcription. Therefore, we have analyzed the effect of caffeine treatment on the mutant strains that lack one of the regulatory factors involve in the TOR signaling or Ty2 regulation. Assuming that the caffeine-triggered autophagy process acts through one of these regulatory factors, we should not see any difference in the transcription of Ty2 in caffeine-treated and untreated mutant yeast cells.

Previous studies have shown that the TOR1 complex (TORC1) is the main factor for the suppression of autophagy in nutrient-replete growth conditions (32, 45). Hence, the inactivation of TORC1 initiates the autophagy process in all eukaryotic cells. Snf1 (also known as AMP-activated kinase) involves in the regulation of numerous metabolic events in eukaryotes (46). Transcription of Ty2 decreased in Δ*tor* and Δ*snf1* mutant yeast strains, indicating that functional TORC1 and Snf1 complex in-

Table 3. Activation of autophagy represses Ty2-754 transcription.

***S. cerevisiae* strains (relevant mutations)**	**Growth Conditions and β-Galactosidase Activities *(± SD)**	
	Sc-Ura+%2 Glucose (Normal growth)	**Autophagy induction (+8 mM Caffein)**
Y0000 (*Wild type*)**	185±15	69±2
Y06864 (Δ*tor1*)**	156±2	86±2
Y14311 (Δ*snf1*)**	116±1	30±1
Y07155 (Δ*tec1*)**	157±1	54±4
Y01641 (Δ*sgc1*)**	74±4	29±1

(± SD): Standard deviations.
*Numbers indicate β-Galactosidase Units which are expressed in nano moles of ONPG cleaved per minute per mg of protein.
**Transcription levels were found significantly different ($p<0.05$).

volved in the transcriptional activation of Ty2 under nutrient-replete conditions (Table 3). Caffeine treatment of these mutant strains resulted in a further decrease in Ty2 transcription. It is noticeable that Ty2 transcription was repressed nearly fourfold in the Δ*snf1* strain (Table 3). In addition to these protein kinases, we have also tested the effects of transcription factors Tec1 and Sgc1 on the Ty2 transcription in caffeine-treated and untreated yeast transformants. Deletion of the *TEC1* gene had a slight effect on Ty2 transcription in untreated cells. But Ty2 transcription decreased more than twofold in Δ*sgc1* mutant cells, indicating that this transcription activator is an essential component of Ty2 transcription. Caffeine treatment of Δ*sgc1* and Δ*tec1* mutants also resulted in a two to threefold decrease in Ty2 transcription. However, when compared to the Ty2 expression level in the untreated wild type cells, Ty2 transcription is sixfold lower (185 units versus 29 units) in Δ*sgc1* mutants than the normal expression level in the wild type yeast (Table 3). Altogether, these results indicated that protein kinase Snf1 and transcription factor Sgc1 are required for the optimal level transcription of Ty2 under nutrient-replete standard growth conditions. Caffeine treatment of yeast cells represses Ty2 expression approximately three to fourfold. Caffeine is a specific inhibitor of TOR1 kinase. A *p*-value which is less than 0.05 (($p<0.05$) indicates that there are statistically significant differences in the expression levels of Ty2-917 gene fusions in the untreated and caffeine-treated yeast cells. However, it is clear that caffeine-dependent repression of Ty2 is largely independent of TORC1, Snf1 kinases, and transcription factors Sgc1 and Tec1.

Effects of Autophagy Signaling on Enhancer Element of Ty2 retrotransposon

Transcriptional regulatory regions of Ty2-917 are located both upstream and downstream of the transcription initiation site. The transcription activation region, an enhancer element, locates between 249 bp and 555bp of Ty2 (Figure 1). Downstream of an enhancer element, the negative regulatory region of Ty2 locates between 555 and 754 bp with respect to the first nucleotide of Ty2-917. An enhancer element activates transcription of any heterologous promoter when inserted upstream of the TATA box (13, 17). We wanted to analyze whether or not autophagy signaling acts on the enhancer element, independent from the negative regulatory region of Ty2. Transcription from the Ty2-555-LacZ reporter gene yielded 2158 units of activity as expected. The lack of negative regulatory region of Ty2 resulted in a more than tenfold increase in Ty2 transcription in normal growth conditions (Table 4). But caffeine treatment of the yeast

Table 4. Autophagy signaling targets Ty2 enhancer dependent transcription in wild type *S. cerevisiae* strain.

Gene Fusions	**Growth Conditions and β-Galactosidase Activities *(± SD)**	
	Sc-Ura+%2 Glucose (Normal growth)	**Autophagy induction (+8 mM Caffein)**
Ty2-555-LacZ**	2158±200	965±77
p-ENC-LacZ	852±55	516±29

(± SD): Standard deviations.
*Numbers indicate β-Galactosidase Units which are expressed in nano moles of ONPG cleaved per minute per mg of protein.
**Transcription levels were found significantly different ($p<0.05$).

cells resulted in a nearly twofold decrease in the transcription of Ty2. Enhancer element-dependent transcription from a heterologous promoter yielded 852 units of activity in normally growing yeast transformants. Caffeine treatment of the yeast transformants resulted in a less than twofold decrease in enhancer element-dependent transcription. These results showed that autophagy activation by caffeine treatment targets regulatory factors, directly or indirectly, that are associated with transcription activation of Ty2, albeit not as high as in Ty2-754 that has a whole-length regulatory region (Table 4). A *p*-value that is less than 0.05 ($p<0.05$) indicates that there are statistically significant differences in the expression levels of Ty2-555-LacZ gene fusions in the untreated and caffeine treated yeast cells.

Amino Acid Starvation Represses Ty2-917 Transcription Independent of *GCN4* Pathway

Amino acid starvation that inactivates TOR1 signaling triggers the autophagy process in *S. cerevisiae*. We wanted to investigate if the Ty2 transcription will be affected by amino acid starvation. Previously constructed expression vectors that contain Ty2-555-LacZ and pEnh-LacZ gene fusions were transformed into F212 and F113 yeast strains. pST1 and pFN8X-n plasmids were also transformed into the same yeast strains as negative and positive controls, respectively. A portion of the yeast transformants was treated with 3-AT, a competitive inhibitor of the *HIS3* gene product, to trigger amino acid starvation in these transformants.

Transcription of Ty2-555-LacZ decreased eightfold in 3-AT treated wild type *S. cerevisiae* F113 strain (1282 units to 162 units) (Table 5). Ty2 enhancer element-dependent transcription of a heterologous promoter (pEnh-LacZ) was repressed sixfold in amino acid starved yeast cells (Table 5). Amino acid starvation that inactivates TORC1 was probably acting on the regulatory factors that bind to the Ty2 enhancer element since it also affects the enhancer activated transcription of a heterologous promoter. As expected, transcription of *HIS4* gene activated threefold by amino acid starvation (from 812 units to 2388 units) (Table 5). Transcription from cloning vector pST1 that contains only the TATA box region is not affected by amino acid starvation.

It is well-known that transcription factor Gcn4 is activated by amino acid starvation in the wild type yeast strains (29). It was conceivable that Gcn4 could activate a kind of repressor protein that represses Ty2 transcription in amino acid-starved yeast cells by acting on the Ty2 enhancer element either directly or indirectly. To test this possibility, we have measured the effect of amino acid starvation on the Ty2 transcription in *gcn4* mutant *S. cerevisiae* F212 strain, isogenic to the wild type yeast strain. We found that Ty2 enhancer element-dependent transcription of a heterologous promoter and Ty2-555-LacZ was still repressible by amino acid starvation independent of the *GCN4* pathway (Table 5). Transcription of Ty2-555-LacZ and the Ty2 enhancer-activated transcription of a heterologous promoter was repressed approximately four to fivefold in 3-AT treated *gcn4* mutant F212 yeast strain (Table 5). As we expected, transcription of the His4-LacZ fusion gene in the pFN8x-n vector was activated in response to amino acid starvation in the wild type and decreased dramatically in the *gcn4* mutant yeast cells due to the disruption of the *GCN4* pathway. Transcription of the His4-LacZ fusion gene was further decreased in the amino acid-starved *gcn4* mutant yeast cells (Table 5). Transcription of the UAS-less His4-LacZ fusion gene on pST1 is not affected by the *gcn4* mutation as expected. A *p*-value that is less than 0.05 ($p<0.05$) indicates that there are statistically significant differences in the expression levels of Ty2-555-LacZ gene fusions in the untreated and 3-AT treated yeast cells. These results clearly indicated that amino acid starvation acts on Ty2 transcription, but is independent of the *GCN4* pathway.

GATA Factors Activity is Essential for Ty2 Transcription

TOR1 kinase is the master regulator of autophagy in yeast. It also controls the activities of a group of transcription factors

Table 5. Amino acid starvation represses the Ty2-917 transcription independent of *GCN4* pathway.

Gene fusions	Growth Conditions and β-Galactosidase Activities *(± SD)			
	F113 (*GCN4*$^+$)		F212 (Δ*gcn4*)	
	Normal growth	Amino acid starvation (+3-AT)	Normal growth	Amino acid starvation (+3-AT)
pST1**	1.8± 0.5	1.9± 0.7	1.8± 1	1.8± 0.6
p-ENC-LacZ**	309± 25	49± 7	251± 23	41± 2
Ty2-555-LacZ**	1282± 59	162± 12	220± 23	111± 16
HIS4-LacZ**	812± 22	2388± 118	164± 14	80± 9

(± SD): Standard deviations.
*Numbers indicate β-Galactosidase Units which are expressed in nano moles of ONPG cleaved per minute per mg of protein.
**Except pST1 expression levels, transcription levels were found significantly different ($p<0.05$).

known as GATA factors (30). TOR1 kinase phosphorylates Gln3 and keeps it in the cytoplasm as Gln3-Ure2 complex in nutrient-replete conditions. Under nutrient starvation conditions, TOR kinase is inactivated and Gln3 is dephosphorylated. After that Gln3 is transferred to the nucleus and regulates nitrogen-regulated genes (30). GATA factors bind to the GATAA related sequences on the promoter regions of targeted genes. Gln3 and Gat1 are the activator factors. Dal80 and Gzf3 (Deh1) act as a transcriptional repressor on targeted genes depending on the nitrogen sources (30, 47).

In order to analyze whether the transcriptional activators Gln3 and Gat1 have a function in Ty2 transcription, we have analyzed the transcription of Ty2-754-LacZ in the wild type and mutant yeast strain that do not contain Gln3 and Gat1 factors. Transcription of Ty2-754-LacZ gene fusion in the wild type yeast grown in a medium containing preferred nitrogen sources (0.2% glutamine) yielded 188 units of activity. When the yeast transformants are grown in a proline medium that results in the activation of Gln3/Gat1, it results in the high level of activation in Ty2-754 gene expression. But, the expression level of Ty2-754-LacZ in the double mutant strain that does not contain the Gln3/Gat1 factor resulted in only 15 units of activity (Table 6). A significant level of decrease (from 309 units to 15 units) in the Ty2 transcription in the Δgln3/Δgat1 mutant strain clearly indicates that Ty2 transcription is controlled by GATA factors. A *p*-value that is less than 0.05 ($p<0.05$) indicates that there are statistically significant differences in the expression levels of Ty2-754-LacZ gene fusions in the glutamine and proline treated yeast cells.

Ty2 and *GCR1* Gene Promoter Regions have Multiple Putative Binding Sites for GATA Factors and Gcr1

It was previously shown that the *GCR1* gene's transcription is autoregulated by itself. Gcr1, as a transcriptional activator, controls the regulation of 75% of *S. cerevisiae* genes (19). Transcription of Ty2 is also regulated by a Gcr1-dependent manner. Gcr1 binding sites (5'-CTTCC-3') on the promoter regions of Ty2 and *GCR1* gene were analyzed in detail in previous studies (17, 48).

After seeing the effects of the Δ*gln3*/Δ*gat1* mutations on the transcription of Ty2, we have decided to analyze potential binding sites for the GATA factors on the Ty2 promoter regions. To analyze if there is any putative Gcr1 and GATA factor binding sites on the Ty2 and the *GCR1* gene promoter regions, in-silico analyses were carried out using search tools and information provided by SGD and YEASTRACT databases. Analyses of the Ty2 promoter regions for the GATA factor binding sites revealed that it contains at least 6 putative binding sites (GATAAC) (Table 7). Interestingly, three of the GATA factor binding sites locate on the Crick strand (reverse direction to transcription) of Ty2 promoter regions, and two of the perfect consensus binding sites (GATAAT) for GATA factors locate within the negative regulatory region of Ty2 (Table 7). Additional binding sites for Gcr1 (5'-CTTCC-3') were also identified on the Ty2 promoter regions, in addition to previously determined Gcr1 binding sites (17). This result suggests that GATA factors (Gln3, Gat1, Deh80, and Gzf3) may directly bind to the Ty2 promoter.

Transcription of the *GCR1* gene is highly dependent on the growth rate and growth conditions (19, 49). *GCR1* mRNA completely diminished at a post-diauxic stage of yeast growth (19). Hence, there is a possibility that TORC1 may regulate *GCR1* transcription, and transcription activator Gln3 (or other GATA factors) may involve in the regulation of *GCR1* gene expression in a growth rate, and TORC1-dependent manner. Therefore, we have analyzed the promoter region of the *GCR1* gene for the putative binding sites for GATA factors. *In-silico* analysis using YEASTRACT tools indicated that *GCR1* gene promoter regions have at least 5 putative binding sites for GATA factors (Table 7). These results suggest that GATA factors are involved in the *GCR1* gene regulation.

DISCUSSION

Gene expression in yeast Ty elements is controlled at the transcriptional and translational levels. Results presented in this study showed that transcription of the yeast retrotransposon Ty2-917 is repressed up to eightfold in amino acid starved yeast cells. Moreover, caffeine treatment of yeast cells also leads to three to fourfold repression of Ty2 transcription. However, our results indicated that caffeine treatment represses Ty2 transcription, independent from TORC1 and Snf1 pathways. Caffeine has multiple effects on eukaryotic cells. Although it is a specific inhibitor of TOR1 kinase, it also triggers ERAD mediated apoptosis (31). It also has a dramatic effect on DNA repair, cell wall integrity, and telomerase activity (31). Therefore, we think that the repression of Ty2 transcription resulting from caffeine

Table 6. GATA factors are essential for Ty2 transcription.

Nitrogen source	β-Galactosidase Activities *(± SD)	
	Wild type (YST182)	Δgln3/gat1 mutant (YST184)
0.2 % Glutamin**	188±10	15±3
0.2 % Proline**	309±6	15±2

(± SD): Standard deviations.
*Numbers indicate β-Galactosidase Units which are expressed in nano moles of ONPG cleaved per minute per mg of protein.
**Transcription levels were found significantly different ($p<0.05$).

Table 7. *In-silico* analysis of putative binding sites of Gcr1 and GATA factors on the Ty2 and *GCR1* gene promoters.

GATA factors' putative binding sites on the Ty2 promoter region*		***GATA factors' putative binding sites on the GCR1 promoter regions****	
TF consensus binding sites**	**Localization***	**TF consensus binding sites****	**Localization***
GATAAT	56-60 (R)	GATTAG	59-64 (F)
GATAAT	136-142 (F)	GATAAT	163-167 (R)
GATAAT	178-183 (F)	GATAAT	507-512 (F)
GATTAG	425-430 (F)	GATAAG	610-615 (R)
GATAAT	632-637 (R)	GATAAA	764-769 (R)
GATAAT	654-658 (R)		
Gcr1 binding sites on the Ty2 promoter region **		***Gcr1 binding sites on the GCR1 promoter regions *****	
CTTCC	115-119 (R)	CTTCC	112-116 (F)
ATTCC	293-297 (R)	CTTCC	472-476 (F)
CTTCC	363-367 (R)	CTTCC	751-755 (F)
CTTCC	401-405 (F)	CTTCC	809-813 (F)
CTTCC	707-711 (F)	CTTCC	893-897 (F)

*Numbers for the *GCR1* promoter region indicate the position of the first nucleotide of the consensus binding sequence of a transcription factor with respect to the first nucleotide of the promoter region of GCR1 gene. Numbers for the binding sites on Ty2 indicate the position of the consensus binding sequences of relevant transcription factors with respect to the first nucleotide of Ty2-917. (R) indicates the localization of given binding sites at reverse direction (Crick strand, template strand), and (F) indicates the forward localization of relevant transcription factor consensus binding sites on the given promoters.
**Consensus binding sequences of GATA factors and Gcr1 are taken from YEASTRACT database (www.yeastract.com).
***Gcr1 binding sites on the Ty2 and *GCR1* promoter regions were experimentally proven previously (17,48).

treatment is the result of the combinatorial effects of caffeine on the various cellular components. We have already shown that activation of apoptosis by acetic acid treatment represses Ty1 and Ty2 transcription (21).

TOR1 kinase inhibits the autophagy process by directly acting on Atg13 factors. Nitrogen limitation and amino acid starvation inhibit TOR1 kinase activity. Therefore, it seems that nitrogen limitation and amino acid starvation are the better way of autophagy activation. Amino acid starvation leads to an eightfold decrease in Ty2 transcription. Amino acid starvation activates the expression of transcription activator Gcn4. Gcn4 is the master regulator of the general amino acid control (GAAC) pathway (29). However, our results clearly show that amino acid starvation has a negative effect on Ty2 transcription, independent of Gcn4. It is known that prolonged amino acid starvation causes a significant decrease in growth rate, and leads to cell cycle arrest in the G1 stage (50). Previously we have shown that transcription of Ty2 is also regulated in a growth rate-dependent manner. Its transcription decreases by more than 50% in the stationary stage (51). It was also shown that Gcr1 itself controls cell growth by acting on nutrient-regulated gene expression on a global level (49). Gcr1 transcription is autoregulated by itself and its transcription completely stops once the glucose is consumed in the growth medium at the late logarithmic/diauxic stage (19). Hence it is also possible that prolonged incubation of the yeast cells during amino acid starvation, which results in cell cycle arrest, and consumption of glucose in the growth medium leads to inhibition of *GCR1* expression, and this results in the downregulation of Ty2 transcription in the yeast cells.

Gcr1 is a phosphoprotein and recent evidence indicated that Gcr1 isoforms are phosphorylated and pyrophosphorylated depending on the growth conditions (19, 49, 52). It was shown that once Gcr1 is pyrophosphorylated by inositol hexakisphosphate kinase (KCSI), its transcription decreases at a significant level (52). TOR1 kinase and inositol hexakisphosphates synergistically control nutrient-sensing and growth control. Moreover, new evidence indicates that increased levels of 5-diphosphoinositol pentakisphosphate upon stress conditions result in the increased nuclear localization of the transcriptional activators Msn2 and Gln3 (53). New reports indicate that inositol hexakisphosphates also promote autophagy in tissue culture cells (54). Hence, repression of Ty2 transcription in amino acid-starved yeast cells may result from the combinatorial effects of the autophagy signaling and nutrient-dependent down regulation of Gcr1 activity.

Nitrogen limitation, or use of poor nitrogen sources such as urea, proline, or allantoin, also inhibit TOR1 kinase activity (30, 47). TORC1 phosphorylates Gln3 in nutrient-replete conditions.

Phosphorylated Gln3 forms a heterodimer with Ure2 and remains in the cytoplasm. When TOR1 kinase activity is inhibited, Gln3 dephosphorylates and enters nuclei to activate targeted genes (30, 47). But recent evidence indicated that Gln3 also functions independent of TOR kinase activity, independent from Ure2 interaction. Therefore, there is always Gln3-dependent activation of targeted yeast genes, albeit at low levels. Growth of yeast cells in proline medium as a sole nitrogen source leads to approximately threefold activation of Ty2 transcription. Lack of same level activity in Δ*gln3*/Δ*gat1* mutants reveals that even under standard growth conditions (in glutamine medium), GATA factors Gln3/Gat1 are the significant parts of Ty2 transcription activation components. This result also emphasizes that in addition to transcription factor Gcr1, Ty2 transcription is dependent on Gln3/Gat1.

Genetic evidence that we have provided using Δgln3/Δgat mutant strains indicates that at least two of the GATA factors, Gln3 and Gat1, are involved in the activation of Ty2 transcription. Dal80 is another member of the GATA group transcription factors. Contrary to Gln3/Gat1, Dal80 is a repressor protein. Recently published results indicate that Dal80 represses a large group of genes in yeast genes. It turned out that two of these genes are *TEC1* and *SGC1* (TYE7) (55). This new evidence suggests that Dal80 could also repress Ty2 transcription indirectly by interfering with transcription of the *TEC1* and *SGC1* genes. GATA factors directly bind to GATAA related sequences on the targeted promoters. Gln3 and Gat1 are activator factors while Dal80 and Gzf3 (Deh1) are the repressor group of GATA family transcription factors. It was proposed that the GATA factor competes for their binding sites on the targeted promoters (56).

In-silico analysis of the Ty2 regulatory region for the transcription factor binding sites using the YEASTRACT database confirms that there are multiple potential binding sites for GATA factors in the regulatory region of Ty2. It is also possible that Dal80 or Gzf3 is one of the regulatory factors involving Ty2 repression by interacting with GATAA sequences in the negative regulatory region of Ty2. Our *in-silico* analyses results indicated that transcription of the *GCR1* gene might be regulated by GATA factors. Knowing that the *GCR1* gene transcription is regulated growth rate and growth stage dependent-manner, it seems reasonable to suggest that TOR1 kinase affects the expression of Gcr1-dependent gene regulation by modulating the *GCR1* gene transcription via GATA factors. Nonetheless, functional analysis of GATA factors' involvement in the regulation of *GCR1* transcription is necessary to experimentally validate these hypotheses. Deletion of GATA factor binding sites on the *GCR1* promoter, *in-vitro* binding assays (such as EMSA and/or DNaseI Footprint) with the DNA fragments from the *GCR1* promoter region and purified GATA factors would provide conclusive in-vivo and intro evidence as to whether GATA factors control the transcription of *GCR1* gene and Ty2 retrotransposon (17, 37, 56).

Based on our experimental and *in-silico* analyses results, we propose the following model on the regulation of Ty2 transcription in response to the autophagy signaling. Under nutrient-replete conditions at the logarithmic stage of the cell growth, in which TORC1 complex is active and autophagy is repressed, Ty2 transcription is activated mainly by Gcr1, Sgc1, and Tec1. Gln3, Gat1 which are expressed at a basal level, might also contribute to Ty2 transcription in nutrient-replete growth conditions (Figure 2a). In amino acid starved yeast cells, the growth rate slows and

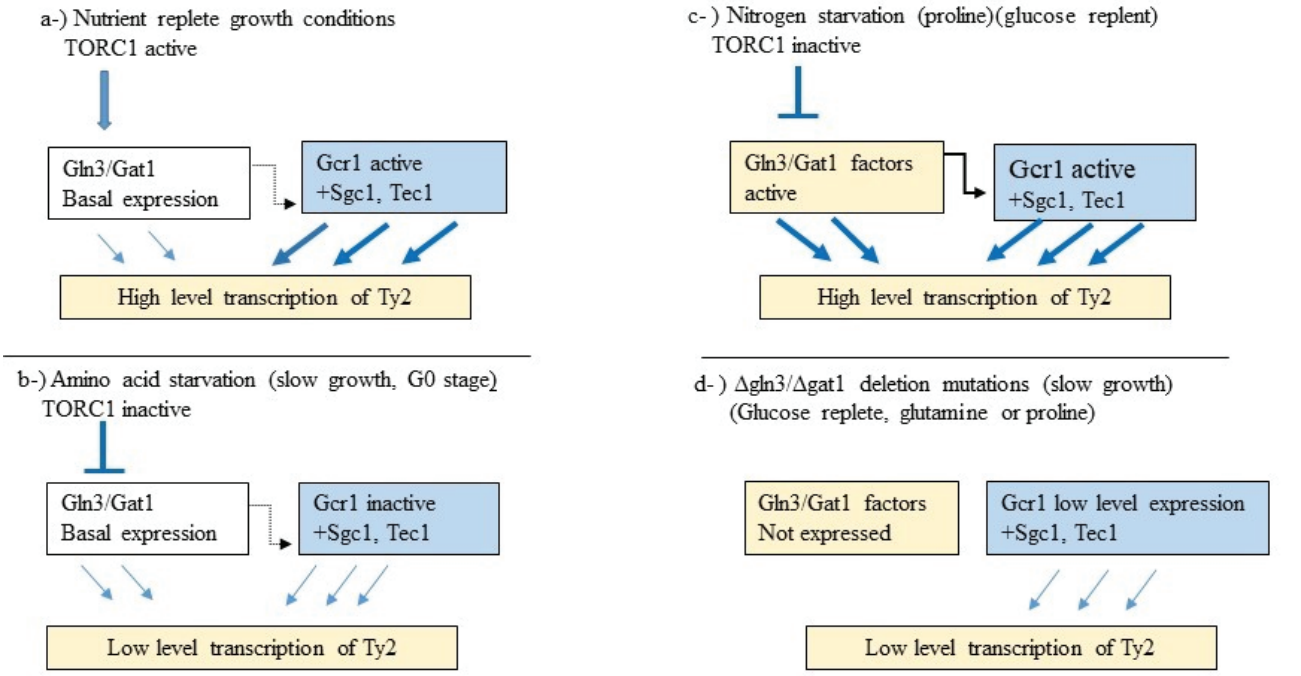

Figure 2. Proposed model on the regulation of Ty2 transcription in response to various growth conditions in yeast.

yeast cells enter G0 stage as the result of prolonged starvation. This situation results in the complete inactivation of the *GCR1* expression. TOR1 kinase is inactivated and the autophagy process initiates due to amino acid starvation. This metabolic situation leads to a significant level decrease in Ty2 transcription. On the other hand, caffeine treatment also inactivates TORC1. But, in caffeine-treated yeast cultures, the nitrogen source and glucose are not consumed completely. Therefore, we think that the autophagy process does not operate at full scale in the caffeine-treated, nutrient-replete yeast cells during the 5-hour incubation period. Under these circumstances, Ty2 transcription occurs at moderate to low levels using relevant transcription factors (Figure 2b). If the cells are grown in proline medium as sole nitrogen sources in glucose replete medium, TORC1 is inactivated. This results in the full-scale activation of GATA factors Gln3/Gat1. In turn, these GATA factors activate Ty2 transcription by directly targeting the Ty2 promoter, and also by further activating *GCR1* expression (Figure 2c). In Δ*gln3*/Δ*gat1* double mutant yeast, Ty2 transcription decreases at a significant level. This decrease might be the result of multiple events, such as lack of functional active Gln3/Gat1 factors and low-level expression of *GCR1* or slow growth phenotypes of the mutant strain (49, 57) (Figure 2d).

Overall, it appears that Ty2 retrotransposon acquired multiple regulatory factors to adjust its expression levels in response to various metabolic changes for its existence in its host cells. The involvement of the autophagy process in viral infections amplification and/or eradication underscores the different applications of autophagy in clinical fields (34, 35). It seems that regulation of the copy number of Ty retrotransposons by degradation of Ty-VLP within autophagosomes and repression of Ty2 transcription in response to autophagy signals makes Ty retrotransposons a potentially good model system to analyze the effects of the autophagy process on the viral propagation in eukaryotic cells.

CONCLUSION

Previously, it was shown that activation of autophagy condition results in the elimination of cytoplasmic Ty2-VLP by autophagosomes. Results of this study indicated that the transcription of retrotransposon Ty2 is also repressed in response to autophagy signaling. It seems that autophagy signaling represses Ty2 transcription by multiple mechanisms including direct binding of repressors and inhibition of activator functions such as Gcr1, Gln3, and Gat1 that are involved in Ty2 transcription. In addition to TY-VLP elimination by autophagy, nutrient limitations could also restrict Ty2 retrotransposon's transcription to limit Ty mobility in the yeast genome under stressful, nutrient-restricted growth conditions.

Informed Consent: Written consent was obtained from the participants.

Peer Review: Externally peer-reviewed.

Author Contributions: Conception/Design of Study- S.T., C.C.; Data Acquisition- C.C., S.T., T.K.; Data Analysis/Interpretation- S.T., C.C.; Drafting Manuscript- S.T., C.C.; Critical Revision of Manuscript- S.T.; Final Approval and Accountability- C.C., S.T., T.K.

Conflict of Interest: Authors declared no conflict of interest.

Financial Disclosure: Authors declared no financial support.

REFERENCES

1. Kim JM, Vanguri S, Boeke JD, Gabriel A, Voytas DF. Transposable Elements and Genome Organization: A Comprehensive survey of retrotransposons revealed by the complete *Saccharomyces cerevisiae* genome sequence. Genome Res 1998; 8: 464-78.
2. Boeke J, Garfinkel DJ, Styles CA, Fink G. Ty elements transpose through an RNA intermediate. Cell 1985; 40: 491-500.
3. Curcio MJ, Lutz S, Lesage P. The Ty1 LTR-retrotransposon of budding yeast, *Saccharomyces cerevisiae*. Microbiol Spectr 2015; 3: 1-35.
4. Capy P. Classification and nomenclature of retrotransposable elements. Cytogenet Genome Res 2005; 110: 457-61.
5. Roeder GS, Farabaugh PJ, Chalef DT, Fink GR. The origin of gene instability in yeast. Science 1980; 209: 1375-80.
6. Garfinkel DJ, Tucker JM, Saha A, Nishida Y, Pachulska-Wieczorek K, Błaszczyk L, et al. A self-encoded capsid derivative restricts Ty1 retrotransposition in *Saccharomyces*. Curr Genet 2016; 62: 321-9.
7. Saha A, Mitchell JA, Nishida Y, Hildreth JE, Ariberre JA, Gilbert WV, et al. A trans-dominant form of Gag restricts Ty1 retrotransposition and mediates copy number control. J Virol 2015; 89: 3922-38.
8. Curcio MJ, Hedge AM, Boeke JD, Garfinkel DJ. 1990. Ty RNA levels determine the spectrum of retrotransposition events that activate gene expression in *Saccharomyces cerevisiae*. Mol Gen Genet 1990; 220: 213-21.
9. Belcourt MF, Farabaugh PJ. Ribosomal frameshifting in the yeast retrotransposon Ty: tRNAs induce slippage on a 7 nucleotide minimal site. Cell 1990; 62: 339-52.
10. Farabaugh PJ. Programmed translational frameshifting. Microbiol Rev 1996; 60: 103-134.
11. Farabaugh PJ, XB. Liao, Belcourt M, Zhao H, Kapakos J, Clare J. Enhancer and silencer-like sites within the transcribed portion of a Ty2 transposable element of *S. cerevisiae*. Mol Cell Biol 1989; 9: 4824-34.
12. Farabaugh PJ, Vimaladithan A, Türkel S, Johnson R, Zhao H. Three downstream sites repress transcription of a Ty2 retrotransposon in *Saccharomyces cerevisiae*. Mol Cell Biol 1993; 13: 2081-90.
13. Türkel S, Farabaugh PJ. Interspersion of an unusual GCN4 activation site with a complex transcriptional repression site in Ty elements of *Saccharomyces cerevisiae*. Mol Cell Biol 1993; 13: 2091-103.
14. Laloux I, Dubois E ,Dewerchin M, Jacobs E. TEC1, a gene involved in the activation of Tyl and Tyl-mediated gene expression in *Saccharomyces cerevisiae*: Cloning and molecular analysis. Mol Cell Biol 1990; 10: 3541-50.
15. Löhning C, Ciriacy M. The TYE7 gene of *Saccharomyces cerevisiae* encodes a putative bHLH-LZ transcription factor required for Ty1-mediated gene expression. Yeast 1994; 10: 1329-39.
16. Türkel S, Yenice B. Analysis of the effects of chromatin modifying complexes on the transcription of retrotransposon Ty2-917 in *Saccharomyces cerevisiae*. Turk J Biol 2006; 30: 101-6.
17. Türkel S, Liao XB, Farabaugh PJ. Gcr1-dependent transcriptional activation of yeast retrotransposon Ty2-917. Yeast 1997; 13: 917-30.

18. Cha S, Hong CP, Kang HA, Hahn J-S. Differential activation mechanisms of two isoforms of Gcr1 transcription factor generated from spliced and un-spliced transcripts in *Saccharomyces cerevisiae*. Nucleic Acids Res 2021; 49: 745-59.
19. Hossain MA, Claggett JM, Edwards S, Shi A, Pennebaker S, Cheng M, et al. Post-transcriptional regulation of Gcr1 expression and activity are crucial for metabolic adjustment in response to glucose availability. Mol Cell 2016; 62: 346-58.
20. Suzuki K, Morimoto M, Kondo C, Ohsumi Y. Selective autophagy regulates insertional mutagenesis by the Ty1 retrotransposon in *Saccharomyces cerevisiae*. Developmental Cell 2011; 21: 358-65.
21. Çolakoğlu C, Türkel S. Apoptosis signaling pathway regulates the gene expression in the yeast retrotransposons Ty1 and Ty2. Eur J Biology 2020; 79: 36-42.
22. Ohsumi Y. Historical landmarks of autophagy research. Cell Research 2014; 24: 9-23.
23. Suzuki K, Ohsumi Y. Molecular machinery of autophagosome formation in yeast, *Saccharomyces cerevisiae*. 2007; FEBS Lett 581: 2156-61.
24. Yin Z, Pascual C, Klionsky DJ. Autophagy: machinery and regulation. Microb Cell 2016; 3: 588-96.
25. Delorme-Axford E, Daniel J. Klionsky DJ. Transcriptional and post-transcriptional regulation of autophagy in the yeast *Saccharomyces cerevisiae*. J Biol Chem 2018; 293: 5396-403.
26. Wen X, Klionsky DJ. An overview of macroautophagy in yeast. J Mol Biol 2016; 428: 1681-99.
27. Kamada Y, Funakoshi T, Shintani T, Nagano K, Ohsumi M, Ohsumi Y. Tor-mediated induction of autophagy via an Apg1 protein kinase complex. J Cell Biol 2000; 150: 1507-13.
28. Yoshiaki Kamada Y, Yoshino K-İ, Kondo C, Kawamata T, Oshiro N, Yonezawa K, et al. Tor directly controls the Atg1 kinase complex to regulate autophagy. Mol Cell Biol 2010; 30: 1049-58.
29. Hinnebusch, AG, Natarajan K. 2002. Gcn4p, a master regulator of gene expression, is controlled at multiple levels by diverse signals of starvation and stress. Eukaryotic Cell 2002; 1: 22-32.
30. Cooper TG. Transmitting the signal of excess nitrogen in *Saccharomyces cerevisiae* from the Tor proteins to the GATA factors: connecting the dots. FEMS Microbiol Rev 2002; 26: 223-38.
31. Ruta LL, Farcasanu IC. *Saccharomyces cerevisiae* and caffeine implications on the eukaryotic cell. Nutrients 2020; 12: 2440; doi:10.3390/nu12082440.
32. Galluzzi L, Baehrecke EH, Ballabio A, Boya P, Bravo-San Pedro JM, Cecconi F, et al. Molecular definitions of autophagy and related processes. EMBO J 2017; 13: 1811-36.
33. Scott SV, Guan J, Hutchins MU, Kim J, Klionsky DJ. Cvt19 is a receptor for the Cytoplasm-to-Vacuole targeting pathway. Mol Cell 2001; 7: 1131-41.
34. Choi Y, Bowman JW, Jung JU. Autophagy during viral infection— a double-edged sword. Nat Rev Microbiol 2018; 16: 341-54.
35. Campbell GR, Spector SA. Induction of autophagy to achieve a human immunodeficiency virus type 1 cure. Cells 2021; 10: 1798. doi.org/10.3390/cells10071798.
36. Brachmann CB, Davies A, Cost GJ, Caputo E, Li J, Hieter P, Boeke JD. Designer deletion strains derived from *Saccharomyces cerevisiae* S288C: a useful set of strains and plasmids for PCR-mediated gene disruption and other applications. Yeast 1998; 14: 115-32.
37. Scherens B, Feller A, Vierendeels F, Messenguy F, Dubois E. Identification of direct and indirect targets of the Gln3 and Gat1 activators by transcriptional profiling in response to nitrogen availability in the short and long term. FEMS Yeast Research 2006; 6: 777-91.
38. Nagawa F, Fink GR. 1985. The relationship between the "TATA" sequence and transcription initiation sites at the *HIS4* gene of *Saccharomyces cerevisiae*. Proc Natl Acad Sci (USA) 1985; 82: 8557-61.
39. Arndt KT, Styles C, Fink GR. Multiple global regulators control *HIS4* transcription in Yeast. Science 1987; 237: 874-80.
40. Christianson TW, Sikorski RS, Dante M, Shero JH, Hieter P. 1992. Multifunctional yeast high-copy-number shuttle vectors. Gene 1992; 110: 119-22.
41. Gietz R., Schiestl R. High-efficiency yeast transformation using the LiAc/SS carrier DNA/PEG method. Nat Protoc 2007; 2: 31-4.
42. Kuranda K, Leberre V, Sokol S, Palamarczyk G, Francois J. Investigating the caffeine effects in the yeast *Saccharomyces cerevisiae* brings new insights into the connection between TOR, PKC and Ras/cAMP signalling pathways. Molecular Microbiol 2006; 61: 1147-66.
43. Guarente L, Patashe M. Fusion of *Escherichia coli* lacZ to the cytochrome c gene of *Saccharomyces cerevisiae*. Proc Natl Acad Sci (USA) 1981; 78: 2199-203.
44. Lowry OH, Rosebrough NJ, Farr AL, Randall RJ. Protein measurement with the Folin phenol reagent. J Biol Chem 1951; 193: 265-75.
45. Schmelzle T, Hall MN. TOR, a central controller of cell growth. Cell 2000; 103: 253-262.
46. Coccetti P, Nicastro R, Tripodi F. Conventional and emerging roles of the energy sensor Snf1/AMPK in *Saccharomyces cerevisiae*. Microb Cell 2018; 5: 482-94.
47. Georis I, A. Feller A, Tate JJ, Cooper TG, Dubois E. Nitrogen catabolite repression-sensitive transcription as a readout of Tor pathway regulation: the genetic background, reporter gene and GATA factor assayed determine the outcomes. Genetics 2009; 181: 861-74.
48. Sasaki H, Kishimoto T, Mizuno T, Shinzato T, Uemura H. Expression of GCR1, the transcriptional activator of glycolytic enzyme genes in the yeast Saccharomyces cerevisiae, is positively autoregulated by Gcr1p. Yeast 2005; 22: 305-19.
49. Barbara KE, Haley TM, Willis KA, Santangelo GM. The transcription factor Gcr1 stimulates cell growth by participating in nutrient-responsive gene expression on a global level. Mol Genet Genomics 2007; 277: 171-88.
50. Gonzalez A, Hall MN. Nutrient sensing and TOR signaling in yeast and mammals. EMBO J 2017; 36: 397-408.
51. Türkel S, Bayram Ö, Arık E. Glucose signaling pathway and growth conditions regulate gene expression in retrotransposon Ty2. Z. Naturforsch 2009; 64 c: 526-32.
52. Szijgyarto Z, Garedew A, Azevedo C, Saiardi A. Influence of inositol pyrophosphates on cellular energy dynamics. Science 2011; 334: 802-5.
53. Morrissette VA, Rolfes RJ. The intersection between stress responses and inositol pyrophosphates in *Saccharomyces cerevisiae*. Curr Genet 2020; 66: 901-10.
54. Nagata E, Saiardi A, Tsukamoto H, Satoh T, Itoh Y, Itoh J, et al. Inositol hexakisphosphate kinases promote autophagy. Int J Biochem Cell Biol 2010; 42: 2065-71.
55. Ronsmans A, Wery M, Szachnowski U, Gautier C, Descrimes M, Dubois E, et al. Transcription-dependent spreading of the Dal80 yeast GATA factor across the body of highly expressed genes. PLoS Genet 2019; 15: e1007999. doi.org/10.1371/journal.pgen.1007999.
56. Coffman JA, Rai R, Loprete DM, Cunningham T, Svetlov V, Cooper TG. Cross regulation of four GATA factors that control nitrogen catabolic gene expression in *Saccharomyces cerevi*siae. J Bacteriol 1997; 179: 3416-29.
57. Lopez MC, Baker HV. Understanding the growth phenotype of the yeast *gcr1* mutant in terms of global genomic expression patterns. J Bacteriol 2000; 182: 4970-8.

ISTANBUL UNIVERSITY PRESS

RESEARCH ARTICLE

Eur J Biol 2021; 80(2): 119-128

Therapeutic Effects of *Momordica charantia* L. Ethanolic Extract on Acetic Acid-Induced Ulcerative Colitis in Rats

Dilek Ozbeyli[1], Ali Sen[2], Asli Aykac[3], Kerem Terali[4], Ozlem Tugce Cilingir-Kaya[5], Ismail Senkardes[6], Goksel Sener[7]

[1]Marmara University, Vocational School of Health Services, Department of Pathology, Laboratory Techniques, Istanbul, Turkey
[2]Marmara University, Faculty of Pharmacy, Department of Pharmacognosy, Istanbul, Turkey
[3]Near East University, Department of Biophysics, Northern Cyprus KKTC
[4]Girne American University, Faculty of Medicine, Department of Medical Biochemistry, Northern Cyprus KKTC
[5]Marmara University, School of Medicine, Department of Histology and Embryology, Istanbul, Turkey
[6]Marmara University, Faculty of Pharmacy, Department of Pharmaceutical Botany, Istanbul, Turkey
[7]Fenerbahce University, Vocational School of Health Services, Istanbul, Turkey

ORCID IDs of the authors: D.O. 0000-0002-4141-6913; A.S. 0000-0002-2144-5741; A.A. 0000-0002-4885-5070; K.T. 0000-0002-9964-6383; O.T.C.K. 0000-0002-2591-9174; I.S. 0000-0002-2656-0319; G.S. 0000-0001-7444-6193

Please cite this article as: Ozbeyli D, Sen A, Aykac A, Terali K, Cilingir-Kaya OT, Senkardes I, Sener G. Therapeutic Effects of *Momordica charantia* L. Ethanolic Extract on Acetic Acid-Induced Ulcerative Colitis in Rats. Eur J Biol 2021; 80(2): 119-128. DOI: 10.26650/EurJBiol.2021.1016222

ABSTRACT

Objective: This study aims to investigate the effect of *Momordica charantia* L. (MoC) ethanolic extract on ulcerative colitis (UC) and was explored *in vitro* and *in vivo*.

Materials and Methods: The rats were divided into control (C), saline-treated colitis (AA), MoC extract-treated colitis (AA+MoC), and sulfasalazine (SS)-treated colitis (AA+SS) groups. Colitis was induced by acetic acid. MoC extract, SS or saline were given to the related groups for 3 days. Interleukine-1β, malondialdehyde, glutathione levels, myeloperoxidase activity, bax/bcl-2 ratio, caspase-9 and caspase-3 levels were measured in colon and macroscopic and histopathologic examinations were done. Total phenolic/flavonoid content and biological activity of MoC were evaluated by *in vitro* analysis.

Results: Compared to the control group, with acetic acid application interleukin-1β levels, myeloperoxidase activity, malondialdehyde levels, bax/bcl-2 ratio, caspase-9 and caspase-3 levels were significantly upregulated, while glutathione levels were significantly decreased in the AA group. In contrast, MoC and SS treatments reduced interleukin-1β, malondialdehyde levels, myeloperoxidase activity, bax/bcl-2 ratio, and caspase-9 and caspase-3 levels. Glutathione levels increased upon MoC or SS treatment. Increased macroscopic and microscopic scoring with AA improved with MoC or SS treatment, but the MoC or SS treated groups had higher score values than the control. Also, *in vitro* results showed that MoC exhibited 2,2-diphenyl-1-picrylhydrazyl and 2,2'-azino-bis-3-ethylbenzothiazoline-6-sulfonic acid radical scavenging activity as well as significant anti-lipoxygenase activity. In addition, MoC extract showed a potent anti-inflammatory activity compared to standard indomethacin.

Conclusion: Our biochemical, *in vitro* and histopathologic analysis indicate that MoC is likely to prove beneficial in UC therapy.

Keywords: *Momordica charantia* L., ulcerative colitis, apoptosis, oxidative stress, radical scavenging activity, anti-lipoxygenase activity

INTRODUCTION

Ulcerative colitis (UC) affects millions of people worldwide and is characterized by recurrent mucosal inflammation and ulceration of the large intestine (1). Although the exact aetiology of UC is not well documented, it involves a dysregulated immune system as well as environmental effects. Current UC treatments are based on the suppression of inflammation (2). The

Corresponding Author: Dilek Ozbeyli E-mail: dilekozbeyli@marmara.edu.tr
Submitted: 30.10.2021 • **Revision Requested:** 09.11.2021 • **Last Revision Received:** 15.11.2021 • **Accepted:** 16.11.2021 • **Published Online:** 06.12.2021

acetic acid (AA)-induced UC model represents a good model for clinical, biochemical, and histological examinations in colonic inflammation (3). AA causes major epithelial damage and is characterized by increased leukocyte infiltration, increased inflammatory mediators, vascular dilatation, oedema, and large, massive ulceration of the non-transmural large intestine (4). Several cytokines are involved in the pathogenesis of UC, including tumour necrosis factor (TNF)-α and interleukin1β (IL-1β) (5). Oxidative stress plays a significant role in the aetiology of UC in such a way that reactive oxygen species (ROS) formation during inflammation causes apoptosis-mediated cellular death and loss of epithelial cells. However, an increase in the apoptotic cells leads to a deterioration of the epithelial defence in the colon and accelerates mucosal inflammation (6).

Current therapies mainly aim at decreasing inflammation using anti-inflammatory drugs as well as at reducing oxidative stress (3). Aminosalicylates, corticosteroids, and immunosuppressants that are used in the treatment of mild and moderate UC provide regression of disease symptoms. One of them, sulfasalazine (SS), which is utilized as standard therapy in the disease, corresponds to an aminosalicylate derivative. The 5-aminosalicylic acid component of SS is liable for its therapeutic effect, and the majority of its side effects are linked to the sulphapyridine portion (5). However, treatments using these agents have drug-related side effects that can lead to some problems (7). On the other hand, natural plants have long been used to treat various diseases and to avoid the side effects of drugs. *Momordica charantia* L. (MoC), also known as bitter gourd, bitter apple, or bitter melon, is a green to yellow-coloured flowering plant and a member of the Cucurbitaceae family. MoC widely grows in Asia and the Mediterranean area, and the main phytochemical ingredients of MoC include essentially flavonoids, phenolic acids, cucurbitane-type triterpenoid saponins (momordicine, momordin, and momordicoside (8-10). Standard constituents of MoC are charantin (a mixture of 5. 25-stigmasteryl glucoside and β-sitosteryl glucoside) and momordicine, which are steroidal saponins (8-11). Momordicine and charantin are mainly responsible for the beneficial activities and bitterness of MoC (8-12). MoC has been reported to have more biological effects such as antioxidant, anti-apoptotic and anti-inflammatory (9, 12, 13). In addition, MoC fruit is used externally for the quick healing of abrasions and internally for the cure of peptic ulcers in Turkish folk medicine (14). MoC has been shown to alleviate dextran sulfate sodium (DSS)-induced colitis in mice by depressing inflammatory cytokines and increasing regulatory T cells (15). Additionally, MoC has been demonstrated to have significant anti-inflammatory effects on trinitrobenzene (TNBS)-induced colitis that mimics Crohn's disease by reducing myeloperoxidase (MPO) activity and cytokine levels in rats (10).

During colitis induction, administered MoC therapy can improve colonic damage ameliorated by decreased colonic oxidative stress and apoptosis. Therefore, the present study was designed to assess the potential antioxidant, anti-inflammatory and anti-apoptotic effects of MoC on AA-induced ulcerative rat models through *in vitro* and *in vivo* analysis.

MATERIALS AND METHODS

Chemicals

Acetic acid, dimethyl sulfoxide (DMSO), 2-(4-(2-hydroxyethyl) piperazin-1-yl) ethanesulfonic acid (HEPES), hexadecyltrimethylammonium bromide (HETAB), N-(2-Hydroxyethyl) piperazine-N'-(2-ethanesulfonic acid), trichloroacetic acid (TCA), thiobarbituric acid (TBA), 5,5'-dithiobis(2-nitrobenzoic acid) (DTNB), o-Dianisidine, $Na_2HPO_4.2H_2O$, K_2HPO_4, 2,2-diphenyl-1-picrylhydrazyl (DPPH), 2,2-azino-bis-3-ethylbenzothiazoline-6-sulfonic acid (ABTS), potassium persulfate, indomethacine, ascorbic acid, trolox, lipoxidase from Glycine max (soybean), Folin-Ciocalteu reagent, linoleic acid, formaldehyde, dithiothreitol (DTT), glycerol, Tris-HCl, Ethylenediaminetetraacetic acid (EDTA), and Triton X-100, $NaNO_2$, $AlCl_3{\cdot}6H_2O$, NaOH, methanol, and ethanol were supplied by Sigma (Sigma-Aldrich, St. Louis, MO, USA). All antibodies for immunoblotting were purchased from Santa Cruz Biotechnology Inc (Santa Cruz, CA, USA). Sodium pentobarbital was purchased from IE Ulagay (Istanbul, Turkey). All other chemicals were of the purest grade commercially available.

MoC Extract Preparation

MoC fruits were collected from the rural district of Gemlik in Bursa, Turkey in August 2019 and identified by Dr. İsmail Şenkardeş from the Department of Pharmaceutical Botany, Faculty of Pharmacy, Marmara University. The voucher specimens were deposited in the Herbarium Faculty of Pharmacy, Marmara University (Marmara No: 22446). Fresh fruit with seeds was blended and then were macerated by 95% ethanol (1000 mL) for 48 h. The extraction process was repeated until the solvent became colourless. The filtrate was evaporated and concentrated at 40°C. The obtained dried ethanol extract of MoC was stored at +4°C until further analysis.

In Vitro Antioxidant and Anti-inflammatory Activity of MoC

The DPPH radical scavenging capacity measurement of MoC extract was performed in line with a previously reported procedure by Zou et al. (16). In short, 10 µL of extract or standard ascorbic acid in DMSO at different concentrations were mixed with 190 µL of 0.1 mM DPPH solution in methanol in a 96-well plate. Mixtures were left to incubate for 30 min in the dark at room temperature. Then, the absorbance was taken at 517 nm. Tests were carried out in triplicate.

The radical scavenging activity percentage of extracts and compounds against DPPH radicals were calculated according to the following: DPPH radical-scavenging activity (%) = $[(A_0\text{-}A_1)/A_0] \times 100$, where A_0 is the absorbance of the control (containing all reagents except the test extracts/compounds) and A_1 is the absorbance of the extracts/compounds. The extract (or standard) concentration resulting in a 50% inhibition (IC_{50}) was calculated by regression equations (by plotting the extract/standard solution concentration versus percentage of inhibition). Lower IC50 values indicate higher inhibitory potential of the tested extract (16).

ABTS radical cation scavenging activity was tested according to Zou et al. (16). ABTS radical cations were produced by mixing

equal volumes of ABTS (7 mM in H_2O) and potassium persulfate (4.9 mM in H_2O) and allowing them to react for 12-16 h at room temperature in the dark. The ABTS radical solution was then diluted with 96% ethanol to obtain an absorbance of about 0.7 at 734 nm using a spectrophotometer. 10 µL of extract, or standard trolox, was added to 190 µL of ABTS radical solution in a 96-well microplate. The mixture was incubated at room temperature in the dark for 30 min. Then, absorbance readings were taken at 734 nm. Tests were carried out in triplicate.

The percent radical scavenging activity of extracts and compounds against ABTS radical were calculated according to the following: ABTS radical-scavenging activity (%) = $[(A_0-A_1)/A_0] \times 100$ where A_0 is the absorbance of the control (containing all reagents except the test extracts/compounds) and A_1 is the absorbance of the extracts/compounds. The extract (or standard) concentration resulting in a 50% inhibition (IC_{50}) was calculated by regression equations (by plotting the extract/standard solution concentration versus percentage of inhibition). Lower IC_{50} values indicate higher inhibitory potential of the tested extract (16).

The anti-lipoxygenase activity was evaluated as described by Phosrithong and Nuchtavorn (17) with slight modifications described by Yıldırım et al. (18). 10 µL of extract or standard indomethacin were added to 20 µL ethanol, 20 µL pure water, 25 µL of sodium borate buffer solution (0.1 M, pH 9) followed by an addition of 25 µL of type V soybean lipoxygenase solution in buffer (pH 9, 20.000 U/mL). The mixture was preincubated at 25 °C for 5 min. Then, 100 µL of 0.6 mM linoleic acid solution was added, mixed well and the change in absorbance at 234 nm was recorded for 6 min. Tests were carried out in triplicate. The inhibition percentage was calculated from the following equation: % inhibition= $[(A_{control}–A_{sample}) / A_{control}] \times 100$.

The extract (or standard) concentration resulting in a 50% inhibition (IC_{50}) was calculated by regression equations (by plotting the extract/standard solution concentration versus percentage of inhibition). Lower IC_{50} values indicate higher inhibitory potential of the tested extract (16).

Determination of the Total Phenolic and Flavonoid Contents

The total phenolic content of the extract was measured as described by Gao et al. (19) with slight modifications described by Yıldırım et al. (18) Ten µL of the extract in various concentrations was mixed with 20 µL of the Folin-Ciocalteu reagent, 200 µL of H_2O, and 100 µL of 15% Na_2CO_3, and the absorbance was measured at 765 nm after 2 h of incubation at room temperature. The total phenolic content was calculated on the basis of the calibration curve of standard gallic acid and expressed as mg gallic acid equivalent (GAE) per g dried extract.

Total flavonoid content was determined following a method by Zhang et al. (20) with slight modifications described by Yıldırım et al. (18). 25 µL extract in various concentrations was mixed with 125 µL of ultra-pure water and 7.5 µL of 5 % $NaNO_2$. After 6 min, 15 µL of 10% $AlCl_3 \cdot 6H_2O$ was added. After 5 min, 50 µL NaOH (1 M) was added and the solution completed with 250 µL of ultra-pure water. The absorbance was measured against the reagent blank at 510 nm. The total flavonoid content was calculated on the basis of the calibration curve of standard quercetin and expressed as mg quercetin equivalent (QE) per g dried extract.

Animals

A total of 24 female Sprague-Dawley rats (250-260 g; 4-5 months) were obtained from the Animal Centre (DEHAMER, Istanbul). The animals were housed in laboratory conditions and fed *ad libitum*. All protocols were carried out following the project submitted to the Marmara University Animal Care and Use Committee (Protocol number: 46.2020.mar). All animal experiments complied with the guidance of the Council of International Organization of Medical Sciences (WHO/UNESCO), NIH and PHS.

Animal Experimental Procedure

After 20 h of fasting, colitis was induced under anaesthesia, where an 8-cm soft cannula was inserted into the rectal hole and pushed forward. Subsequently, 5% (v/v) AA diluted in saline (pH 2.3) was administered in a volume of 1 mL (2). The control group was administered 1 mL saline intrarectally in lieu of AA. The rats were divided into two main groups: the control group and the AA-induced colitis group. The colitis group was further divided into three subgroups: the saline-treated (AA), the MoC extract-treated (AA+MoC), and SS-treated (AA+SS) groups, with each group consisting of 6 rats. Immediately after colitis induction and for the next 2 days, while saline was given to the control and AA groups, MoC extract (300 mg/kg) was given to the AA+MoC group and SS (100 mg/kg) was given to the AA+SS group. Thus, all treatments were given a total of 3 times. MoC extract and dissolved SS were administered to the rats using an oral gavage tube (p.o.) The dose of the MoC extract was selected based on a former study that demonstrated the protective effect of MoC on the Crohn's colitis model (10). However, SS, which is the standard drug for the treatment of ulcerative colitis, was used as a reference to evaluate the effectiveness of MoC (2). All treatments were given at around 11: 00 am. The rats were euthanized (Thiopenthal sodium, 50 mg/kg/i.p.) at the 72nd h of the colitis induction. The last 8 cm of the distal part of the colon was harvested. Colon tissues were taken for macroscopic and histological examinations, while the remaining parts were kept at -80°C until biochemical experiments were performed.

IL-1β, Malondialdehyde (MDA) and Glutathione (GSH) Levels and MPO Activity Measurement in Colonic Tissues

An enzyme-linked immunosorbent assay (ELISA) test was performed to determine IL-1β levels in the colonic samples following the manufacturer's instructions (EBIOSCIENCE, Thermo Fisher Scientific, MA, USA). MDA levels were defined for end products of membrane lipid oxidation by capturing the generation of thiobarbituric acid-sensitive substances as previously described by Buege and Aust (21) and the data were expressed as nmol MDA/g tissue. Cellular antioxidant GSH levels were determined using a modified Ellman procedure (22) and the data

were expressed as μmol GSH/g tissue. MPO activity assays were used in the evaluation of tissue neutrophil recruitment in line with Bradley et al. (23) and the data were expressed as U/g.

Immunoblotting

Frozen tissues were prepared in a 20 mM Tris-HCl buffer containing protease inhibitors. Following centrifugation, the pellets were incubated in the protease inhibitor solution (which includes DTT, glycerol, Tris-HCl, EDTA, and Triton X-100) for 1h. After determining the amount of protein in each of the colon tissues by the Lowry method (24), samples containing 100 mg of protein were prepared for SDS-PAGE separation. The prepared samples were loaded onto the gel and subsequently transferred to nitrocellulose membranes (at 90 V for 1 h). The transferred samples were incubated with primary antibodies [β-actin (sc-130657, 1: 200), bax (sc-20067, 1: 100), bcl-2 (sc-7382, 1: 200), casp-3 (sc-56053, 1: 200) and casp-9 (sc-56076, 1: 200] for 14 h, and then the membranes were incubated with rabbit monoclonal anti-goat IgG secondary antibodies (1: 1500) for an additional 1 h. All incubations with antibodies were carried out at +4 °C. A publicly available software was used for the densitometric analysis of the resulting membranes (Bio-Rad Molecular Analyst, www.totallab.com).

Morphological and Histopathological Analysis

Macroscopic scoring of the colonic damage was performed using the criteria outlined in Table 1, with a maximum score of 10, and photographed according to Karakoyun et al. (2). The colonic tissue samples were processed for light microscopic investigations. In short, the tissues were fixed in 10% formaldehyde, dehydrated in ethanol series with ascending alcohol concentrations, cleared in xylene, and embedded in paraffin blocks. The cut tissue sections (5 μm thick) were stained with hematoxylin and eosin (H&E) and photographed using a light microscope with its dedicated camera (Olympus BX51; Olympus DP72; Olympus, Tokyo, Japan). Semi-quantitative histological scoring was performed according to the method modified from the previous study (2) The relevant scoring criteria are stated in Table 2.

Table 1. Criteria of the macroscopic scoring of the colonic injury.

Score View
0 Normal view
1 Local hyperaemia, no ulcers
2 Non-hyperaemic ulceration and bowel wall thickening
3 Ulceration with inflammation at one region
4 Ulceration and inflammation in two or more regions
5 Colonic damage more than 1 cm
6-10 Damage is increased by 1 point for each cm
(Maximum score 10)

Table 2. Criteria of the microscopic scoring of the colonic injury.

Score	Appearance
0 None; 1 Mild; 2 Moderate; 3 Severe	Submucosal oedema
0 None; 1 Localized; 2 Moderate; 3 Severe	Damage/necrosis
0 None; 1 Mild; 2 Moderate; 3 Severe	Inflammatory cell infiltration
0 None; 1 Mild; 2 Moderate; 3 Severe	Haemorrhage
0 Absent; 1 Present	Perforation
(Maximum score 13)	

Statistical Analysis

GraphPad software (Prism 6.0; GraphPad Software, San Diego, CA, USA) was used for statistical analysis. The comparisons through all groups were made with analysis of one-way variance followed by Bonferroni multiple comparison post-hoc tests. All data were expressed as mean±SD, and $p<0.05$ was conceded to be statistically significant.

RESULTS

Extraction Yield, *In Vitro* Biological Activity, and Total Phenol and Flavonoid Content of MoC Extract

22.04 g dried MoC extract was obtained from 411.71 g fresh fruit (extraction yield: 5.35%). MoC extract displayed moderate DPPH radical scavenging activity with an IC_{50} of 222.70±12.16 μg/mL when compared to an IC_{50} value of 17.6±0.37 μg/mL of standard ascorbic acid ($p<0.05$). The extract showed moderate ABTS radical scavenging activity with an IC_{50} value of 349.30±3.47 μg/mL when compared to standard Trolox (IC_{50}=13.00±0.21 μg/mL; $p<0.05$). MoC extract with an IC_{50} value of 14.46±1.33 μg/mL showed potent anti-inflammatory activity compared to standard Indomethacin (IC_{50}=22.39±0.26 μg/mL; $p<0.05$). The total phenolic and total flavonoid contents of the extract were 26.16±2.01 mg GAE and 1.88±0.02 mg QE per g extract, respectively (Table 3).

IL-1β, MDA and GSH Levels, MPO Activity

The pro-inflammatory cytokine IL-1β levels of the saline-treated AA group were found to be significantly higher than those of the control group ($p<0.001$). The treatment of the rats with MoC and SS decreased IL-1β elevation ($p<0.01$-$p<0.001$, respectively; Figure 1a).

In comparison to the control group, while a significant elevation was observed in the MDA levels which indicate lipid peroxidation of the saline-treated AA group ($p<0.01$), this elevation significantly decreased in the MoC and SS treated colitis groups ($p<0.01$; Figure 1b). The cellular antioxidant molecule GSH levels were markedly diminished in the saline-treated AA group in comparison to the control group ($p<0.01$); however, a significant elevation of GSH levels was detected in the MoC and SS-treated colitis groups ($p<0.01$ and $p<0.01$,

Table 3. Anti-inflammatory, antioxidant activity and total compound content of MoC extract.

Assays	MoC*	Trolox	Ascorbic acid	Indomethacin
ABTS radical scavenging activity (IC_{50}, µg/mL)	349.30±3.47[b]	13.00±0.21[a]		
DPPH radical scavenging activity (IC_{50}, µg/mL)	222.70±12.16[b]		17.6±0.37[a]	
Anti-lipoxgenase activity (IC_{50}, µg/mL)	14.46±1.33[a]			22.39±0.26[b]
Total phenolic content (mg GAE/g extract)**	26.16±2.01			
Total flavonoid content (mg QE/g extract)***	1.88±0.02			

*MoC: Ethanol extract of *Momordica charantia* L. fruits
**Total phenolic content was expressed as gallic acid equivalent (GAE).
***Total flavonoid content was expressed as quercetin equivalent (QE).
****Each value in the table is represented as mean±SD (n=3). Different letter superscripts in the same line indicate significant differences (p<0.05).

respectively; Figure 1c). MPO activity, which indicates tissue neutrophil recruitment, was found to be significantly increased in the saline-treated AA group in comparison to the control group (p<0.001). The colonic MPO activity was decreased upon MoC and SS treatments in comparison to the saline-treated AA group (p<0.01 and p<0.001, respectively; Figure 1d). There was no statistical difference between MoC and SS treatments.

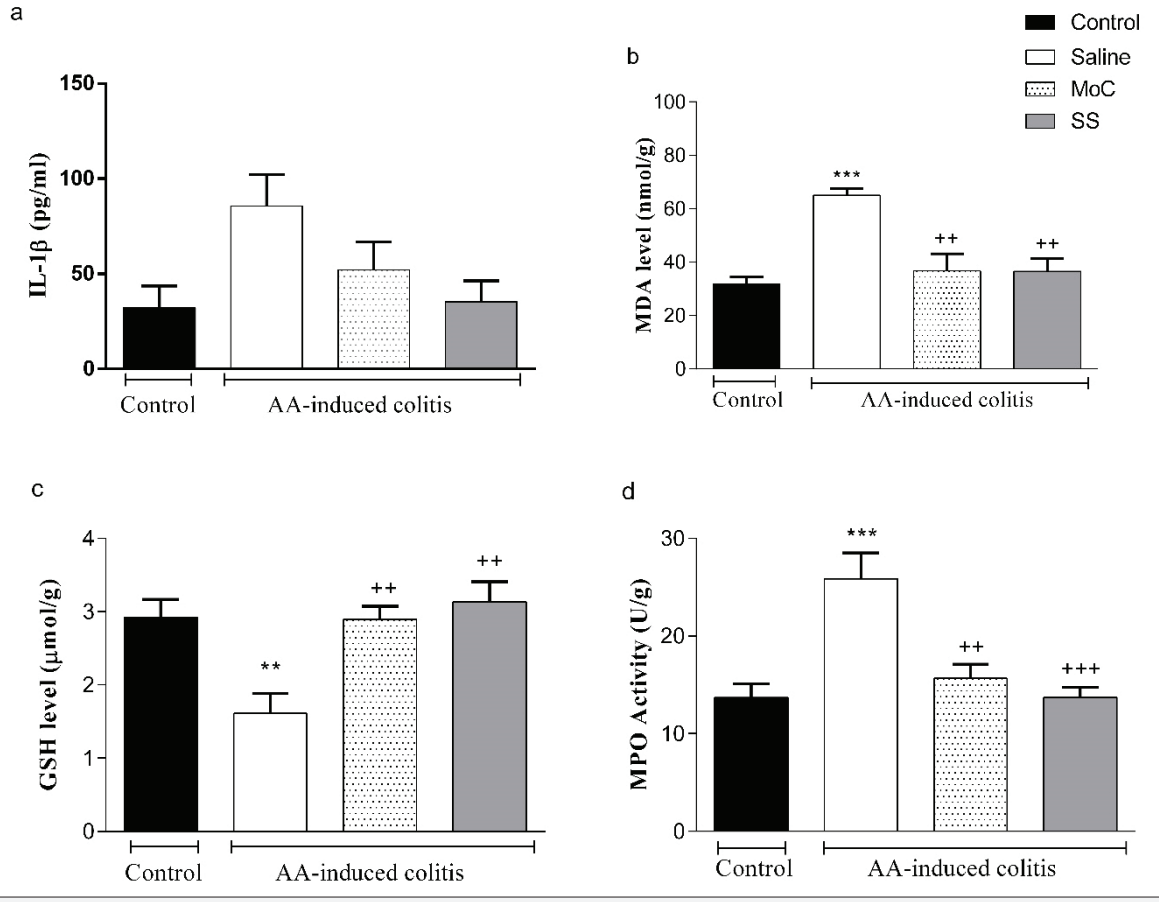

Figure 1. Tissue IL-1β (a), MDA (b), GSH levels (c), and MPO activity (d). $^{**}p<0.01$, and $^{***}p<0.001$ Comparisons according to the control group, $^{++}p<0.01$ and $^{+++}p<0.001$ Comparisons according to the saline-treated AA-induced colitis group. Control: Saline-treated control group, AA: Saline-treated AA-induced colitis group, MoC: *MoC* extract-treated AA-induced colitis group, SS: SS-treated AA-induced colitis group (for each group, n=6). Abbreviations: Interleukin 1-β (IL-1β); Malondialdehyde (MDA); Glutathione (GSH); Myeloperoxidase (MPO); Acetic acid (AA); Sulfasalazine (SS); *Momordica charantia* L. (MoC).

Immunoblotting

The representative immunoblotting membranes of the colon tissues were illustrated in Figure 2a. Changes in the bax/bcl-2 expression ratio and casp-9, casp-3 levels were used to determine the mitochondrial apoptosis evaluation for each group (*n*=4).

The bax/bcl-2 ratio was increased in the saline-treated AA-induced colitis group compared to the control group (p<0.001). The changes in the expression of bax/bcl-2 ratio in the AA-induced colitis group were restored upon MoC and SS treatments (p<0.01 and p<0.001, respectively; Figure 2b). Casp-9 and casp-3 levels were also significantly increased in the saline-treated AA-induced colitis group compared to the control group (p<0.05 and p<0.01, respectively). MoC and SS treatments decreased casp-9 and casp-3 levels compared to the saline-treated AA group (p<0.05; Figure 2c and 2d).

Morphological and Histopathological Analysis

At 72 h after colitis induction, macroscopic scoring was found to be significantly higher in the saline-treated AA group compared to the control group (p<0.001), while this scoring was significantly decreased in the MoC and SS-treated colitis groups (p<0.001; Figures 3a and c).

As a result of light microscopic examinations, colon tissues of the control group had histological layers with regular morphology and the total microscopic damage score was the lowest (mean 1.46; Figure 3b). In the saline-treated AA group, severe loss of epithelial lining, extensive submucosal oedema, massive inflammatory cell infiltration, and haemorrhage were observed with the highest total damage score (mean 12.4). MoC and SS-treated colitis groups showed similar histological appearance, such as more regular epithelial surfaces, decreased inflammatory cell infiltration, and submucosal oedema (Figure 4). Microscopic scoring was found to be markedly higher in the AA group compared to the control group (p<0.001), while this scoring was significantly decreased upon MoC and SS treatment (p<0.001). When compared to the control group, there were still high scores in the MoC and SS groups (p<0.01 and p<0.001, respectively), whereas the difference between these treatment groups was not significant (Figure 3b, Table 4).

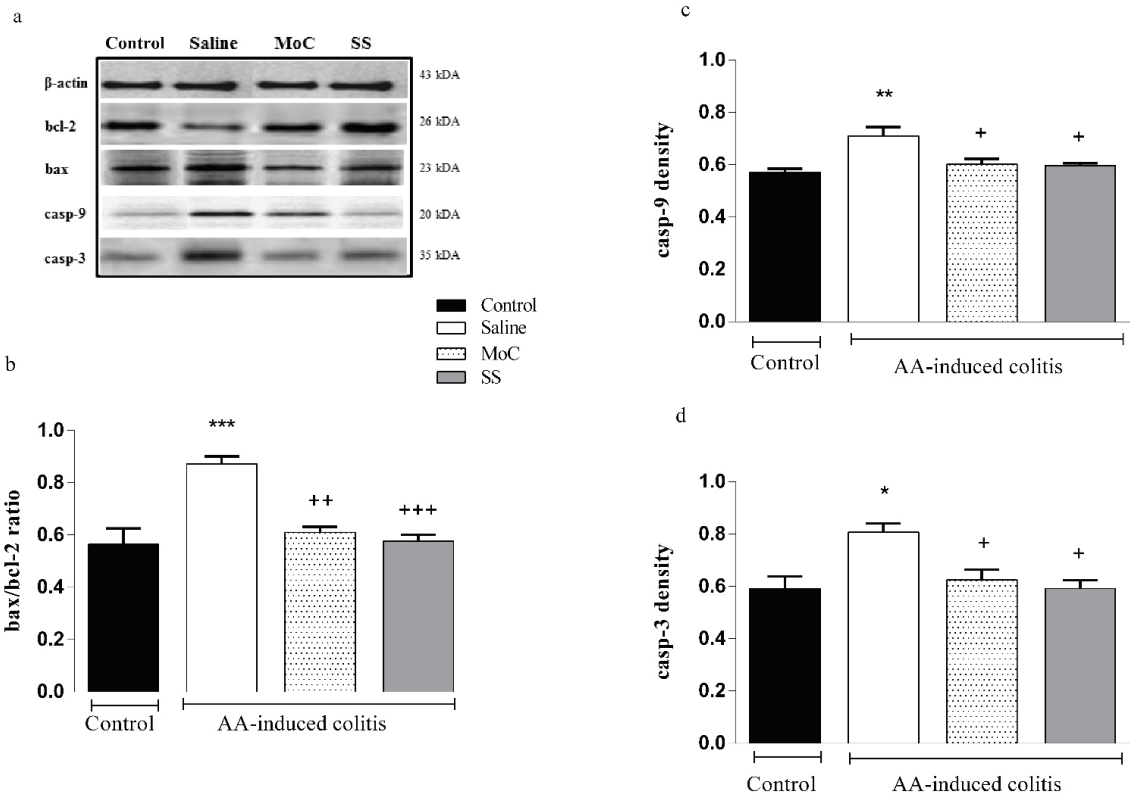

Figure 2. The representative images of membranes obtained from western blotting assays showing protein expressions of β-actin, bax, bcl 2, casp-9, and casp-3 (a), the expression levels of bax/bcl-2 ratio (b), casp-9 (c) and casp-3 (d) in colon.
All membranes (for each group, n=4) were normalized by using β-actin antibodies . *p<0.05, **p<0.01, and ***p<0.001 Comparisons according to control group, +p<0.05, ++p<0.01 and +++p<0.001 Comparisons according to saline treated AA-induced colitis group. Control: Saline-treated control group, AA: Saline-treated AA-induced colitis group, MoC: Momordica charantia extract-treated AA-induced colitis group, SS: SS-treated AA-induced colitis group (for each group, n=6). Abbreviations: Bcl-2-associated X protein (bax); B-cell lymphoma 2 (bcl-2); Caspase-9 (casp-9); Caspase-3 (casp-3); Acetic acid (AA); Sulfasalazine (SS); *Momordica charantia* L. (MoC).

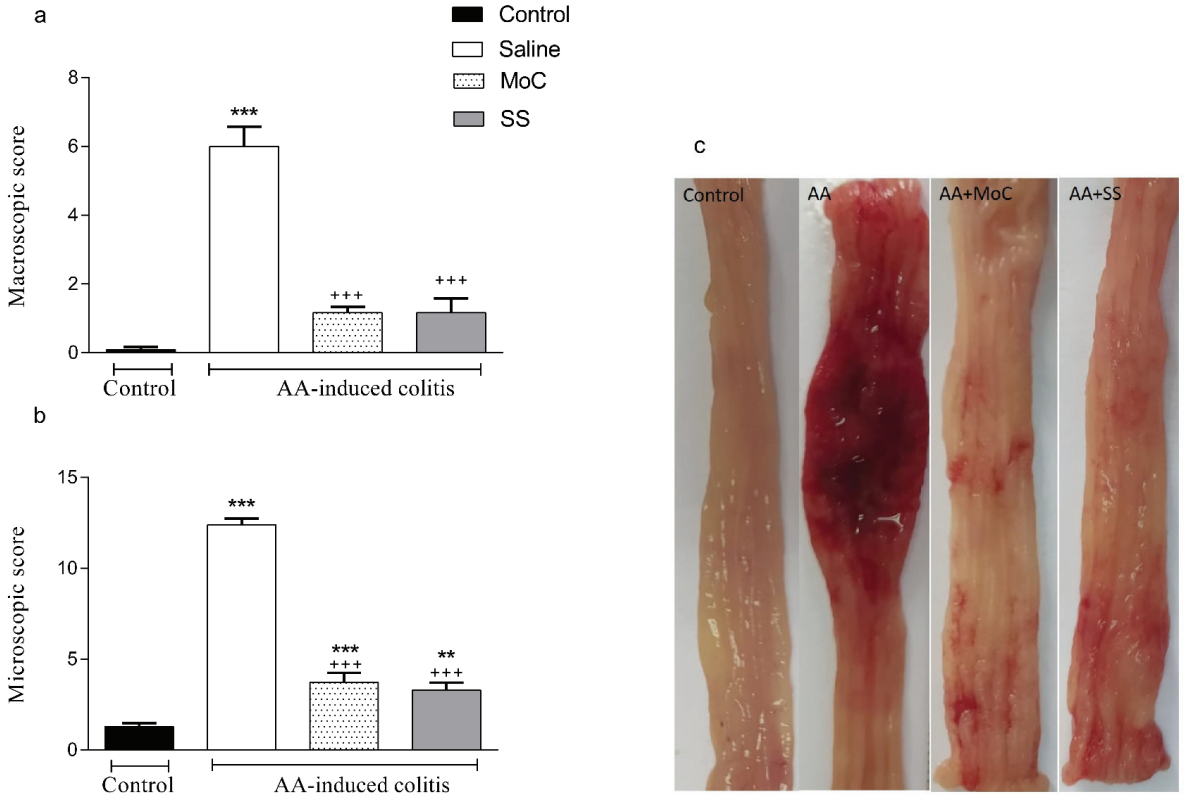

Figure 3. Macroscopic (a), microscopic scoring (b), and representative photographs of the colonic tissues (c). **p<0.01, and ***p<0.001 Comparisons according to control group, $^{+++}$p<0.001 Comparisons according to saline-treated AA-induced colitis group. Control: Saline-treated control group, AA: Saline-treated AA-induced colitis group, MoC: MoC extract-treated AA-induced colitis group, SS: SS-treated AA-induced colitis group (for each group, n=6). Abbreviations: Acetic acid (AA); Sulfasalazine (SS); *Momordica charantia* L. (MoC).

Table 4. Predominant histological grading of each sign of colonic damage in each experimental group of animals.

	Oedema	Damage/Necrosis	Inflammatory cell	Haemorrhage	Perforation	Total Score
Control	0.38	0.42	0.44	0.02	0.20	1.46
Saline+AA	3.00	2.70	3.00	2.90	0.80	12.40
MoC+AA	0.90	0.86	1.22	0.56	0.20	3.74
SS+AA	0.80	0.65	1.125	0.50	0.25	3.30

Abbreviations: Acetic acid (AA); Sulfasalazine (SS); *Momordica charantia* L. (MoC).

DISCUSSION

The results of the current study reveal that MoC extract ameliorates colonic damage, as assessed by decreased pro-inflammatory cytokine IL-1β levels, bax/bcl-2 ratios, caspase-3 and -9 levels, MPO activity, lipid peroxidation and increased GSH levels. Also, macroscopic and histopathologic evaluation suggests significant colonic healing.

In the present study *in vitro* DPPH and ABTS radical scavenging activity and lipoxygenase inhibitory activity, and *in vivo* MPO enzyme activity of MoC extract were investigated. The antioxidant and anti-lipoxygenic effects of MoC extract detected *in vitro* confirmed its in vivo antioxidant and anti-inflammatory activity. Previous studies have shown that MoC contained cucurbitane-type triterpenes as the main compounds (8, 9, 25-27). Furthermore, some of these triterpene compounds have been reported to have significant antioxidant and anti-inflammatory activities (27, 28). Therefore, these cucurbitane-type triterpenes together with other compounds in MoC may be responsible for the antioxidant and anti-inflammatory activity of MoC. In our *in vitro* analysis MoC exhibited a strong anti-inflammatory activity compared to standard Indomethacin, which is an important

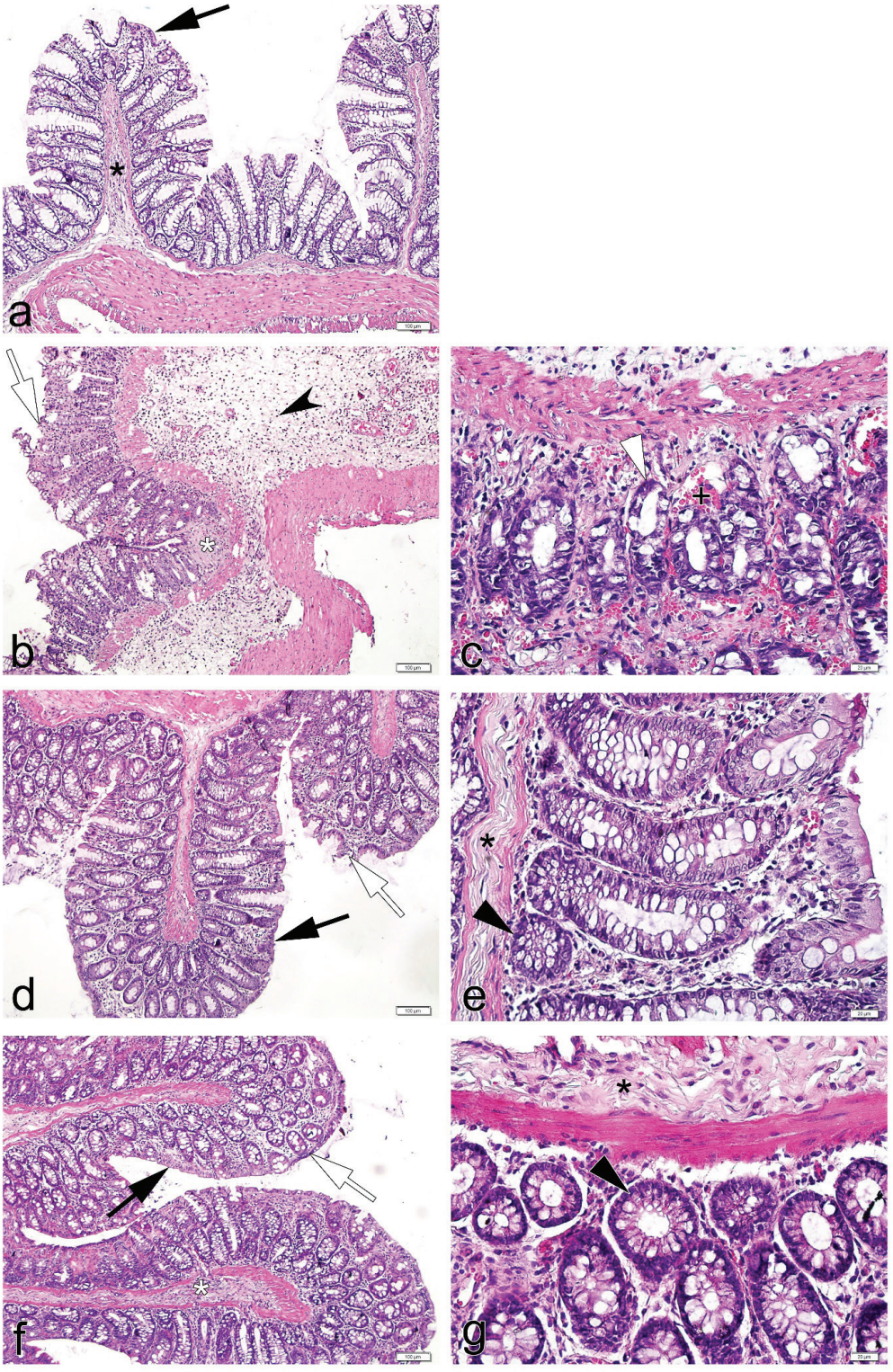

Figure 4. Representative light microscopic photographs of the colonic tissues from all experimental groups. (a) Saline-treated control group, (b-c) Saline-treated AA-induced colitis group (AA), (d-e) MoC extract-treated AA-induced colitis group (AA+MoC) group. (f-g) SS-treated AA-induced colitis group (AA+SS) group. Arrow: Normal colon mucosa with regular surface epithelium. Arrowhead: Regular Lieberkuhn crypts. Asterisk (*): Regular submucosa. Notched arrow: Inflammatory cell infiltration. Plus (+): Vascular dilatation/haemorrhage. White arrow: Colon mucosa with damaged epithelium. White arrowhead: Lieberkuhn crypts with the abnormal organization. H&E staining. Bar size a,b,d,f: 100 µm and c,e,g: 20 µm. Abbreviations: Acetic acid (AA); Sulfasalazine (SS); *Momordica charantia* L. (MoC).

reason for colonic healing. However, in the present study, the total phenolic and flavonoid contents of MoC were found to be low. The fact that MoC is rich in cucurbitane-type triterpene compounds overlaps with this result.

Here, we established an AA-induced colitis model because it is highly similar to human inflammatory bowel disease (IBD) in terms of pathophysiological, histopathologic, and inflammatory mediator profiles (29). AA-induced UC has been shown to initiate physical and chemical damage in colon tissue, causing inflammation and an increase in ROS levels and a subsequent decrease in GSH levels. Besides, neutrophils that infiltrate the damaged colon mucosa, which leads to oxidative stress, also increase inflammation (4, 30, 31). In the present study, impaired epithelial integrity, which was demonstrated macroscopically and microscopically, facilitated neutrophil infiltration from blood to colon tissue. Our *in vitro* biological activity results indicate that MoC extract has free radical scavenging and anti-inflammatory activities. Scavenging of free radicals and depletion of inflammation diminishes lipid peroxidation and restores cellular GSH stores. Decreased MDA levels and increased GSH levels observed upon MoC treatment in this study may be due to such activities of MoC. In addition, MoC therapy reduced MPO activity, which increased oxidative damage, and inflammation caused by AA increased neutrophil infiltration into the colon, mucosal and submucosal necrosis, oedema, vascular dilation, immense epithelial damage, and submucosal ulceration, which are main features of human colitis (29). Our macroscopic scoring showed that AA caused excessive damage to the colon tissue, but the MoC and SS treatments had significant ameliorative effects. Our macroscopic and microscopic results were in agreement with our biochemical results. Compared to the control group, there was still microscopic damage in the MoC and SS-treatment groups; however, these treatment groups were similar and the results correlated with macroscopic scoring. IL-1β proinflammatory cytokine is released from the colonic macrophage early in inflammation after AA administration and exacerbates mucosal inflammation (32, 33) and directly proportional to the severity of inflammation (34). Functional foods are beneficial by reducing pro-inflammatory cytokine expression in models of IBD (35). MoC reduced IL-1β levels in DSS-induced colitis and TNBS-induced colitis models (10, 15, 34).

In line with these studies, our result showed that colitis caused a significant increase in colonic IL-1β levels and that MoC and SS treatments were effective in reversing this trend. However, in those studies, the preparation methods of the plant sample, the treatment durations, treatment ways, and the chemical agents used for model induction were different from our study.

Colitis has previously been shown to cause increased apoptosis in colonic epithelial cells (36-38). Overproduction of ROS in cells can disrupt cellular parts, such as lipids and proteins, which can eventually cause cell death by apoptosis (39). Anti-apoptotic protein bcl-2 is localized on the mitochondrial membrane and inhibits apoptosis by stabilizing this membrane (40). However, bax inhibits the anti-apoptotic function of bcl-2 (41). Zhu et al. demonstrated the increased expression of bax/bcl-2, casp-3, and casp-9 in a UC rat model (38). Consistent with this report, our data showed that AA increased bax/bcl-2 ratio, casp-3, and casp-9 levels in the colon. In previous studies, MoC has been reported to reduce pro-apoptotic protein casp-3 and casp-9 levels of uterine tissue in ovariectomized rats (42). The results presented herein revealed that MoC extract attenuated AA-induced colonic cell apoptosis by decreasing casp-9 and casp-3 levels and bax/bcl-2 ratio, thereby improving the epithelial barrier integrity and colonic architecture.

CONCLUSION

Our *in vivo* and *in vitro* examinations proved that MoC extract had a protective role in AA-induced inflammation, apoptosis, and oxidative damage. MoC reduced the severity of colitis. Our results point out that MoC extract treatment appears to be as effective as SS treatment. According to our study results, we suggest that MoC has a protective role in AA-induced colitis.

Acknowledgement: We thank Deniz Mukaddes Turet for taking pictures of the colon and Seren Ede for helping arrange the references.

Ethics Committee Approval: This study was approved by the Marmara University Animal Experiments Local Ethics Committee (14.09.2020 / 45.2020.mar).

Informed Consent: Written consent was obtained from the participants.

Peer Review: Externally peer-reviewed.

Author contributions: Conception/Design of study- D.O., G.S.; Data Acquisition- D.O., A.S.; Data Analysis/Interpretation- D.O., A.S., A.A., K.T., O.T.C.K., I.S.; Drafting Manuscript- D.O., A.S., A.A., O.T.C.K.; Critical Revision of Manuscript- K.T, G.S.; All the authors reviewed the manuscript and after their respective inputs gave their final approval for submission/publication.

Conflict of Interest: Authors declared no conflict of interest.

Financial Disclosure: Authors declared no financial support.

REFERENCES

1. Yadav V, Varum F, Bravo R, Furrer E, Bojic D, Basit AW. Inflammatory bowel disease: exploring gut pathophysiology for novel therapeutic targets. Transl Res 2016; 176: 38-68.
2. Karakoyun B, Ertaş B, Yüksel M, Akakin D, Çevik Ö, Şener G. Ameliorative effects of riboflavin on acetic acid-induced colonic injury in rats. Clin Exp Pharmacol Physiol 2018; 45: 563-72.
3. Fabia R, Willen R, Arrajab A, Andersson R, Ahren B, Bengmark S. Acetic acid-induced colitis in the rat: a reproducible experimental model for acute ulcerative colitis. Eur Surg Res 1992; 24: 211-25.
4. El-Akabawy G, El-Sherif NM. Zeaxanthin exerts protective effects on acetic acid-induced colitis in rats via modulation of pro-inflammatory cytokines and oxidative stress. Biomed Pharmacother 2019; 111: 841-51.
5. Shalkami AS, Hassan MIA, Bakr AG. Anti-inflammatory, antioxidant and anti-apoptotic activity of diosmin in acetic acid-induced ulcerative colitis. Hum Exp Toxicol 2018; 37: 78-86.

6. Hagiwara C, Tanaka M, Kudo H. Increase in colorectal epithelial apoptotic cells in patients with ulcerative colitis ultimately requiring surgery. J Gastroenterol Hepatol 2002; 17: 758-64.
7. Rosenberg LN, Peppercorn MA. Efficacy and safety of drugs for ulcerative colitis. Expert Opin Drug Saf 2010; 9: 573-92.
8. Saeed F, Afzaal M, Niaz B, Arshad Mu, Tufail T, Hussain MB, et al. Bitter Melon (Momordica Charantia): A Natural Healthy Vegetable. Int J Food Prop 2018; 21: 1270-90.
9. Huang Ht, Zhang LJ, Huang HC, Hwang SY, Wu Cl, Lin YC, et al. Cucurbitane-type triterpenoids from the vines of Momordica charantia and their anti-inflammatory activities. J Nat Prod 2020; 83: 1400-08.
10. Ünal NG, Kozak A, Karakaya S, Oruç N, Barutçuoğlu B, Aktan Ç, et al. Anti-inflammatory effect of crude Momordica charantia l. extract on 2,4,6-trinitrobenzene sulfonic acid-induced colitis model in rat and the bioaccessibility of its carotenoid content. J Med Food 2020; 23: 641-8.
11. Patel S, Patel T, Parmar K, Bhatt Y. Patel NM. Isolation, characterization and antimicrobial activity of charantin from Momordica charantia linn. fruit. Int J Drug Dev Res 2010; 2: 629-34.
12. Kumar R, Balaji S, Sripriya R, Nithya N, Uma TS, Sehgal PK. *In vitro* evaluation of antioxidants of fruit extract of Momordica charantia l. On fibroblasts and keratinocytes. J Agric Food Chem 2010; 58: 1518-22.
13. Jia S, Shen M, Zhang F, Xie J. Recent advances in Momordica charantia: functional components and biological activities. Int J Mol Sci 2017; 18: 2555.
14. Gürbüz I, Akyüz Ç, Yeşilada E, Şener B. Anti-ulcerogenic effect of Momordica charantia l. fruits on various ulcer models in rats. J Ethnopharmacol 2000; 71: 77-82.
15. Lu HY, Lin BF. Wild bitter melon alleviates dextran sulphate sodium-induced murine colitis by suppressing inflammatory responses and enhancing intestinal regulatory t cells. J Funct Foods 2016; 23: 590-600.
16. Zou Y, Chang SK, Gu Y, Qian SY. Antioxidant activity and phenolic compositions of lentil (Lens culinaris var. morton) extract and its fractions. J Agric Food Chem 2011; 59: 2268-76.
17. Phosrithong N, Nuchtavorn N. Antioxidant and anti-inflammatory activities of Clerodendrum leaf extracts collected in Thailand. Eur J Integr Med 2016; 8(3): 281-85.
18. Yildirim A, Şen A, Dogan A. Bitis L. Antioxidant and anti-inflammatory activity of capitula, leaf and stem extracts of tanacetum cilicicum (boiss.) Grierson. Int J Second Metab 2019; 6: 211-22.
19. Gao, X, Ohlander M, Jeppsson N, Björk L, Trajkovski V. Changes in Antioxidant Effects and Their Relationship to Phytonutrients in Fruits of Sea Buckthorn (Hippophae rhamnoides L.) during Maturation. J Agric Food Chem 2000; 48(5): 1485-90.
20. Zhang R, Zeng Q, Deng Y, Zhang M, Wei Z, Zhang Y, et al. Phenolic profiles and antioxidant activity of litchipulp of different cultivars cultivated in Southern China. Food Chem. 2013; 136: 169-76.
21. Buege JA, Aust SD. Microsomal lipid peroxidation. Meth Enzymol 1978; 52: 302-10.
22. Beutler E. Red Cell Metabolism. A manual of biochemical methods. In B ergmeyen HV (ed.), annals of internal medicine 1975 2nd Ed. Issue 6. Grune & Stratton.
23. Bradley PP, Priebat DA, Christensen RD, Rothstein G. Measurement of cutaneous inflammation: estimation of neutrophil content with an enzyme marker. J Investig Dermatol 1982; 78: 206-9.
24. Lowry OH, Rosebrough NJ, Farr AL, Randall RJ. Protein measurement with the folin phenol reagent. J Biol Chem 1951;193: 265-75.
25. Wurtz NR, Viet A, Shaw SA, Dilger A, Valente MN, Khan JA, et al. Potent triazolopyridine myeloperoxidase inhibitors. Acs Med Chem Lett 2018; 9: 1175-80.
26. Chang CI, Chen CR, Liao YW, Cheng HI, Chen YC, Chou CH. Cucurbitane-type triterpenoids from Momordica charantia. J Nat Prod 2006; 69: 1168-71.
27. Lin Kw, Yang Sc, Lin Cn. Antioxidant constituents from the stems and fruits of Momordica charantia. Food Chem 2011; 127: 609-14.
28. Shivanagoudra SR, Perera WH, Perez JL, Athrey G, Sun Y, Jayaprakasha GK, et al. Cucurbitane-type compounds from Momordica charantia: Isolation, *in vitro* antidiabetic, anti-inflammatory activities and in silico modeling approaches. Bioorg Chem 2019; 87: 31-42.
29. Randhawa PK, Singh K, Singh N, Jaggi AS. 2014. A review on chemical-induced inflammatory bowel disease models in rodents. Korean J Physiol Pharmacol 2014; 18: 279-88.
30. Iseri SO, Ersoy Y, Ercan F, Yuksel M, Atukeren P, Gumustas K, et al. The effect of sildenafil, a phosphodiesterase-5 inhibitor, on acetic acid-induced colonic inflammation in the rat. J Gastroenterol Hepatol (Australia) 2009; 24: 1142-48.
31. Kolgazi M, Uslu U, Yuksel M, Velioglu-Ogunc A, Ercan F, Alican I. The role of cholinergic anti-inflammatory pathway in acetic acid-induced colonic inflammation in the rat. Chem Biol Interact 2013; 205(1): 72-80.
32. Soliman NA, Keshk WA, Rizk FH, Ibrahim MA. The possible ameliorative effect of simvastatin versus sulfasalazine on acetic acid induced ulcerative colitis in adult rats. Chem Biol Interact 2019; 298: 57-65.
33. Tahan G, Gramignoli R, Marongiu F, Aktolga S, Cetinkaya A, Tahan V, et al. Melatonin expresses powerful anti-inflammatory and antioxidant activities resulting in complete improvement of acetic-acid-induced colitis in rats. Dig Dis Sci 2011; 56: 715-20.
34. Semiz A, Ozgun Acar O, Cetin H, Semiz G, Sen, A. Suppression of inflammatory cytokines expression with Bitter melon (Momordica charantia) in tnbs-instigated ulcerative colitis. J Transl Int Med 2020; 8: 177-87.
35. Hossen I, Hua W, Ting L, Mehmood A, Jingyi S, Duoxia X, et al. Phytochemicals and inflammatory bowel disease: A review. Critical Reviews in Food Science and Nutrition 2020; 60(8): 1321-45.
36. Guven B, Can M, Piskin O, Aydin BG, Karakaya K, Elmas O, et al. Flavonoids protect colon against radiation induced colitis. Regul Toxicol Pharmacol 2019; 104: 128-32.
37. Yao J, Cao X, Zhang R, Li YX, Xu Zl, Zhang DG, et al. Protective effect of baicalin against experimental colitis via suppression of oxidant stress and apoptosis. Pharmacogn Mag 2016; 12: 225-34.
38. Zhu L, Dai LM, Shen H, Gu PQ, Zheng K, Liu YJ, et al. Qing Chang Hua Shi granule ameliorate inflammation in experimental rats and cell model of ulcerative colitis through Mek/Erk signaling pathway. Biomed Pharmacother 2019; 116: 108967.
39. Kannan K, Jain SK. Oxidative stress and apoptosis. Pathophysiology 2000; 7: 153-63.
40. Haeberlein SLB. Mitochondrial function in apoptotic neuronal cell death. Neurochem Res 2004; 29: 521-30.
41. Tan KO, Fu NY, Sukumaran SK, Chan SL, Kang JH, Poon KL, et. Map-1 is a mitochondrial effector of bax. Proc Natl Acad Sci USA. 2005; 102(41): 14623-8.
42. Cevik O, Akpinar H, Oba R, Cilingir OT, Ozdemir ZN, Cetinel S, et al. The effect of Momordica charantia intake on the estrogen receptors ESRα/ESRβ gene levels and apoptosis on uterine tissue in ovariectomy rats. Mol Biol Rep 2015; 42: 167-77.

ISTANBUL UNIVERSITY PRESS

RESEARCH ARTICLE

Eur J Biol 2021; 80(2): 129-137

Antitumoral Properties of a Pincer-Type Isonicotinohydrazone-Hg(II) Complex

Burcu Saygıdeğer Demir[1], Aycan Sezan[1], Ezgi Derinoz[1], Eylem Nas[1], Mehmet Ozerten[1], Ghodrat Mahmoudi[2], Yasemin Saygideger[1,3]

[1]Çukurova University, Departmant of Biotechnology, Institute of Natural and Applied Sciences, Adana, Turkey
[2]University of Maragheh, Department of Chemistry, Faculty of Science, Maragheh, Iran
[3]Cukurova University, Department of Pulmonary, Faculty of Medicine, Adana, Turkey

ORCID IDs of the authors: B.S.D. 0000-0001-5179-0522; A.S. 0000-0003-1506-7083; E.D. 0000-0002-1951-6862; E.N. 0000-0003-3799-9172; M.O. 0000-0003-4868-0212; G.M. 0000-0002-4846-5283; Y.S. 0000-0003-3293-373X

Please cite this article as: Saygideger Demir B, Sezan A, Derinoz E, Nas E, Ozerten M, Mahmoudi G, Saygideger Y. Antitumoral Properties of a Pincer-Type Isonicotinohydrazone-Hg(II) Complex. Eur J Biol 2021; 80(2): 129-137.
DOI: 10.26650/EurJBiol.2021.1010029

ABSTRACT

Objective: The aim of this study was to evaluate the antitumoral properties of the novel $Hg(SCN)_2$ complex of a pincer-type isonicotinohyrazone ligand (PTIH).

Materials and Methods: Hydrazine ligands were prepared through a Schiff base condensation between the 2-Acetylpyridine and isonicotinoyl acid hydrazide. PTIH was synthetized by a branch tube method using $Hg(SCN)_2$. In vitro cell killing activity, the induction of apoptosis, the influence on motility, and the effects on mRNA expression to a motility-related gene (E-cadherin) of PTIH were evaluated in A549, HepG2, HUH7 cancer cell lines, and BEAS2B non-cancer cell line.

Results: PTIH was found to be cytotoxic to cancer cells, compared to non-cancers, and induced apoptosis. Additionally, it suppressed cell migration in A549 cells, leading to an increase in the levels of E-cadherin mRNA expression, and decreased colony formation in HepG2 and HUH7 cells. Through UV titration studies, it was determined that PTIH showed albumin binding and interacted with DNA by electrostatically and/or groove binding.

Conclusion: PTIH exerted more cytotoxic effects in some cancer cells than in normal cells. This feature and other anticancer properties make it a promising agent.

Keywords: Antitumor, cytotoxicity, apoptosis, isonicotinohydrazone, Hg(II) complex, E-cadherin

INTRODUCTION

Hydrazones are called N-N-O donor Schiff bases pincer type ligands, which are derived by the one-pot condensation reaction of substituted hydrazides with aldehydes and ketones in high yields (1-2). In general, metal complexes including hydrazones, by adding new structural and electronic properties to the organic skeleton, can add different biological binding properties to the compound (3). The biological activity of these metal complexes is influenced by the oxidation level and the other features of the metal as well as the structure of the ligand (4-6).

Charming chemical behaviors (ability to chelate, structural flexibility, etc.) and biological activities such as antibacterial, antiproliferative, antimalarial, and antitumoral make hydrazone ligands remarkable for drug design (7-9). There are less anti-tumor studies with Hg complexes compared to other transition metal complexes. However, recently, the superior cytotoxic effects of Hg(II) compounds have been recognized and have been the subject of new drug studies (10-12). Thimerosal (Ethyl (2-mercaptobenzoato- (2 -) - O, S) mercurate (1-) sodium), known as an antibacterial and antifungal, has been used for a long time in vaccines, eye drops,

Corresponding Author: Burcu Saygıdeğer Demir E-mail: burcusaygidemir@gmail.com
Submitted: 15.10.2021 • **Revision Requested:** 28.10.2021 • **Last Revision Received:** 15.11.2021 • **Accepted:** 16.11.2021 • **Published Online:** 07.12.2021

and contact lens solutions. Now, it has been discovered to have anti-cancer properties. In a study conducted on the TPC-1 thyroid cancer cell line, its in vitro cytotoxic effect was proven, and it was seen as a potential chemotherapeutic agent (10). In another study, the Hg(II) complex was found to cause significantly higher mitochondrial damage and ROS-induced cell death in A549 and MCF-7 cells compared to cisplatin (12).

The chemotherapeutic drugs of metal complexes are effectively used clinically despite their widely recognized side effects and increasing reports of resistance to these drugs (1, 2). The discovery of new metal complexes is important in overcoming the potential side effects of existing anticancer agents and in developing more effective and targeted cancer drugs (3, 13, 14).

Recent studies on hydrazone-based metal complexes have shown that the presence of a methyl substituent in the imine carbon atom has a remarkable effect on the cytotoxicity of the complexes (15-17). Therefore, in our study, we chose a hydrazone ligand methyl-substitution in the imine carbon atom and the Hg(II) complex of this ligand to further increase its anticancer activity.

MATERIALS AND METHODS

Materials and Physical Techniques

All reagents and solvents were commercially available and used without further purification. To evaluate anticancer activities, three different cancer cell lines were used, of which one was non-small cell lung carcinoma (A549) and the other two were hepatocellular carcinoma (HepG2, Huh7). The A549 cell line was provided by Gaziantep University, and the HepG2 and Huh7 cell lines were from IBG Izmir. All cells were maintained in RPMI 1640 (HyClone Cat. No: SH30027.01), supplemented with 10% FBS (fetal bovine serum) (HyClone Cat. No: SV30160.03) and 1% antibiotics (HyClone Cat. No: SV30079.01) in a CO_2 incubator (Thermo Sci.) at 5% CO_2 and 21% O_2. Cells were harvested using Trypsin (HyClone Cat. No: SH30042.01), and a phosphate buffer solution (PBS) 1X (HyClone Cat. No: SH30256.01) was used to wash the plated cells or cell pellets when necessary. PTIH was dissolved in dimethyl sulphoxide (DMSO) with a 10 mM stock concentration and was further diluted in the cell culture media during the experiments.

Hydrazine ligands were arranged through a Schiff base condensation between the 2-Acetylpyridine and isonicotinoyl acid hydrazide. These ligands were prepared as described previously (18).

Infrared spectra (KBr pellets) were documented with a Perkin-Elmer spectrometer in the range of 400-4000 cm^{-1}. Microanalyses were done through a Heraeus CHN-O-Rapid analyzer. Melting points are not corrected although they were measured on an Electrothermal 9100 instrument. *HL: melting point (m.p). 240 C, Infrared (IR) (cm^{-1}) chosen bands:* 3189 (w), 3073 (w), 1671 (s), 1563 (w), 1382 (s), 1302 (m), 1216 (s), 1144 (m), and 985(m), 836 (m), 789 (m), 735 (m), 669 (m) and 566 (s).

Synthesis of $[Hg(SCN)_2(HL)]$ (PTIH)

A simple formula (branched tube glass) was used to synthesize and purify PTIH, as explained before (19), and is summarized in Figure 1. In this way, organic ligand and the related metal salt were placed in the main arm of the branched tube. Ethanol was carefully added to fill the arms, the tube was sealed, and the ligand-containing arm was plunged in a bath containing oil heated to 60°C while the branched arm was kept at room temperature. After an appropriate time, crystals were retrieved from the cool arm and washed with acetone and ether after filtration and allowed to dry in the air.

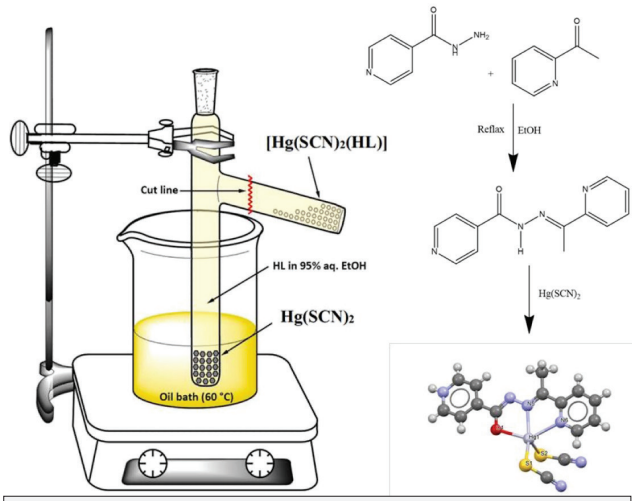

Figure 1. Graphical representation of the apparatus used in the syntheses of PTIH ($[Hg(SCN)_2(HL)]$), synthesis reaction and crystal structure of the PTIH.

Reactant materials: HL=2-Acetylpyridine isonicotinoyl hydrazone, mercury(II) thiocyanate.

Product: yellow-green, m.p. 180° C.

Yield (based on $Hg(SCN)_2$): 0.240 g, (84%). Anal. Calcd for $C_{15}H_{12}HgN_6OS_2$: C, 32.34; H, 2.17; N, 15.09%. Fund: C, 32.60; H, 2.22; N, 15.29%.

IR (cm^{-1}) selected bands: 3368(w), 2993 (w), 2061(vs), 1622(m) 1593 (m), 1534(s), 1481 (s), 1438 (m), 1288 (s), 1157 (m), 948 (m), 834 (m), 787 (m) and 699 (m).

Cytotoxicity Assay

PTIH was dissolved in DMSO at 10mM concentration and tested for its cytotoxicity across four distinct cell lines (A549, HepG2, HUH7, and BEAS2B) using MTT (Thiazolyl Blue Tetrazolium Bromide) as described earlier (20). Briefly, the cells (1.0×10^4/200 mL/well) were split into 96-well plates and incubated overnight at 37°C, 5% CO_2, and 80% humidity in their respective medium (RPMI for A549 and, BEAS2B and DMEM for HUH7 and HEPG2, respectively) containing 10% FBS and 1% antibiotics. The media were replaced with increasing concentration of PTIH, ranging between 0-100µM and containing even amounts of DMSO for 24h at similar incubation conditions. MTT was added to the

wells at 0.5 mg/mL final concentration before being maintained in the incubator for another 4hrs. At the end of the incubation time, the supernatants were carefully removed, 50µL DMSO was added to each well, and then, absorbance was measured at 570nm and 630nm (for background) in a microplate reader (Biochrom EZ Read 400). The way of calculating the percentage of living cells was done by using the equation (A) sample/ (A) control × 100. In this process, the sample can be compared with control cells by ignoring PTIH.

Flow Cytometric Apoptosis Detection Assay

Biolegend apoptosis detection kit protocol was used to perform Annexin-V/PI staining and apoptotic cell detection (21) in A549, HepG2, and HUH7 cells. Cells (1.0×10^5 cells/mL) were either treated with PTIH or DMSO (control) for 24hrs before harvesting, and the suspensions of the cells and harvested cells were collected and centrifuged. The pellets were washed with PBS two times. After incubation with the indicated dyes according to the kit's protocol, the fluorescence emission was detected at 633 nm in a flow cytometer (Beckman Coulter/CytoFLEX, United States).

Cell Motility Assay

A549 cells were plated in 6-well plates in a regular growth medium containing 10% FBS. After 24 hrs (when the cells were 100% confluent), a straight-line scratch was formed on cell layers with a sterile 200 µL disposable pipette tip and washed with PBS. In turn, the cells were treated either with IC_{50} concentration of the PTIH or with DMSO as a control. Images of cell migration were taken using an inverted microscope at times between 0 and 24hrs after the scratch. The percent closure ratio was measured using Image J software (NIH, USA, Version 1.53a).

Colony Formation Assay

A colony-forming efficiency assay was performed in 6 well plates. The cells were seeded at a quantity of 200 cells/well (for HepG2 and HUH 7) and of 300 cells/well (for A549) in a 3mL complete culture medium. Two different concentrations of PTIH were applied to cells for 72 hours. Then, the old medium was removed, and a new fresh complete medium (not containing PTIH) was added to the cells. The medium was changed with the new one twice a week. After a total of three weeks, the colonies formed were dyed with a methylene blue solution (50% Methanol, 50% distilled water, and 0.4 g methylene blue) and were counted.

Quantitative Polymerase Chain Reaction (qPCR)

Cells, either treated with PTIH or an equal amount of DMSO for 4 hours, underwent RNA extraction using a commercially available RNA isolation kit (Macherey-Nagel) and reverse-transcribed (Thermo Fisher) according to the manufacturer's protocols. A quantitative PCR was performed in 3 replicates on a 96-well plate using a SYBR Green qPCR Master Mix (Ampliqon). 18S rRNA was used as an internal control gene, and fold differences in the expression levels of the genes between the samples were calculated using the comparative Cycle threshold (CT) method, as previously described (20). 18S rRNA: sense: 5'-cttagagggacaagtggcg-3 ', non-sense: 5'-acgctgagccagtcagtgta-3 '; E-cadherin: sense: 5'-acactgccaactggctggagatta-3 ', antisense: 5'-tgattagggctgtgtacgtgctgt-3 ' primer pairs were used.

BSA Binding Assay

BSA was used to examine the protein binding kinetic of the PTIH. Bovine serum albumin (BSA) was chosen for studying the drug interaction because of its structural similarity to human serum albumin (HSA) and for being easily available and inexpensive. 1 µM BSA was dissolved in PBS (PH: 7.0), and the change in absorbance was monitored in a UV-visible spectrophotometer at 200-400 nm wavelength by increasing the concentration of PTIH (0-10 µM) (UV titration) against the constant amount of BSA.

DNA Binding Assay

Experiments of PTIH binding with CT-DNA (Calf Thymus-DNA) were carried out within 1mM trizma hydrochloric acid (Tris-HCl) with 1mM EDTA, pH 7.5 buffer solution. The CT-DNA solution in this buffer showed a UV absorption rate of about 2.5 at 260 and 280 nm, which means that the DNA did not contain sufficient proteins, i.e., it was pure (22). The DNA concentration was identified by an absorption spectroscopy using a molar extinction coefficient value of 6600 $dm^3mol^{-1}cm^{-1}$ at 260 nm. PTIH was dissolved in a solvent consisting of 5% DMSO and 95% pH 7.5 Tris buffer. With the constant concentration of PTIH (25 µM), the DNA concentration was gradually increased (2.5-25 µM), and absorption titration was performed. The study aim was to eliminate DNA self-absorption at wavelengths. Therefore, an equal amount of DNA was added to both the test solution and the reference solution. The Kb (intrinsic binding constant) value was calculated using the Wolfe-Shimmer equation (23) with the absorption titration method: [DNA] / (| εb-εa |) = [DNA] / (| εb-εf |) + 1 / {Kb (| εb-εf |)} where [DNA] is the DNA concentration in base pairs; εa, εf, and εb represent Aobsd/[PTIH], the extinction coefficient of the free complex (PTIH), and the extinction coefficient of PTIH in the fully DNA-bound form, respectively. The Kb value is described by the ratio of the slope to intercept in the graph [DNA] / (| εa - εf |) versus [DNA].

Statistical Analysis

Statistical analysis was shown with Prism V.8 Software. (GraphPad, USA). Non-linear regression analysis was performed for IC_{50} calculations, and Pearson's chi-square tests were used for the comparison of two different conditions or treatments. $p<0.05$ was considered significant.

RESULTS

We evaluated the cytotoxicity of the PTIH in 4 different cell lines by MTT test. Cells were treated with 8 different concentrations of PTIH containing equal amounts of DMSO in each well. After absorbance measurements, we calculated the IC_{50} values of PTIH for A549, HepG2, and HUH7 cells, and the results were 24, 24 and 17 µM, respectively (Figure 2). We also evaluated the cytotoxicity of PTIH on BEAS2B, which is a non-cancerous bronchial epithelial cell line, and the IC_{50} value of PTIH was found to be higher (87 µM) in these cells (Figure 2), which indicated that it might be less toxic to normal cells.

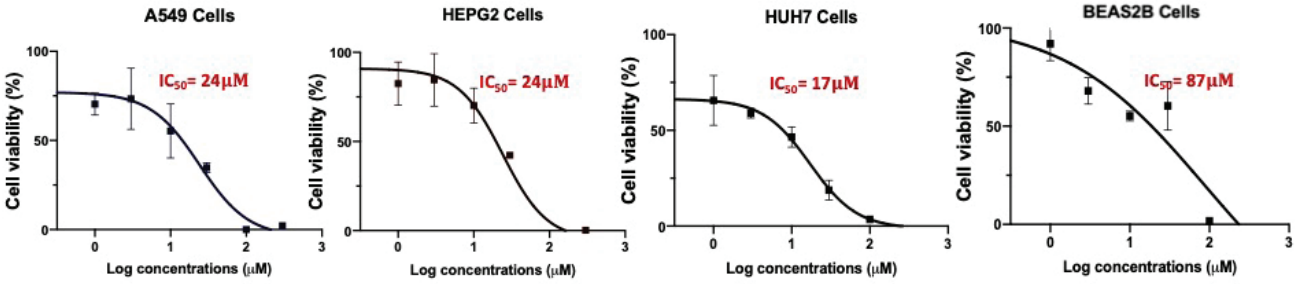

Figure 2. Cytotoxic effects of PTIH ([$Hg(SCN)_2(HL)$])on cancer and non-cancer cells. MTT (Thiazolyl Blue Tetrazolium Bromide) test was performed to evaluate cytotoxicity with the increased concentrations of PTIH (0-0.3-1-3-10-30-100 and 300 µM) for 24 hrs. Graphs show the best curve fit of non-linear regression analysis of 24h PTIH treated A549, HepG2, HUH7, and BEAS2B cells respectively. Calculated IC_{50} values of the PTIH on these cell lines are also given above each curve.

After determining the cytotoxicity of PTIH, we tested the apoptotic effect of PTIH in cancer cells. We performed a flow cytometry experiment to detect apoptotic cells after 48-hour incubation with 50 µM PTIH. The apoptotic cell ratio was calculated as 28.36% in the A549 cells, 99.30% in HepG2 cells, and 61.82% in HUH7 cells (Figure 3). There is a statistically significant difference between the apoptosis percentages of the control and the PTIH-treated cells.

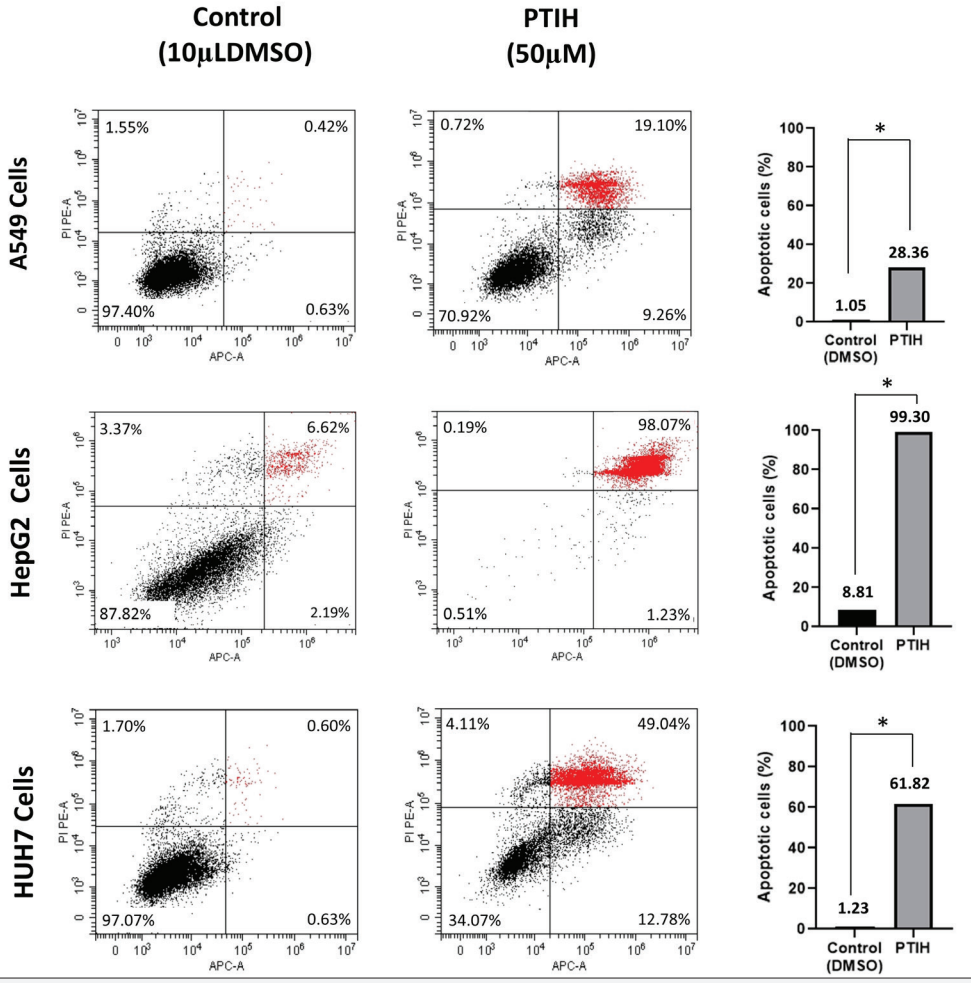

Figure 3. Apoptotic cell rates of A549, HepG2, and HUH7 cells treated with PTIH ([$Hg(SCN)_2(HL)$]) (50 µM) and equal amount of DMSO (Dimethyl Sulfoxide) as a control. Living and apoptotic cells were determined by flow cytometry. Both right quadrants (upper (late) and lower (early)) indicate the apoptotic cells of the population, while the left lower quadrant gives the percentage of viable cells. Percentages of entire (early and late) apoptotic cells in the A549, HepG2 and HUH7 cells are showed by bar diagrams (*$p<0.05$).

In addition, we performed a motility assay and demonstrated that PTIH strongly suppressed the migration of A549 cells. While 75.50±1.26% of the wound was closed in the control plate, there was 4.40±0.80% closure in the PTIH treated plate at the end of the 24-hour treatment (Figures 4 a-b). We also extracted RNA from the cells and ran a quantitative PCR analysis to detect E-cadherin mRNA level differences in DMSO and PTIH treated cells (Figure 4c). E-cadherin expression of cells treated with PTIH increased 9-fold (9.03±5.99) compared to the control.

We further assessed the effect of PTIH on the colony-forming ability of the cells, which the results showed that it significantly led to decreased colony formation in HepG2 and Huh7 cells in increasing concentrations (Figure 5).

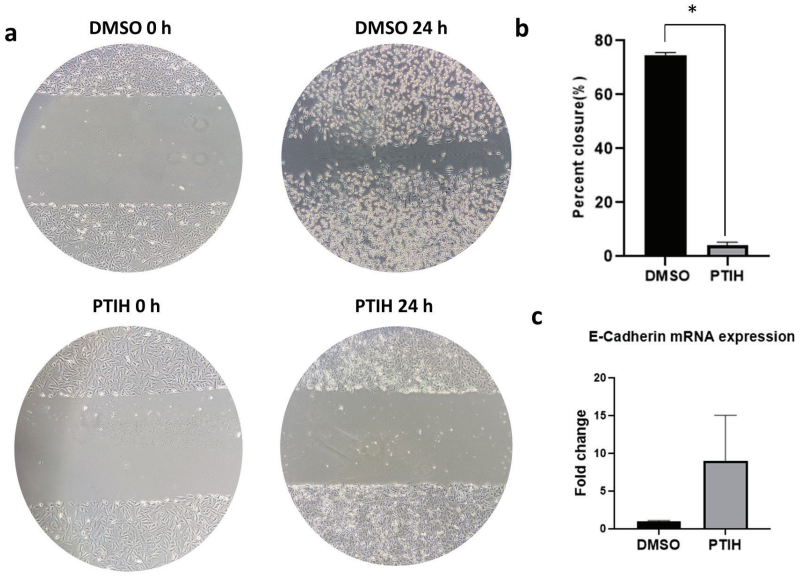

Figure 4. **a:** 0 and 24-hours representative images from the wound healing (motility) assay in the presence of DMSO, the solvent of PTIH ($[Hg(SCN)_2(HL)]$) and 50 micromolar PTIH ($[Hg(SCN)_2(HL)]$) as controls, **b:** shows percent wound closure bar graph (*p<0.05), **c:** shows a bar graph where gene expression of E-cadherin is normalized to 18S rRNA and fold differences are calculated using the comparative CT method.

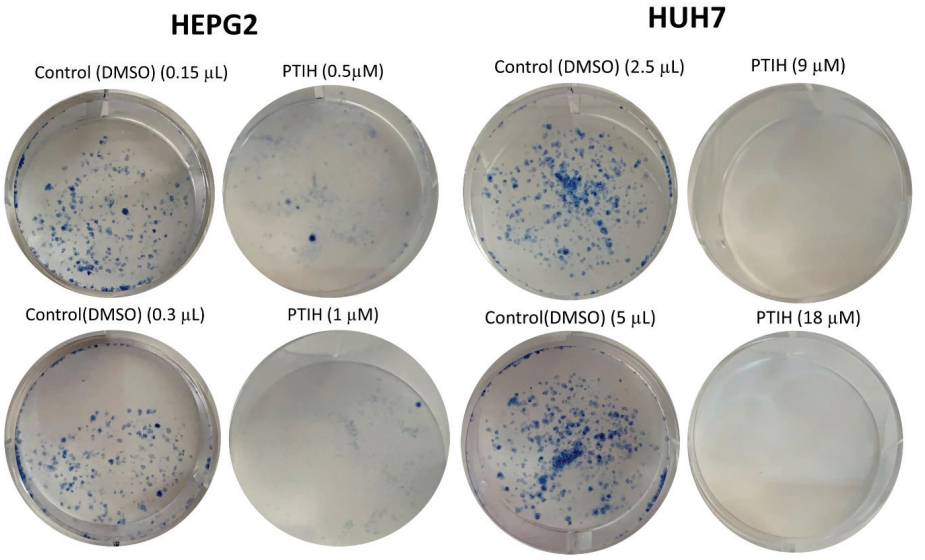

Figure 5. Colony formation assay was performed in HepG2 and HUH7 cells. Cells exposed to PTIH ($[Hg(SCN)_2(HL)]$) at two different concentrations. The results were compared to the negative control (DMSO) (Dimethyl Sulfoxide). Cells were allowed to grow for 10-14 days before staining with methylene blue solution to visualize colonies.

The addition of PTIH causes the intensity of pure BSA to increase in the absorption band at 280 nm and also the blue shift of about 5nm at 1 μM BSA with 10 μM PTIH (Figure 6). This result shows that PTIH changes the polarity of the microenvironment around the Trp and Tyr amino acids of BSA. The change in the absorption band of BSA in the presence of PTIH indicates that the PTIH-BSA interaction is in the form of static quenching (24-26).

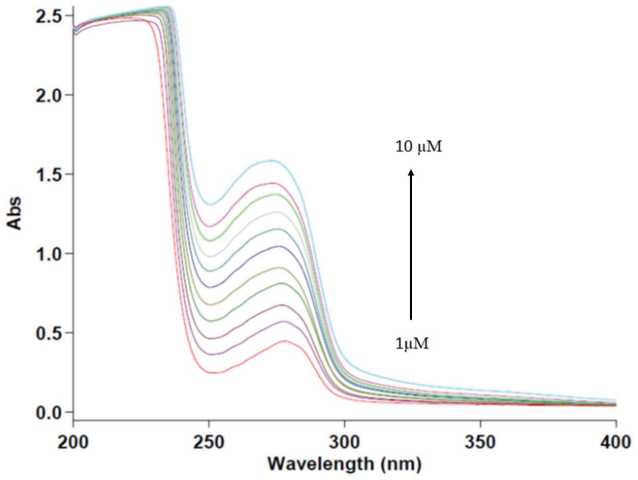

Figure 6. Absorption spectra of BSA (Bovine serum albumin) (1 μM) and with PTIH ([$Hg(SCN)_2(HL)$]) (0-10μM).

The UV absorption spectrum of PTIH as a result of increasing CT- DNA concentrations are shown in Figure 7. In the absence of DNA, PTIH exhibited maximum absorbance at 289 nm can be assigned to the π-π* transition. The hyperchromic effect was observed upon the addition of CT-DNA. Additionally, small blueshifts have been accompanied by the increase in peaks. This indicates an interaction between PTIH and CT-DNA (Kb $8.35x10^5$ L mol^{-1}).

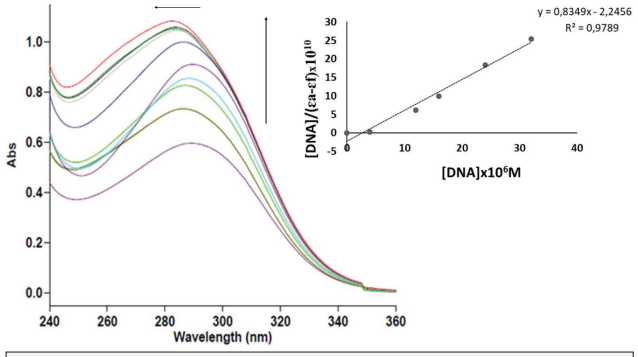

Figure 7. Absorption spectra of PTIH([$Hg(SCN)_2(HL)$]) (80 μM) in the presence of increasing amounts of CT-DNA (Calf Thymus-DNA) (in the range of 0-40 μM). Arrows show the absorbance changes upon increasing DNA concentration. (E) Plots of [DNA]/(εa - εf) versus [DNA] for the PTIH ([$Hg(SCN)_2(HL)$]) with CT-DNA (Kb = $8.35 x10^5$ M^{-1}).

DISCUSSION

According to the cytotoxicity results, PTIH was more effective than cisplatin in HUH7 cells compared to previous reports in the literature (IC_{50}= 58.77 μM (27) and 20.5 μM (28)) in the means of cell killing activity. The efficiency of PTIH in HepG2 cells was also substantially good compared to previous studies on some hydrazone metal complexes (15, 29). PTIH showed good cytotoxic activity in the A549 cell when compared to the effects of some similar hydrazone metal complexes in A549 cells (30, 31). In HUH7 cells, PTIH also showed good anticancer activity compared to some similar molecules in the literature (32, 33). In this study, we have not performed flow cytometric analyses on BEAS2B cells, which may be counted as a limitation, but the fact that the IC_{50} value of PTIH is higher in BEAS2B cells than in cancer cells indicate that PTIH will specifically kill cancer cells at low doses if it is used as a drug.

The biological activity of a metal complex is determined as much as the metal itself, the number of valence electrons, the conformational and electronic nature of the organic ligand it is in, and other groups attached to that ligand. The HL ligand has a flexible conformational structure and multiple hydrogen bonding sites. Aromatic rings at either end of the HL gain the ability to form π … π stacking interactions into the structure (34).

The anticancer activity mechanisms of Hg(II) complexes were not studied until 2016 (35). According to an *in silico* docking study with a Hg(II) complex, the binding energy to the epidermal growth factor receptor (EGFR protein) was calculated as -5.79 kcal/mol, and it was theoretically claimed that apoptosis could be induced with the complex in cells with EGFR mutations (11). In a recent study, it has been shown by docking studies that a Hg(II) complex binds to DNA, and it has been experimentally shown that it displays nuclease activity. Besides this, the same study claimed that Hg(II) activated G0/G1 cell arrest and apoptotic cell death in cancer cells (12). The thiocyanate groups (SCN) in its structure give some properties to PTIH. It is known that thiocyanates cause DNA damage by creating oxidative stress (36), and it has been reported that they inhibit some enzymes whose expression is increased in cancer due to the potential of binding to the cysteine amino acids of the sulfur atom in their structure (36, 37). In a study comparing different groups attached to the same metal complex, it was revealed that the SCN group had a better cytotoxic effect than the compounds containing other side groups (38).

In addition to cytotoxic activity, PTIH showed apoptosis induction as well as suppressed cell migration in cancer cells. In the repeated experiments, we obtained similar results that while apoptotic cell rate was lower in A549 cells, it showed very high apoptotic activity in HepG2 and HUH7 cells, which indicate that a possible active pathway was affected in hepatocellular carcinoma cells or a resistance mechanism might be in charge in A549 lung cancer cells. Different apoptotic activities of Hg(II) or hydrazone-based compounds in different cell lines are also encountered in the literature (12, 15). Which molecules in the

apoptotic pathway the drug candidate targets may be a new area of research. The deficiency of E-cadherin-induced cell-cell adhesion in tumor cells and its transformation from epithelial to mesenchymal characteristics and gaining invasive properties are the core of the metastasis pathways in most solid tumors (39). Therefore, we performed a motility assay and demonstrated that PTIH statistically significantly and strongly suppressed the migration of A549 cells. As a result, PTIH increased 9-fold (9.03±5.99) the expression of E-cadherin compared to DMSO in the A549 cell supporting motility assay results.

It is very important to examine the interaction mechanism of serum albumin, the most abundant protein in plasma, and drug candidates because the interactions of drugs with serum albumin may cause them to lose their biological properties or gain better biological activity while being transported in the body. BSA, which is similar to human serum albumin, is widely used in such drug studies. BSA binding studies are performed by the spectrophotometric titration method (UV-visible absorption). The absorption of BSA at 280 nm is monitored. The changes in the structure of aromatic amino acids tyrosine (Tyr), tryptophan (Trp), and phenylalanine (Phe) asa result of binding are reflected in the spectrum. Whether potent drugs bind statically or dynamically to BSA is determined by comparing the characteristic absorption spectra of pure BSA and BSA-drug solutions. Since the dynamic coupling only affects the excited state of the fluorophore group, no change is observed in the absorption spectra. Static bonding, on the other hand, causes a change in the absorption spectrum of the fluorophore group with the formation of PTIH with BSA (24-26).

The most common method used to examine the binding potential of metal complexes with DNA is electronic absorption titration (40, 41). If there is an interaction between the metal complexes and DNA, changes occur in the spectrum transitions of the complex. As a result of intercalative interactions between DNA and small molecules, hypochromism and redshift are usually observed in the spectrum (42). If DNA and small molecules perform groove bonding or electrostatic attraction between them, a hyperchromic effect showing conformational changes in the structure is observed, and a slight redshift can be observed. The hyperchromic effect and blueshift observed in the figure indicate that PTIH interacts with CT-DNA via groove binding and/or electrostatic attraction (42-45). Kb value of PTIH indicates that it has a good binding affinity with DNA in comparison with the Kb value for classical intercalator ethidium bromide ($Kb=1.4x10^5\ M^{-1}$) (46) and resembles studies in the literature (47, 48).

One of the limitations of this study is that we did not perform any experiment to analyze the possible molecular alterations of the compound in cell culture conditions, which may need further evaluation in future studies.

CONCLUSION

According to in vitro experiments on A549, HepG2, and HUH7 lung cancer cells, PTIH has been found to exert dose-dependent cytotoxic effects in cell lines. It has also been shown to induce apoptotic cell death. It was less cytotoxic to BEAS2B, a non-cancerous lung epithelial cell line. It was also determined by PCR analysis that it induces E-cadherin expression in A549 cells, indicating prevention of metastasis that was confirmed by cell motility assay. Moreover, PTIH has been proven to effectively stop colony generation in cancer cells. PTIH performed its antitumoral activity by interacting with DNA in grooves and/or electrostatically. Therefore, it may be a promising anti-tumor agent.

Acknowledgements: We thank Gaziantep University and Izmir Biomedicine and Genome Center (İBG) for providing the cell lines. We are also greatful to Çukurova University genetic diseases diagnosis and treatment center (AGENTEM) for device usage support.

Informed Consent: Written consent was obtained from the participants.

Peer Review: Externally peer-reviewed.

Author Contributions: Conception/Design of Study- B.S.D., Y.S.; Data Acquisition- B.S.D., A.S., E.D., E.N., M.O., G.M., Y.S.; Data Analysis/Interpretation- B.S.D., A.S., E.D., G.M., Y.S.; Drafting Manuscript- B.S.D., Y.S.; Critical Revision of Manuscript- Y.S.; Final Approval and Accountability- B.S.D., A.S., E.D., E.N., M.O., G.M., Y.S.

Conflict of Interest: Authors declared no conflict of interest.

Financial Disclosure: Authors declared no financial support.

REFERENCES

1. Szabó KJ, Wendt OF. Pincer and pincer type complexes, applications in synthesis and catalysis: Wiley-VCH, Weinheim, Germany, 2014.
2. Mahmoudi G, Bauzá A, Gurbanov AV, Zubkov FI, Maniukiewicz W, Rodríguez-Diéguez A, et al. The role of unconventional stacking interactions in the supramolecular assemblies of Hg(II) coordination compounds. CrystEngComm 2016; 18: 9056-66.
3. Mahmoudi G, Zareba JK, Bauzá A, Kubicki M, Bartyzel A, Keramidas A, et al. Recurrent supramolecular motifs in discrete complexes and coordination polymers based on mercury halides: prevalence of chelate ring stacking and substituent effects. CrystEngComm 2018; 20: 1065-76.
4. Blake AJ, Champness NR, Hubberstey P, Li WS, Withersby MA, Schröder M. Two- and three-dimensional CuSCN co-ordination networks including new CuSCN structural motifs. Coord Chem Rev 1999; 183: 117-38.
5. Sarkar M, Biradha K. Crystal engineering of metal-organic frameworks containing amide functionalities: Studies on network recognition, transformations, and exchange dynamics of guests and anions. Cryst Growth Des 2007; 7: 1318-31.
6. Beheshti A, Clegg W. Nobakht V, Harrington RW. Metal-to-ligand ratio as a design factor in the one-pot synthesis of coordination polymers with $[MS_4Cu_n]$ (M=W or Mo, n=3or 5) cluster nodes and a flexible pyrazole-based bridging ligand. Cryst Growth Des 2013; 13: 1023-32.
7. Angelusiu MV, Barbuceanu SF, Draghici C, Almajan GL. New Cu(II), Co(II), Ni(II) complexes with aroyl-hydrazone based ligand. Synthesis, spectroscopic characterization, and in vitro antibacterial evaluation. Eur J Med Chem 2010; 45: 2055-62.

8. Aslan HG, Ozcan S, Karacan N. Synthesis, characterization and antimicrobial activity of salicylaldehyde benzenesulfonylhydrazone (Hsalbsmh) and its Nickel(II), Palladium(II), Platinum(II), Copper(II), Cobalt(II) complexes. Inorg Chem Commun 2011; 14: 1550-53.
9. Xu Z, Zhang X, Zhang W, Gao Y, Zeng Z. Synthesis characterization DNA interaction and antibacterial activities of two tetranuclear cobalt(II) and nickel(II) complexes with salicylaldehyde 2-phenylquinoline-4-carboylhydrazone. Inorg Chem Commun 2011; 14: 1569-73.
10. Zhang L, He M, Zhang Y, Nilubol N, Shen M, Kebebew E. Quantitative high-throughput drug screening identifies novel classes of drugs with anticancer activity in thyroid cancer cells: opportunities for repurposing. J Clin Endocrinol Metab 2012; 97(3): E319-28.
11. Malella R, Konkanchi R, Guda R, Munirathinam N, Gandamalla D, Yellu NR, et al. Zn(II), Cd(II), and Hg(II) metal complexes of 2-aminonicotinaldehyde: Synthesis, crystal structure, biological evaluation, and molecular docking study. Inorganica Chim. Acta 2017; 469: 66-75.
12. Icsel C, Yilmaz VT, Aydinlik S, Aygün M. Zn(II), Cd(II) and Hg(II) saccharinate complexes with 2,6-bis(2- benzimidazolyl)pyridine as promising anticancer agents in breast and lung cancer cell lines via ROS-induced apoptosis. Dalton Trans 2020; 49: 7842-51.
13. Yumnan S, Rajkumari L. Thermodynamics of the complexation of N-(Pyridin-2-ylmethylene) isonicotinohydrazide with lighter lanthanides. J Chem Eng Data 2009; 54: 28-34.
14. Wolff SK, Grimwood DJ, McKinnon JJ, Turner MJ, Jayatilaka D, Spackman MA. Visualization and characterization of voids in crystalline materials. Dalton Trans 2011; 13: 1804-13.
15. Megger DA, Rosowski K, Radunsky C, Kösters J, Siteka B, Müller J. Structurally related hydrazone-based metal complexes with different antitumor activites variably induce apoptotic cell death. Dalton Trans 2017; 46: 4759-67.
16. Pape VFS, Türk D, Szabo P, Wiese M, Enyedy EA. Cook G, Synthesis and characterization of the anticancer and metal-binding properties of novel pyrimidinylhydrazone derivatives. Inorg Biochem 2015; 144: 18-30.
17. Pape VFS, Torh S, Füredi A, Szebenyi K, Lovrics A, Szabo P, et al. Design, synthesis and biological evaluation of thiosemicarbazones, hydrazinobenzothiazoles and arylhydrazones as anticancer agents with a potential to overcome multidrug resistance. Eur J Med Chem 2016; 117: 335-54.
18. Afkhami FA, Mahmoudi G, Qu F, Gupta A, Zangrando E, Fronteral A. Supramolecular architecture constructed from the hemidirected lead(II) complex with N'-(4-hydroxybenzylidene)isonicotinohydrazide. Inorganica Chim. Acta 2020; 502: 119350.
19. Mahmoudi G, Khandar AA, Afkhami AF, Miroslaw B, Gurbanov VA, Zubkov F, et al. Modulation of coordination in pincer-type isonicotinohydrazone Schiff base ligands by proton transfer. CrystEngComm 2019; 21: 108-17.
20. Saygideger Y, Saygıdeğer Demir B, Taskin Tok, Avci A, Sezan A, Baydar O, et al. Antitumoral effects of Santolina chameacyparissus on non-small cell lung cancer cells. J Exp Clin Med 2021; 38(3): 294-300.
21. https://www.biolegend.com/nl-be/products/apc-annexin-v-apoptosis-detection-kit-with-pi-9788.
22. Marmur J, Doty P. Determination of the base composition of deoxyribonucleic acid from its thermal denaturation temperature. J Mol Biol 1983; 5: 109-18.
23. Wolfe A, Shimer GH, Meehan T. Polycyclic aromatic hydrocarbons physically intercalate into duplex regions of denatured DNA. Biochemistry 1987; 26: 6392-96.
24. Raja DS, Bhuvanesh NSP, Natarajan K. Biological evaluation of a novel water- soluble sulfur bridged binuclear copper (II) thiosemicarbazone complex. Eur J Med Chem 2011; 46: 4584-94. (b)
25. Raja DS, Paramaguru G, Bhuvanesh NSP, Reibensipes JH, Reanganathan R, Natarajan K. Effect of terminal N-substitution in 2-oxo-1, 2-dihydroquinoline-3-carbaldehyde thiosemicarbazones on the mode of coordination, structure, interaction with protein, radical scavenging, and cytotoxic activity of copper(II) complexes. Dalton Trans 2011; 40: 4548-59. (a)
26. Gupta RK, Sharma G, Pandey R, Kumar A, Koch B, Li P-Z, et al. DNA/Protein binding, molecular docking, and in vitro anticancer activity of some thioether-dipyrrinato complexes. Inorg Chem 2013; 52: 13984-96.
27. Brito AF, Abrantes AM, Pinto-Costa C, Gomes AR, Mamede AC, Casalta-Lopes J, et al. Hepatocellular carcinoma and chemotherapy: the role of p53. Chemotherapy 2012; 58: 381-86.
28. Ye R-R, Peng W, Chen B-C, Jiang N, Chen X-Q, Mao Z-W, et al. Mitochondria-targeted artesunate conjugated cyclometalated iridium(III) complexes as potent anti-HepG2 hepatocellular carcinoma agents. Metallomics 2020; 12: 1131-41.
29. Machakanur SS, Patil BR, Badiger DS, Bakale RP, Gudasi KB, Bligh SWA. Synthesis characterization and anticancer evaluation of novel tri-arm star shaped 1, 3, 5-triazine hydrazones. J Mole Struct 2012; 1011: 121-27.
30. Dasgupta S, Karim S, Banerjee S, Saha M, Saha KD, Das D. Designing of novel zinc (II) Schiff base complexes having acyl hydrazone linkage: Study of phosphatates and anti-cancer activity. Dalton Trans 2020; 49: 1232-40.
31. Wang F, Yin H, Cui J, Zhang Y, Geng H, Hong M. DNA-binding and BSA interaction of diorganotin (IV) complexes derived from hydrazone Schiff base. J Organomet Chem 2014; 759: 83-91.
32. Balaji S, Subarkhan MKM, Ramesh R, Wang H, Semeril D. Synthesis and structure of arene Ru (II) N^O chelating complexes: In vitro cytotoxicity and cancer cell death mechanism. Organometallics, 2020; 39 (8): 1366-75.
33. Li Z-H, Yang D-X, Geng PF, Zhang J, Wei HM, Hu B, et al. Design, synthesis and biological evaluation of [1,2,3] triazolo[4,5-d] pyrimidine derivatives possessing a hydrazone moiety as antiproliferative agents. Eur J Med Chem 2016; 124: 967-80.
34. Saygıdeger Demir B, Mahmoudi G, Sezan A, Derinoz E, Nas E, Saygideger Y, et al. Evaluation of the antitumor activity of a series of the pincer-type metallocomplexes produced from isonicotinohydrazide derivative. J Inorg Biochem 2021; 223: 111525.
35. Marloye M, Berger G, Gelbcke M, Dufrasne F. A survey of the mechanisms of action anticancer transition metal complexes. Future Med Chem 2016; 8 (18): 2263-86.
36. Hać A, Brokowska J, Rintz E, Bartkowski M, Węgrzyn G, Antosiewicz AH. Mechanism of selective anticancer activity of isothiocyanates relies on diferences in DNA damage repair between cancer and healthy cells. Eur J Nutr 2020; 59: 1421-32.
37. Lin RK, Zhou N, Lyu YL, Tsai YC, Lu CH, Kerrigan J, et al. Dietary isothiocyanate induced apoptosis via thiol modifcation of DNA topoisomerase IIalpha. J Biol Chem 2011; 286: 33591-600.
38. El-bendary MM, Arshad MN, Asiri AM. Structure characterization and antitumor activity of palladium pseudo halide complexes with 4-acetylpyridine. J Coord Chem 2019; 72(18): 3088-101.
39. Ribatti D, Tamma R, Annese T, Epithelial-mesenchymal transition in cancer: A historical overview. Transl Oncol 2020; 13(6): 100773.
40. Kelly JM, Tossi AB, McConnell DJ, Uigin CO. A study of the interactions of some polypyridylruthenium(II) complexes with DNA using fluorescence spectroscopy, topoisomerisation, and thermal denaturation. Nucl Acids Res 1985; 13: 6017-34.

41. Abdel-Rahman LH, El-Khatib RM, Nassr LA, Abu-Dief AM, Ismael M, Seleem AA. Metal based pharmacologically active agents: synthesis, structural characterization, molecular modeling, CT-DNA binding studies and in vitro antimicrobial screening of iron(II) bromosalicylidene amino acid chelates. Spectrochim Acta A Mol Biomol Spectrosc 2014; 117: 366-78.
42. Rahban M, Divsalar A, Saboury AA, Golestani A. Nanotoxicity and spectroscopy studies of silver nanoparticle: calf thymus DNA and K562 as targets. J Phys Chem 2010; 114: 5798-803.
43. Sarwar T, Husain MA, Rehman SU, Ishqi, HM, Tabish M. Multi-spectroscopic and molecular modeling studies on the interaction of esculetin with calf thymus DNA. Mol Biosyst 2015; 11(2): 522-31.
44. Liu R, Yan H, Jiang J, Li J, Liang X, Yang D, et al. Synthesis, characterization, photoluminescence, molecular docking and bioactivity of Zinc (II) compounds based on different substituents. Molecules, 2020; 25(15): 3459.
45. Draksharap A, Boersma AJ, Leising M, Meetsma A, Browne WR, Roelfes G. Binding of copper(II) polypyridyl complexes to DNA and consequences for DNA-based asymmetric catalysis. Dalton Trans 2015; 44: 3647-55.
46. Li W, Ji YY, Wang JW, Zhu YM. Cytotoxic activities and DNA binding properties of 1-methyl-7H-indeno[1,2-b] quinolinium-7-(4-dimethylamino) benzylidene triflate. DNA Cell Biol 2012; 31(6): 1046-53.
47. Franich AA, Živković MD, Milovanović J, Arsenijević D, Arsenijević A, Milovanović M, et al. In vitro cytotoxic activities, DNA- and BSA-binding studies of dinuclear palladium(II) complexes with different pyridine-based bridging ligands. J Inorg Biochem 2020; 210: 111-58.
48. Li Y, Li Y, Wang N, Lin D, Liu X, Yang Y. Et al. Synthesis, DNA/BSA binding studies and in vitro biological assay of nickel(II) complexes incorporating tridentate aroylhydrazone and triphenylphosphine ligands. J Biomol Struct Dyn 2019; 38(17): 4977-96.

ISTANBUL UNIVERSITY PRESS

RESEARCH ARTICLE

Eur J Biol 2021; 80(2): 138-144

The Activation of PI3K/AKT/mTOR Signaling Pathway in Response to Cabazitaxel Treatment in Metastatic Castration-Resistant Prostate Cancer Cells

Isil Ezgi Eryilmaz[1], Gamze Guney Eskiler[2], Ceyda Colakoglu[1], Unal Egeli[1*], Gulsah Cecener[1]

[1]Bursa Uludag University, Faculty of Medicine, Medical Biology Department, Bursa, Turkey
[2]Sakarya University, Faculty of Medicine, Medical Biology Department, Sakarya, Turkey

ORCID IDs of the authors: I.E.E. 0000-0002-3316-316X; G.G.E. 0000-0002-2088-9914; C.C. 0000-0002-7471-5071; U.E. 0000-0001-7904-883X; G.C. 0000-0002-3820-424X

Please cite this article as: Eryilmaz IE, Guney Eskiler G, Colakoglu C, Egeli U, Cecener G. The Activation of PI3K/AKT/mTOR Signaling Pathway in Response to Cabazitaxel Treatment in Metastatic Castration-Resistant Prostate Cancer Cells. Eur J Biol 2021; 80(2): 138-144. DOI: 10.26650/EurJBiol.2021.1018938

ABSTRACT

Objective: Despite advances in treatment approaches, metastatic castration-resistant prostate cancer (mCRPC) remains a clinical challenge to treat. Cabazitaxel (Cab), a third-line chemotherapy option for mCRPC, exhibits limited efficiency due to the activation of different signaling pathways associated with drug resistance. The PI3K/AKT/mTOR activation has led to mCRPC progression, and long-term acquired Cab resistance. However, we aimed to assess the association of apoptotic efficiency of Cab with the PI3K/AKT/mTOR activation in mCRPC cells in the present study.

Materials and Methods: Cell viability, cell death, morphological analysis, PI3K/AKT/mTOR pathway activation by PI3K/MAPK dual activation assay, mRNA and miRNA expression analysis and immunofluorescence staining were performed in the Cab-treated PC3 cells.

Results: Cab caused a significant reduction in PC3 cell viability and triggered apoptotic death at 1 and 5 nM for 72 h. Cab significantly induced PI3K/AKT/mTOR activation, and increased mRNA and activated protein levels of AKT and mTOR in PC3 cells, despite its increased apoptotic effect. Furthermore, the expressions of miR-205 and miR-579, the PI3K/AKT/mTOR-targeted miRNAs, were upregulated after Cab treatment. Our findings have shown that the Cab treatment activated PI3K/AKT/mTOR pathway is associated with its apoptotic effect in mCRPC cells.

Conclusion: Although further studies are required to investigate the molecular mechanisms accompanying the Cab response in detail, the PI3K/AKT/mTOR activation, as an alteration related to the apoptotic effect of the drug, may play a role in Cab resistance in mCRPC cells, suggesting that combined therapy with PI3K/AKT/mTOR inhibitors may improve the Cab therapeutic efficiency.

Keywords: Cabazitaxel, Castration-resistant Prostate Cancer, AKT, mTOR, miRNAs

INTRODUCTION

Prostate cancer (PCa), the second most common solid tumor, is the fifth leading cause of cancer-related deaths in men (1). The recurrent form of the disease, castration-resistant prostate cancer (CRPC), frequently occurs after castration by surgery (orchiectomy) or chemically, with androgen deprivation therapy (ADT), which is the first-line treatment option in advanced PCa (2). Although there is a wide range of treatment options, including next-generation antiandrogens, autologous immunotherapy and internal radiotherapy for metastatic CRPC (mCRPC), chemotherapy with microtubule-targeting drugs, Paclitaxel (Pac) or Docetaxel

Corresponding Author: Unal Egeli E-mail: egeli@uludag.edu.tr
Submitted: 04.11.2021 • **Revision Requested:** 17.11.2021 • **Last Revision Received:** 22.11.2021 • **Accepted:** 22.11.2021 • **Published Online:** 07.12.2021

(Doc), is used as a standard first-line option (3). One class of these agents that is only approved for the patients with ADT- and Doc-resistant mCRPC is also the newer one, Cabazitaxel (Cab) (4). Despite these advances in mCRPC treatment over the past decade, long-term survival rates remain low, and there are no effective treatment options for mCRPC (5-8).

One of the molecular mechanisms, the activation of phosphatidylinositol-3-kinase (PI3K)/serine-threonine protein kinase B (AKT)/mammalian target of rapamycin (mTOR) pathway, has been strongly implicated in mCRPC progression and the acquired resistance to both conventional and targeted anticancer drugs (9-11). Liu et al. (2015) also indicate that PI3K/AKT/mTOR and mitogen-activated protein kinase (MAPK) signaling pathways play a role in the development of Pac resistance in mCRPC cells (12). Although Cab has a different chemical structure containing extra methyl groups compared to Pac and Doc, which enables it to be more effective in Doc-resistant mCRPC (13), mCRPC patients eventually show clinical resistance, and the underlying mechanism of Cab-resistance is poorly understood. A recent study regarding *in vitro* Cab resistance mechanisms has shown that Cab-resistant mCRPC cells exhibit altered expression in gene clusters of mitotic cells and nuclear division. Additionally, Cab-resistant cells (DU145CR and PC3CR) exhibit a different PI3K/AKT/mTOR and MAPK activity (14). However, these studies have focused on the role of signaling pathways in Doc-, Pac- and Cab-resistant PCa cells. Thus, the activation of these pathways in response to Cab treatment remains unclear at the genetic and epigenetic levels. The relationship between the apoptotic efficacy of Cab and the Cab-targeted signaling pathways needs further investigation in mCRPC cells.

In the present study, we report the relationship between the apoptotic efficacy of Cab and the PI3K/AKT/mTOR activation in PC3 mCRPC cells through the determination of *Akt* and *mTOR* gene expression, activated protein levels, and associated miRNAs' (miR-205-3p, miR-340-5p, miR-579-3p, and miR-429) levels in the Cab-treated cells.

MATERIALS AND METHODS

Cell Line and Culture Conditions

The mCRPC cell line PC3 (ATCC® CRL-1435™) was purchased from the American Type Culture Collection (ATCC) and cultured at 37°C and 5% CO_2 in a humid incubator (Panasonic, Japan). The Roswell Park Memorial Institute (RPMI)-1640 medium w/ sodium pyruvate and L-glutamine (Thermo Fisher Scientific, USA) supplemented with 10% fetal bovine serum (FBS, Thermo Fisher Scientific, USA), and 1% antibiotic-antimycotic solution (Wisent Bio Products, USA) was used as a growth medium and changed every 2 days. Cells were passaged with a Trypsin-EDTA 0.25% solution (Thermo Fisher Scientific, USA) as needed.

Drug Treatment

Cab (Catalog No: S3022) was purchased from Selleck Chemicals (Houston, TX) in a lyophilized powder form. The drug was prepared in dimethyl-sulphoxide (DMSO) to obtain a 5 mM stock solution as indicated in the datasheet and stored at -80°C. An intermediate solution of 100 nM was freshly diluted with a growth medium just before the experiments. The Cab doses were applied directly to the cultured cells on the plates. The amount of DMSO (Sigma-Aldrich, Germany) applied to cells was always kept below the toxic concentration [<0.01% (v/v)].

Cell Viability

The seeded cells, into 96-well plates at a density of $2x10^4$/well, were incubated for attachment. Two concentrations of Cab, 1 and 5 nM, were exposed to the cells for 72 h. After 10 µl WST-1 reagent (BioVision, San Francisco, CA) was applied to each well, the cells were incubated until they metabolized the dye in a growth atmosphere. Relative cell viability was detected by obtaining absorbances for color intensity at 450 nm in a TriStar² S LB 942 microplate reader (Berthold Technologies, Germany). Each treatment included three replicates for statistical data analysis.

Apoptotic and Morphological Evaluation

For determining the apoptotic effect of Cab, the cells ($5x10^5$cells/well) were seeded into 6-well plates and the drug treatment at 1 and 5 nM was applied for 72 h. After the indicated time, the cell staining was performed with a Muse Annexin V & Dead Cell Kit (Merck Millipore, Germany) reagent for 30 min in the dark. Then, apoptotic cells were analyzed in three replicates in a Muse Cell Analyzer (Merck Millipore, Germany). For morphological assessment, the cells were stained with acridine orange dye after the fixation step with a 4% paraformaldehyde (PFA) solution (Sigma-Aldrich, Germany). Morphological changes in Cab-treated cells were observed under a cell imaging system (Thermo Fisher Scientific, Waltham, MA, USA).

PI3K/MAPK Dual Activation Assay

Activation of PI3K/MAPK pathways was examined simultaneously in the Cab-treated cells using a Muse PI3K/MAPK Dual Pathway Activation Kit that included two antibodies, a phospho-specific AKT (Ser473) and a phospho-specific ERK1/2 (Thr202/Tyr204, Thr185/Tyr187). Briefly, the cells were cultured in 6-well plates at an appropriate density and treated with 1 and 5 nM Cab for 72 h. After, the drug administration, fixation and permeabilization steps were performed according to the manufacturer's instructions. The staining was carried out with an antibody cocktail solution for 30 min and kept in the dark. Then, the pathway examination was obtained in triplicate in a Muse Cell Analyzer (Merck Millipore, Germany).

Gene and miRNA Expression

After treatment with 1 and 5 nM Cab for 72 h, total RNA samples and miRNAs were separately isolated from PC3 cells with a Total RNA I kit (Omega Bio-Tek Inc, Norcross, GA) and NucleoSpin miRNA Small RNA isolation kit (Macherey-Nagel, Germany), respectively. All RNA samples were checked for A_{260}/A_{280} value and quantity with a spectrophotometer (Beckman Coulter, Inc., Fullerton, CA, USA). The reverse-transcription step was performed using a High-Capacity cDNA Reverse Transcription Kit (Applied Biosystems, Foster City, CA) and a miScript II RT Kit (Qiagen, Hilden, Germany). Then, RT-qPCR was done in an amplification

mix containing miScript SYBR Green PCR Kit (Qiagen, Hilden, Germany) for miScript Primer Assays (Qiagen, Hilden, Germany) and TaqMan Gene Expression Master Mix for mRNAs (Hs00178289_m1 *AKT* and Hs00234508_m1 *mTOR*) in a StepOnePlus Real-Time PCR System (Applied Biosystems, Foster City, CA). The miRNAs used in the study with their catalog numbers were miR-205-3p (MS00016793), miR-340-5p (MS00031759), miR-579-3p (MS00007805) and miR-429 (MS00004193). In this way, relative gene and miRNA expression levels were determined in Cab-treated cells. As internal controls, Hs_RNU6-2_11 (MS00033740) and *Actin beta* (Hs01060665_g1 *ACTB*) were used for normalization. All expression analysis was performed in triplicate.

Immunofluorescence Staining for Phosphorylated AKT and mTOR

To visualize the subcellular localization of phosphorylated AKT and mTOR proteins, the Cab-treated PC3 cells were fixed with 4% PFA and blocked with 5% normal goat serum. Then, the cells were incubated with primary antibodies (Santa Cruz Biotechnology, Germany), mouse p-AKT1/2/3 (sc-514021), and mouse p-mTOR (sc-293133). Subsequently, the cells were treated with goat anti-mouse Alexa Fluor 488 seconder antibody (Abcam, Cambridge, UK). DAPI (Sigma Aldrich, St. Louis, Missouri, USA) staining was performed for nuclear visualization. Finally, the cells were examined under a cell imaging system (Thermo Fisher Scientific, Waltham, MA, USA).

Statistical Analysis

The GraphPad Prism 6.0 software (La Jolla, CA, USA) was used for statistics. The results were presented as the mean ± standard deviation (SD). The significance of differences between the groups was assessed using an analysis of variance (ANOVA) with a Post-hoc test. Relative expressions of indicated genes and miRNAs were evaluated by using the 2^-(ΔΔCt) method in a web-based tool at https://geneglobe.qiagen.com/us/analyze/. In all analyses, a p-value less than 0.05 was considered statistically significant.

RESULTS

Cytotoxic and Apoptotic Effect of Cab on PC3 Cells

Firstly, we evaluated the effective Cab concentrations inducing apoptosis in PC3 mCRPC cells. No significant cytotoxic effect was detected for 24 and 48 h. However, as shown in Figure 1A, the 1

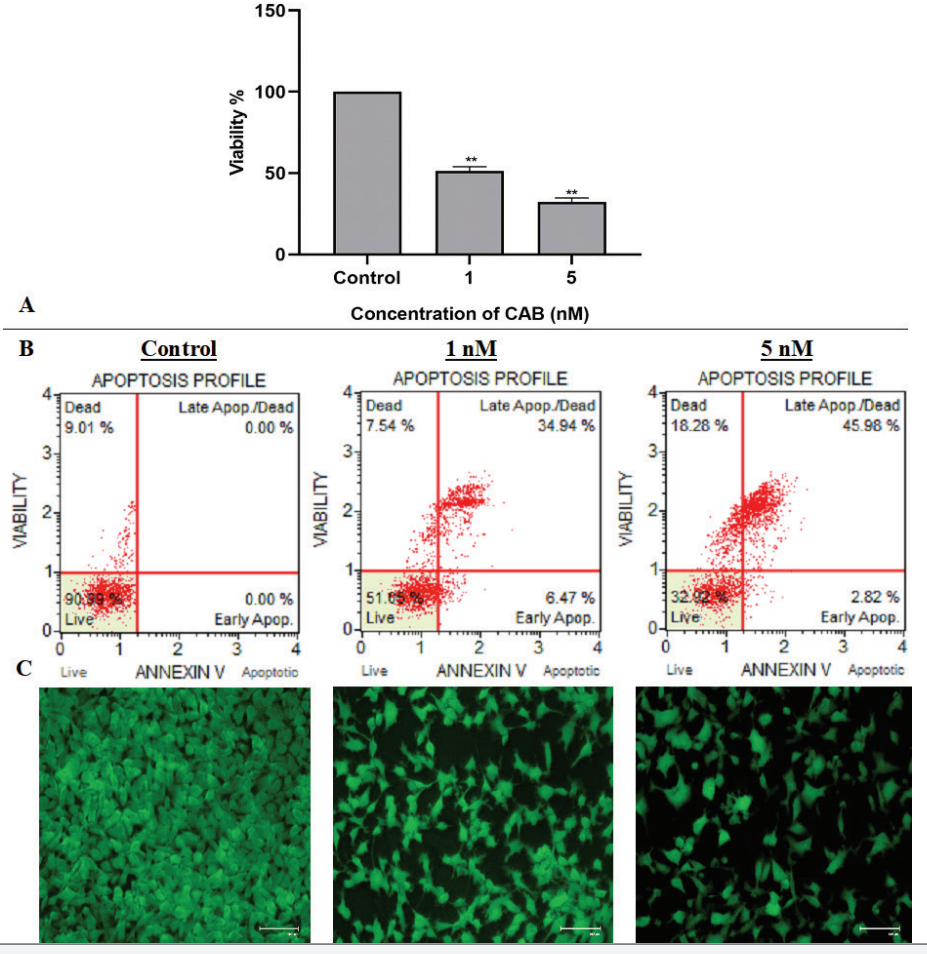

Figure 1. **(A)** Cytotoxic and **(B)** apoptotic effects of 1 and 5 nM Cabazitaxel treatment for 72 h in PC3 metastatic castration-resistant prostate cancer cells, $^{**}p<0.01$ **(C)** Morphological changes of the cells treated with 1 and 5 nM Cabazitaxel for 72 h, respectively at 100 µm scale.

and 5 nM Cab treatment significantly decreased the cell viability to 51.2±2.7% and 32.3±2.3% for 72 h, respectively (p<0.01). The IC_{50} value of Cab was calculated as 1.25 nM for PC3 cells at 72 h. When the apoptotic effect of Cab was evaluated, the total apoptotic cells were found to increase by 41.4% and 48.8% after the 1 and 5 nM Cab treatment, respectively (Figure 1B). Additionally, morphological changes regarding apoptotic cell death were observed in the Cab-treated cells. Disappeared cytoplasmic extension, cell disassembly, and bleb formation were more prominent in the 5 nM Cab-treated group, as shown in Figure 1C.

The Activation of MAPK/PI3K Pathways Upon Treatment with Cab

We also examined the alterations in dual MAPK/PI3K pathway activation in response to apoptotic effect in the 1 and 5 nM Cab treatments in PC3 cells for 72 h. As represented in Figure 2A, our findings revealed that ERK activation was not affected by any of the Cab treatments. However, the percentage of AKT activated cells significantly increased from 27.16±0.05% to 59.9±0.07% and 62.01±0.33% in the 1 and 5 nM Cab-treated groups, respectively (p<0.01). The negative cell population percentage decrease was also consistent with the increase in the AKT-activated cells (Figure 2B). Thus, we showed that the PI3K/AKT/mTOR pathway, rather than MAPK, was activated in PC3 cells despite the apoptotic effect of Cab.

The Effect of Cab on the Expression Levels of AKT and mTOR

Cab treatments caused a significant increase in the mRNA levels of *AKT* and *mTOR* compared with the untreated control group (Figure 3A). The 1 nM Cab treatment upregulated the *AKT* level

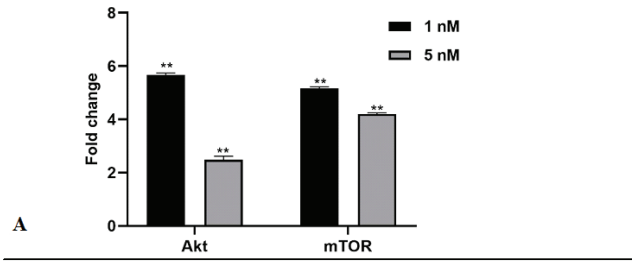

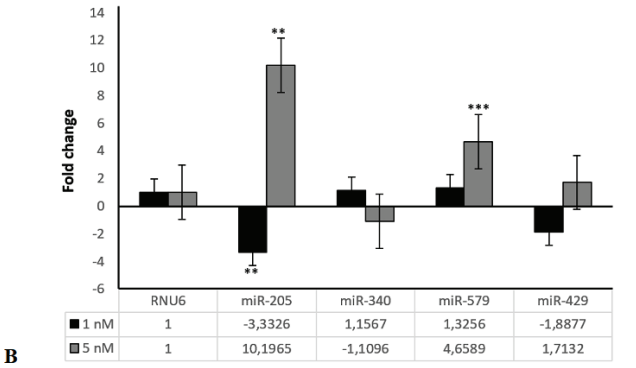

	RNU6	miR-205	miR-340	miR-579	miR-429
1 nM	1	-3,3326	1,1567	1,3256	-1,8877
5 nM	1	10,1965	-1,1096	4,6589	1,7132

Figure 3. The relative fold changes in the RNA expression level of **(A)** Serine/threonine protein kinase B (*Akt*) and mammalian target of rapamycin (*mTOR*) **(B)** Phosphatidylinositol-3-kinase (PI3K)/serine-threonine protein kinase B (AKT)/mammalian target of rapamycin (mTOR) pathway targeting microRNAs (miRNAs) after Cabazitaxel treatment with 1 and 5 nM for 72 h in PC3 cells. **p<0.01, ***p<0.001.

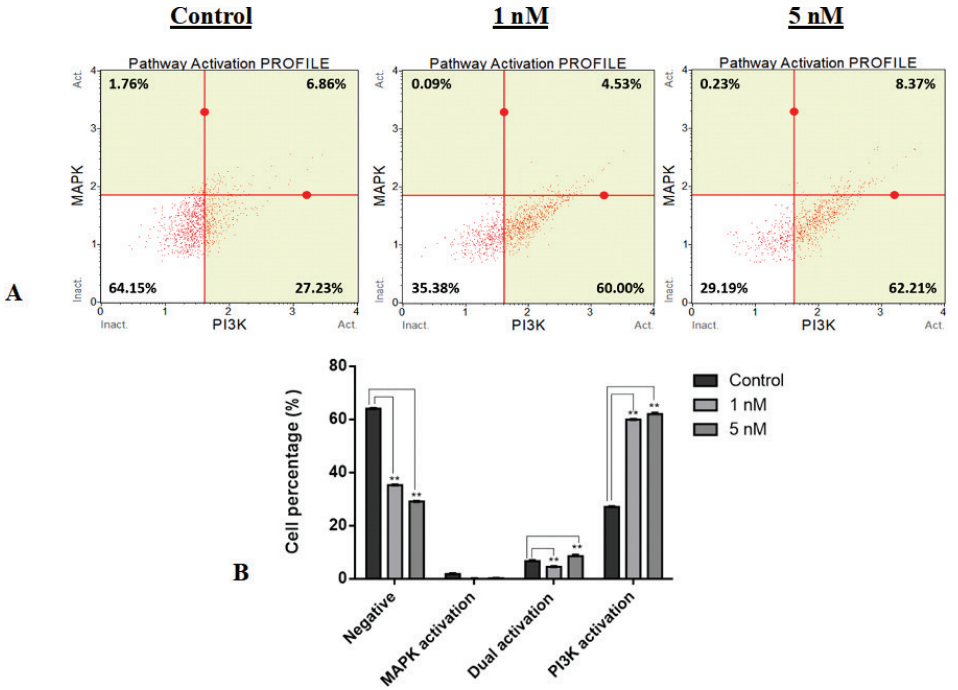

Figure 2. The results of mitogen-activated protein kinase (MAPK)/phosphatidylinositol-3-kinase (PI3K) activation in Cabazitaxel-treated PC3 cells. **(A)** Histograms of PI3K/MAPK dual pathway activation assay. **(B)** Statistical comparison of the MAPK/PI3K activated cell populations after 1 and 5 nM Cabazitaxel treatment for 72 h compared to the untreated control group, **p<0.01.

by 5.67-fold (p<0.01). A noticeable increase (5.17-fold, p<0.01) was also detected in *mTOR* expression for the 1 nM Cab-treated cells. Additionally, a significant upregulation of the indicated genes was detected in the 5 nM treatment groups, as shown in Figure 3A. However, higher expression levels of *AKT* and *mTOR* were observed in the 1 nM treatment group.

The Effect of Cab on the Expression Levels of miRNAs

Through a web-based tool, DIANA-miRPath, we selected four miRNAs that target the PI3K/AKT/mTOR signaling (miR-205-3p, miR-340-5p, miR-579-3p, and miR-429), and showed that neither miR-340 nor miR-429 levels changed after Cab treatment. However, the expression level of miR-205 was significantly down-regulated 3.33-fold (p<0.01) after the 1 nM Cab treatment. However, the expression levels of miR-205 and miR-579 were significantly upregulated 10.19- (p<0.01) and 4.65- (p<0.001) folds in the 5 nM Cab-treated group, respectively (Figure 3B).

The Effect of Cab on the Subcellular Localization of Phosphorylated AKT and mTOR

Cab treatment changed the subcellular localization of p-AKT and p-mTOR, as shown in Figure 4. The cytoplasmic expression of the activated form of AKT, p-AKT, increased after the 1 and 5 nM Cab treatments for 72 h, compared with the levels in the untreated cells (Figure 4A). Moreover, in connection with the activation of p-AKT, a higher nuclear and cytoplasmic expression of p-mTOR was visualized in the Cab-treated cells (Figure 4B). These results were consistent with the AKT/mTOR activation in the Cab-treated PC3 cells, as shown in Figure 2.

DISCUSSION

Our study determined that Cab induced the PI3K/AKT/mTOR signaling activation in PC3 mCRPC cells despite its significant apoptotic effect. The findings showed that Cab treatment led to a significant increase in AKT activation and mRNA level of *AKT* and *mTOR*. These findings were supported by immunofluores-

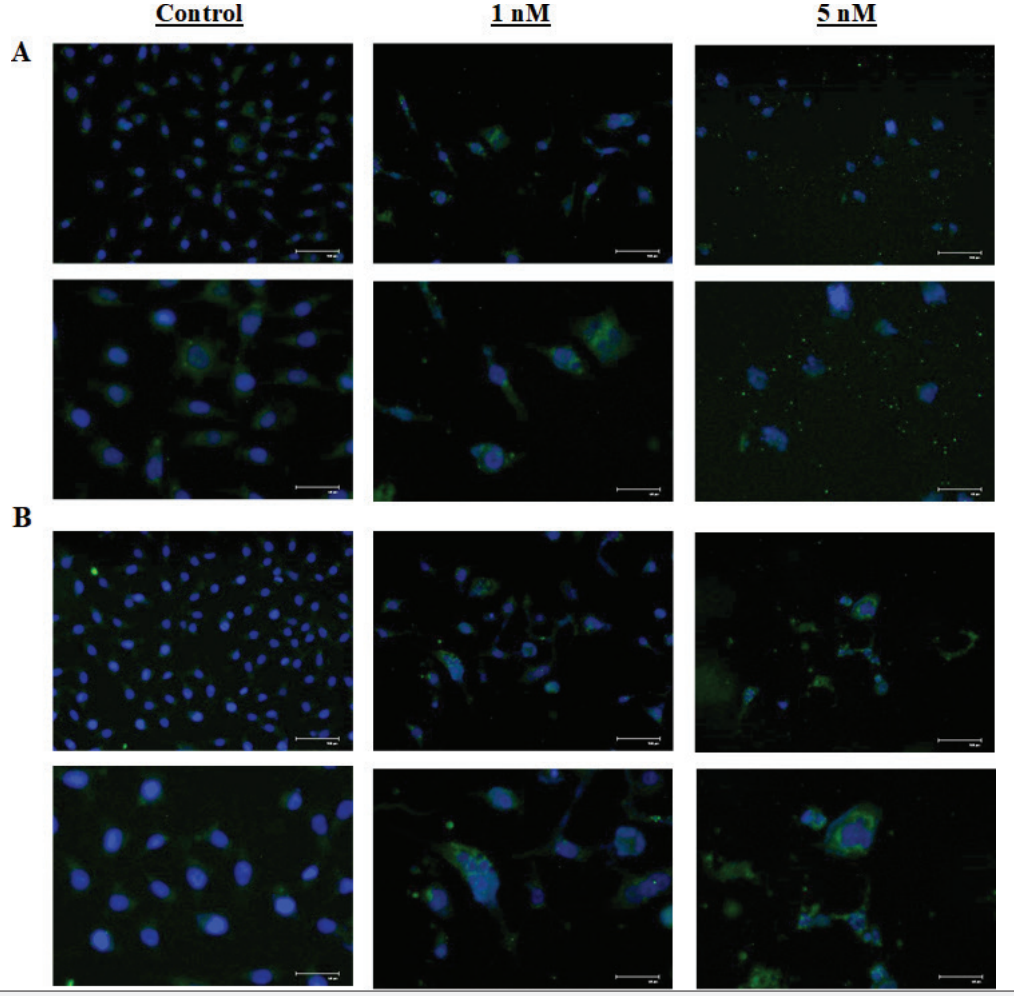

Figure 4. Observation of the differences in the subcellular localization of phosphorylated **(A)** Serine/threonine protein kinase B (AKT) and **(B)** Mammalian target of rapamycin (mTOR) by immunofluorescence staining in 1 and 5 nM Cabazitaxel-treated PC3 cells at two different scales (100 and 50 µm).

cence staining of p-AKT and p-mTOR protein levels. Additionally, the PI3K/AKT/mTOR activation was mediated by the upregulation of miR-205 and miR-579 in the Cab-treated PC3 cells.

Metastatic CRPC exhibits a poor prognosis due to decreased therapy response and drug resistance (15). Microtubule-targeting drugs are used as first-line options for mCRPC patients who have progressed after ADT, surgical or medical castration (16,17). Cab, the new generation taxane, has been more active due to its improved structure than the other taxane-based chemotherapeutics (7,13,18,19). Thus, it has been approved for mCRPC patients progressing after Doc treatment. Although Cab is a promising alternative, mCRPC remains a significant therapeutic challenge (7,8,14,20).

PI3K/AKT/mTOR is one of the major oncogenic pathways for PCa (21). The phosphorylated AKT (p-AKT) is reported to be upregulated in advanced PCa, directly linked to androgen receptor signaling, and contributes to CRPC progression (22-24). Moreover, recent reports have also indicated that the activation of PI3K/AKT/mTOR might be one of the resistance mechanisms after prolonged treatment, approximately two years, with taxane-based chemotherapeutics (12,14,15). However, the alterations in this pathway accompanied by the apoptotic effect of Cab in mCRPC cells have not been investigated yet.

Herein, we first investigated the role of the PI3K/AKT/mTOR signaling pathway in the response of Cab in mCRPC cells. Our results showed that Cab significantly triggered late apoptosis in the treated cells for 72 h. Interestingly, the Cab-mediated PI3K/AKT activation increased with the apoptotic effect of the drug. In the 5 nM Cab-treated cells, apoptosis and PI3K/AKT activation were more prominent than in the 1 nM treatment group. Cab treatment also resulted in the upregulation of AKT and mTOR at both mRNA and protein levels in PC3 cells at 72 h. These results suggest that, despite its apoptotic effect, Cab plays a role in the upregulation of the PI3K/AKT, which contributes to the survival and progression of PCa cells, as contributing to a previous study (12). Although the findings point to the role of PI3K/AKT/mTOR signaling in the Cab therapy response, the underlying molecular mechanisms of *in vitro* Cab-induced PI3K/AKT/mTOR signaling need further investigation.

Moreover, Cab significantly altered the expression levels of miR-205 and miR-579. A decreased level of miR-205 as an up-regulator of PI3K/AKT signaling has been associated with the worse clinical outcome in PCa patients (25,26). Besides, miR-579 has been reported to be related to PCa recurrence (27). However, in glioblastomas, miR-579 has also been shown to directly target the 3'UTR of mTOR, exhibiting a tumor-suppressive effect (28). We found that, as compatible with the AKT activation, 1 nM Cab significantly down-regulated miR-205. However, 5 nM Cab caused a significant upregulation of miR-205 and miR-579 levels. Thus, the alterations of miR-205 and miR-579 could be mediated by Cab-induced PI3K/AKT activation. The Cab also increased the cytoplasmic and nuclear expression of p-AKT and p-mTOR in PC3 cells. Besides being a cytoplasmic kinase, the active form of mTOR is also found in the nucleus of many cancer cells (29). The nuclear-localized mTOR involves transcription of rDNA and tRNA genes with RNA polymerase I and III, which contribute to cell growth, protein synthesis, and proliferation (30,31). Therefore, we concluded that the activated p-AKT and p-mTOR might contribute to the survival of PC3 cells, which are not undergoing apoptotic death after 72 h Cab treatment. However, further investigations are required to identify the relationship between Cab efficacy and PI3K/AKT/mTOR pathway activation and related target genes or transcription factors, including GSK3β and FOXO1.

CONCLUSION

Consequently, Cab treatment induced apoptotic cell death in PC3 mCRPC cells. However, Cab simultaneously activated the PI3K/AKT/mTOR signaling pathway in the cells. Based on the results, we suggest that the PI3K/AKT/mTOR signaling pathway alterations may represent an early resistance mechanism for Cab treatment in mCRPC cells. Thus, further *in vitro* and *in vivo* studies should focus on combined or subsequent therapy with Cab and PI3K/AKT/mTOR inhibitors in mCRPC cells and PI3K/AKT/mTOR pathway-associated genes or transcription factors.

Informed Consent: Written consent was obtained from the participants.

Peer Review: Externally peer-reviewed.

Author Contributions: Conception/Design of Study- I.E.E., G.G.E., U.E.; Data Acquisition- I.E.E., G.G.E.; Data Analysis/Interpretation- I.E.E., G.G.E., U.E., C.C.; Drafting Manuscript- I.E.E., G.G.E., C.C.; Critical Revision of Manuscript- U.E., G.C.; Final Approval and Accountability- I.E.E., G.G.E., U.E., C.C., G.C.

Conflict of Interest: Authors declared no conflict of interest.

Financial Disclosure: This study was supported by a grant from the Scientific Research Projects Foundation of Bursa Uludag University, Bursa, Turkey [Project No. BUAP(T)-2015/4].

REFERENCES

1. Ferlay J, Ervik M, Lam F, Colombet M, Mery L, Piñeros M, et al. Global cancer observatory: cancer today 2020. Lyon, France: International Agency for Research on Cancer 2018. https://gco.iarc.fr/today. Accessed May 27, 2021.
2. Huang Y, Jiang X, Liang X, Jiang G. Molecular and cellular mechanisms of castration resistant prostate cancer. Oncol Lett 2018; 15: 6063-76.
3. Lowrance WT, Roth BJ, Kirkby E, Murad MH, Cookson MS. Castration-Resistant Prostate Cancer: AUA Guideline Amendment 2015. J Urol 2015; 195: 1444-52.
4. Abidi A. Cabazitaxel: A novel taxane for metastatic castration-resistant prostate cancer-current implications and future prospects. J Pharmacol Pharmacother 2013; 4: 230-7.
5. de Bono JS, Oudard S, Ozguroglu M, Hansen S, Machiels JP, Kocak I, et al. Prednisone plus cabazitaxel or mitoxantrone for metastatic castration-resistant prostate cancer progressing after docetaxel treatment: a randomised open-label trial. Lancet 2010; 376: 1147-54.

6. Nuhn P, De Bono JS, Fizazi K, Freedland SJ, Grilli M, Kantoff PW, et al. Update on Systemic Prostate Cancer Therapies: Management of Metastatic Castration-resistant Prostate Cancer in the Era of Precision Oncology. Eur Urol 2019; 75: 88-99.
7. Tsao CK, Cutting E, Martin J, Oh WK. The role of cabazitaxel in the treatment of metastatic castration-resistant prostate cancer. Ther Adv Urol 2014; 6:97-104.
8. Rouyer M, Oudard S, Joly F, Fizazi K, Tubach F, Jove J, et al. Overall and progression-free survival with cabazitaxel in metastatic castration-resistant prostate cancer in routine clinical practice: the FUJI cohort. Br J Cancer 2019; 121: 1001-8.
9. Taylor BS, Schultz N, Hieronymus H, Gopalan A, Xiao Y, Carver BS, et al. Integrative genomic profiling of human prostate cancer. Cancer Cell 2010; 18: 11-22.
10. Bitting RL, Armstrong AJ. Targeting the PI3K/Akt/mTOR pathway in castration-resistant prostate cancer. Endocr Relat Cancer 2013; 20: R83-99.
11. Martini M, De Santis MC, Braccini L, Gulluni F, Hirsch E. PI3K/AKT signaling pathway and cancer: an updated review. Ann Med 2014; 46: 372-83.
12. Liu Z, Zhu G, Getzenberg RH, Veltri RW. The Upregulation of PI3K/Akt and MAP Kinase Pathways is Associated with Resistance of Microtubule-Targeting Drugs in Prostate Cancer. J Cell Biochem 2015; 116: 1341-9.
13. Paller CJ, Antonarakis ES. Cabazitaxel: a novel second-line treatment for metastatic castration-resistant prostate cancer. Drug Des Devel Ther 2011; 5: 117-24.
14. Hongo H, Kosaka T, Oya M. Analysis of cabazitaxel-resistant mechanism in human castration-resistant prostate cancer. Cancer Sci 2018; 109: 2937-45.
15. Bumbaca B, Li W. Taxane resistance in castration-resistant prostate cancer: mechanisms and therapeutic strategies. Acta Pharm Sin B 2018; 8: 518-29.
16. Tannock IF, de Wit R, Berry WR, Horti J, Pluzanska A, Chi KN, et al. Docetaxel plus prednisone or mitoxantrone plus prednisone for advanced prostate cancer. N Engl J Med 2004; 351: 1502-12.
17. Petrylak DP, Tangen CM, Hussain MH, Lara PN Jr, Jones JA, Taplin ME, et al. Docetaxel and estramustine compared with mitoxantrone and prednisone for advanced refractory prostate cancer. N Engl J Med 2004; 351: 1513-20.
18. Gottesman MM, Fojo T, Bates SE. Multidrug resistance in cancer: role of ATP-dependent transporters. Nat Rev Cancer 2002; 2: 48-58.
19. Duran GE, Derdau V, Weitz D. Cabazitaxel is more active than first-generation taxanes in ABCB1(+) cell lines due to its reduced affinity for P-glycoprotein. Cancer Chemother Pharmacol 2018; 81: 1095-103.
20. de Wit R, de Bono J, Sternberg CN, Fizazi K, Tombal B, Wülfing C, et al. Cabazitaxel versus Abiraterone or Enzalutamide in Metastatic Prostate Cancer. N Engl J Med 2019; 381: 2506-18.
21. Janku F, Yap TA, Meric-Bernstam F. Targeting the PI3K pathway in cancer: are we making headway? Nat Rev Clin Oncol 2018; 15: 273-91.
22. Malik SN, Brattain M, Ghosh PM, Troyer DA, Prihoda T, Bedolla R, et al. Immunohistochemical demonstration of phospho-Akt in high Gleason grade prostate cancer. Clin Cancer Res 2002; 8: 1168-71.
23. Kosaka T, Miyajima A, Shirotake S, Suzuki E, Kikuchi E, Oya M. Long-term androgen ablation and docetaxel up-regulate phosphorylated Akt in castration resistant prostate cancer. J Urol 2011; 185: 2376-81.
24. Mulholland DJ, Tran LM, Li Y, Cai H, Morim A, Wang S. et al. Cell autonomous role of PTEN in regulating castration-resistant prostate cancer growth. Cancer Cell 2011; 19: 792-804.
25. Bhatnagar N, Li X, Padi SKR, Zhang Q, Thang M-S, Guo B. Downregulation of miR-205 and miR-31 confers resistance to chemotherapy-induced apoptosis in prostate cancer cells. Cell Death Dis 2010; 1: e105.
26. Hagman Z, Haflidadóttir BS, Ceder JA, Larne O, Bjartell A, Lilja H, et al. miR-205 negatively regulates the androgen receptor and is associated with adverse outcome of prostate cancer patients. Br J Cancer 2003; 108: 1668-76.
27. Pashaei E, Pashaei E, Ahmady M, Ozen M, Aydin N. Meta-analysis of miRNA expression profiles for prostate cancer recurrence following radical prostatectomy. PLoS One 2017; 12: e0179543.
28. Kalhori MR, Irani S, Soleimani M, Arefian E, Kouhkan F. The effect of miR-579 on the PI3K/AKT pathway in human glioblastoma PTEN mutant cell lines. J Cell Biochem 2019; 120: 16760-74.
29. Zhang X, Shu L, Hosoi H, Murti KG, Houghton PJ. Predominant nuclear localization of mammalian target of rapamycin in normal and malignant cells in culture. J Biol Chem 2002; 277: 28127-34.
30. Tsang CK, Liu H, Zheng XF. mTOR binds to the promoters of RNA polymerase I- and III-transcribed genes. Cell Cycle 2010; 953-7.
31. Warner JR, Vilardell J, Sohn JH. Economics of ribosome biosynthesis. Cold Spring Harb Symp Quant Biol 2001; 66: 567-74.

ISTANBUL UNIVERSITY PRESS

RESEARCH ARTICLE

Eur J Biol 2021; 80(2): 145-153

Proteomic Analysis Revealed Underlying Biological Pathways Associated with Hormetic Response of Hormone-Positive Breast Cancer Cell Line Exposed to Low-Dose Flavonoid Mixture

Mete Bora Tuzuner[1], Ayse Begum Ceviz[2]

[1]Acıbadem Labmed Medical Laboratories, Research and Development Center, Istanbul, Turkey
[2]Istanbul Health and Technology University, Faculty of Medicine, Department of Medical Genetics, Istanbul, Turkey

ORCID IDs of the authors: M.B.T. 0000-0001-8924-4850; A.B.C. 0000-0002-3635-8421

Please cite this article as: Tuzuner MB, Ceviz AB. Proteomic Analysis Revealed Underlying Biological Pathways Associated with Hormetic Response of Hormone-Positive Breast Cancer Cell Line Exposed to Low-Dose Flavonoid Mixture. Eur J Biol 2021; 80(2): 145-153. DOI: 10.26650/EurJBiol.2021.1017807

ABSTRACT

Objective: A considerable level of evidence has accumulated about the breast cancer risk-reducing effect of consuming specific flavonoids, through the increasing amount of research and epidemiologic studies. Different flavonoids may have different cellular bioavailability and favor, i.e., the occurrence of a hormetic effect, thus it is important to evaluate breast cancer cells' response to different doses of flavonoids. This study aims to investigate the alterations of the biological pathways in a hormone-positive (HR+) breast cancer cell line as a resemblance for the most common breast cancer subtype, related to the low-dose exposure of the flavonoids.

Materials and Methods: Different levels of doses were applied to MCF-7 breast cancer cells. In order to determine cellular proliferation, WST-1 analysis was conducted. The highest proliferation was observed with cell lines exposed to a low-dose flavonoid mixture and these were selected for further analysis. Intracellular protein expression were investigated by peptide analysis on a nano LC-MS/MS platform. A protein-protein interaction network and pathway analysis were conducted for the proteins expressed differently between the groups.

Results: A total of 214 proteins were identified and 36 proteins with significant alterations (≥1.2-fold change, $p \leq 0.05$) were detected. Significant changes were observed in the pathways related to carbon metabolism, amino acid biosynthesis, splicing mechanism, mitochondrial protein import and translation elongation pathways.

Conclusion: Our study demonstrated that flavonoids can have a hormetic effect which can initially alter metabolic pathways vital for cell proliferation and survival. These pathways may include potential targets for enhancing the anticancer activity of the flavonoids.

Keywords: Flavonoids, breast cancer, hormesis, proteomics

INTRODUCTION

Breast cancer has the highest incidence rate and occupies second place after lung cancer for the mortality rates in women worldwide (1). One of the best ways to reduce the global burden of breast cancer is prevention. Maintaining a healthy diet which is rich in flavonoids has been suggested to achieve that goal (2). Flavonoids are polyphenolic compounds which are highly represented in many plants, fruits, vegetables and propolis. Especially, propolis has a very important place as a medicine in Eastern Europe and Asian regions (3). Because of the wide range of pharmacological properties, it is commonly used by people as a dietary supplement whether being in good health or suffering from a disease like cancer (4).

Corresponding Author: Mete Bora Tuzuner E-mail: bora.tuzuner@acibadem.com
Submitted: 02.11.2021 • **Revision Requested:** 10.11.2021 • **Last Revision Received:** 17.11.2021 • **Accepted:** 21.11.2021 • **Published Online:** 09.12.2021

Studies have shown a significant difference between the breast cancer incidence rates of Asian and Western populations (5). Thus, the differences of dietary habits, regarding the flavonoid consumption tendencies among populations can be suggested as a factor for this phenomenon. Furthermore, the breast cancer prevalence increase, among Asian women who migrate to western countries, may also be considered as evidence for the protective effect of flavonoids against breast cancer (6).

Despite the anticancer effects of flavonoids, their bioavailability is generally low and can vary dramatically among different flavonoid classes as a consequence of Phase 2 metabolism. Most flavonoids go through several steps of ingestion such as glucuronidation, methylation and sulfation in the small intestine and liver before their conjugated metabolites can be found in plasma (7). Overall, flavonoids' metabolites have lower bioactivity than the parent molecules. Having a high molecular weight and a complex molecular structure are also factors for the attenuated bioavailability levels (8). Therefore, *in vivo* bioavailability of flavonoids must be taken into consideration while assessing their anticancer bioactivity via *in vitro* systems.

Several studies have reported the anticancer action of different flavonoids with cell culture and animal models (9,10). However, when the dose-response relationship is considered, an increase of tumor cell proliferation was observed at low-dose flavonoid exposures (11). This biphasic effect, so called "hormesis", of some flavonoids such as daidzein, genistein, kaempferol, quercetin, luteolin and resveratrol, have been demonstrated in several studies (12,13). Up to date literature points out that exposure to such flavonoids may cause cells to synthesize protective proteins against upcoming stress, including increased energy demand, free radical production and ion fluxes via triggering adaptive response pathways (12). Furthermore, studies have suggested that the transactivation of the estrogen receptor may be one of the reasons for the hormetic effect (13). However, there is still insufficient data presented to elucidate the responsible biphasic response mechanisms of the breast cancer cells exposed to multiple flavonoids.

In the current study, we investigated the hormetic effect of a selected mixture of flavonoids (henceforth referred to as "Flavonoid Mix") which we have the patent for pending formulation regarding our research group's previous studies (9,14). By investigating the proliferation part of the hormetic effect on the MCF-7 cell line, we aimed to provide insights about hormone driven breast cancer cells' response mechanisms for the non-cytotoxic dose of the Flavonoid Mix (FM). Our findings will provide important understanding on how the commonest molecular subtype of breast cancer rewires its metabolic pathways in response to the initial stress caused by flavonoid exposure that may not be obtained from high-dose studies alone.

MATERIALS AND METHODS

Materials

Acetonitrile (LC-MS grade) and water (LC-MS grade) were purchased from Merck (EMD Millipore). Dithiothreitol (DTT) and iodoacetamide (IAA) were purchased from Sigma-Aldrich. Formic acid (FA) was obtained from Fluka. Sequencing grade modified trypsin (proteomic grade) was acquired from Thermo Scientific. The MCF-7 cell line was obtained from American Type Cell Collection (MD, USA). Dulbecco's Modified Eagle's Medium (DMEM) was purchased from Sigma Aldrich. Trypsin-EDTA (0.05%), penicillin/streptomycin and FBS were obtained from Biochrome.

Culture of MCF-7 Cells

The ER/PR (+), HER2 (–) human breast cancer cell line, MCF-7, was purchased from American Type Culture Collection (ATCC, Rockville, MD) and the rest of the cell culture related materials were obtained from Biochrome (Berlin, Germany). Cells were maintained in high glucose DMEM and all were supplemented with 10% fetal bovine serum (FBS), 1% glutamine, and 1% penicillin/streptomycin. They were incubated at 37°C in a 5% CO_2 humidified atmosphere. When the density of the cells reached 70-80%, subculturing was done and sixth-eighth passages were used in the experiment.

Preparation of the Flavonoid Mix

The "Flavonoid Mix" (FM) was originated from our research group's previous studies on propolis extracts (9,14). Seven flavonoids, including apigenin and luteolin (>95% HPLC, Sigma-Aldrich, Germany) were used in the preparation of the FM (patent pending). Master stock solutions were created by dissolving object in 60% ethanol with a sonicator. Then, the doses to be administered in the experiment were prepared by diluting object in a medium containing 3% FBS. FBS of 3% was preferred since high percentages of FBS such as 10%, although appropriate for rapid cell growth, deflects the WST-1 reading results (15). Before the solutions were administered, they were made ready for use by passing them through 0.22 µm filters. The FM was formed by combining the compounds of which the IC_{50} values were determined by applying object to the cells one by one, each containing the IC_{50} concentration, and this mixture contained 117 µg/ml flavonoids in total. Other doses (16, 26, 63, 90 µg/ml) were then prepared with dilutions.

Cell Proliferation Analysis

The cell proliferation reagent WST-1 (Roche, Manheim, Germany) was used for the cell proliferation analysis. Vi-Cell XR Cell Viability Analyzer (Beckman Coulter, Brea, CA, USA) was employed for the cell counting process. $1x10^4$ cells were seeded per well with medium supplemented with 3% FBS in 96 well plates (Greiner Bio-one, Kremsmünster, Austria). Fresh medium replacement was done after overnight adherence of the cells. Then, doses (16, 26, 63, 90, 116 µg/mL) of FM were applied to the cells to determine the effects at different time intervals (24^{th}, 48^{th}, and 72^{nd} h). WST-1 reagent (10 µL) was added to each well at the designated time intervals and afterwards 2 hours of incubation was carried out at 37°C in 5% CO_2. Multiscan ELISA reader (Thermo Fisher Scientific, Waltham, MA, USA) was used to measure the absorbance of the wells at 450 nm with the reference wavelength set at 620 nm in order to detect the formazan formation. Control cells' viability were accepted as 100%. Data are expressed as percentages of

absorbance readings compared to control wells on a relative proliferation index scale (Mean ± standard deviation). All tests were performed in triplicate.

LC-MSMS Analysis

Tryptic peptides were generated according to the Filter Aided Sample Preparation Protocol (FASP) (16). Cells were scraped from cell culture plates and washed twice with cold 50 mM ammonium bicarbonate and lysed in a 50 mM ammonium bicarbonate solution via ultrasonic homogenization (5 s on, 5 s off, 3 cycles). The mixture was centrifuged at 15,000 rpm and the protein concentration in the supernatant was measured based on NanoDrop. Thirty µL of protein mixture containing 100 µg protein was transferred to a 30 kDa cut-off spin filter and mixed with 200 µL of 6M urea and centrifuged at 14,000 x g for 15 min. The process was repeated twice. The flow through was discarded and the proteins were alkylated with 10 mM iodoacetamide in the dark at room temperature (RT) for 20 min. The protein mixture was washed first with 200 µL of 6M urea and later twice with 100 µL of 50 mM AmBic solution. The mixture was incubated with 1:100 (trypsin:protein) ratio of MS grade trypsin overnight. Peptides were eluted from the spin column first with 50 mM Ambic solution and later with 0.5 M NaCl. The flow through was collected and lyophilized. The concentration of the tryptic peptides was measured with a NanoDrop spectrophotometer and samples were prepared at a concentration of 100 ng/µL.

In LC-MS/MS analysis, Symmetry C18 (5µm, 180µm i.d. × 20 mm) column was used for trapping tryptic peptides. Sixty minutes of ACN gradient (4% to 40% ACN, 0.3 µL /min flow rate) was applied for elution on a CSH C18 (1.7 µm, 75 µm i.d. × 250 mm) analytical nano column. Data collection and processing was performed as it is stated in our previous studies (17).

Bioinformatic Analysis

To seek potential interactions between identified proteins according to low-dose flavonoid exposure, the STRING database (http://string-db.org/, v11.0) was employed. In order to construct the PPI network, text mining, experiments, database co-expression, neighborhood, gene fusion, and co-occurrence were selected as active interaction sources. Results with a high confidence level (high confidence=0.70) were taken into consideration. Interpretation and analysis of pathways were performed with REACTOME (http://www.reactome.org, v76.0) and KEGG (Kyoto Encyclopedia of Genes and Genomes, https://www.genome.jp/kegg/, Release 98.0) databases. Proteins showing significant differences were categorized based on biological processes and molecular function using AmiGO (18).

RESULTS

Effects of the FM on Cell Viability and Proliferation

Normal growth features expected under standard in vitro culture conditions were observed among all MCF-7 cells. Cells were grown in increasing concentration of FM, ranging from 16 µg/mL to 117 µg/mL for up to 3 days and cell viability was determined using the standard WST-1 assay. Our analysis showed that FM had a hormetic dose response on MCF-7 cells. We observed the highest viability relative to the untreated cells at the 24th hour with a dose of 16 µg/ml FM (~135%, Figure 1), as well as the highest viability difference (~97%) compared to the next dose. Therefore, cells exposed to 16 µg/mL for 24 hours were selected for further proteomic analysis.

Proteome Analysis of the MCF-7 Cells with Maximum Hormetic Response

In order to analyze the protein expression differences between FM treated MCF-7 cell line and controls, mass spectrometry-based proteomics methods were used. Progenesis QI-P was employed to perform charge state deconvolution and deisotoping and 214 proteins were identified (data not shown) and 36 of them were detected as being significantly altered (fold change >1.2 and p<0.05) in the MCF-7 cell line treated with 16 µg /mL flavonoid mixture at the 24th hour compared to controls (Table 1). Stress-70 protein (HSPA9) was ranked top amongst the upregulated proteins. On the other hand, Anterior gradient protein 2 homolog (AGR2) was found to be the most downregulated compared to control samples. Overall, the majority of downregulated proteins assume roles in the response to unfolded proteins, RNA binding and catalytic step 2 spliceosome. Ribose phosphate biosynthetic process, cadherin binding and

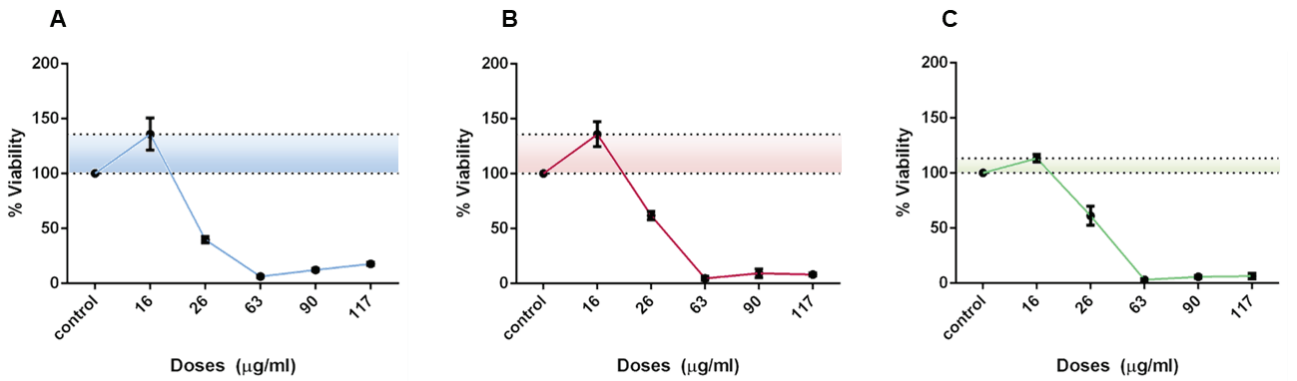

Figure 1. Effects of the flavonoid mixture on the viability of MCF-7 breast cancer cells. 24 hours (A), 48 hours (B), and 72 hours (C) of exposure are represented.

Table 1. Significantly altered proteins in MCF-7 cell line exposed to low-dose FM for 24 hours

Accession no	Gene symbol	Description	Fold Change	Anova (p value)
UPREGULATED *(TREATED vs CONTROL)*				
P38646	*HSPA9*	Stress-70 protein	7.87	0.0002
P38919	*EIF4A3*	Eukaryotic initiation factor 4A-III	3.95	0.0109
Q5T200	*ZC3H13*	Zinc finger CCCH domain-containing protein 13	3.06	0.0139
P34897	*SHMT2*	Serine hydroxymethyltransferase	2.48	0.0079
P62910	*RPL32*	60S ribosomal protein L32	2.44	0.0142
P22626	*HNRNPA2B1*	Heterogeneous nuclear ribonucleoproteins A2/B1	1.71	0.0315
P02545	*LMNA*	Prelamin-A/C	1.70	0.0257
P06733	*ENO1*	Alpha-enolase	1.65	0.0305
P10809	*HSPD1*	60 kDa heat shock protein	1.62	0.0123
Q13263	*TRIM28*	Transcription intermediary factor 1-beta	1.61	0.0037
P05787	*KRT8*	Keratin type II	1.58	0.0166
P09651	*HNRNPA1*	Heterogeneous nuclear ribonucleoprotein A1	1.40	0.0206
P04792	*HSPB1*	Heat shock protein beta-1	1.39	0.0131
P25705	*ATP5A1*	ATP synthase subunit alpha	1.27	0.0425
DOWNREGULATED *(TREATED vs CONTROL)*				
O95994	*AGR2*	Anterior gradient protein 2 homolog	12.41	0.0004
Q15365	*PCBP1*	Poly(rC)-binding protein 1	7.77	0.0008
O14745	*SLC9A3R1*	Na(+)/H(+) exchange regulatory cofactor NHE-RF1	4.67	0.0083
P11413	*G6PD*	Glucose-6-phosphate 1-dehydrogenase	4.30	0.0009
P31939	*ATIC*	Bifunctional purine biosynthesis protein	2.98	0.0053
O60361	*NME2P1*	Putative nucleoside diphosphate kinase	2.61	0.0077
P14625	*HSP90B1*	Endoplasmin	2.36	0.0325
P07910	*HNRNPC*	Heterogeneous nuclear ribonucleoproteins C1/C2	2.32	0.0016
P55786	*NPEPPS*	Puromycin-sensitive aminopeptidase	2.24	0.0149
P61978	*HNRNPK*	Heterogeneous nuclear ribonucleoprotein K	2.06	0.0092
P14649	*MYL6B*	Myosin light chain 6B	2.03	0.0148
P13639	*EEF2*	Elongation factor	2.02	0.0002
P12004	*PCNA*	Proliferating cell nuclear antigen	1.99	0.0289
P00558	*PGK1*	Phosphoglycerate kinase	1.94	0.0011
P49327	*FASN*	Fatty acid synthase	1.74	0.0039
P60709	*ACTB*	Actin	1.68	0.0006
P07355	*ANXA2*	Annexin A2	1.67	0.0060
P23527	*HIST1H2BO*	Histone H2B type 1-O	1.63	0.0470
P29692	*EEF1D*	Elongation factor 1-delta	1.61	0.0162
P04908	*HIST1H2AB*	Histone H2A type 1-B/E	1.52	0.0208
P14618	*PKM*	Pyruvate kinase	1.43	0.0260
P29401	*TKT*	Transketolase	1.32	0.0096
P06576	*ATP5B*	ATP synthase subunit beta	1.31	0.0025

chromatin were observed to be the most enriched biological process, molecular function and cellular compartment respectively among the upregulated proteins (Figure 2).

Protein-Protein Interaction and Pathway Analysis of Differentially Expressed Proteins

In order to uncover underlying signaling pathways and associated proteins affected by flavonoid treated hormone positive breast cancer cells during their hormetic response, we carried out STRING, Reactome and KEGG pathway analysis with differentially expressed proteins. STRING results indicated three significant clusters related to carbon metabolism, biosynthesis of amino acids and spliceosome (Figures 3 and 4). In addition, Reactome analysis reported two more significantly altered pathways: mitochondrial protein import and eukaryotic translation elongation. The analysis revealed that the protein expressions (including proteins; G6PD: Glucose-6-phosphate 1-dehydrogenase, PGK1: Phosphoglycerate kinase, TKT: Transketolase, PKM: Pyruvate kinase) involved in carbon metabolism, amino acid synthesis (same proteins except G6PD) and eukaryotic translation elongation (EEF1D: Elongation factor 1-delta and EEF2: Elongation factor) were downregulated (except SHMT2: Serine

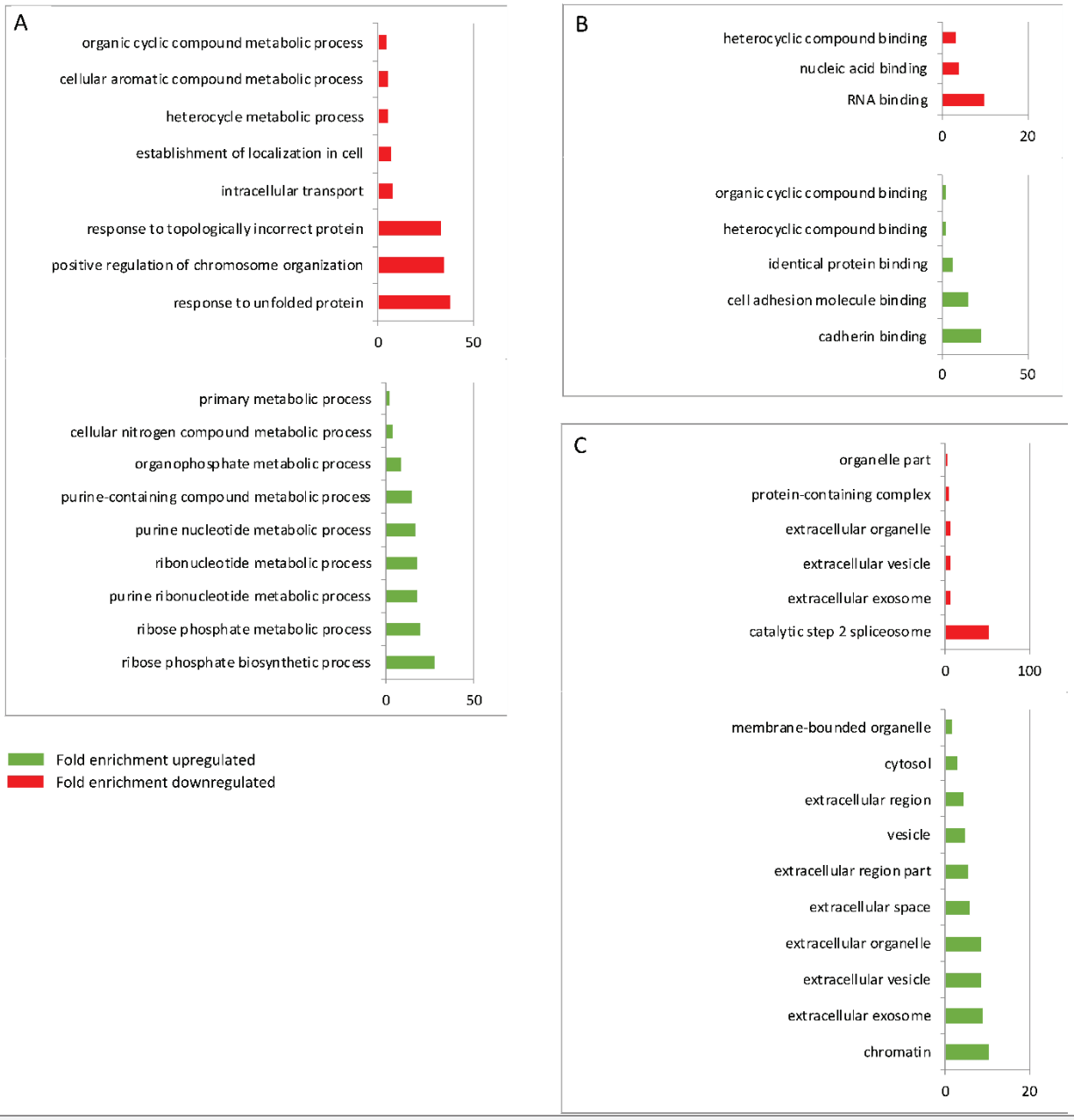

Figure 2. Gene Ontology (GO) enrichment analysis of significantly altered proteins. Biological process (A), molecular function (B) and cellular component (A) are represented. Displaying only results for Bonferroni-corrected for $p<0.05$.

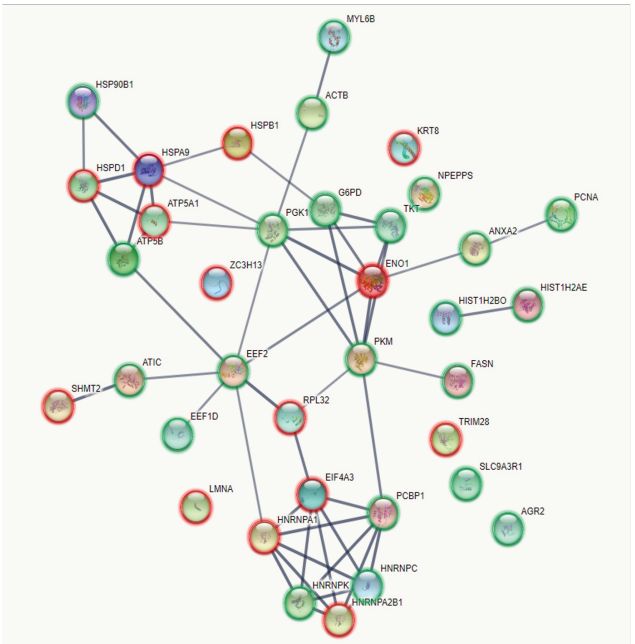

NETWORK STATS				
number of nodes:	36		avg. local clustering coefficient:	0,484
number of edges:	53		expected number of edges:	17
average node degree:	2,94		PPI enrichment p-value:	1,47E-12

DOWNREGULATED UPREGULATED

Figure 3. STRING network of differentially expressed proteins. Network stats are shown below. Down/upregulated proteins are shown as green and red nodes, respectively. Connections reflect protein interactions where the line thickness indicates strength of the data support.

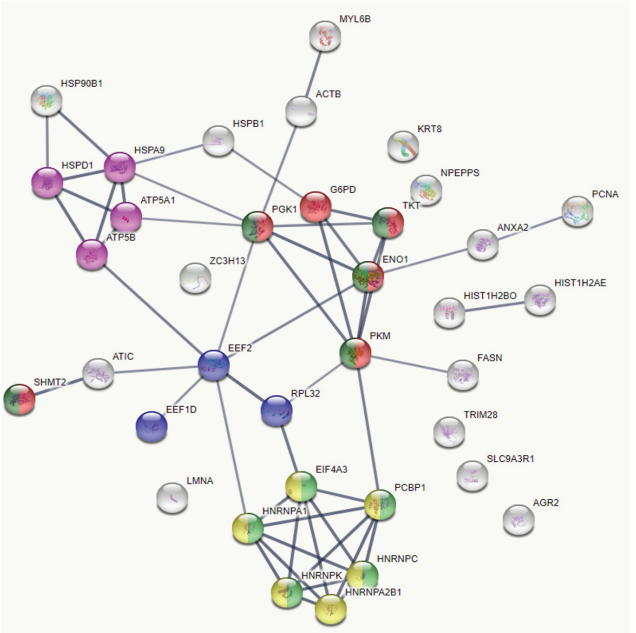

KEGG			
Pathway	Description	Count in gene set	False discovery rate
hsa01200	Carbon metabolism	6 of 116	7,30E-06
hsa01230	Biosynthesis of amino acids	5 of 72	1,19E-05
hsa03040	Spliceosome	5 of 130	0,00013

REACTOME			
Pathway	Description	Count in gene set	False discovery rate
HSA-72163	mRNA Splicing - Major Pathway	6 of 178	0,00029
HSA-1268020	Mitochondrial protein import	4 of 64	0,00053
HSA-156842	Eukaryotic Translation Elongation	3 of 90	0,0122

Figure 4. Significantly enriched pathways associated with proteins among the STRING network are shown. Top 3 pathways for KEGG and Reactome analysis are shown.

hydroxymethyl transferase, ENO1: Alpha enolase and RPL32: 60S ribosomal protein L32) in cells exposed to the low-dose FM. On the other hand, the proteins involved in the mitochondrial protein import pathway (HSPD1: 60 kDa heat shock protein, HSPA9: Stress-70 protein, ATP5A1: ATP synthase subunit alpha) were observed to be upregulated (except ATP5B: ATP synthase subunit beta). Splicing mechanism was also observed to be altered, but not towards a specific direction.

DISCUSSION

Secondary metabolites originating from dietary flavonoids are well recognized for their wide range of pharmacological activities and even for their anticancer potential. Studies have shown that there is a positive correlation between a diet rich in flavonoids and a decrease in the risk of colon, prostate and breast cancer (19). In the light of these findings, it has raised the question whether flavonoids can be effective in the prevention and treatment of cancer by interacting with different genes and proteins. Therefore, the investigation of their effect on biological pathways along with their significant protein interactions is of utmost important.

Dietary flavonoids are also known to be among hormetic factors. Hormesis can simply be described as an observed biphasic dose response, which is stimulation at low doses and inhibition at high doses. When a cell receives a low dose of toxin, it tries to compensate with the disruption of cell homeostasis. In this process the cell activates its pathways for survival and promotes proliferation. In summary, hormesis is a stress response. Environmental factors such as heat and low-dose chemicals cause this effect.

In our study, a hormetic effect was observed as a result of the application of our patent-stage standardized flavonoid mixture, consisting of the flavonoids in propolis, on the MCF-7 cell line at a dose range of 16-117 µg/mL. Due to the 16 µg/mL dose application, an increase of up to 35% in viability was observed in the cells, and a cytotoxic effect was observed in correlation with the increasing dose. The proteome analysis we performed to elucidate the mechanism of the hormetic effect observed at this dose indicated significant changes in carbon metabolism, amino acid biosynthesis, splicing mechanism, mitochondrial protein import and translation elongation pathways.

Today, the perception that cancer is a metabolic disease is getting stronger (20). Tumor cells are known to modulate their metabolism for growth, survival and proliferation (21). Since the times of Otto Warburg, the central carbon metabolism is known to have an impact in the progression of different types of cancers, in-

cluding breast carcinomas (22,23). High glucose uptake and lactate production under aerobic conditions in the tumor cells are supported by glycolysis and the pentose phosphate pathways (PPP). Regarding these dysregulated pathways, flavonoids are known to have anti-Warburg effects on cancer cells (24). Thus, it was not a surprise that we have identified altered expressions of proteins related to glycolysis and PPP. We observed expressions of the enzymes responsible for substrate level phosphorylation were downregulated (PGK1 FC=1.9, PKM FC=1.4) as well as PPP enzymes G6PD and TKT at the hormetic condition compared to the FM free cultured MCF-7 cells. In contrast, ENO1 and SHMT2 protein expressions were found to be upregulated.

Up to date data related to ENO1 expression levels in breast cancer cells/tissues were associated with the PI3K/Akt signaling pathway. Downregulation of ENO1 was shown to decrease the proliferation in breast cancer cells via the PI3K/Akt signaling pathway which is crucial for a series of cellular activities such as glycolysis (25). Carbon metabolism and amino acid metabolism are intimately connected to each other and share many proteins that have a role in both pathways. In this regard, SHMT2 is another key metabolic enzyme that converts serine to glycine.

Serine is necessary for synthesis of biomolecules such as proteins that are required for cell proliferation. By the activity of SHMT2, mitochondrial one-carbon metabolism produces 1C units from serine. After the oxidation of these 1C units, they are exported to the cytoplasm for the induction of one-carbon metabolism. Thus, one carbon metabolism serves as a set of reactions that supply methyl groups (one-carbon moiety) for *de novo* nucleotide biosynthesis and DNA methylation (26). It has been reported that SHMT2 was overexpressed in breast cancer as in many cancers. In addition, this situation was associated with tumorigenesis and progression (27,28). Under the stress of low-dose FM, MCF-7 cells may reprogram their carbon and amino acid metabolism. Our findings correlate in the same direction with previous studies in which ENO1 and SMHT2 upregulation may be one of the responsible players that cause the hormetic effect of the FM.

Messenger RNA processing is a principal step for expression of eukaryotic genes that helps cells maintain various biological processes, such as proliferation, survival, and differentiation (29-31). Many diseases, such as cancer development and progression, have been linked to anomalies in mRNA splicing (32). In breast cancer, unusual alternative splicing has been shown to be one of the risk factors. Furthermore, flavonoids such as apigenin and luteolin were shown to bind spliceosome components and therefore have an effect on splicing molecular mechanisms (33).

According to our analysis, expression levels of eukaryotic translation initiation factor 4A3 (EIF4A3) together with the heterogeneous nuclear ribonucleoproteins (hnRNPs) altered where the FM showed its hormetic effect. Deregulation of these alternative splicing elements have already been established as factors for breast cancer development (34,35). Although the exact molecular mechanism is not known, spliceosome (HSA-03040) and the mRNA splicing pathway (HSA-72163) have a role where low-dose FM shows its hormetic effect on hormone positive breast cancer cells.

Many mitochondrial proteins encoded by nuclear genes are synthesized in the cytosol. These proteins are transported to the mitochondria in order to go through a delivery and sorting process by the mitochondrial import mechanism. Heat shock proteins (HSPs) acting as molecular protein chaperones have important roles in mitochondrial protein import. Specifically, after the cells have experienced different kinds of cellular stress, HSPs assist correct protein folding and sustain protein stability. They are also related with cancer development, progression, metastasis and drug resistance (36). Although flavonoids are known as inhibitors of HSPs expression (37), our data indicates that they can also induce expression of some of the proteins in this family at low doses because of their biphasic nature. A noteworthy hit in this pathway, mitochondrial stress protein 70 (HSPA9, mtHsp70, or mortalin), is a member of the heat shock protein 70 family. HSPA9 is known to prevent apoptosis via interacting with p53 and inactivating the tumor suppressor feature of p53 (38). In addition, it has been determined that increased expression of HSPA9 contributes to tumor formation (39,40). Studies have shown that HSPA9 is a certain factor in breast cancer occurrence and development (41).

Moreover, HSPA9 plays an important role in the synthesis of iron-sulfur clusters (ISC) in mitochondria. Its function is to interact with and stabilize ISC cluster-assembly proteins which are used for various functions such as substrate binding and activation, electron transport, radical generation, regulation of gene expression, and DNA repair. Therefore, it can be speculated that the initial stress state caused by the low dose FM leads to a significant upregulation (7.8-fold) of this protein which may have contributed to MCF7 cell proliferation.

Mitochondrial protein import is fueled by ATP hydrolysis thus it is not surprising ATP synthase complex is affected from the FM treatment.

An upregulation of ATP synthase was detected in breast tumors, where also a correlation was observed between the α subunits (ATP5A1) and high stage, poorly differentiated and larger tumors (42,43). However, according to Isidoro et al., there is no significant change in the expression levels of β subunits (ATP5B) in breast cancer cells compared to normal breast cells (44). Nonetheless, decreased catalytic β subunit expression has been associated with cancer development (45-47). Although we cannot suggest a certain direction of the expression (ATP5A1 1.3-fold up, ATP5B 1.3-fold down), it is possible to say that impairment of ATP synthesis takes part in the molecular mechanism of hormesis together with mitochondrial transport of proteins.

Translation is a complicated process that is disrupted through different mechanisms in cancer. (48). EEF2 and EEF1D, which were identified in our MS analysis, are such factors that play essential roles in the polypeptide chain elongation step. Ex-

pression of elongation factors were shown to be significantly different within the subtypes of breast cancers, suggesting they have a potential of being therapeutic targets and prognostic biomarkers (49).

Increased EEF2 levels have been linked to poor outcome of HR (+) breast cancer (50). Furthermore, flavonoid structures can specifically bind to these elongation factors and can inhibit proliferation of breast cancer cells (51). We observed downregulation of EEF2 and EEF1D compared to untreated cells which favors antiproliferative effects of FM; however, it can be hypothesized that MCF-7 cells tend to overcome this via increasing ribosomal proteins such as RPL32 expression. RPL32 overexpression in breast cancer cells and tissues have been associated with cell migration and invasion (52). Although there has been no evidence of RPL32 protein and flavonoids interaction to our knowledge, we may suggest low-dose FM alters the translation elongation pathway through ribosomal protein expression levels in order to support the proliferation response of hormone positive breast cancer cells.

CONCLUSION

In our study we investigated the underlying biological pathways of the hormetic effect which was observed in FM treated MCF-7 cells. We have shown that multiple mechanisms are involved in the proliferation outcome of low-dose FM exposure. We suggest that the modulation of biological pathways, such as carbon metabolism, amino acid biosynthesis, splicing mechanism, mitochondrial protein import and translation elongation pathways are essential for the response of hormone positive breast cancer cells to flavonoids. Further studies on the hormetic effect of flavonoids on breast cancer in association with dietary intake values extrapolated from in vivo conditions are required to validate these preliminary findings. Elucidating the mechanisms that lie beneath the hormetic effect of flavonoids on HR (+) breast cancers, particularly the ones triggering the intrinsic adaptive response that leads to proliferation, may highlight some potential targets for better preventive and prophylactic interventions.

Acknowledgements: We thank Hülya Yılmaz Aydoğan and Oğuz Öztürk for useful discussions and invaluable opinions during the preparation of the manuscript. We also thank Emel Akgün for her support in wet-lab experiments.

Peer Review: Externally peer-reviewed.

Author Contributions: Conception/Design of Study- M.B.T.; Data Acquisition- A.B.C.; Data Analysis/Interpretation- M.B.T.; Drafting Manuscript- M.B.T.; Critical Revision of Manuscript- M.B.T.; Final Approval and Accountability- M.B.T., A.B.C.

Conflict of Interest: Authors declared no conflict of interest.

Financial Disclosure: This study was funded by the Scientific Projects Coordination Unit, Istanbul University (Project No. 22859).

REFERENCES

1. Sung H, Ferlay J, Siegel RL, Laversanne M, Soerjomataram I, Jemal A, et al. Global cancer statistics 2020: GLOBOCAN estimates of incidence and mortality worldwide for 36 cancers in 185 countries. CA Cancer J Clin 2021; 71: 209-49.
2. Rodríguez-García C, Sánchez-Quesada C, J Gaforio J. Dietary Flavonoids as Cancer Chemopreventive Agents: An Updated Review of Human Studies. Antioxidants 2019; 8(5): 137.
3. Toreti VC, Sato HH, Pastore GM, Park YK, Recent progress of propolis for its biological and chemical compositions and its botanical origin, Evid Based Complement Alternat Med 2013; 697390.
4. Banskota AH, Tezuka Y, Kadota S. Recent progress in pharmacological research of propolis. Phytother Res 2001; 15(7): 561-71.
5. Peeters PH, Keinan-Boker L, van der Schouw YT, Grobbee DE. Phytoestrogens and breast cancer risk: Review of the epidemiological evidence. Breast Cancer Res Treat 2003; 77: 171-83.
6. Lim DW, Giannakeas V, Narod SA. Survival Differences in Chinese Versus White Women With Breast Cancer in the United States: A SEER-Based Analysis. JCO Glob Oncol 2020; 6: 1582-92.
7. Rupasinghe HP, Ronalds CM, Rathgeber B, Robinson RA. Absorption and tissue distribution of dietary quercetin and quercetin glycosides of apple skin in broiler chickens. J Sci Food Agric 2010; 90(7): 1172-8.
8. Gonzales GB, Smagghe G, Grootaert C, Zotti M, Raes K, Van Camp J. Flavonoid interactions during digestion, absorption, distribution and metabolism: a sequential structure-activity/property relationship-based approach in the study of bioavailability and bioactivity. Drug Metab Rev 2015; 47(2): 175-90.
9. Seyhan MF, Yılmaz E, Timirci-Kahraman Ö, Saygılı N, Kısakesen Hİ, Gazioğlu S, et al. Different propolis samples, phenolic content, and breast cancer cell lines: Variable cytotoxicity ranging from ineffective to potent. IUBMB Life 2019; 71(5): 619-31.
10. Bonofiglio D, Giordano C, De Amicis F, Lanzino M, Andò S. Natural Products as Promising Antitumoral Agents in Breast Cancer: Mechanisms of Action and Molecular Targets. Mini Rev Med Chem 2016; 16(8): 596-604.
11. Pal S, Konkimalla VB. Hormetic Potential of Sulforaphane (SFN) in Switching Cells' Fate Towards Survival or Death. Mini Rev Med Chem 2016; 16(12): 980-95.
12. Son TG, Camandola S, Mattson MP. Hormetic dietary phytochemicals. Neuromolecular Med 2008; 10(4): 236-46.
13. Jodynis-Liebert J, Kujawska M. Biphasic Dose-Response Induced by Phytochemicals: Experimental Evidence. Journal of Clinical Medicine 2020; 9(3): 718.
14. Narter F, Diren A, Kafkasli A, Eronat AP, Seyhan MF, Yilmaz-Aydogan H, et al. Anatolian Propolis Prevents Oxalate Kidney Stones: Dramatic Reduction of Crystal Deposition in Ethylene-Glycol-Induced Rat Model. Rec Nat Prod 2018; 12(5): 445-59.
15. Huang KT, Chen YH, Walker AM. Inaccuracies in MTS assays: major distorting effects of medium, serum albumin, and fatty acids. Biotechniques 2004 Sep; 37(3): 406, 408, 410-2.
16. Wiśniewski JR, Zougman A, Nagaraj N, Mann M. Universal sample preparation method for proteome analysis. Nat Methods 2009; 6(5): 359-62.
17. Akgun E, Tuzuner MB, Sahin B, Kilercik M, Kulah C, Cakiroglu HN, et al. Proteins associated with neutrophil degranulation are upregulated in nasopharyngeal swabs from SARS-CoV-2 patients. PLoS One 2020; 15(10): e0240012
18. Carbon S, Ireland A, Mungall CJ, Shu S, Marshall B, Lewis S, AmiGO Hub; Web Presence Working Group. AmiGO: online access to ontology and annotation data. Bioinformatics 2009; 25(2): 288-9.

19. Batra P, Sharma AK. Anti-cancer potential of flavonoids: recent trends and future perspectives. 3 Biotech 2013; 3(6): 439-59.
20. Coller HA. Is cancer a metabolic disease? Am J Pathol 2014; 184(1): 4-17.
21. Pavlova NN, Thompson CB. The emerging hallmarks of cancer metabolism. Cell Metab 2016; 23(1): 27-47.
22. Liberti MV, Locasale JW. The Warburg effect: how does it benefit cancer cells? Trends Biochem Sci 2016; 41(3): 211-8.
23. Richardson AD, Yang C, Osterman A, Smith JW. Central carbon metabolism in the progression of mammary carcinoma. Breast Cancer Res Treat 2008; 110(2): 297-307.
24. Samec M, Liskova A, Koklesova L, Samuel SM, Zhai K, Buhrmann C, et al. Flavonoids against the Warburg phenotype-concepts of predictive, preventive and personalised medicine to cut the Gordian knot of cancer cell metabolism. EPMA J 2020; 11(3): 377-98.
25. Zang HY, Gong LG, Li SY, Hao JG. Inhibition of α-enolase affects the biological activity of breast cancer cells by attenuating PI3K/Akt signaling pathway. Eur Rev Med Pharmacol Sci 2020; 24(1): 249-57.
26. Locasale JW. Serine, glycine and one-carbon units: cancer metabolism in full circle. Nat Rev Cancer 2013; 13: 572-83.
27. Possemato R, Marks KM, Shaul YD, Pacold ME, Kim D, Birsoy K, et al. Functional genomics reveal that the serine synthesis pathway is essential in breast cancer. Nature 2011; 476(7360): 346-50.
28. Liu C, Wang L, Liu X, Tan Y, Tao L, Xiao Y, et al. Cytoplasmic SHMT2 drives the progression and metastasis of colorectal cancer by inhibiting β-catenin degradation. Theranostics 2021; 11(6): 2966-86.
29. Maniatis T, Reed R. An extensive network of coupling among gene expression machines. Nature 2002; 416: 499-506.
30. Millevoi S, Vagner S. Molecular mechanisms of eukaryotic pre-mRNA 3′ end processing regulation. Nucleic Acids Res 2009; 38: 2757-74.
31. Orphanides G, Reinberg D. A unified theory of gene expression. Cell 2002; 108: 439-51.
32. Scotti MM, Swanson MS. RNA mis-splicing in disease. Nat Rev Genet 2016; 17(1): 19-32.
33. Kurata M, Fujiwara N, Fujita KI, Yamanaka Y, Seno S, Kobayashi H, et al. Food-Derived Compounds Apigenin and Luteolin Modulate mRNA Splicing of Introns with Weak Splice Sites. iScience 2019; 22: 336-52.
34. Geuens T, Bouhy D, Timmerman V. The hnRNP family: insights into their role in health and disease. Hum Genet 2016; 135(8): 851-67.
35. Silipo M, Gautrey H, Tyson-Capper A. Deregulation of splicing factors and breast cancer development. J Mol Cell Biol 2015; 7(5): 388-401.
36. Calderwood SK, Gong J. Heat Shock Proteins Promote Cancer: It's a Protection Racket. Trends Biochem Sci 2016; 41(4): 311-23.
37. Hosokawa N, Hirayoshi K, Nakai A, Hosokawa Y, Marui N, Yoshida M, et al. Flavonoids inhibit the expression of heat shock proteins. Cell Struct Funct 1990; 15(6): 393-401.
38. Wadhwa R, Yaguchi T, Hasan MK, Mitsui Y, Reddel RR, Kaul SC. Hsp70 family member, mot-2/mthsp70/GRP75, binds to the cytoplasmic sequestration domain of the p53 protein. Exp Cell Res 2002; 274(2): 246-53.
39. Wadhwa R, Takano S, Kaur K, Deocaris CC, Pereira-Smith OM, Reddel RR, et al. Upregulation of mortalin/mthsp70/Grp75 contributes to human carcinogenesis. Int J Cancer 2006; 118(12): 2973-80.
40. Na Y, Kaul SC, Ryu J, Lee JS, Ahn HM, Kaul Z et al. Stress chaperone mortalin contributes to epithelial-mesenchymal transition and cancer metastasis. Cancer Res 2016; 76(9): 2754-65.
41. Zhang R, Meng Z, Wu X, Zhang M, Zhang S, Jin T. Mortalin promotes breast cancer malignancy. Exp Mol Pathol 2021;118:104593.
42. Huang TC, Chang HY, Hsu CH, Kuo WH, Chang KJ, Juan HF. Targeting therapy for breast carcinoma by ATP synthase inhibitor aurovertin B. J Proteome Res 2008; 7: 1433-44.
43. Pan J, Sun LC, Tao YF, Zhou Z, Du XL, Peng L, et al. ATP synthase ecto-alpha subunit: a novel therapeutic target for breast cancer. J Transl Med 2011; 9: 211.
44. Isidoro A, Casado E, Redondo A, Acebo P, Espinosa E, Alonso AM, et al. Breast carcinomas fulfill the Warburg hypothesis and provide metabolic markers of cancer prognosis. Carcinogenesis 2005; 26: 2095-104.
45. Willers IM, Cuezva JM. Post-transcriptional regulation of the mitochondrial H(+)-ATP synthase: a key regulator of the metabolic phenotype in cancer. Biochim Biophys Acta 2011; 1807: 543-51.
46. Cuezva JM, Krajewska M, de Heredia ML, Krajewski S, Santamaría G, Kim H, et al. The bioenergetic signature of cancer: a marker of tumor progression. Cancer Res 2002; 62: 6674-81.
47. Zheng SQ, Li YX, Zhang Y, Li X, Tang H. MiR-101 regulates HSV-1 replication by targeting ATP5B. Antiviral Res 2011; 89: 219-26.
48. Bilanges B, Stokoe D. Mechanism of translational deregulation in human tumors and therapeutic intervention strategies. Oncogene 2007; 26: 5973-90.
49. Hassan MK, Kumar D, Naik M, Dixit M. The expression profile and prognostic significance of eukaryotic translation elongation factors in different cancers. PLoS One 2018; 13(1): e0191377.
50. Meric-Bernstam F, Chen H, Akcakanat A, Do KA, Lluch A, Hennessy BT, Hortobagyi GN, Mills GB, et al. Aberrations in translational regulation are associated with poor prognosis in hormone receptor-positive breast cancer. Breast Cancer Res 2012; 14: R138.
51. Yao N, Chen CY, Wu CY, Motonishi K, Kung HJ, Lam KS. Novel flavonoids with antiproliferative activities against breast cancer cells. J Med Chem 2011; 54(13): 4339-49.
52. Xu L, Wang L, Jiang C, Zhu Q, Chen R, Wang J, et al. Biological effect of ribosomal protein L32 on human breast cancer cell behavior. Mol Med Rep 2020; 22(3): 2478-86.

ISTANBUL UNIVERSITY PRESS

RESEARCH ARTICLE

Eur J Biol 2021; 80(2): 154-163

Antioxidant Activities of *Eremurus spectabilis* M. Bieb. Extracts and Sulfur Compounds

Bertan Boran Bayrak[1], **Refiye Yanardag**[1]

[1]Istanbul University-Cerrahpasa, Faculty of Engineering, Department of Chemistry, Istanbul, Turkey

ORCID IDs of the authors: B.B.B. 0000-0002-0700-5096; R.Y. 0000-0003-4185-4363

Please cite this article as: Bayrak BB, Yanardag R. Antioxidant Activities of *Eremurus spectabilis* M. Bieb. Extracts and Sulfur Compounds. Eur J Biol 2021; 80(2): 154-163. DOI: 10.26650/EurJBiol.2021.1028656

ABSTRACT

Objective: *Eremurus spectabilis* M. Bieb. is grown in East and Southeast Mediterranean regions of Turkey, and is commonly used as an edible plant in these regions. The aim of the current study was to determine the antioxidant activities of different *E. spectabilis* M. Bieb. extracts and some sulfur compounds.

Materials and Methods: In this study, the antioxidant activities of aqueous, ethanolic, and ethyl acetate extracts of *E. spectabilis* M. Bieb. and sulfur compounds (α-lipoic acid, cysteamine, cysteine, diallyl sulfide, glutathione, homocysteine, N-acetyl cysteine, vitamin U and 1,4-dithioerythritol) were assessed in several antioxidant tests. These tests included reducing power, cupric ion reducing antioxidant capacity, 2,2'-azino-bis (3-ethylbenzothiazoline-6-sulfonic acid) radical scavenging, 2,2-diphenyl-1-picrylhydrazyl radical scavenging, N,N-dimethyl-4-phenylenediamine dihydrochloride radical scavenging, superoxide anion radical scavenging, hydroxyl radical scavenging, metal chelating activities and ferric ion reducing antioxidant power. The phytochemical profiles and total phenolic and flavonoid contents of all extracts were investigated.

Results: It was found out that the antioxidant activities of all the extracts and sulfur compounds generally increased with concentration increases, the highest antioxidant activity was found in ethyl acetate extract, while the aqueous extract was found to have the lowest antioxidant activity. Diallyl sulfide was found to have the highest antioxidant activity, whereas vitamin U had the lowest antioxidant activity. It was observed that all extracts of *E. spectabilis* M. Bieb. and the sulfur compounds showed antioxidant activity.

Conclusion: The *E. spectabilis* M. Bieb. and sulfur compounds investigated in this study could be considered as a source of antioxidants.

Keywords: *Eremurus spectabilis* M. Bieb., antioxidant potential, sulfur compounds, free radicals, phytochemical screening

INTRODUCTION

Plants produce a variety of chemicals known as secondary metabolites. Many of these metabolites have been used by humans both nutritionally and for the treatment of illness or drug production. Most of the ancient civilizations in Anatolia produced many food and medicinal plants (1). Turkey is one of the richest countries in Europe and the Middle East in terms of natural flora. It has more than eleven thousand plant species due to its climate and geographical location. Approximately thirty-three percent of these plant species identified within the borders of Turkey are endemic (2).

The genus *Eremurus* (an important genus of *Xanthorrhoeaceae* that comprises 62 species) is widely known as foxtail lily or desert candles (3). It is found on dry and stony grazed hillside. This plant is naturally grown and geographically distributed in the regions of Central Asia, South Asia, East Asia, and the Middle East, including Turkey (4). Two *Eremurus* species, namely *Eremurus spectabilis* M. Bieb. and *Eremurus cappadocicus*, grow naturally and are localized in the Mediterranean, East and Southeast regions of Turkey (Eastern Anatolian part of Turkey). It is popularly referred to as "çiriş", "gulik", "gülük" and "sarı çiriş" in

Corresponding Author: Bertan Boran Bayrak E-mail: bertanb@iuc.edu.tr

Submitted: 26.11.2021 • **Revision Requested:** 27.11.2021 • **Last Revision Received:** 28.11.2021 • **Accepted:** 06.12.2021 • **Published Online:** 14.12.2021

these regions (5). The plant has traditionally been consumed fresh and/or dried as a wild edible vegetable and as a traditional medicine/folk drug. Additionally, it has been shown in both ethnobotanical and ethnopharmacological studies that it is used for traditional treatment of gastrointestinal pain, liver diseases, diabetes, scabies and syphilis, rheumatism and various inflammations (6). In addition, a study by Abubaker and Hidayat showed that both water and hexane-ethanol extracts of *E. spectabilis* M. Bieb. exhibited antiproliferative effects against different cancer cell lines via its bioactive compounds (e.g., carvacrol, valence, cadelene) (7). These effects have been attributed to its richness in phenolics and flavonoids (8). In a recent study, it was shown that ethanolic and ethyl acetate extracts of *E. spectabilis* M. Bieb. have an inhibitive action against histone deacetylase, xanthine oxidase, and urease enzymes (9). In addition, the aqueous extract of this plant exhibits inhibitory effects on diabetes mellitus and skin-associated enzymes (i.e., α-amylase, α-glucosidase, elastase, hyaluronidase, and tyrosinase, respectively) (10).

Mopping up both reactive oxygen and nitrogen species (ROS and RNS) has been put forward as a crucial strategy in the suppression of the deleterious effects of oxidative stress, which give rise to the development of diseases, including cancer. Antioxidants are complex molecules, abundant in medicinal plants. They act as a protective shield for cells against the deleterious effects of ROS and RNS. In addition, antioxidants may easily neutralize free radicals (i.e., hydroxyl, peroxyl, and superoxide radicals) retarding them from binding with bioactive macromolecules (proteins, lipids, and DNA) in normal cells (11). The formation and elimination of free radicals are well-balanced, shifting of this balance to overproduction of free radicals causes oxidative stress, thus playing a crucial role in many diseases including tissue damage, inflammation, neurodegenerative diseases, cancer, and aging (8). It is also known that there are many antioxidant substances (especially synthetic ones) that fight against these negative effects of free radicals. On the other hand, it has been shown that the usage of synthetic antioxidants such as butylated hydroxyanisole and butylated hydroxytoluene cause potential health risks and toxicity as a result of their side effects (12). For this reason, there is currently an upsurge of interest in phytochemicals as a new source of both natural and novel antioxidants to be used in foods and pharmaceutical preparations to replace synthetic antioxidants (13).

Sulfur, one of the most essential chemical elements, is necessary for biochemical functions in all living organisms owing to its involvement in the structures of proteins, enzymes, amino acids (e.g., methionine and cysteine), and certain vitamins (e.g., thiamine and biotin) (14). In contrast to mammals (e.g., humans and monogastric animals), plants can utilise inorganic sulfur for synthesizing sulfur amino acids. Accordingly, plants are important sources of sulfur for most animals (15). These sulfur molecules can also be referred to as organosulfur compounds [for example, α-lipoic acid (ALA), cysteine (Cys), cystin, homocysteine (HCys), glutathione (GSH), taurine, vitamin U (Vit U), and allylic sulfur compounds] which are found in cruciferous plants. In addition, they provide beneficial health effects by maintaining the redox balance through transmethylation/transsulfuration pathways in the cell (16).

All over the world, the number of side effects of treatment with herbal drugs is very low compared to synthetic drugs. They are also more accessible in terms of having a lower cost, thereby making these treatments/plants more attractive. Therefore, the usage and importance of herbal preparations that contain bioactive constituents such as organosulfur compounds in the treatment of various diseases is increasing. The aim of the current study was to determine the antioxidant activities of different *E. spectabilis* M. Bieb. extracts and sulfur compounds by using different methods.

MATERIALS AND METHODS

Chemicals

All chemicals used in the preparation of the extracts, and in the experiments were supplied by Sigma-Aldrich (St. Louis, MO, USA) or Merck (KGaA, Darmstadt, Germany). All other chemicals were of analytical grade.

Herbal Material

The fresh *E. spectabilis* M. Bieb. specimens (both roots and leaves) were obtained from local markets in the Eyup district of Istanbul/Turkey. The plant was inspected and identified by Prof. Dr. Emine Akalin (Faculty of Pharmacy, Istanbul University). A specimen was deposited at the Faculty of Pharmacy Herbarium of Istanbul University (ISTE 93132). The plant samples were carefully washed three times with distilled water and then dried at room temperature. The dried plant was stored at −20°C until required for use.

Preparation of Extracts

Dried and ground plant materials were used for extract preparation. The reflux system was used to for preparing an aqueous extract for 6 h, which was then lyophilized. The amount of aqueous extract obtained was found to be 323.1 % mg dry weight (d.w.). Alongside this, both ethanolic and ethyl acetate extracts of the plant were prepared using the Soxhlet extractor for 6 h. Thereafter, these extracts were evaporated under low pressure. The ethanolic and ethyl acetate extract amounts were found to be 436.6 % mg d.w. and 439.2 % mg d.w., respectively. All extracts were kept in a freezer at -20°C before use.

Phytochemical Analysis

Phytochemical analysis of extracts was employed to investigate various major classes of secondary metabolites (e.g., alkaloids, anthraquinones, carbohydrates, diterpenes, flavonoids, phenolics, phytosterols, proteins, sulfurs, and tannins) using standard qualitative analysis methods (17).

Assesment of Total Phenolic Contents (TPCs)

To determine TPCs in all extracts of *E. spectabilis* M. Bieb., the method of Slinkard and Singleton was employed using Folin-Ciocalteau reagent (18). A reference solution of catechin (25-200 µg/mL) was employed to obtain the calibration curve. Thereafter, the TPCs in the *E. spectabilis* M. Bieb. extracts were calculated as µg of catechin equivalent per mL of extract.

Assesment of Total Flavonoid Contents (TFCs)

TFCs in all extracts of *E. spectabilis* M. Bieb. were assessed employing the aluminum chloride colorometric method according to Zhishen et al., (19). A reference solution of pyrocatechin (25-300 µg/mL) was used to obtain the calibration curve. Thereafter, the TFCs in the *E. spectabilis* M. Bieb. extracts were calculated as µg of pyrocatechin equivalent per mL of extract.

Reducing Power Assay

The reducing power of *E. spectabilis* M. Bieb. extracts and sulfur compounds was determined using the method described by Oyaizu (20). As a reference solution, 6-hydroxy-2,5,7,8-tetramethylchromane-2-carboxylic acid (Trolox) was used. The intensity of the blue color is directly proportional to the reducing power of the tested samples. A high absorbance of the reaction mixture indicates a greater reducing power of the tested samples.

Cupric Ions (Cu^{2+}) Reducing Antioxidant Capacity (CUPRAC) Assay

Total antioxidant capacities of *E. spectabilis* M. Bieb. extracts and sulfur compounds were obtained using Cu(II)-neocuproine reagent according to Apak et al., (21). Trolox was used as a reference solution. The intensity of the yellow-orange color is directly proportional to the total antioxidant capacity of the tested samples. A high absorbance of the reaction mixture indicates a greater total antioxidant capacity of the tested samples.

Ferric Reducing Antioxidant Power (FRAP) Assay

The FRAP assay was carried out utilizing 2,4,6-tri(2-pyridyl)-S-triazine -$FeCl_3$ complex system according to Benzie and Strain (22). Reference solutions of $FeSO_4.7H_2O$ were employed to obtain the calibration curve. L-ascorbic acid and α-tocopherol were used as positive controls. The results were expressed as µM Fe^{2+} per 100 mL sample.

ABTS Radical Scavenging Activity Assay

ABTS [2,2'-azino-bis (3-ethylbenzothiazoline-6-sulfonic acid)] radical scavenging activities of the extracts of *E. spectabilis* M. Bieb., sulfur compounds and reference antioxidant were completed using 2,2'-azino-bis (3-ethylbenzothiazoline-6-sulfonic acid) diammonium salt according to the discolorizing procedure of Arnao et al., (23). α-Tocopherol was used as a reference antioxidant. The ABTS radical scavenging activity was calculated using the following equation:

$$\text{ABTS radical scavenging activity (\%)} = \left[\frac{(A_0 - A_1)}{A_0}\right] \times 100 \quad (1)$$

A_0 is the absorbance of the initial concentration of ABTS

A_1 is the absorbance of the remaining concentration of ABTS in the presence of samples (or reference antioxidant).

DPPH Radical Scavenging Activity Assay

DPPH (2,2-diphenyl-1-picrylhydrazyl) radical scavenging activities of the extracts of *E. spectabilis* M. Bieb., sulfur compounds and reference antioxidant were estimated utilizing 2,2-diphenyl-1-picrylhydrazyl (DPPH) (24). Trolox was used as a reference antioxidant. The DPPH radical scavenging activity was calculated using the following equation:

$$\text{DPPH radical scavenging activity (\%)} = \left[\frac{(A_0 - A_1)}{A_0}\right] \times 100 \quad (2)$$

A_0 is the absorbance of the initial concentration of DPPH

A_1 is the absorbance of the remaining concentration of DPPH in the presence of samples (or reference antioxidant).

DMPD Radical Scavenging Activity Assay

The determination of DMPD (N,N-dimethyl-4-phenylenediamine) radical scavenging activity was performed using the N,N-dimethyl-4-phenylenediamine decolorization method developed by Fogliano et al., (25). Trolox was used as a reference antioxidant. The DMPD radical scavenging activity was calculated using the following equation:

$$\text{DMPD radical scavenging activity (\%)} = \left[\frac{(A_0 - A_1)}{A_0}\right] \times 100 \quad (3)$$

A_0 is the absorbance of the initial concentration of DMPD

A_1 is the absorbance of the remaining concentration of DMPD in the presence of samples (or reference antioxidant).

Superoxide Radical Scavenging Activity Assay

Superoxide radical scavenging activity of the extracts of *E. spectabilis* M. Bieb., sulfur compounds and reference antioxidant were employed according to Liu et al., (26) using the phenazine methosulfate -reduced nicotinamide adenine dinucleotide -nitroblue tetrazolium system. As a reference antioxidant, Trolox was used. The superoxide radical scavenging activity was calculated using the following equation:

$$\text{The superoxide radical scavenging activity (\%)} = \left[\frac{(A_0 - A_1)}{A_0}\right] \times 100 \quad (4)$$

A_0 is the absorbance of control

A_1 is the absorbance of the sample (or reference antioxidant).

Hydroxyl Radical Scavenging Activity Assay

Hydroxyl radical scavenging activities of the extracts of *E. spectabilis* M. Bieb. and sulfur compounds were measured by the oxidation of 2-deoxy-D-ribose by the hydroxyl radical (27). Gallic acid (GA) was employed as a reference solution. The hydroxyl radical scavenging activity was calculated using the following equation:

$$\text{Hydroxy radical scavenging activity (\%)} = \left[\frac{(A_0 - A_1)}{A_0}\right] \times 100 \quad (5)$$

A_0 is the absorbance of the control

A_1 is the absorbance of the sample (or reference antioxidant).

Metal Chelating Activity Assay

The metal chelating activities of the extracts of *E. spectabilis* M. Bieb., sulfur compounds and reference antioxidants were determined using the 3-(2-pyridyl)-5,6-diphenyl-1,2,4-triazine-4',4''-disulfonic acid sodium salt (ferrozine)-Fe^{2+} complex method described by Decker and Welch (28). As reference antioxidants, a mixture containing ethylenediaminetetraacetic acid (EDTA) (or GA) was used instead of the sample. A low ab-

sorbance indicates a higher chelating activity of the tested samples. The percentage inhibition of ferrozine-Fe^{2+} complex formation was calculated using the formula:

$$\text{Metal chelating activity (\%)} = \left[\frac{(A_0 - A_1)}{A_0}\right] \times 100 \quad (6)$$

A_0 is the absorbance of the control

A_1 is the absorbance of the samples (or reference antioxidants).

For all antioxidant activities, the extracts and sulfur compounds (or standards) concentration providing half maximum (50 %) inhibitions (IC_{50}) was calculated using regression equations (by plotting extract solution concentration versus percentage inhibition). A low IC_{50} indicates a higher inhibitory potential of the tested plant extracts and sulfur compounds.

RESULTS

Phytochemical Analysis

The results of phytochemical analysis of all the extracts of *E. spectabilis* M. Bieb. are depicted in Table 1. The ethyl acetate extract of *E. spectabilis* M. Bieb. is rich in anthraquinones, diterpenes, flavonoids, phenolics, and proteins. On the other hand, anthraquinones and diterpenes were higher in the ethanolic extract, while the aqueous extract was only rich in phenolics. All other phytochemical constituents in the three extracts were detected in moderate or low quantities (Table 1).

TPCs and TFCs of *E. spectabilis* M.Bieb.

The TPCs and TFCs of all the extracts of *E. spectabilis* M. Bieb. are summarized in Table 2. It was found that the TPCs and TFCs of all extracts became elevated as the concentration increased. The highest TPCs and TFCs in all extracts was found at a concentration of 2500 µg/mL (Table 2). Meanwhile, in this concentration, the TPCs in all extracts of this plant (assessed using Folin-Ciocalteau reagent), were close to each other while the TFCs ranged from 34.64±0.55 to 183.99±3.55 µg/mL. The order for TPCs and TFCs of the extracts is as follows: ethanolic > ethyl acetate > aqueous extract and ethyl acetate > ethanolic > aqueous extract, respectively (Table 2).

Table 1. Phytochemical analysis of all extracts of *Eremurus spectabilis* M. Bieb.*

Phytochemicals	Aqueous Extract	Ethanolic Extract	Ethyl Acetate Extract	Methods
Alkaloids	+	++	++	Hager's test
Anthraquinones	+	+++	+++	Bornträger Test
Carbohydrates	+	+	+	Molisch test
Diterpenes	+	+++	+++	Cupric acetate test
Flavonoids	+	++	+++	Zhishen's test
Phenolics	+++	+	+++	Millon's test
Phytosterols	-	+	++	Lieberman Burchard's Test
Proteins	+	++	+++	Xanthoproteic test
Sulfurs	+	+	++	Lead acetate test
Tannins	+	++	++	Braemar's test

*(+): Present in poor; (++): Present in moderate; (+++): Present in more quantity; (-): Absent.

Table 2. Total phenolic contents and total flavonoid contents of all extracts of *Eremurus spectabilis* M. Bieb.

Extracts	Concentrations (µg/mL)	TPCs (µg Catechin eq/mL)*	TFCs (µg Pyrocatechin eq/mL)*
Aqueous extract	1500	46.53±0.79	20.90±0.79
	2000	52.80±0.26	27.81±0.26
	2500	62.80±0.55	34.64±0.55
Ethanolic extract	1500	56.53±0.69	42.09±0.69
	2000	62.19±0.65	61.38±0.65
	2500	80.37±2.27	71.54±2.27
Ethyl acetate extract	1500	52.60±0.18	107.25±1.78
	2000	61.68±1.22	138.13±3.17
	2500	73.00±1.09	183.99±3.55

*Mean±standard deviation (n=3), TPCs: Total phenolic contents, TFCs: Total flavonoid contents.

Reducing Power, CUPRAC Levels, and FRAP Values of *E. spectabilis* M.Bieb. Extracts and Sulfur Compounds

The reducing power, CUPRAC levels, and FRAP values of all the extracts of *E. spectabilis* M. Bieb., sulfur compounds and reference antioxidants are presented in Table 3. In the current study, it was found that reducing power, CUPRAC levels, and FRAP values of all tested samples elevated with an increase in concentration (Table 3). At 1000 µg/mL for all extracts and Trolox, it was observed that reducing power and CUPRAC levels decreased as follows, respectively: Trolox (1.705±0.009 and 2.705±0.144) > ethyl acetate (0.822±0.002 and 0.225±0.006) > ethanolic (0.684±0.002 and 0.185±0.004) > aqueous extract (0.318±0.011 and 0.050±0.002) (Table 3). When the sulfur compounds were compared, it was seen that their reducing power and CUPRAC values diminished in the order of: Diallyl sulfide (DAS) > HCys > N-Acetylcysteine (NAC) > GSH > Cys > ALA > Vit U and $CysNH_2$ > Cys > HCys > 1,4-DTE > NAC > GSH > DAS > ALA > Vit U, respectively (Table 3). At 250 µg/mL concentration, FRAP values of aqueous, ethanolic, and ethyl acetate extracts were found to be very close (15.92±0.76 µM Fe^{2+}, 13.33±0.90 µM Fe^{2+}, and 17.94±0.49 µM Fe^{2+}, respectively), they exhibited weak FRAP values as compared to standard (350.21±1.12 µM Fe^{2+} for L-ascorbic acid). Of the sulfur compounds, ALA had a much better FRAP value than the standard compound (Table 3).

ABTS, DPPH and DMPD Radical Scavenging Activities of *E. spectabilis* M.Bieb. Extracts and Sulfur Compounds

The ABTS, DPPH and DMPD radical scavenging activities of *E. spectabilis* M. Bieb. extracts and sulfur compounds are shown in Table 4. The results depict half-maximal inhibition concentrations (IC_{50}) values of the ABTS, DPPH and DMPD radical scavenging activities of the samples. The IC_{50} values were calculated by plotting the inhibition percentage values as a function of their concentrations. IC_{50} is defined as the concentration of a sample that gives rise to 50 % of free radicals neutralization. Thus, the lower the IC_{50} value, the higher the radical scavenging activity. In our study, the IC_{50} values ranging from 312.71±6.74 to 469.43±13.24 µg/mL for ABTS, 0.409±0.004 to 0.843±0.019 mg/mL for DPPH, and $75.43x10^{-9}$±$1.61x10^{-9}$ mg/mL to 0.100±0.0006 mg/mL for DMPD were recorded for aqueous, ethanolic and ethyl acetate extracts, while the IC_{50} values of 102.45±1.90 µg/mL and 0.012±0.0002 mg/mL and 0.001±0.0001 mg/mL were found for α-tocopherol and Trolox, respectively (Table 4). Considering the high antioxidant activities (associated with the lower IC_{50} values), it was found that the IC_{50} values of all extracts had been higher ABTS and DPPH radical scavenging activities than standards (α-tocopherol and Trolox, respectively). In contrast, both ethanolic and ethyl acetate extracts were found to be stronger DMPD radical scavengers than aqueous extract and Trolox (Table 4). Comparisons show that the sulfur compounds (excluding Vit U and DAS) exhibited greater ABTS radical scavenging activities than α-tocopherol, while only $CysNH_2$ exhibited better DPPH radical scavenging activity than Trolox. On the other hand, of the sulfur compounds, it was seen that DAS had the best DMPD scavenging activity. In addition to our DMPD results, GSH, NAC, and 1,4-DTE had the same IC_{50} values as Trolox (Table 4).

Superoxide Radical, Hydroxyl Radical Scavenging, and Metal Chelating Activities of *E. spectabilis* M.Bieb. Extracts and Sulfur Compounds

Superoxide radical, hydroxyl radical scavenging, and metal chelating activities of all the extracts of *E. spectabilis* M. Bieb. and sulfur compounds are summarized in Table 5. In the current study, the IC_{50} values of superoxide radical scavenging activities of extracts were found to be as follows: aqueous (17.62±0.65 µg/mL), ethanolic (21.77±0.64 µg/mL), and ethyl acetate (8.83±1.64 µg/mL) extracts. As seen in Table 5, all extracts were stronger superoxide radical scavengers than Trolox (Table 5). Of the sulfur compounds, both DAS and HCys exhibited almost the same strong IC_{50} values as superoxide radicals (0.026±0.0003 µg/mL for DAS and 0.027±0.0004 µg/mL for HCys) (Table 5). The superoxide radical scavenging activities decreased in the order of: DAS > HCys > NAC > GSH > 1,4-DTE > $CysNH_2$ > Cys > Vit U > ALA (Table 5). Herein, the hydroxyl radicals scavenging activities of extracts decreased in the order of: ethanolic ($7.82x10^{-3}$±$0.09x10^{-3}$ mg/mL) > ethyl acetate ($8.93x10^{-3}$±$0.33x10^{-3}$ mg/mL) > aqueous (44.41±0.03 mg/mL) extracts. Comparisons show that the hydroxyl radical scavenging activities for the sulfur compounds (excluding ALA and DAS) were higher than that of the standard (GA), whereas Vit U had low hydroxyl radical scavenging activity (Table 5). As for metal chelating activities, all extracts had a greater tendency to metal chelation as compared to GA. The metal chelating activities of sulfur compounds decreased as follows: EDTA > $CysNH_2$ > DAS > 1,4-DTE > Cys > ALA > Vit U > NAC > HCys > GSH (Table 5).

DISCUSSION

The value of medicinal herbs is associated with having the major biologically active constituents known as secondary metabolites. This makes them an important natural source for usage in either traditional or conventional medicine. However, their values can be specified by the diversity of their phytochemical constituents which produce a certain physiological effect on the organism (29). These phytochemicals may be distinguished in several ways, which are based on their biosynthetic origin, solubility properties, and the presence of key chemical groups (30). In a recent study, Güler et al., reported that wild medicinal plants were more preferred than cultivated species (2).

Wild edible and medicinal plants like *E. spectabilis* M. Bieb., which contain natural ingredients rich in bioactive compounds (such as phenolics and flavonoids), have attracted attention due to their biological properties. They exhibit antioxidant activity and are considered as a good alternative to synthetic antioxidants (12). From this point of view, this work was designed to investigate the antioxidant activities of the aqueous, ethanolic and ethyl acetate extracts of *E. spectabilis* M. Bieb. and certain sulfur compounds.

Phytochemicals are the essence of plant-based drugs; the efficacy of their therapeutic role is directly proportional to the richness of these constituents in plants (31). In this study, the phytochemical consituents (e.g., alkaloids, flavonoids, phenolics etc.)

Table 3. Reducing power, total antioxidant capacity levels, and ferric reducing antioxidant power values of all extracts of *Eremurus spectabilis* M. Bieb. and sulfur compounds.

Extracts /Sulfur Comp. /Standards	Conc. (µg/mL)	Reducing Power*,#	Conc. (µg/mL)	CUPRAC*,#	Conc. (µg/mL)	FRAP (µM Fe^{2+})*
Aqueous extract	600	0.248±0.001	600	0.023±0.005	250	15.92±0.76
	800	0.292±0.001	800	0.034±0.003	500	23.89±0.43
	1000	0.318±0.011	1000	0.050±0.002	1000	44.09±1.49
Ethanolic extract	600	0.485±0.007	600	0.122±0.003	250	13.33±0.90
	800	0.592±0.008	800	0.154±0.003	500	18.95±0.79
	1000	0.684±0.002	1000	0.185±0.004	1000	31.99±0.52
Ethyl acetate extract	600	0.619±0.005	600	0.147±0.002	250	17.94±0.49
	800	0.735±0.001	800	0.181±0.006	500	28.96±0.76
	1000	0.822±0.002	1000	0.225±0.006	1000	50.43±1.05
ALA	600	0.104±0.002	500	0.012±0.001	2.5	35.73±0.58
	800	0.114±0.002	750	0.025±0.002	5	65.60±0.88
	1000	0.132±0.003	1000	0.031±0.003	10	127.65±0.58
Cys	60	0.229±0.002	50	0.406±0.002	25	9.23±0.29
	80	0.274±0.001	75	0.564±0.006	50	12.01±0.32
	100	0.331±0.003	100	0.688±0.003	100	18.73±0.58
$CysNH_2$	60	0.131±0.001	50	0.460±0.004	250	9.22±0.29
	80	0.171±0.002	75	0.556±0.006	500	11.33±0.44
	100	0.188±0.004	100	0.731±0.004	1000	18.73±0.58
DAS	0.001	0.081±0.004	50	0.006±0.002	250	12.77±0.17
	0.01	0.091±0.001	75	0.009±0.001	500	14.31±0.44
	0.1	0.099±0.002	100	0.014±0.001	1000	17.00±0.58
GSH	60	0.245±0.003	50	0.140±0.003	250	23.34±1.15
	80	0.294±0.002	75	0.216±0.005	500	41.40±1.16
	100	0.355±0.004	100	0.302±0.003	1000	77.03±1.01
HCys	60	0.522±0.005	50	0.303±0.004	250	34.67±1.76
	80	0.641±0.002	75	0.430±0.006	500	64.45±1.92
	100	0.736±0.004	100	0.600±0.004	1000	122.66±2.04
NAC	60	0.326±0.001	50	0.290±0.007	25	31.22±0.72
	80	0.404±0.002	75	0.360±0.004	50	60.03±0.72
	100	0.433±0.003	100	0.502±0.005	100	114.28±1.45
Vit U	600	0.094±0.002	5000	0.024±0.002	2.5	6.79±0.03
	800	0.101±0.002	7500	0.035±0.003	5	7.00±0.03
	1000	0.108±0.001	10000	0.042±0.001	10	7.38±0.05
1,4-DTE	60	0.456±0.001	50	0.348±0.003	25	61.38±0.86
	80	0.558±0.001	75	0.474±0.006	50	122.47±1.75
	100	0.704±0.004	100	0.585±0.004	100	225.63±1.44
Trolox[a]	600	1.602±0.003	600	2.568±0.046	-	-
	800	1.661±0.010	800	2.636±0.041		
	1000	1.705±0.009	1000	2.705±0.144		
α-Tocopherol[b]	-	-	-	-	50	31.12±1.24
					100	56.38±1.66
					250	146.77±1.59
L-Ascorbic acid[b]	-	-	-	-	50	93.94±0.91
					100	186.54±1.23
					250	350.21±1.12

*Mean±standard deviation (n=3), ALA: α-Lipoic acid, $CysNH_2$: Cysteamine, Cys: Cysteine, DAS: Diallyl sulfide, GSH: Glutathione, HCys: Homocysteine, NAC: N-Acetyl cysteine, Vit U: Vitamin U, 1,4-DTE: 1,4-Dithioerythritol, CUPRAC: Cupric ions (Cu^{2+}) reducing antioxidant capacity, FRAP: Ferric ion reducing antioxidant power, #Absorbance; [a]Standard for reducing power and CUPRAC; [b]Standards for FRAP.

Table 4. 2,2'-Azino-bis(3-ethylbenzothiazoline-6-sulfonic acid), 2,2-Diphenyl-1-picrylhydrazyl, N,N-dimethyl-4-phenylenediamine radical scavenging activities of all extracts of *Eremurus spectabilis* M. Bieb. and sulfur compounds.

Extracts /Sulfur Compounds /Standards	ABTS IC_{50} (µg/mL)*	DPPH IC_{50} (mg/mL)*	DMPD IC_{50} (mg/mL)*
Aqueous extract	469.43±13.24	0.409±0.004	0.100±0.0006
Ethanolic extract	312.71±19.94	0.482±0.003	$75.43x10^{-9}$±$1.61x10^{-9}$
Ethyl acetate extract	375.01±6.74	0.843±0.019	$80.20x10^{-9}$±$1.31x10^{-9}$
ALA	98.18±0.15	126.33±12.83	0.88±0.01
Cys	31.74±0.53	0.015±0.0002	0.005±0.0001
$CysNH_2$	9.12±0.06	0.009±.0002	0.004±0.0001
DAS	290.92±31.94	0.198±0.016	$7.96 x10^{-9}$±$0.82x10^{-9}$
GSH	58.65±0.92	0.081±0.003	0.001±0.0002
HCys	25.66±0.21	0.041±0.002	0.005±0.0002
NAC	13.96±0.68	0.025±0.0002	0.001± 0.0001
Vit U	153.11±4.12	0.232±0.0002	50.04±1.48
1,4-DTE	35.30±1.13	0.029±0.0002	0.001±0.0001
α-Tocopherol[a]	102.45±1.90	-	-
Trolox[b,c]	-	0.012±0.0002	0.001±0.0001

*Mean±standard deviation (n=3). ALA: α-Lipoic acid, $CysNH_2$: Cysteamine, Cys: Cysteine, DAS: Diallyl sulfide, GSH: Glutathione, HCys: Homocysteine, NAC: N-Acetyl cysteine, Vit U: Vitamin U, 1,4-DTE: 1,4-Dithioerythritol, ABTS: 2,2'-Azino-bis(3-ethylbenzothiazoline-6-sulfonic acid), DPPH: 2,2-Diphenyl-1-picrylhydrazyl, DMPD: N,N-dimethyl-4-phenylenediamine, [a]Standard for ABTS radical scavenging activity, [b,c]Standard for DPPH and DMPD radical scavenging activities.

Table 5. Superoxide radical, hydroxyl radical scavenging, and metal chelating activities of all extracts of *Eremurus spectabilis* M. Bieb. and sulfur compounds.

Extracts /Sulfur Compounds /Standards	Superoxide Radical Scavenging Activities IC_{50} (µg/mL)*	Hydroxyl Radical Scavenging Activities IC_{50} (mg/mL)*	Metal Chelating Activities IC_{50} (mg/mL)*
Aqueous extract	17.62±0.65	44.41±0.03	0.74±0.01
Ethanolic extract	21.77±0.64	$7.82x10^{-3}$±$0.09x10^{-3}$	0.82±0.03
Ethyl acetate extract	8.83±1.64	$8.93x10^{-3}$±$0.33x10^{-3}$	1.01±0.01
ALA	157.25±4.71	$7.99x10^{-9}$±$1.25x10^{-9}$	23.38±0.79
Cys	37.10±2.32	50.05±1.26	8.71±0.09
$CysNH_2$	20.09±1.57	48.14±0.99	0.038±0.002
DAS	0.026±0.0003	$8.39 x10^{-9}$±$0.05 x10^{-9}$	0.38±0.04
GSH	5.11±0.28	36.42±0.76	110.37±5.38
HCys	0.027±0.0004	0.55±0.02	55.61±6.51
NAC	0.78±0.01	29.07±1.04	46.65±2.47
Vit U	52.16±1.73	92.00±2.16	39.50±0.06
1,4-DTE	19.81±0.91	42.16±1.08	0.47±0.01
Trolox[a]	25.34±1.07	-	-
α-Tocopherol[b]	-	$9.24x10^{-3}$±$0.14x10^{-3}$	-
GA[b,c]	-	77.13±5.56	35.57±0.87
EDTA[c]	-	-	0.034±0.003

*Mean±standard deviation (n=3). ALA: α-Lipoic acid, $CysNH_2$: Cysteamine, Cys: Cysteine, DAS: Diallyl sulfide, GSH: Glutathione, HCys: Homocysteine, NAC: N-Acetyl cysteine, Vit U: Vitamin U, 1,4-DTE: 1,4-Dithioerythritol, [a]Standard for superoxide radical scavenging activity, [b]Standard for hydroxyl radical scavenging activity, [c]Standard for metal chelating activity.

present in *E. spectabilis* M. Bieb. varied in quantity. According to our results, it was found that the aqueous extract had the poor, the ethanolic extract had the moderate, and the ethyl acetate extract had the more quantity of alkaloids, flavonoids, protein, and tannins, respectively. On the other hand, anthraquinones and diterpenes were found to be of a higher degree in the ethanolic extract, while the aqueous extract was only rich in phenolics. All other phytochemical constituents in three extracts were detected in low or moderate quantities. The present findings are in line with the results on phytochemical screening wild plants previously published (13, 32).

In general, phenolics and flavonoids, ubiquitous in plants such as *E. spectabilis* M. Bieb., may play crucial roles owing to their antioxidant potentials as well as having beneficial health effects in the prevention of several diseases such as diabetes, cancer, gastrointestinal illnesses, and aging-related disorders (33, 34). In the current study, TPCs were found to be at their highest level in ethanolic extract, whereas TFCs were at their lowest level in aqueous extract of *E. spectabilis* M. Bieb. The present findings were inconsistent with those of Ozsoy et al., who reported that the aqueous extracts of *Smilax excelsa* L. and *Amaranthus lividus* L. had the highest TPC levels (35, 36). On the other hand, it was revealed by Peksel et al., that TPC levels of the alcoholic extract of *Pistacia atlantica* Desf. leaves were higher than those of ethyl acetate extracts (37). A study by Falahi et al., reported that *E. spectabilis* M.Bieb. extract had the highest TPC levels (591.00±111.73 mg GA equivalent) and TFC levels (18.32±2.30 mg GA equivalent) of the other five traditional Iranian wild edible plants (12). In the study conducted on *E. himalaicus*, it was reported that the aqueous extract contained more TPCs and TFCs than ethanolic extract (8). The discrepancies between the aforementioned reports and the current study regarding TPCs and TFCs of these extracts may be due to the different geographical origins of the plants as well as the tested part of the herbs.

The reducing power and CUPRAC tests provide a convenient, fast, and simple estimation of total phenolics in plant extracts, as well as the overall antioxidant capacity of plant tissue extracts (21). The FRAP test is also a simple, fast, cost-effective and widely used method that directly assesses the antioxidant potentials of the samples (38). According to our findings, the reducing power and CUPRAC values of both ethanolic and ethyl acetate extracts were higher than those of the aqueous extract. This is in line with the TPCs and TFCs of the same extracts. On the other hand, an increase in FRAP values of all extracts in terms of dose was consistent with TPCs of all extracts in this study. This is similar to the findings of Bernaert et al., (39). Of the sulfur compounds, ALA had a much better FRAP value than the standard compound. A possible explanation for this may be associated with the redox potential of ALA being lower than the ferric-ferrous couple (40). Other sulfur compounds showed weaker ferrous ion reducing capacity. This may be due to the low pH (pH 3.6) compared to the physiological pH. This low pH in the FRAP protocol may result in reducing capacity being suppressed depending on protonation on antioxidant compounds, hence providing lower antioxidant activity (41).

Free radical scavenging assays (ABTS, DPPH, and DMPD) are accepted as standard methods (which are simple, rapid, convenient, and fast techniques) based on decolorization reaction for estimation of antioxidant capacities of foods, beverages, pharmaceuticals as well as biological fluids (38). In the present study, it was seen that there was compliance between the TPCs and TFCs of these plant extracts and their free radical scavenging activities. These observations were in line with the previously published outcomes of Mushtaq et al., (8) However, studies on some Indian medicinal plants have also been reported a strong correlation between TPCs and antiradical activity (42). In addition, Gaggeri et al., reported that ethanolic root extracts of two *Eremurus* species had very close antiradical activities (43). As for comparisons of sulfur compounds and standard antioxidants, $CysNH_2$ exhibited a better DPPH radical scavenging activity and GSH, NAC, and 1,4-DTE showed the same DMPD radical scavenging activities compared to their respective standards. NAC has also been reported to have better antiradical activity than the standard (44).

The superoxide anion is the main precursor molecule that underpins the formation of H_2O_2, and the hydroxyl radical, which triggers oxidative damage in lipids, proteins, and DNA (11). Metal ions in the organism such as free Fe(II) ion can provide an unwanted increase in the production of ROS via distinct reactions viz., Fenton reactions (45). Any substance having the ability to chelate iron can be valuable in terms of antioxidant properties by delaying metal-catalyzed oxidation of ROS (46). In a study on the radical mopping effects of *Asphodelus aestivus* Brot. extracts conducted by Peksel and her colleagues, 1 mg/mL of methanolic extract exhibited a strong scavenging effect on superoxide radicals (47). These findings were found to be lower than the outcomes of the current study. Similar results were reported by Eddine et al., (48). In the current study, all extracts exhibited more effective hydroxyl radical scavenging activities than GA. These observations were higher than previously published article by Sacan et al., who reported that the extract of *Eruca sativa* Mill. also had hydroxyl radical scavenging activity (49). On the other hand, both ALA and DAS exhibited the best hydroxyl radical scavenging activities among all the tested samples (extracts, sulfur compounds, and standards). When the extracts were compared in terms of metal chelating activities, it was found that all extracts showed strong metal chelating activities when compared to GA, but they exhibited weak metal chelating activities in comparison with EDTA. This may be attributed to its richness in varied amounts of bioactive constituents, which reportedly include resveratrol and flavonoids (e.g., rutin, morin, and quercetin) (50). In addition, due to their hydroxyl groups or carbonyl moieties in structure, these flavonoids may contribute to the higher chelating ability of the extracts (51). In contrast, among the sulfur compounds, only $CysNH_2$ was observed to have almost the same metal chelating activity as EDTA. The reason that $CysNH_2$ has the highest metal chelating activity among other sulfur compounds may be due to the free thiol group in its structure.

CONCLUSIONS

In the current study, the antioxidant activities of different extracts of *E. spectabilis* M. Bieb. and important sulfur compounds were investigated. Taken together, the present findings revealed that all extracts of *E. spectabilis* M. Bieb. exerted considerable antioxidant potential against different radicals *in vitro.* Moreover, it was observed that the ethyl acetate extract had a better radical scavenging effect than the other extracts. On the other hand, DAS was found to have the highest antioxidant activity out of the studied sulfur compounds. From this point of view, it may be considered that *E. spectabilis* M. Bieb. may be a good source of potent antioxidants in the prevention of oxidative stress-mediated disorders. In addition, more research should be done to determine the possible beneficial effects of these sulfur compounds on health.

Acknowledgement: This study was supported by Istanbul University-Cerrahpaşa Scientific Research Projects Units with the grant numbers 22605 and UDP-55170.

Informed Consent: Written consent was obtained from the participants.

Peer Review: Externally peer-reviewed.

Author Contributions: Conception/Design of Study- B.B.B., R.Y.; Data Acquisition- B.B.B.; Data Analysis/Interpretation- B.B.B., R.Y.; Drafting Manuscript- B.B.B., R.Y.; Critical Revision of Manuscript- B.B.B., R.Y.; Final Approval and Accountability- B.B.B., R.Y.

Conflict of Interest: Authors declared no conflict of interest.

Financial Disclosure: Authors declared no financial support.

REFERENCES

1. Hayta S, Polat R, Selvi S. Traditional uses of medicinal plants in Elazığ (Turkey). J Ethnopharmacol 2014; 154(3): 613-23.
2. Güler B, Erkan Y, Uğurlu E. Traditional uses and ecological resemblance of medicinal plants in two districts of the Western Aegean Region (Turkey). Environ Dev Sustain 2020; 22(3): 2099-120.
3. Beiranvand M, Beiranvand F. Iranian plant *Eremurus persicus*: An overview of botany, traditional uses, phytochemistry and pharmacology. Nat Prod Res 2021; doi: 10.1080/14786419.2021.1916744 [Epub ahead of print].
4. Mehdiyeva N, Fayvush G, Aleksanyan A, Alizade V, Paniagua Zambrana NY, Bussmann RW. *Eremurus spectabilis* M. Bieb. Xanthorrhoeaceae. Bussmann RW, editor. Ethnobotany of the Caucasus. Cham: Springer International Publishing; 2017.p. 285-88.
5. Baytop T. Türkiye'de Bitkiler ile Tedavi: Geçmişte ve Bugün. Ankara: Nobel Tıp Kitabevleri 1999.s.185.
6. Karaoğlan ES, Albayrak A, Kutlu Z, Bayır Y. Gastroprotective and antioxidant effects of *Eremurus spectabilis* Bieb. methanol extract and its isolated component isoorientin on indomethacin induced gastric ulcers in rats. Acta Cir Bras 2018; 33: 609-18.
7. Abubaker SR, Hidayat HJ. Anti-tumor potential of local aslerk (*Eremurus spectabilis*) leaf extracts by HPLC and applying on cancer cell lines *in vitro.* Iraqi J Cancer Med Genet 2015; 8(2): 123-8.
8. Mushtaq A, Masoodi MH, Wali AF, Ganai BA. Total phenolic content, total flavonoid content, *in vitro* antioxidant activity and antimicrobial activity against human pathogenic bacteria of *Eremurus himalaicus*–An edible herb of North Western Himalayas. Free Radic Antioxid 2017; 7(1): 90-4.
9. Bayrak BB, Yanardag R. Histone deacetylase, xanthine oxidase and urease inhibitory activities of *Eremurus spectabilis* M. Bieb. extracts. Experimed 2021a; 11(2): doi: 10.26650/experimed.2021.913680 [Epub ahead of print].
10. Bayrak BB, Yanardag R. Inhibitory effects of aqueous extract of *Eremurus spectabilis* M. Bieb. on diabetes mellitus and skin related enzymes. Istanbul J Pharm 2021b; 51(2): doi: 10.26650/IstanbulJPharm.2021.934461 [Epub ahead of print].
11. Njoya E. Medicinal plants, antioxidant potential, and cancer. Preedy VR, Pattel VB, editors. 2nd ed., Cancer: Oxidative Stress and Dietary Antioxidants. London: Academic Press; 2021.p. 349-57.
12. Falahi E, Delshadian Z, Ahmadvand H, Jokar S. Head space volatile constituents and antioxidant properties of five traditional Iranian wild edible plants grown in west of Iran. AIMS Agric Food 2019; 4(4): 1034-53.
13. Adawia K, Rawaa AK, Ghalia S. Phytochemical screening and antioxidant activity of selected wild plants in *Liliaceae* family growing Syria. Int J Pharmacogn Phytochem Res 2016; 8(12): 2025-32.
14. Zhu H, Dronamraju V, Xie W, More SS. Sulfur-containing therapeutics in the treatment of Alzheimer's disease. Med Chem Res 2021; 30: 305-52.
15. Komarnisky LA, Christopherson RJ, Basu TK. Sulfur: Its clinical and toxicologic aspects. Nutrition 2003; 19(1): 54-61.
16. Francioso A, Baseggio Conrado A, Mosca L, Fontana M. Chemistry and biochemistry of sulfur natural compounds: Key intermediates of metabolism and redox biology. Oxid Med Cell Longev 2020; 2020: 8294158.
17. Aiyelaagbe OO, Osamudiamen PM. Phytochemical screening for active compounds in *Magnifera indica* leaves from Ibadan, Oyo State. Plant Sci Res 2009; 2(1): 11-3.
18. Slinkard K, Singleton VL. Total phenols analysis: Automation and comparison with manual methods. Am J Enol Vitic 1997; 28(1): 49-55.
19. Zhishen J, Mengcheng T, Jianming W. The determination of flavonoid contents in mulberry and their scavenging effects on superoxide radicals. Food Chem 1999; 64(4): 555-9.
20. Oyaizu M. Studies on products of browning reaction: Antioxidative activities of browning reaction prepared from glucose amine. Jpn J Nutr Diet 1986; 44(6): 307-15.
21. Apak R, Güçlü K, Özyürek M Karademir SE. Novel antioxidant capacity index for dietary polyphenols and vitamin C and E, using their cupric ion reducing capability in the presence of neocuproine: CUPRAC method. J Agric Food Chem 2004; 52(26): 7970-81.
22. Benzie IFF, Strain JJ. The ferric reducing ability of plasma (FRAP) as a measure of antioxidant power": The FRAP assay. Anal Biochem 1996; 239(1): 70-6.
23. Arnao MB, Cano A, Acosta M. The hydrophilic and lipophilic contribution to total antioxidant activity. Food Chem 2001; 73(2): 239-44.
24. Brand-Williams W, Cuvelier ME, Berset C. Use of a free radical method to evaluate antioxidant activity. LWT-Food Sci Technol 1995; 28(1): 25-30.
25. Fogliano V, Verde V, Randazzo G, Ritieni A. Method for measuring antioxidant activity and its application to monitoring the antioxidant capacity of wines. J Agric Food Chem 1999; 47(3): 1035-40.
26. Liu F, Ooi VEC, Chang ST. Free radical scavenging activities of mushroom polysaccharide extracts. Life Sci 1997; 60(10): 763-71.

27. Sakanaka S, Tachibana Y, Okada Y. Preparation and antioxidant properties of Japanese persimnon leaf tea (kakinoha-cha). Food Chem 2005; 89(4): 569-75.
28. Decker EA, Welch B. Role of ferritin as a lipid oxidation catalyst in muscle food. J Agric Food Chem. 1990; 38(3): 674-7.
29. Alqethami A, Aldhebiani AY. Medicinal plants used in Jeddah, Saudi Arabia: Phytochemical screening. Saudi J Biol Sci 2021; 28(1): 805-12.
30. Bandiola TMB. Extraction and qualitative phytochemical screening of medicinal plants: A brief summary. Int J Pharm 2018; 8(1): 137-43.
31. Velu G, Palanichamy V, Rajan AP. Phytochemical and pharmacological importance of plant secondary metabolites in modern medicine. Roopan S, Madhumitha G, editors. Bioorganic Phase in Natural Food: An Overview. Cham: Springer; 2018.p.135-56.
32. Benzidia B, Barbouchi M, Hammouch H, Belahbib N, et al. Chemical composition and antioxidant activity of tannins extract from green rind of *Aloe vera* (L.) Burm. F. J King Saud Univ Sci 2019; 31(4): 1175-81.
33. Salehi B, Ayatollahi SA, Segura-Carretero A, Kobarfard F, Contreras MDM, Faizi M, et al. Bioactive chemical compounds in *Eremurus persicus* (Joub. & Spach) Boiss. essential oil and their health implications. Cell Mol Biol 2017; 63(9): 1-7.
34. Dhalaria R, Verma R, Kumar D, Puri S, Tapwal A, Kumar V, et al. Bioactive compounds of edible fruits with their anti-aging properties: A comprehensive review to prolong human life. Antioxidants, 2020; 9(11): 1123.
35. Ozsoy N, Can A, Yanardag R, Akev N. Antioxidant activity of *Smilax excelsa* L. leaf extracts. Food Chem 2008; 110(3): 571-83.
36. Ozsoy N, Yilmaz T, Kurt O, Can A, Yanardag R. *In vitro* antioxidant activity of *Amaranthus lividus* L. Food Chem 2009; 116(4): 867-72.
37. Peksel A, Arisan-Atac I, Yanardag R. Evaluation of antioxidant and antiacetylcholinesterase activities of the extracts of *Pistacia atlantica* Desf. Leaves. J Food Biochem 2010; 34(3): 451-76.
38. Munteanu IG, Apetrei C. Analytical methods used in determining antioxidant activity: A review. Int J Mol Sci 2021; 22(7): 3380.
39. Bernaert N, De Paepe D, Bouten C, De Clercq H, Stewart D, Van Bockstaele E et al. Antioxidant capacity, total phenolic and ascorbate content as a function of the genetic diversity of leek (*Allium ampeloprasum* var. *porrum*). Food Chem 2012; 134(2): 669-77.
40. Moini H, Packer L, Saris NEL. Antioxidant and prooxidant activities of α-lipoic acid and dihydrolipoic acid. Toxicol Appl Pharmacol 2002; 182(1): 84-90.
41. Güngör N, Özyürek M, Güçlü K, Demirci Çekiç S, Apak R. Comparative evaluation of antioxidant capacities of thiol-based antioxidants measured by different *in vitro* methods. Talanta 2011; 83(5): 1650-8.
42. Surveswaran S, Cai YZ, Corke H, Sun M. Systematic evaluation of natural phenolic antioxidants from 133 Indian medicinal plants. Food Chem 2007; 102(3): 938-53.
43. Gaggeri R, Rossi D, Mahmood K, Gozzini D, Mannucci B, Corana F, et al. Towards elucidating Eremurus root remedy: Chemical profiling and preliminary biological investigations of *Eremurus persicus* and *Eremurus spectabilis* root ethanolic extracts. J Med Plant Res 2015; 9(41): 1038-48.
44. Ates B, Abraham L, Ercal N. Antioxidant and free radical scavenging properties of N-acetylcysteine amide (NACA) and comparison with N-acetylcysteine (NAC). Free Radic Res 2008; 42(4): 372-7.
45. Sánchez, M, Sabio L, Gálvez N, Capdevila M, Dominguez-Vera JM. Iron chemistry at the service of life. IUBMB Life 2017; 69(6): 382-8.
46. Sabraoui T, Khider T, Nasser B, Eddoha R, Moujahid A, Benbachir M. et al. Determination of punicalagins content, metal chelating, and antioxidant properties of edible pomegranate (*Punica granatum* L) peels and seeds grown in Morocco. Int J Food Sci 2020; 2020: 8885889.
47. Peksel A, Imamoglu S, Altas Kiymaz N, Orhan N. Antioxidant and radical scavenging activities of *Asphodelus aestivus* Brot. extracts. Int J Food Prop 2013; 16(6): 1339-50.
48. Eddine LS, Segni L, Redha OM, Noureddine G. Free radical scavenging activity of leaf extract of *Rumex vesicarius* L. obtained by different methods. Int J Toxicol Pharmacol Res 2015; 7(3): 140-6.
49. Sacan O, Orak H, Yanardag R. Antioxidant activity of water extract of *Eruca sativa* Mill. Asian J Chem 2008; 20(5): 3462-74.
50. Bircan B, Kırbağ S. Determination of antioxidant and antimicrobial properties of *Eremurus spectabilis* Bieb. ACU J For Fac 2015; 16(2): 176-186.
51. Kejík Z, Kaplánek R, Masařík M, Babula P, Matkowski A, Filipenský P, et al. Iron complexes of flavonoids-antioxidant capacity and beyond. Int J Mol Sci 2021; 22(2): 646.

ISTANBUL UNIVERSITY PRESS

RESEARCH ARTICLE

Eur J Biol 2021; 80(2): 164-172

Scape, Rhizome and Root Anatomy of *Polygonatum* Species from Turkey

Yeter Yesil[1], Fatma Neriman Ozhatay[2]

[1]Istanbul University, Faculty of Pharmacy, Istanbul, Turkey
[2]Eastern Mediterranean University, Faculty of Pharmacy, Gazimağusa, North Cyprus, Turkey

ORCID IDs of the authors: Y.Y. 0000-0002-4458-7881; F.N.O. 0000-0003-4062-7492

Please cite this article as: Yesil Y, Ozhatay FN. Scape, Rhizome and Root Anatomy of *Polygonatum* Species from Turkey. Eur J Biol 2021; 80(2): 164-172. DOI: 10.26650/EurJBiol.2021.1026981

ABSTRACT

Objective: *Polygonatum* (Asparagaceae) is a rhizomatous monocotyledon genus that is distributed in the temperate regions of the Northern Hemisphere. The genus is represented by 5 species in Turkey (*P. glaberrimum, P. latifolium, P. multiflorum, P. verticillatum* and *P. orientale*). Karyological, palynological, phylogenic, chemotaxonomical and some anatomical studies of *Polygonatum* species have been carried out previously. However, the detailed anatomical features of the scape, rhizome and root of *Polygonatum* species grown in Turkey have not been examined before and so the aim of this study is to determine their anatomical characteristics. Also, the study compares the species with each other according to obtained anatomical characteristics and comparing them with previous anatomical studies.

Materials and Methods: Investigations were carried out on fresh material collected from wild habitats during July 2009-2012 in Turkey. Cross-sections of scape, rhizome and roots were cut by hand, detailed photographs were taken under a light microscope, and anatomical structures were drawn in detail with an isograph pen.

Results: The anatomical structures of *Polygonatum* species have monocotyledones features. Significant differences between species were observed, such as the number of costas in the scape, number of xylem arms in the root and the types of vascular bundle in the rhizome. Also, the anatomical characteristics of the species were compared with previous anatomical studies.

Conclusion: The anatomical features determined by this study will be useful at the species level as well as at the genus and family level. Hence the obtained data will contribute to the literature.

Keywords: *Polygonatum, Asparagaceae,* Anatomy, Solomans seal, Turkey

INTRODUCTION

Polygonatum Miller. species grow in warm temperate regions in the boreal zones of the northern hemisphere and are represented by a total of 71 species and 4 varieties (1-3) across the world and by 5 species in Turkey (4). *Polygonatum* is a rhizomatous herb and the biggest genus of the family Asparagaceae. Early on it was classified as a member of the Liliaceae family (or in some countries the Convallariaceae family) and was later classified into the Asparagaceae family (5-7).

The genus *Polygonatum* is seperated into tree sections according to leaf sequences, size of perianth, whether bracts are present or not and the chromosome bases number; sect. *Polygonatum,* sect. *Oppocitifolia* and sect. *Verticillata* (8-12). Also, sect. *Verticillata* has shouting stamen filaments, perforated pollen exines, and most of the pollen has opposite or vertical leaves with slender type filaments (13).

Tamura (14) subdivided the genus into two sections, sect. *Polygonatum* (*Alternifolia*) and sect. *Verticillata* Baker., Sect. *Polygonatum* possesses alternate leaves, stout staminal filaments, perforated pollen exines, x = 9, 10 or 11 as chromosome base number. Sect. *Verticillata* has mostly opposite or verticillate leaves,

Corresponding Author: Yeter Yesil E-mail: yesily@istanbul.edu.tr
Submitted: 22.11.2021 • **Revision Requested:** 28.11.2021 • **Last Revision Received:** 01.12.2021 • **Accepted:** 02.12.2021 • **Published Online:** 15.12.2021

slender filaments, mostly reticulate pollen exines, x = 14 or 15 as base chromosome number (14,15). Also, Tamura (14) divided sect. *Polygonatum* into three series, ser. *Bracteata* L. Abramova, ser. *Polygonatum* and ser. *Inflata* (Satake) M. N. Tamura based on the karyological and micromorphological characters of the staminal filaments.

The phylogenetic studies (16) have primarily focused on relationships at the tribal level. Meng and friends (13) studied the phylogenetic analysis of the *Polygonatum* species using data from two plastid coding regions, *rbcL* and *trnK* (*matK*), and two non-coding regions, *psbA-trnH* and *trnC-petN*. They also, tested the monophyly of *Polygonatum*, reconstruct phylogenetic relationships and examined the character evolution of phyllotaxis in the genus. Moreover, a recent phylogenetic study provided support for the recognition of *Polygonatum, Disporopsis* and *Heteropolygonatum* within *Polygonatum* genus (17).

The leaf anatomy of *Polygonatum* species grown in China was studied and it was noted that leaf thickness, the appearance of raffite or other crystals and size of stoma are significant features. Also, it has been noted that there is no sponge and palisade parenchyma differentiation in the mesophyll tissue (18-22). Foliar epidermal characteristics, such as, thickness of cell wall, different types of stomata, and epidermis of the *Polygonatum* species have been used for the classification of the Asparagaceae taxa (23,24), additionally the micromorphological characteristics of the epidermis of six species of the *Polygonatum* have been studied from different geographic populations of China (25). The anatomical structure of *Polygonatum* Mill. species in the Precarpathian region were studied recently (26), although the *Polygonatum* species is mentioned in the article, only the features of *P. multiflorum* are shown with photographs.

Also, the used parts of two medicinal *Polygonatum* species (*P. verticillatum* and *P. cirrhifolium*) were studied, but mostly the pharmacognostic properties of the species were indicated in this study (27).

Kauff and friends (28) studied the root anatomy of several taxa of Asparagales and certain taxa formerly included in Asparagales described in a systematic context together with a literature review. However, there is no detailed systematic study on root, scape and rhizome anatomy of *Polygonatum* species. This study aimed to investigate the scape, rhizome and root anatomical features of *Polygonatum* species grown in Turkey.

MATERIALS AND METHODS

The study materials were collected during the doctoral dissertation study 'Pharmaceutic Botanical Investigation on *Polygonatum* Mill., *Paris* L., *Veratrum* L. genera in Turkey'. The studied *Polygonatum* samples were gathered from different regions of Turkey during July 2010 and July 2012. The herbarium numbers, locations and collection dates of the samples are given in Table 1. The Latin name of species were verified by Kew's vascular plant database (3), Flora of Turkey (29), the Illustrated Flora of Turkey database (30) and the Turkey Plant list (Vascular Plants) (31). The voucher specimens were kept in the herbarium of Istanbul University Faculty of Pharmacy (ISTE). The collected specimens for anatomical study were stored in 70% ethyl alcohol in the field trips.

The transverse sections of the *Polygonatum* species were cut by hand, the samples were investigated in Sartur reagent (a compound reagent of Sudan III, lactic acid, iodine, aniline, alcohol, potassium iodide and water) (32). Photographs were taken with the Canon Power shot A640.

The cross-sections of the rhizome were taken from the knuckle of the scapular and the knee of the previous year. The cross sections of the root were taken from the root of the scapulae and the roots of the previous year's stranglehold. Observations were made with a BH2 Olympus Light Microscope-Philips camera and a Leica DFC 295 stereo microscope.

The anatomical investigations referred to were: "Applied Plant Anatomy" (33), "Plant Anatomy Part 1-2" (34,35), "Anatomy of Flowering Plant" (36) and "Bitki Anatomisi" (37).

RESULTS

The scape, rhizome and root anatomy of the *Polygonatum* species were documented and represented in Figures.

Table 1. The list of studied species and some label information.

Species	Herbarium Number	Locations	Collection date
Polygonatum glaberrimum	ISTE 97684	Ardahan: Çıldır, 1405 m.	06 vii 2011
Polygonatum latifolium	ISTE 97530	Kırklareli: Dereköy, 454 m.	10 v 2011
Polygonatum multiflorum	ISTE 97507	Artvin: Borçka, 426 m.	08 viii 2010
Polygonatum orientale	ISTE 97464	Kastamonu: Taşköprü, 1183 m	28 vii 2010
Polygonatum verticillatum	ISTE 97486	Trabzon: Maçka, 1534 m.	28 iii 2010

Scape Anatomy

The scape of the *Polygonatum* species show anatomical characteristics of the stem (Figures 1-3).

Epidermis, epidermis cells are single layered, isodiametric and have a thick cell wall. The cuticle is thick and stomata are present. Papilla and small trichomes are present in *P. verticillatum*. 2-4 small trichomes or 1-2 (-3) scabride trichomes are present on costas and papilla and small trichome and stomata are present in between the costas of *P. orientale*. In the costas of *P. latifolium* there is unicellular trichome. *P. glaberrimum* does not have trichomes (Figures 1A, 2A and 2B).

Cortex, *P. multiflorum* does not have costas and has 2 or 3 layers of lignifiedcells under the epidermis. Parenchymatous tissue is 2 or 3 layered cells, in a rounded or polygonal shape and very big. The species which have costas, have 2-5 layers of collenchymatous tissues under the epidermis cells (Figures 1 and 2).

Central cylinder, vascular bundles, and the tissue in which they are contained are surrounded by 3-6 layers of sclerenchymatous tissue. Vascular bundles are small in the sclerenchyma ring, but central vascular bundles are larger and rarely have sclerenchymatous tissues. Also, the surrounded phloem are in the form of a U or V shape in central vascular bundles xylem. *Pith* is unspecified or parenchymatous (Figure 2).

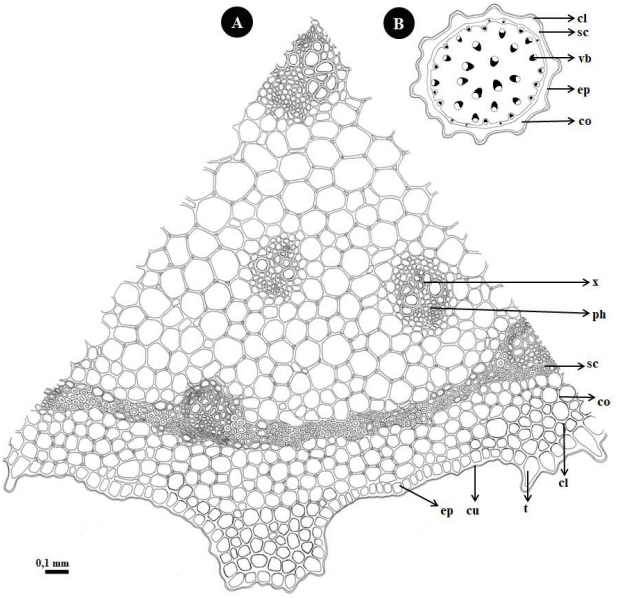

Figure 1. The illustrations of scape cross section of *Polgonatum orientale* (ISTE 97464); (A) detailed illustration, (B) schematic illustration, cl: collenchyma, co: cortex, cu: cuticule, ep: epidermis, ph: phloem, sc: sclerenchyma, t: trichome, vb: vascular bundle, x: xylem.

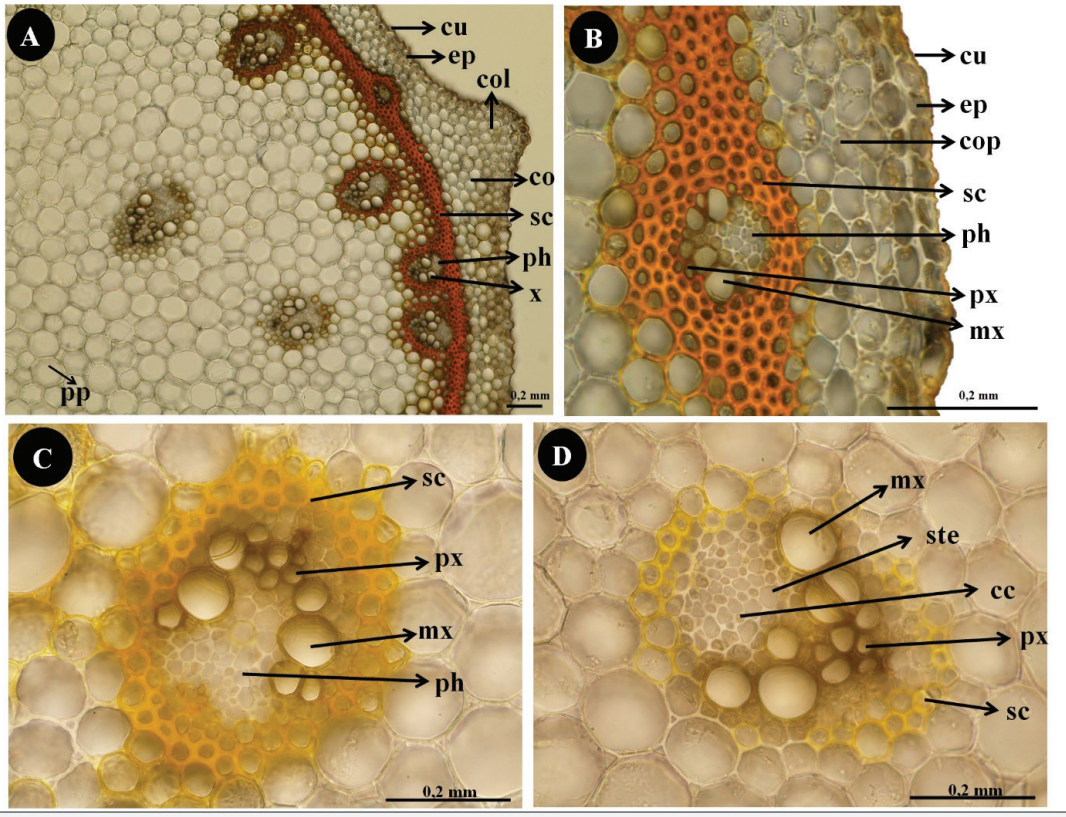

Figure 2. Cross section of scape of *Polygonatum glaberrimum*; (A) general view, (B) cortex and vascular bundle, (C) marginal vascular bundle, (D) central vascular bundle, cc: companion cell, co: cortex, col: collenchyma, cop: cortex parenchyma, cu: cuticule, ep: epidermis, mx: metaxylem, ph: phloem, px: protoxylem, sc: sclerenchyma, ste: sieve tube element, x: xylem.

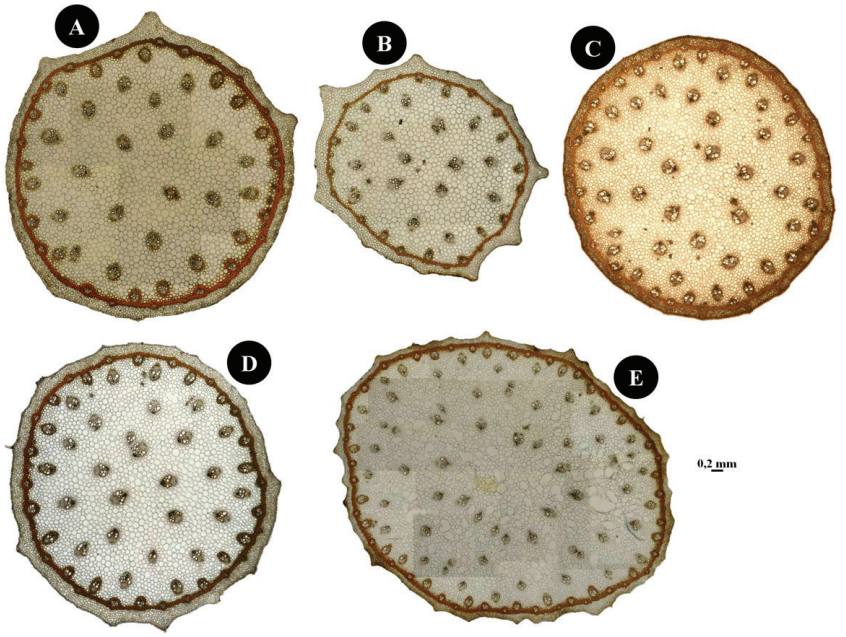

Figure 3. Cross section of scapes of the speceis; (A) *Polygonatum glaberrimum*, (B) *Polygonatum latifolium*, (C) *Polygonatum multiflorum*, (D) Polygonatum orientale, (E) Polygonatum verticillatum..

Although scape anatomy has the characteristics of a monocotyledon stem anatomy, the sclerenchyma tissue formed a circle under the cortex as in a dicotyledon stem. Some vascular bundles are also located at a distance in this tissue. Other vascular bundles are irregular in the central cylinder. Central vascular bundles are larger and less numerous than those close to the cortex. Therefore, the scape shows typical monocotyledonous stem anatomy. The bundles are collateral (Figures 1, 2A, and 3).

In addition, the presence of costas in the scapes of *Polygonatum* species and, if any, the size of the costas differ according to the species. *P. glaberrium* and *P. latifolium* species have big costas, *P. verticillatum* and *P. orientale* species have smaller costas, *P. multiflorum* species do not have costas. In the central cylinder, bands of raphide are rarely seen. Detailed examination results are given below (Figure 3).

Rhizome Anatomy

The rhizomes of the *Polygonatum* species show characteristics of monocotyledones rhizome anatomy. Raphides and starch grains are present.

Epidermis cells are single layered, rectangular and have a thick cell wall. The cuticle is very thick (Figures 4A and 5B).

Cortex, there are thick-walled, different-sized, polygonal, oval or round parenchymal cells located here. Since there was no endodermis, there was no definite boundary between the cortex and the central cylinder (Figures 4 and 5).

Central cylinder, under the cortex, the vascular bundles are arranged in a circle (Figures 4B and 5A). Some xylem and phlo-

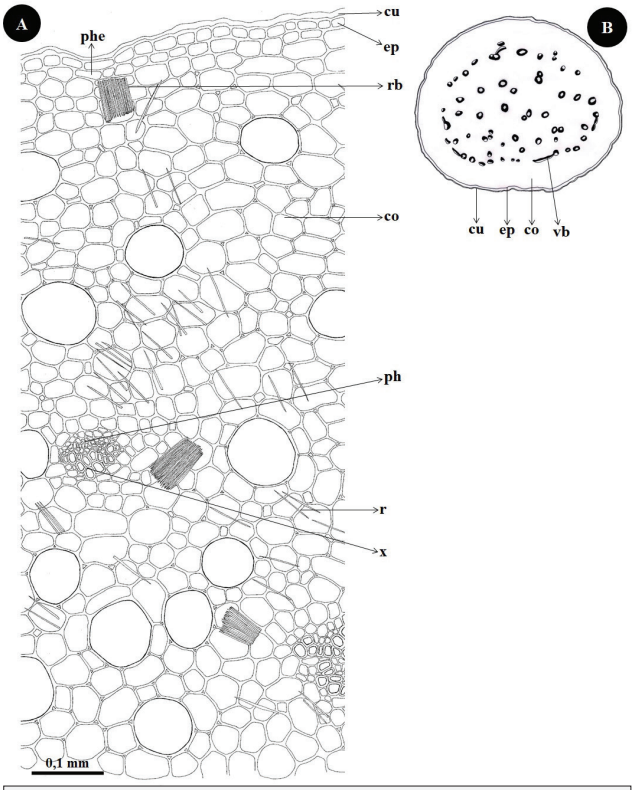

Figure 4. The illustrations of rhizome cross section of *Polgonatum orientale* (ISTE 97464); (A) detailed illustration, (B) schematic illustration, co: coteks, cu: cuticule, ep: epidermis, ph: phloem, phe: phellogen, r: raphide, rb: raphide bundle, vb: vascular bundle, x: xylem.

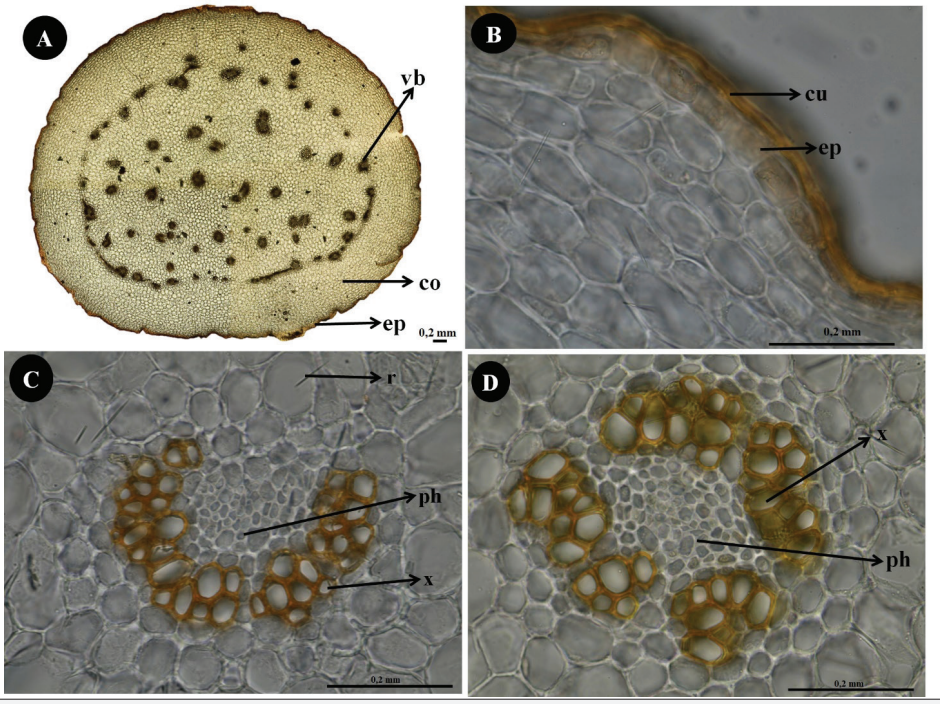

Figure 5. The rhizome cross section of *Polygonatum orentale* (ISTE 97464); (A) general view of rhisome, (B) cortex and epidermis, (C) central vascular bundle with U shaped xylem, (D) central vascular bundle with amfivasal xylem, co: coteks, cu: cuticule, ep: epidermis, ph: phloem, r: raphide, vb: vascular bundle, x: xylem.

em of vascular bundles in the circle are united at long distance. These vascular bundles and close vascular bundles are collateral. But the vascular bundles which are bigger and diffused near the center are amfivasal or the phloem is surrounded by xylem U shaped and particularly amfivasal vascular bundles surrounded by a single layered bundle-sheath (Figures 4B, 5C and 5D). The cell walls of xylem are reticulat. Pith is unspecified, parenchymatous (Figure 4A).

Root anatomy

The roots of *Polygonatum* species do not show characteristics of monocotyledones root anatomy. Raphide crystals are present (Figures 6-8).

Epidermis is replaced by the spongy tissue, the velamen. Velamen is single layered (Figures 6B and 7A).

Cortex has different cells in size and shapes. Endodermis is one layered with 1-3 transition cells, endodermis cells with thickened radial and inner tangential walls (Figures 6B, 7A, 7B and 8).

Central cylinder, pericycle cells are single layered, thin-walled, in different sizes and shapes. Vascular bundles are radial and xylem has 4-9 arm, metaxylem and protoxylem, metaxylem vessels thick walled thickenings on lateral walls of vessels scalariform perforation plates, of vessels simple or scalariform. Phloem has polygonal small thin-walled cells. Pith is sclerenchymatous (Figures 6B, 7 and 8).

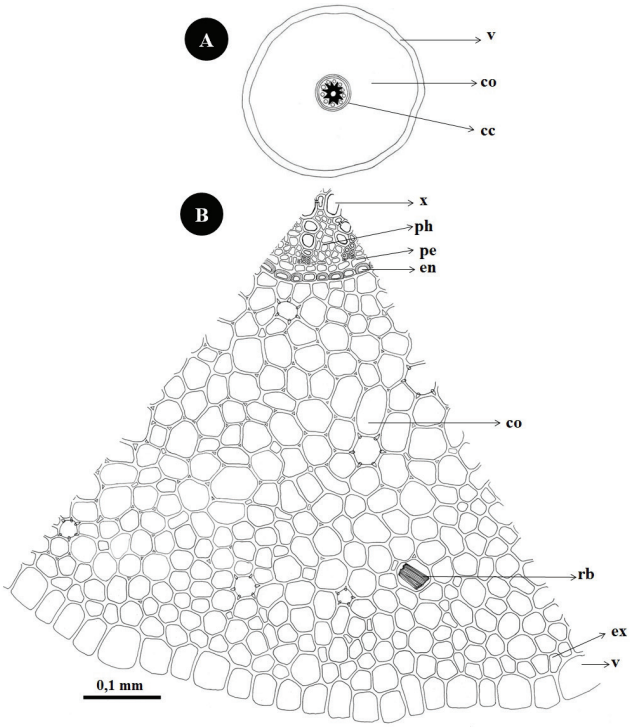

Figure 6. The illustrations of root cross section of *Polgonatum orientale* (ISTE 97464); (A) schematic illustration, (B) detailed illustration, cc: central cylinder, co: cortex, ex exodermis, en: endodermis, pe: pericycle, ph: phloem, rb: raphide bundle, x: xylem, v: velamen.

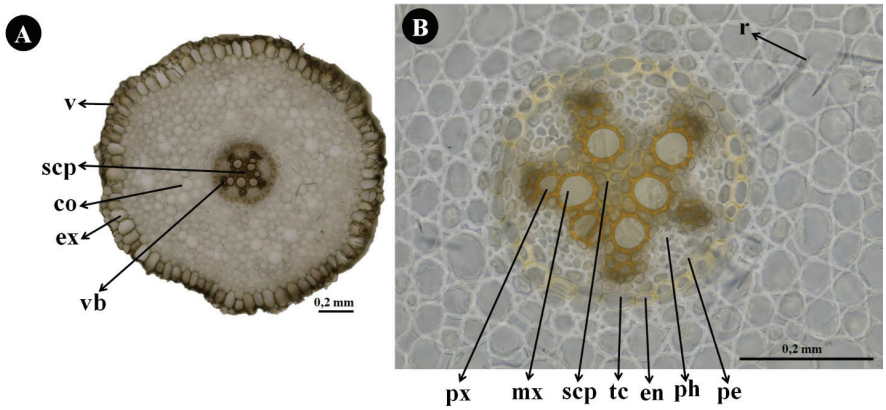

Figure 7. The root cross section of *Polygonatum latifolium* (ISTE 97530); (A) general view of root, (B) the central cylinder, co: cortex, ex: exodermis, en: endodermis, mx: metaxylem, pe: pericycle, ph: phloem, px: protoxylem, tc: transition cell, scp: sclerenchymatious pith, x: xylem, v: velamen.

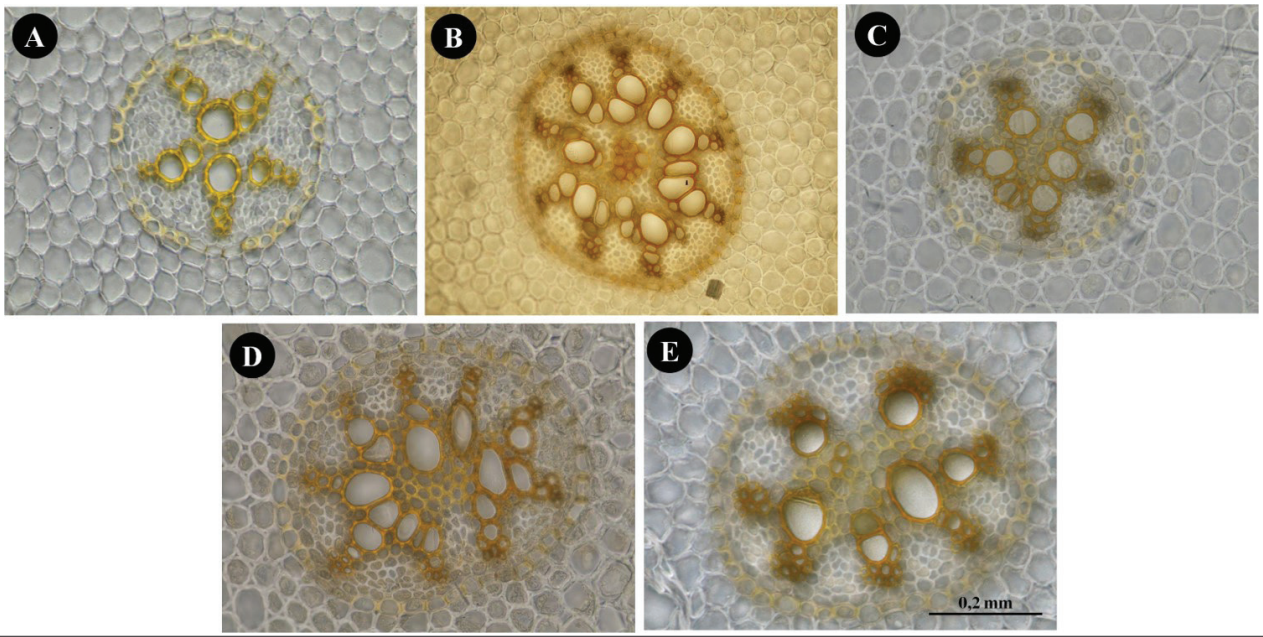

Figure 8. The cross section of root central cylinder of the species; (A) *Polygonatum glaberrimum*, (B) *Polygonatum orientale*, (C) *Polygonatum latifolium*, (D) *Polygonatum multiflorum*, (E) *Polygonatum verticillatum*.

DISCUSSION

This study covers the scape, rhizome and root anatomical features of *Polygonatum* species distributed in Turkey. The samples of 5 species, collected from different regions of Turkey, were studied in detail. An anatomical key was created in light of obtained data and important anatomical features of the studied species can be seen in Table 2.

There is a marked difference in the size of costas between *Polygonatum* species in scape anatomy. Costas are few in number but large in *P. glaberrium* and *P. latifolium* species, for this reason, the cortex of these species are larger. Costas are many and small in *P. verticillatum* and *P. orientale*, no costa was observed in *P. multiflorum* species. Therefore, collenchyma tissue is denser in species with large costa compared to species with small costa. Also, the cortex consists of more parenchymatous layers.

When the study researching the anatomical structures of the scapes and phylloclades of Bulgarian *Ruscus* species were investigated (38), the similarities of *Polygonatum* and *Ruscus* species in scape anatomy were easily observed. These similarities were the presence of costas, a single layer of the epidermis, a well-developed sclerenchyma ring, and the distribution of vascular bundles in central cylinder and type of vascular bundles.

Table 2. Scape, rhizome and root characteristics of *Polygonatum* species.

Characteristics	*P. glaberrimum*	*P. latifolium*	*P. multiflorum*	*P. orientale*	*P. verticillatum*
Number of costas in scapes	3-4	6-7	-	10-17	25-35
Collenchyma layers in scapes	4-5	2-4	-	2-3	1-3
Xylem arms in roots	4-5	5-7	5-10	5-9	5-7
Starch grain in rhizomes	+	+	+	+	++
Types of vascular bundles in rhizomes	Collateral or concentric-amphivasal type	Collateral type	Collateral or concentric-amphivasal type	Collateral or concentric-amphivasal type	Collateral or concentric-amphivasal type

Although these two genera are not completely similar in morphology, the reason for their anatomical similarity may be that they are in the same family (Asparagaceae).

Study of the rhizome revealed characteristics of monocotyledones stem. The rhizome of *P. verticillatum* contains more starch grains than the rhizome of other species. All species contain a large number of raphide bundles. Vascular bundles are collateral or concentric-amphivasal type. Only the *P. latifolium* species does not have amphivasal type vascular bundles.

The root generally has monocotyledones properties in *Polygonatum* species. Endodermis are seen as horseshoe, but not very distinct when compared to other monocotyledones. *Polygonatum* species have different numbers of xylem arms in the central cylinder, in particular *P. multiflorum*, *P. orientale* and *P. verticillatum* species, where as many as 10 were detected.

This study supports the study of Kauf and friends (27) because of the presence of raphide crystals, endodermis cells with thickened radial and internal tangential walls and the presence of sclerenchymatous tissue in the central pith of root. The epidermis layer can often be replaced by the velamen layer or layers in the root. The species with velamentous roots are geophytes and hemicryptophytes that grow in zones with a dry tropical climate or Mediterranean climates. Velamen tissue protects the root tissue and prevents water loss (39). The velamen tissue of *Polygonatum* species growing in Turkey is one layered. Because these species are not distributed in very dry areas, their habitats are mixed forests or mixed needle-leaved forests.

The roots of *Polygonatum* and *Sansevieria* are very similar, but while vascular bundles are absent in the central pith of *Polygonatum*, collateral bundles and vascular bundles are present in the central pith in roots of *Sansevieria* (40).

The types of calcium oxalate crystals were stated as differing by species in a previous study (41). However, no difference in the types of calcium oxalate crystals was observed between the species in this study.

The rhizome and root anatomical features of *Polygonatum verticillatum* have some overlaps with the Pandey and friends study (27). However, in contrast to the study, the periscle was easily observed in the root anatomy of Turkish *P. veriticillatum* species, in addition the endoderma is indistinct in the rhizome, the vascular bundles are particularly amphivasal and they are surrounded by a single layered bundle-sheath.

It has been stated that the difference in the shapes of endodermal cells in the leaves of *Polygonatum* species may be due to temperature and geographical distribution (42). Similarly, In the current study, whether the scapuses of *Polygonatum* species had costas or not, the number or the size of the costs can be explained by temperature and geographical variation.

Tamura (14) divided *Polygonatum* species into two groups - the *Alternifolia* group and the *Verticillata* group - in his classification based on chromosome numbers and filament surface properties. Another study based on numbers of chromosomes, karyological structures and karyotypic constitution also confirmed these results (2). When we evaluated the anatomical features in this study in this scope, although there were differences between *P. verticillatum*, which is a verticillate leaved species, and other species with alternate leaves, there was no significant grouping in these species.

Key for anatomical determination of the investigated species

1. Costas and collenchyma layers absent in scape …… *P. multiflorum*
1. Costas and collenchyma layers present in scape ……2
2. Numbers of costas more than 20, collenchyma layers 1-3… ……*P. verticillatum*
2. Numbers of costas less than 20, collenchyma layers more than 1-3…….3
3. Numbers of costas at least 9……*P. orientale*
3. Numbers of costas maximum 7……4
4. Vascular bundle only collateral in rhizome, xylem arms ≥5……*P. latifolium*
4. Vascular bundle collateral or concentric-amphivasal in rhizome, xylem arms ≤5…… *P. glaberrimum*

CONCLUSION

Polygonatum species can be confused with each other when analysed morphologically, especially *P. orientale* and *P. multiflorum* or *P. multiflorum* and *P. glaberrimum* species if they don't have parts such as flowers or fruit. However, the obtained anatomical characteristics such as the size of the costas show noticeable differences for distinguishing the species. Therefore, the anatomical characteristics of these species play an important role which may be the reference to use as an additional tool for the correct identification.

The anatomical features determined by this study may be useful at the genus level as well as at the species level. Thus, the data obtained in this study may lead to different studies to be conducted on both the *Polygonatum* genus and the genera in the Asparagaceae family.

Acknowledgement: We would like to thank Prof. Dr. Emine Akalın for her valuable suggestions during the writing process of the doctoral thesis.

Informed Consent: Written consent was obtained from the participants.

Peer Review: Externally peer-reviewed.

Author Contributions: Conception/Design of Study- Y.Y., N.O.; Data Acquisition- Y.Y.; Data Analysis/Interpretation- Y.Y.; Drafting Manuscript- Y.Y., N.O.; Critical Revision of Manuscript- Y.Y.; Final Approval and Accountability- Y.Y., N.O.

Conflict of Interest: Authors declared no conflict of interest.

Financial Disclosure: This study was supported by the Scientific Research Projects Unit of Istanbul University within the scope of the thesis project numbered 5923.

REFERENCES

1. Chien-Ti C, Yen-Hsueh T. Revision of *Polygonatum* (Asparagaceae, Nolinoideae, Polygonateae) of Taiwan. PhytoKeys 2019; 117: 99-118.
2. Deng XY, Wang Q, He XJ. Karyotypes of 16 populations of eight species in the genus *Polygonatum* (Asparagaceae) from China. Bot J Linn Soc 2009; 159(2): 245-54.
3. The Plant List, 2021. ⟨http://www.theplantlist.org/⟩. (Accessed 20 September 2021).
4. Yeşil Y. *Polygonatum*, *Paris* ve *Vertarum* cinsleri üzerinde farmasötik botanik çalışmalar. İ.Ü. Sağlık Bilimleri Enstitüsü, Doktora Tezi. 2013.
5. Byng JW, Chase MW, Christenhusz MJM, Fay MF, Judd WS, Mabberley D, et al. An update of the Angiosperm Phylogeny Group classification for the orders and families of flowering plants: APG IV, Bot J Linn Soc 2016; 181(1): 1-20.
6. Reveal JL, Chase MW. Bibliographical Information and Synonymy of Magnoliidae: APG III. Phytotaxa 2011; 19: 71-134.
7. Seberg O, Petersen G, Davis JI, Pires CP, Stevenson DW, Chase MW, et al. Phylogeny of the Asparagales based on three plastids and two mitochondrial genes. Am J Bot 2012; 99: 875-89.
8. Abramova LI. On the taxonomical structure of the genus *Polygonatum* Mill. Botaniceskii Žurnal 1965; 60: 490-7.
9. Baker JG. Revision of the genera and species of Asparagaceae. J Proc Linn Soc Bot 1875; 14: 508-46.
10. Chang GJ, Kim YS. Morphological evolution and relationships of Korean *Polygonatum*. Korean J Plt Taxon 1999; 29: 135-49.
11. Jeffrey C. The genus *Polygonatum* in eastern Asia. Kew Bull 1980; 34: 435-71.
12. Tamura MN. Biosystematic studies on the genus *Polygonatum* (Liliaceae) I. Karyotype analysis of species indigenous to Japan and its adjacent regions. Cytologia 1990; 55: 443-66.
13. Meng Y, Nie ZL, Deng T, Wen J, Yang YP. Phylogenetics and evolution of phyllotaxy in the Solomon's seal genus *Polygonatum* (Asparagaceae: Polygonateae). Bot J Linn Soc 2014; 176(4): 435-51.
14. Tamura MN. Biosystematic studies on the genus *Polygonatum* (Liliaceae) III. Morphology of staminal filaments and karyology of eleven Eurasian species. Bot Jahrb Syst 1993; 115: 1-26.
15. Tamura MN. Taxonomic studies on the genus *Polygonatum* (Liliaceae). Proc Jpn Soc Pl Taxon 1993; 9: 73-81.
16. Tamura MN, Schwarzbach AE, Kruse S, Reski R. Biosystematic studies on the genus *Polygonatum* (Convallariaceae) IV: Molecular phylogenetic analysis based on restriction site mapping of the chloroplast gene trnK. Feddes Repert 1997; 108: 159-68.
17. Floden A, Schilling EE. Using phylogenomics to reconstruct phylogenetic relationships within tribe Polygonateae (Asparagaceae), with a special focus on *Polygonatum*. Mol Phylogenet Evol 2018; 129: 202-13.
18. Chen CW, Li YT, Zhou SB. Comparative investigation on leaf epidermis of five species of *Polygonatum* from Dabieshan. J Anhui Agric Univ 2006; 33(1): 108-12.
19. Li, JH, Zhou SB, Wang CJ, Yu BQ. Comparative Anatomy of the Leaves in *Polygonatum* from Anhui Province. Acta Bot Yunnan 2005; 27(5): 509-16.
20. Li, JH, Zhou SB, Wang Y, Tian, CC. Leaf comparative anatomy of *Polygonatum cyrtonema* from five populations. Guihaia 2007; 27(6): 826-31.
21. Meng Y, Wang JJ, Nie ZL. Comparative morphology of leaf epidermis in 34 species of *Maianthemum* (Asparagaceae, Polygonateae) and their systematic significance. Phytotaxa 2016; 275(2): 81-96.
22. Zheng Y, Wang Y, Zhou H-B, Xu RS, Lian S, Zhang DC. Study on the leaf epidermis of *Polygonatum* from Anhui Province. Guihaia 1999; 19: 263-6.
23. Çitak BY, Dural H, Uysal T. Comparative anatomical and morphological studies on six *Muscari* species (Asparagaceae). Biol Divers Conserv 2019; 12(2): 141-50.
24. Raycheva T, Stojanov K. Comparative anatomical study of five species of genus *Asparagus* in Bulgaria. Trakia J Sci 2013; 11(2): 104-9.
25. Ali M, Bahadur S, Hussain A, Saeed S, Khuram I, Ullah M, et al. Foliar epidermal micromorphology and its taxonomic significance in *Polygonatum* (Asparagaceae) using scanning electron microscopy. Microsc Res Tech 2020; 83: 1381-90.
26. Riznychuk N, Gniezdilova V. Anatomical structure of *Polygonatum* Mill. species in the Precarpathian region. Journal Vasyl Stefanyk Precarpath Nat Uni 2020; 7(4): 53-5.
27. Pandey MM, Govindarajan R, Khatoon S, Singh Rawat AK, Mehrotra S. Pharmacognostical Studies of *Polygonatum cirrifolium* and *Polygonatum verticillatum*. J Herbs Spices Med Plants 2007; 12: 1(2), 37-48.
28. Kauff F, Rudall PJ, Conran JG. Systematic root anatomy of Asparagales and other monocotyledons. Plant Syst Evol 2000; 223: 139-54.
29. Miller R. *Polygonatum* Mill. In: Flora of Turkey and the East Aegean Islands Volume 8. Davis PH, editor. Edinburgh; Edinburgh University Press; 1984.

30. Bizim Bitkiler, 2021. ⟨https://bizimbitkiler.org.tr/yeni/demos/technical/⟩. (Accessed 22 September 2021).
31. Güner A, Aslan S, Ekim T, Vural M, Babaç MT, editors. *Türkiye Bitkileri Listesi (Damarlı Bitkiler)*. İstanbul: Nezahat Gökyiğit Botanik Bahçesi ve Flora Araştırmaları Derneği Yayını: 2012.
32. Çelebioğlu S, Baytop T. A new reagent for microscopical investigation of plant. Publication of the Institute of Pharmacognosy 1949; 10: 301.
33. Cutler DF, Botha T, Stevenson D, editors. Plant Anatomy an applied approach. Oxford, England: Blackwell Publishing; 2007.
34. Cutter EG. Plant Anatomy Part 2. 2nd ed. Newyork: John Wiley & Sons Press; 1971.
35. Cutter EG. *Plant Anatomy* Part 1, 2nd ed. Newyork: Addison-Wesley Press; 1978.
36. Rudall PJ. Anatomy of flowering plants: An introduction to plant structure and development. 3rd ed. Cambridge; Cambridge University Press: 2007.
37. Yentür S. Bitki Anatomisi. İstanbul: İstanbul Üniversitesi Fen Fakültesi Yayınları; 2003.
38. Raycheva T, Stojanov K. Comparative anatomical study of five species of genus *Asparagus* in Bulgaria. Trakia J Sci 2013; 11 (2): 104-9.
39. Zotz G, Schickenberg N, Albach D. The velamen radicum is common among terrestrial monocotyledons. Anal Bot 2017; 120: 625–32.
40. Huber H. Die Samenmerkmale und VerwandtschaftsverMltnisse der Liliifloren. München; Mitteilungen der Botanischen Staatssammlung: 1969.
41. Namba T, Komatsu K, Liu YP, Mikage M. Pharmacognostical studies on the *Polygonatum* plants. I. On the Tibetan crude drug Ra-mnye. Shoyakugaku Zasshi 1991; 45: 99-108.
42. Meng Y, Wang JJ, Nie ZL. Comparative morphology of leaf epidermis in 34 species of *Maianthemum* (Asparagaceae, Polygonateae) and their systematic significance. Phytotaxa 2016; 275(2): 81-96.

ISTANBUL UNIVERSITY PRESS

RESEARCH ARTICLE

Eur J Biol 2021; 80(2): 173-178

Protective Effects of *Petroselinum crispum* (Parsley) Extract Against Methotrexate-Induced Hepatotoxicity

Busra Ertas[1], Feyza Berin Turan[1], Dilek Ozbeyli[2], Refiye Yanardag[3], Ozlem Sacan[3], Goksel Sener[4]

[1]Marmara University, School of Pharmacy, Department of Pharmacology, Istanbul, Turkey
[2]Marmara University, Vocational School of Health Services, Medical Pathology Techniques, Istanbul, Turkey
[3]Istanbul University, Faculty of Engineering, Department of Biochemistry, Istanbul, Turkey
[4]Fenerbahce University, Vocational School of Health Services, Istanbul, Turkey

ORCID IDs of the authors: B.E. 0000-0001-8374-1098; F.B.T. 0000-0002-0436-7876; D.O. 0000-0002-0250-9535; R.Y. 0000-0003-4185-4363; O.S. 0000-0001-6503-4613; G.S. 0000-0001-7444-6193

Please cite this article as: Ertas B, Turan FB, Ozbeyli D, Yanardag R, Sacan O, Sener G. Protective Effects of *Petroselinum crispum* (Parsley) Extract Against Methotrexate-Induced Hepatotoxicity. Eur J Biol 2021; 80(2): 173-178. DOI: 10.26650/EurJBiol.2021.1023136

ABSTRACT

Objective: By inhibiting the synthesis of thymidine and purine, and thereby DNA synthesis, Methotrexate (MTX), suppresses the proliferation of cancer cells. It is thought that the side-effect mechanism is related to oxidant molecules derived from MTX metabolism. In this study, we examined whether the *Petroselinum crispum* extracts (PCr; parsley) of which the antioxidant properties have been previously shown, was protective against MTX induced liver damage.

Materials and Methods: Sprague Dawley rats (female/male; 200-250 g) were used. MTX was injected intraperitoneally and PCr extract was given orally. A single dose of 20mg/kg MTX was administered to the groups that were to experience hepatotoxicity. Then, a physiological saline (MTX group) or PCr (2 g/kg, MTX + PCr group) treatment was applied for 5 days. The same treatments were applied to the other groups (control group, PCr group) for 5 days after a single dose saline injection. At the end of the study, the biochemical parameters were examined in the blood and liver tissues taken from animals sacrificed by decapitation.

Results: MTX caused a significant increase in malondialdehyde and collagen levels and myeloperoxidase and caspase-3 activities, while glutathione levels were found to have decreased. PCr treatment showed protective efficacy by preventing these increases.

Conclusion: It appears that the administration of PCr to MTX treated rats prevented the accumulation of lipid peroxides, inflamatory reactions and depletion of antioxidant glutathione, and thus protected liver tissues against oxidative stress.

Keywords: Methotrexate, *Petroselinum crispum*, hepatotoxicity, oxidative injury, anti-inflammatory

INTRODUCTION

Methotrexate (MTX), a folic acid antagonist, has been used in the chemotherapy of malignant tumors for many years (1). It is also used in treatment of autoimmune diseases and for immunosuppressive therapy (2).

Once MTX enters the cell, it is polyglutamated and binds to dihydrofolate reductase (DHFR) with high affinity, thus it inhibits the conversion of dihydrofolate to tetrahydrofolate. With this mechanism, the biosynthesis of thymidine and purines, which might be important for DNA synthesis, are blocked. Blocking tetrahydrofolate synthesis by methotrexate stops cell division and protein synthesis. It is known that the cytotoxic effect of MTX on the 'S phase' of the cell cycle is a factor that inhibits cell division (3). Moreover, this cytotoxic effect is not limited to only tumor cells; MTX is known to affect

Corresponding Author: Goksel Sener E-mail: goksel.sener@fbu.edu.tr
Submitted: 14.11.2021 • **Revision Requested:** 28.11.2021 • **Last Revision Received:** 28.11.2021 • **Accepted:** 01.12.2021 • **Published Online:** 15.12.2021

vital organs through endogenous oxidant systems and inflammatory pathways (4).

Unfortunately, most of the drugs approved for cancer treatment cause acute toxic effects in organs. The aforementioned toxic effects are more common in organs containing self-renewing cells such as bone marrow, the stomach and intestines, mucous membranes and hair follicles (5). In addition, it is known that oxidative products formed during the metabolism of agents used in cancer treatment are harmful to various organ systems such as the liver, heart, kidneys, lungs. Due to these adverse effects, dose restrictions are needed, but this limits the treatment (6). Similarly, in the liver, MTX is oxidized and converted to 7-hydoxymethotrexate, its major extracellular metabolite (7).

Oxidative stress develops due to the disturbed balance between oxidants and antioxidants, against or in favor of antioxidants. Free radicals are by-products formed during enzymatic events in cells and are cleared by antioxidant systems. However, when this formation exceeds the antioxidant capacity of the organism, oxidant substances damage the organs. Therefore, the use of antioxidants to prevent oxidant damage seems promising in treatment (8).

Petroselinum crispum (Parsley), a natural source of vitamins and minerals, is a green plant with important medicinal properties such as being antioxidant, anti-apoptotic, anti-inflammatory, anti-diabetic, as well as having nutritional properties (9). It contains antioxidant substances such as flavonoids (apigenin, luteolin), carotenoids and ascorbic acid (10). When the therapeutic potential of natural products is evaluated, there are many studies showing that they can be effective in different stress conditions such as oxidation, inflammation and liver disease. Multiple active ingredients extracted from different herbs and plants have potential in the treatment of hepatotoxicity with their potential antioxidant and anti-inflammatory properties (11). In our study, which we designed based on these data, we investigated whether aqueous PC extract was protective against MTX-induced liver damage with biochemical analyses.

MATERIALS AND METHODS

Preparation of Plant Extracts

Parsley (*Petroselinum crispum*, PC) leaves were collected from Istanbul, Turkey. Five grams of plant leaves were extracted with 50 mL distilled water for 30 min by boiling. Aqueous Parsley extract was then lyophilized and the obtained powdered extract was stored at -20°C (12). The extract yield was 31.50% w/w.

Animals and Experimental Design

Both sexes of Sprague Dawley rats (200-250 g) were divided into four groups containing 8 rats in each. The rats were housed in standard laboratory conditions: 22±2°C, 60-63% humidity and 12 hours light-12 hours dark period, and were given water and feed *ad libitum*. All procedures for animals were approved by Marmara University Animal Experiments Local Ethics Commission (Protocol number: 26. 2019.mar). The study was carried out at the Marmara University Experimental Animals Application and Research Center (DEHAMER, Istanbul-Turkey).

Methotrexate was injected intraperitoneally (20 mg/kg) and PCr extract (2 g/kg) was given orally. In the study, which consisted of four groups, the animals were divided into two groups (saline and PCr treatment groups) after a single dose of MTX administration, and a similarly saline and PCr treatment group after a single dose of saline administration. Saline (MTX group) or PCr (MTX+PCr group) was administered for 5 days. Alanine transaminase (ALT) and aspartate transaminase (AST), lactate dehydrogenase (LDH) and proinflammatory cytokines were measured in the plasma while in the liver tissues malondialdehyde (MDA), glutathione (GSH), and collagen levels, and myeloperoxidase (MPO) and Caspase-3 activities were analyzed. Statistical analyses were completed with GraphPad Prism 8.0 (GraphPad Software, San Diego; CA; USA).

Biochemical Analyses in Plasma and Liver Tissues

Plasma AST, ALT and LDH levels were determined using the spectrophotometric method with an automatic analyzer. Plasma levels of tumor necrosis factor-α (TNF-α) and interleukin-1β (IL-1β) were determined with purchased enzyme-linked immunosorbent assay (ELISA) kits specific for these proteins, according to the manufacturer's instructions (Biosource Int., Nivelles, Belgium).

To determine MDA and glutathione levels, the tissues were kept ready by homogenizing them in ice-cold 150 mM KCl (13). GSH determination was performed using a standard spectrophotometric method coupled with the use of Ellman reagent. The results were evaluated in mmol MDA/g tissue and mmol GSH/g tissue units (14).

The MPO activity in tissue was determined following the procedure according to Hillegas et al. (15). Tissues homogenized in potassium phosphate buffer (PB, 50mM pH 6.0) were centrifuged (41,400 g) for 10 min to obtain pellets. The pellets were suspended in 50 mM PB with 0.5% hexadecyltrimethylammonium bromide (HETAB). 2.3 ml volume of 50 mM PB was added from aliquots to the mixture containing o-dianisidine and 20 mM H_2O_2 solution. The MPO activity was expressed as U/g tissue.

The liver tissues were homogenized with 0.9% NaCl and centrifuged at 1500xg 4°C for 10 min. Caspase-3 activities in the collected supenatants were measured using the commercial kit following the manufacturer's procedure (Abbkine Rat Caspase-3 ELISA Kit, Cat. number: KTE100992, China).

Determination of collagen is important as a free radical-derived fibrous marker. The tissues were fixed in 10% formalin with paraffin in 0.1M phosphate buffer (pH; 7.2), then 15 mm thick sections were obtained. This method is an assay based on the selective binding of Sirius Red and Fast Green FCF to collagen and non-collagen components, respectively, when sections are stained with both dyes dissolved in aqueous saturated picric

acid. To determine the amount of collagen and protein, absorbances at 540 and 605 nm were read (16).

Statistical Analysis

Statistical analysis was performed using GraphPad Prism 8.0 (GraphPad Software, San Diego, CA, 230 USA). All data are expressed as the mean±standard error mean (SEM). The results of the all datas were analyzed using one-way ANOVA followed by Tukey's post hoc test. Statistical significance was accepted as $p<0.05$.

Table 1. Plasma aspartate aminotransferase (AST), alanine aminotransferase (ALT), lactate dehydrogenase (LDH), TNF-α, and IL-1β Levels in the control (C), PCr, MTX and MTX+PCr groups.

	C	PCr	MTX	MTX + PCr
AST (U/L)	63.5±4.1	53.5±4.5	158.2±8.4 ***	94.2±12.6^{+++}
ALT (U/L)	44.4±2.8	43.0±3.5	92.0±5.9 ***	53.0 ±7.5 $^{+++}$
LDH (U/L)	362±22.3	331 ±24.2	715±97.6 **	386 ±68.3 $^{++}$
TNF-α (pg/mL)	2.7±0.3	2.6±0.5	7.3±0.6 ***	3.7±0.5 $^{+++}$
IL-1β (pg/mL)	5.8 ±0.4	5.7±0.8	14.3±0.9 ***	9.5±0.9 *, $^{++}$

*p<0.05, **p< 0.01, ***p< 0.001: compared with control group. $^{++}$p<0.01, $^{+++}$p<0.001: compared with MTX group. C: Control, PCr: *Petroselinum crispum*, MTX: Metotreksat.

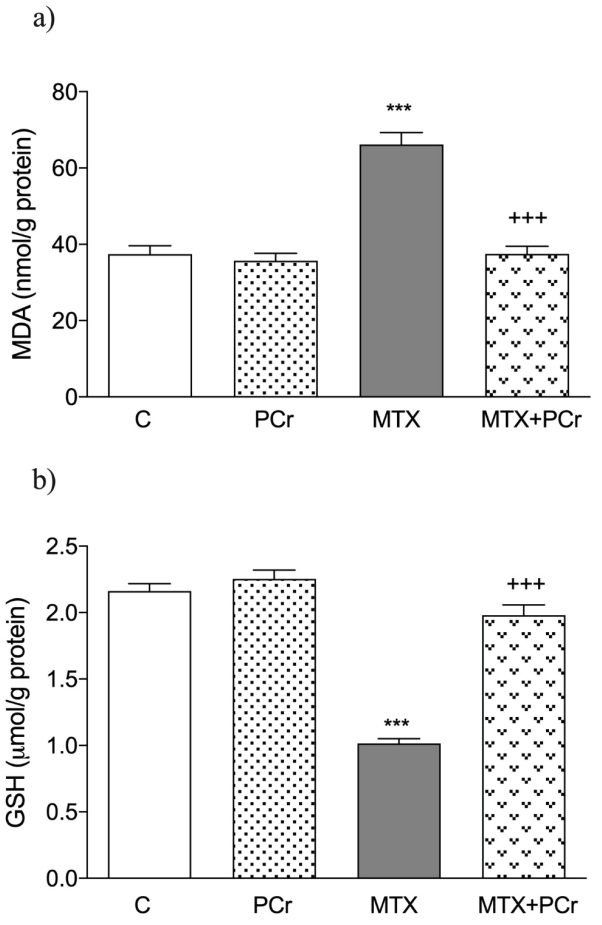

Figure 1. **a)** Malondialdehyde (MDA) and **b)** glutathione (GSH) levels the liver tissues of groups. ***p<0.001: vs control group. $^{+++}$p<0.001: vs saline-treated MTX group. C: Control, PCr: *Petroselinum crispum*, MTX: Metotreksat.

RESULTS

MTX-induced liver damage was evaluated by detecting ALT and AST levels, which are markers of liver function damage in the blood samples. When the results were examined, the level of these proteins increased with MTX application in the plasma samples. In addition to these, the level of tissue damage marker LDH and proinflammatory cytokines (TNF-α, and IL-1β) had also increased compared to the control group. PCr treatment significantly reduced these increased values compared to the MTX group ($p<0.01–0.001$, Table 1).

While MTX application increased the MDA level in the tissue compared to the control, the GSH level decreased significantly. PCr treatment returned these results induced by MTX injection to control group levels ($p<0.001$; Figure 1).

The level of MPO, which is evidence of neutrophil infiltration, increased significantly ($p<0.001$) after MTX injection compared to the control group. The level of MPO, which is evidence of neutrophil infiltration, was significantly increased after MTX injection compared to the control group. On the other hand, the liver MPO level had significantly decreased in the MTX+PCr group compared to the MTX group. This was a consistent result in accordance with the antioxidant and anti-inflammatory properties of PCr ($p<0.001$, Figure 2a).

Similarly, the caspase-3 activity, as an apoptotic marker, was found to have significantly increased ($p<0.001$) due to MTX administration. However, treatment with PCr of the rats given MTX, significantly prevented ($p<0.01$) the increase in caspase-3 activity, and the levels were close to the control group (Figure 2b).

Methotrexate administration caused a significant increase ($p<0.001$) in hepatic tissue collagen levels. However, when PCr was given following MTX, the collagen levels reduced significantly ($p<0.05$, Figure 3).

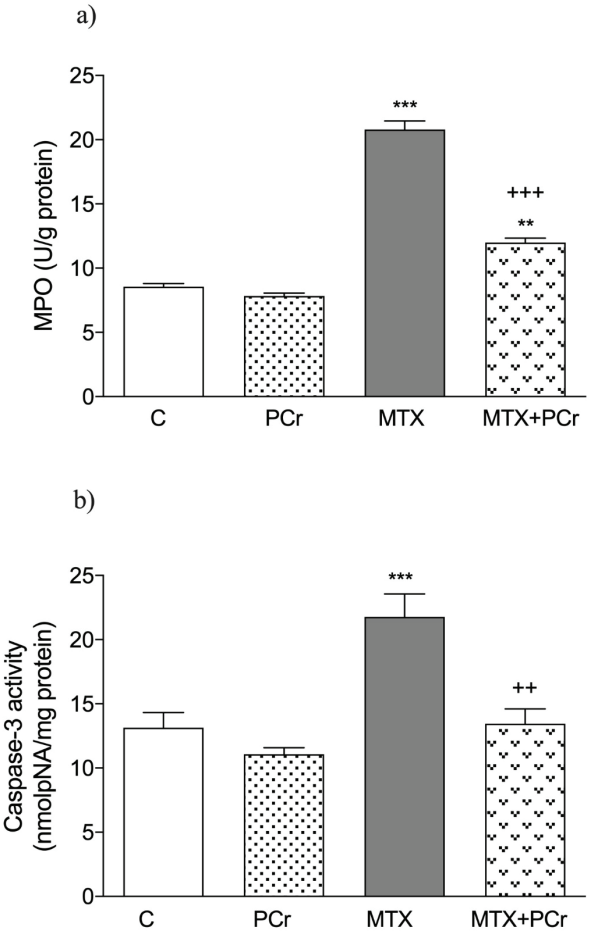

Figure 2. **a)** Myeloperoxidase (MPO) and **b)** caspase-3 activities in the liver tissues of groups. *** p<0.001, ** p<0.01: vs control group. +++p<0.001, ++p<0.01: vs saline-treated MTX group. C: Control, PCr: *Petroselinum crispum*, MTX: Metotreksat.

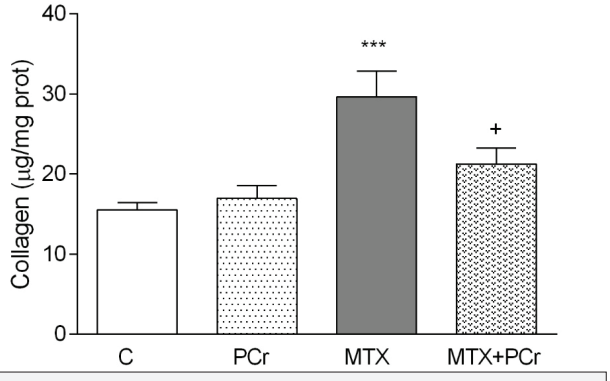

Figure 3. Collagen levels in the liver tissues of groups. ***p<0.001: vs control group. $^{+}$p<0.05; vs saline-treated MTX group. C: Control, PCr: *Petroselinum crispum*, MTX: Metotreksat.

DISCUSSION

With its folate antagonist effect, MTX is a drug that is preferably used clinically in the treatment of leukemia and various other solid tumors (17). Based on our results, the increase in MDA level with MTX application and the increase in caspase-3 activity, which is a marker defining the apoptotic process, indicate a hepatotoxic state accompanied by oxidative damage. It was observed that the level of GSH, an important antioxidant, decreased in parallel with the increased oxidative stress. In addition, the MTX caused a significant inflammation process with an increase in proinflammatory cytokines accompanied by an increase in MPO in the tissue. The known antioxidant and anti-inflammatory activity of parsley has been a therapeutic factor in the treatment of many diseases. We designed our study based on the potential effectiveness of hepatotoxicity through the same properties. In addition, this oxidant and inflammation increase decreased with PCr treatment in the hepatotoxicity group treated with MTX.

The factors responsible for MTX toxicity are the age of the patient, other diseases present in the patient, predisposing factors to toxicity, as well as MTX metabolites. 7-hydoxymethotrexate is the major oxidant metabolite of MTX, which is formed as a result of oxidase-mediated (aldehyde oxidase) biotransformation reactions in the liver (18). In the long-term administration of MTX, another mechanism responsible for hepatic toxicity is its other metabolites which are accumulated as polyglutamates (19). MTX inhibits nicotinamide adenosine diphosphate [NAD(P)]-dependent dehydrogenases and the NADP malic enzyme, which control the production of NADPH (20). By providing a reduced glutathione level, NADPH has played a mediating role in a kind of antioxidant defense mechanism of the cell (21). This mechanism induced by MTX causes a decreased GSH level, leaving cells vulnerable to oxidant stress (22). Since this situation mediates hepatic toxicity and the pathogenesis of organ failure in clinical situations that require treatment with MTX, it is an essential to prevent this effect. Recent studies in the literature have shown that plants and major compounds obtained from plants are protective against this effect, which limits the use of MTX, thanks to their antioxidant effects. It was concluded that treatment with *Ginkgo biloba* extract treats MTX-induced hepatic injury by reducing the level of proinflammatory cytokines (23). A study by Famurewa et al. (24) examined the effect of *Hibiscus sabdariffa* extract on hepatic damage caused by MTX injection. The results obtained were interpreted as oxidant damage in the tissue was treated with the antioxidant properties of *Hibiscus sabdariffa* extract (24).

Petroselinum crispum (parsley), besides its use as a spice, is one of the most beneficial herbs for health due to its vitamins and mineral contents. In addition to its antidiabetic, antihypertensive, cholesterol-lowering, diuretic effects, various mixtures are prepared and used in knee and lower back pain (12). Parsley (*Petroselinum crispum*), which belongs to the Umbellifera plant family, is a widely grown annual herb. Today, herbs are being researched with increasing interest and speed, and those that

have been shown to have benefits are considered as alternative agents as new, safe and effective therapeutics (25). *Petroselinum crispum*, a culinary herb originating from the Mediterranean region, has become a common herb worldwide in modern times and has been studied in many experimental models examining its antioxidant properties (26). Yanardag et al. demonstrated the hypoglycemic effects of PCr extract in streptozotocin-induced diabetic rats (12). Furthermore, Sener et al. showed that PCr extract, besides reducing glucose level, also prevented diabetes-induced oxidant damage in the heart and tissue of diabetic rats through its antioxidant properties (27). Indeed, decreased GSH levels with increasing damage in heart and aorta tissues show that this diabetic damage is related to oxygen radicals. On the other hand, GSH levels were preserved in diabetic animals treated with PCr through with its antioxidant properties (28). Similarly, in this study, it is thought that MTX has a protective effect against liver tissue damage with its antioxidant effect. Similarly, in our study, it is thought that the decreased GSH levels in liver tissue damage caused by MTX are restored with the antioxidant effect of PCr and the tissue is protected.

Free radicals trigger inflammatory reactions, further increasing tissue damage. Thus, it causes an increase in pro-inflammatory cytokines and migration of neutrophils to the tissues (29). Neutrophils have an important role in host defense and innate immune response against harmfull agents (30). However, along with these beneficial effects, in cases of hyperactivity, neutrophils when infiltrating to the tissue, release MPO enzyme, which has an oxygen radical-dependent microbicidal activity, also causes inflammation or tissue damage (31). In accordance with the previous findings, MTX administration caused an increase in the proinflammatory cytokines, TNF-α and IL-1β in blood, and the activity of MPO enzyme in liver tissue (32). PCr extract given to MTX group prevented oxidant damage, and prevented inflammatory reactions Alleviation of tissue damage by PCr extract treatment and decreased AST, ALT and LDH levels increased by MTX suggest that liver functions are also preserved.

As is well known, ROS-mediated DNA damage results in apoptosis (33). In fact, apoptosis, defined as programmed cell death, is induced by MTX activating the mitochondrial extrinsic apoptotic pathway (34). Studies have shown that MTX-mediated apoptosis occurs by the amplified expression of proapoptotic genes such as TNF-α, caspase-3 and COX-2 (35). As a result we found that PCr extract has an anti-inflammatory activity and that MTX-induced caspase-3 and TNF-alpha increase could be prevented by treatment. One of the liver fibrosis parameters is the amount of tissue collagen present (36). It has already been proven by various researchers that MTX tends to increase the level of tissue collagen (37). In our own results, the increase of tissue collagen level by MTX induction is supported by the results obtained. However, treatment with PCr was effective in preventing hepatotoxicity in MTX-induced fibrosis by significantly reducing the level of collagen, which explains the additional antifibrotic mechanism involved in hepatoprotection of PCr.

CONCLUSION

In conclusion, it can be said that PCr treatment has a protective effect against MTX-induced hepatotoxicity by eliminating lipid peroxide accumulation and restoring GSH levels through its antioxidant property. PCr treatment also inhibited inflammatory reactions. According to these results, PCr treatment is thought to be a potential protective factor against organ damage which is encountered in chemotherapy with MTX. Broader research with the major compounds of the plant mediating this activity should be considered.

Ethics Committee Approval: This study was approved by Marmara University Animal Experiments Local Ethics Commission (Protocol number: 26. 2019.mar).

Informed Consent: Written consent was obtained from the participants.

Peer Review: Externally peer-reviewed.

Author Contributions: Conception/Design of Study- B.E., F.B.T., G.S.; Data Acquisition- B.E., F.B.T., G.S.; Data Analysis/Interpretation- B.E., F.B.T., B.E., O.S., G.S.; Drafting Manuscript- B.E., D.O., G.S.; Critical Revision of Manuscript- D.O., R.Y., G.S.; Final Approval and Accountability- B.E., F.B.T., D.O., R.Y., O.S., G.S.

Conflict of Interest: Authors declared no conflict of interest.

Financial Disclosure: Authors declared no financial support.

REFERENCES

1. Wang W, Zhou H, Liu L. Side effects of methotrexate therapy for rheumatoid arthritis: A systematic review. Eur J Med Chem 2018; 158: 502-16.
2. Rizzi R, Curci P, Delia M, Rinaldi E, Chiefa A, Specchia G, et al. Spontaneous remission of "methotrexate-associated lymphoproliferative disorders" after discontinuation of immunosuppressive treatment for autoimmune disease. Review of the literature. Med Oncol 2009; 26 (1): 1-9.
3. Sayılmaz A, Karabulut YY, Özgörgülü A. The histopathological evaluation of healing effects of vitamin C administered before methotrexate therapy on testicular injury induced by methotrexate. Turk J Urol 2016; 42(4): 235-9.
4. El-Sheikh AA, Morsy MA, Al-Taher AY. Multi-drug resistance protein (Mrp) 3 may be involved in resveratrol protection against methotrexate-induced testicular damage. Life Sci 2014; 119(1-2): 40-6.
5. Taguchi T. [Side effects of cancer chemotherapy and steps to deal with them]. Gan To Kagaku Ryoho. 1995; 22(14): 2017-28.
6. Goto E, Hosomi M, Nishihara M, Goto M, Yoshida M, Kii T, et al. [Comparison of chemotherapy side effects between elderly and young subjects]. Gan To Kagaku Ryoho 2012; 39(13): 2527-31.
7. Jahovic N, Cevik H, Sehirli AO, Yeğen BC, Sener G. Melatonin prevents methotrexate-induced hepatorenal oxidative injury in rats. J Pineal Res 2003; 34(4): 282-7.
8. Athreya K, Xavier MF. Antioxidants in the Treatment of Cancer. Nutr Cancer 2017; 69(8): 1099-104.
9. Ozsoy-Sacan O, Yanardag R, Orak H, Ozgey Y, Yarat A, Tunali T. Effects of parsley (Petroselinum crispum) extract versus glibornuride on the liver of streptozotocin-induced diabetic rats. J Ethnopharmacol 2006; 104(1-2): 175-81.

10. Tunali T, Yarat A, Yanardağ R, Ozçelik F, Ozsoy O, Ergenekon G, et al. Effect of parsley (Petroselinum crispum) on the skin of STZ induced diabetic rats. Phytother Res 1999; 13(2): 138-41.
11. Malayeri A, Badparva R, Mombeini MA, Khorsandi L, Goudarzi M. Naringenin: a potential natural remedy against methotrexate-induced hepatotoxicity in rats. Drug Chem Toxicol 2020: 1-8.
12. Yanardağ R, Bolkent S, Tabakoğlu-Oğuz A, Ozsoy-Saçan O. Effects of Petroselinum crispum extract on pancreatic B cells and blood glucose of streptozotocin-induced diabetic rats. Biol Pharm Bull 2003; 26(8): 1206-10.
13. Sener G, Paskaloglu K, Toklu H, Kapucu C, Ayanoglu-Dulger G, Kacmaz A, et al. Melatonin ameliorates chronic renal failure-induced oxidative organ damage in rats. J Pineal Res 2004; 36(4): 232-41.
14. Sener G, Sehirli AO, Ayanoglu-Dülger G. Melatonin protects against mercury(II)-induced oxidative tissue damage in rats. Pharmacol Toxicol 2003; 93(6): 290-6.
15. Hillegass LM, Griswold DE, Brickson B, Albrightson-Winslow C. Assessment of myeloperoxidase activity in whole rat kidney. J Pharmacol Methods 1990; 24(4): 285-95.
16. López-De León A, Rojkind M. A simple micromethod for collagen and total protein determination in formalin-fixed paraffin-embedded sections. J Histochem Cytochem 1985; 33(8): 737-43.
17. Burmester GR, Pope JE. Novel treatment strategies in rheumatoid arthritis. Lancet 2017; 389(10086): 2338-48.
18. Seideman P, Beck O, Eksborg S, Wennberg M. The pharmacokinetics of methotrexate and its 7-hydroxy metabolite in patients with rheumatoid arthritis. Br J Clin Pharmacol 1993; 35(4): 409-12.
19. Conway R, Carey JJ. Risk of liver disease in methotrexate treated patients. World J Hepatol 2017; 9(26): 1092-100.
20. Kim J, Kim KY, Jang HS, Yoshida T, Tsuchiya K, Nitta K, et al. Role of cytosolic NADP+-dependent isocitrate dehydrogenase in ischemia-reperfusion injury in mouse kidney. Am J Physiol Renal Physiol 2009; 296(3): F622-33.
21. Espinosa-Diez C, Miguel V, Mennerich D, Kietzmann T, Sánchez-Pérez P, Cadenas S, et al. Antioxidant responses and cellular adjustments to oxidative stress. Redox Biol 2015; 6: 183-97.
22. Eki Nci-Akdemi R FN, Yildirim S, Kandemi R FM, Gülçi N İ, Küçükler S, Sağlam YS, et al. The effects of casticin and myricetin on liver damage induced by methotrexate in rats. Iran J Basic Med Sci 2018; 21(12): 1281-8.
23. Sherif IO, Al-Shaalan NH. Hepatoprotective effect of Ginkgo biloba extract against methotrexate-induced hepatotoxicity via targeting STAT3/miRNA-21 axis. Drug Chem Toxicol 2020: 1-9.
24. Famurewa AC, Folawiyo AM, Epete MA, Igwe EC, Okike PI, Maduagwuna EK. Abrogation of Hepatic Damage Induced by Anticancer Drug Methotrexate by Zobo (Hibiscus sabdariffa extract) Supplementation via Targeting Oxidative Hepatotoxicity in Rats. J Diet Suppl 2019; 16(3): 318-30.
25. Liberal Â, Fernandes Â, Polyzos N, Petropoulos SA, Dias MI, Pinela J, et al. Bioactive Properties and Phenolic Compound Profiles of Turnip-Rooted, Plain-Leafed and Curly-Leafed Parsley Cultivars. Molecules 2020; 25(23): 5606.
26. Bolkent S, Yanardag R, Ozsoy-Sacan O, Karabulut-Bulan O. Effects of parsley (Petroselinum crispum) on the liver of diabetic rats: a morphological and biochemical study. Phytother Res 2004; 18(12): 996-9.
27. Ozel AB, Cilingir-Kaya OT, Sener G, Ozbeyli D, Sen A, Sacan O, et al. Investigation of possible neuroprotective effects of some plant extracts on brain in bile duct ligated rats. J Food Biochem 2021: e13835.
28. Sener G, Kapucu C, Paskaloglu K, Ayanoglu-Dülger G, Arbak S, Ersoy Y, et al. Melatonin reverses urinary system and aorta damage in the rat due to chronic nicotine administration. J Pharm Pharmacol 2004; 56(3): 359-66.
29. Sener G, Ekşioğlu-Demiralp E, Cetiner M, Ercan F, Yeğen BC. Beta-glucan ameliorates methotrexate-induced oxidative organ injury via its antioxidant and immunomodulatory effects. Eur J Pharmacol 2006; 542(1-3): 170-8.
30. Nauseef WM, Metcalf JA, Root RK. Role of myeloperoxidase in the respiratory burst of human neutrophils. Blood 1983; 61(3): 483-92.
31. Mortaz E, Alipoor SD, Adcock IM, Mumby S, Koenderman L. Update on Neutrophil Function in Severe Inflammation. Front Immunol 2018; 9: 2171.
32. Abdellatief SA, Galal AA, Farouk SM, Abdel-Daim MM. Ameliorative effect of parsley oil on cisplatin-induced hepato-cardiotoxicity: A biochemical, histopathological, and immunohistochemical study. Biomed Pharmacother 2017; 86: 482-91.
33. Al Kury LT, Dayyan F, Ali Shah F, Malik Z, Khalil AAK, Alattar A, et al. Ginkgo biloba Extract Protects against Methotrexate-Induced Hepatotoxicity: A Computational and Pharmacological Approach. Molecules 2020; 25 (11).
34. Ali N, Rashid S, Nafees S, Hasan SK, Sultana S. Beneficial effects of Chrysin against Methotrexate-induced hepatotoxicity via attenuation of oxidative stress and apoptosis. Mol Cell Biochem 2014; 385(1-2): 215-23.
35. Kelleni MT, Ibrahim SA, Abdelrahman AM. Effect of captopril and telmisartan on methotrexate-induced hepatotoxicity in rats: impact of oxidative stress, inflammation and apoptosis. Toxicol Mech Methods 2016; 26(5): 371-7.
36. De S, Kundu S, Chatterjee U, Chattopadhyay S, Chatterjee M. Allylpyrocatechol attenuates methotrexate-induced hepatotoxicity in a collagen-induced model of arthritis. Free Radic Res 2018; 52(6): 698-711.
37. Tawfik MK. Combination of coenzyme Q10 with methotrexate suppresses Freund's complete adjuvant-induced synovial inflammation with reduced hepatotoxicity in rats: Effect on oxidative stress and inflammation. Int Immunopharmacol 2015; 24(1): 80-7.

ISTANBUL UNIVERSITY PRESS

REVIEW ARTICLE

Eur J Biol 2021; 80(2): 179-187

Zebrafish Embryo as an Emerging Model Organism in Neurodevelopmental Toxicity Research

Sukriye Caliskan[1], Ebru Emekli-Alturfan[2]

[1]Marmara University, Institute of Health Sciences, Department of Biochemistry, Istanbul, Turkey
[2]Marmara University, Faculty of Dentistry, Department of Basic Medical Sciences, Istanbul, Turkey

ORCID IDs of the authors: S.C. 0000-0002-7576-4967; E.E.A. 0000-0003-2419-8587

Please cite this article as: Caliskan S, Emekli-Alturfan E. Zebrafish Embryo as an Emerging Model Organism in Neurodevelopmental Toxicity Research. Eur J Biol 2021; 80(2): 179-187. DOI: 10.26650/EurJBiol.2021.1006402

ABSTRACT

Zebrafish is a model organism that has become increasingly popular in recent years due to some of the advantages it has when compared to traditional model organisms. Its genetic similarity with humans has contributed significantly to the elucidation of the molecular mechanisms underlying diseases. Moreover, external fertilization and rapid embryonic development of zebrafish embryos have made it attractive in many research areas. The genome of humans and zebrafish are found to be highly conserved having 76-82 % of the disease genes in humans that are also present in zebrafish. Zebrafish have been used in different studies in several concepts of neurogenesis. Unlike mammals, the external development of a zebrafish embryo makes it accessible for experimental manipulation in central nervous system research. It was observed that neurotoxic agents induced similar responses to other vertebral models in zebrafish embryos, whose brain development and blood-brain barrier were similar to those of other vertebrates. This review provides brief information about the availability of zebrafish embryos in neurodevelopmental toxicity research while giving brief information on embryogenesis and neurogenesis in zebrafish. Evaluation of neurotoxicity and the specific effects of various neurotoxins on motor and dopaminergic neurons, neuronal proliferation, mobility, and neurodevelopment are also explained.

Keywords: Zebrafish, zebrafish embryo, neurotoxicity, neurodevelopment

INTRODUCTION

The zebrafish (*Danio rerio*) is gaining popularity as a model organism in many human diseases as a small tropical freshwater fish. Since the zebrafish shares a high genetic similarity to humans, it is a powerful model for both identifying the actual mechanisms and improving therapeutic strategies in many diseases, including metabolic and neurological diseases (1-3). The genome of humans and zebrafish are found to be highly conserved having 76-82 % of the disease genes in humans that are also present in zebrafish. On the other hand, nearly 20-24 % of genes in zebrafish are duplicated (4). A high genetic similarity to humans enables discoveries of many genetic mutations leading to different hereditary neurological diseases in humans (5). To use the zebrafish as a model organism, it is necessary to understand its physiology and behavioral characteristics well. Zebrafish belong to the class of teleosts, which constitutes 99% of the *Actinopterygii* species and emerged 350 million years ago. It inhabits vegetated freshwater streams and stagnant waters such as rice paddies in South and East Asia (Pakistan, Burma, India, and Nepal). Zebrafish live and lay eggs in shallow water at temperatures ranging from 24°C to 28°C. Appropriate conductivity and pH values are between 10 and 271 µS and pH 6.0-8.0, respectively (6). They feed on mosquito larvae and other insects. In the laboratory, embryos can hatch within 3 days after fertilization and mature within 2-3 months under good conditions (7). Zebrafish differ from previously used vertebrate models because of their external fertilization, transparency in development, small body

Corresponding Author: Ebru Emekli-Alturfan E-mail: ebruemekli@yahoo.com, eiemekli@marmara.edu.tr
Submitted: 08.10.2021 • **Revision Requested:** 15.10.2021 • **Last Revision Received:** 25.10.2021 • **Accepted:** 27.10.2021 • **Published Online:** 16.12.2021

size, short development time, production of a high number of eggs (200/female/week), and low maintenance costs (1).

Neurogenesis is defined as the progress of undifferentiated neural progenitor cells producing neurons that are mature and functional. The neural progenitor induction and the cell division phase are the first steps in neurogenesis that expands the progenitor pool. The specification of progenitors and differentiation into post-mitotic neurons follow the first step. All these steps are regulated to produce the various neuronal and glial cell types that will at the end form the mature central nervous system (CNS). Zebrafish have been used in many different studies on several concepts of neurogenesis. Unlike mammals, the external development of a zebrafish embryo makes zebrafish accessible for experimental manipulation in CNS research (8). Their small size and optical transparency allow observation of all processes in vivo throughout the early developmental stages, the early development of measurable behaviors, and the simplicity of the zebrafish nervous system compared to other model organisms provide advantages in nervous system studies (9,10). Thanks to major advances in genetic, embryological, and optical techniques in recent years, zebrafish have become a unique vertebrate model for studying neurogenesis (8).

To date, most of the studies have focused on neurogenesis in the embryonic stages of zebrafish (8-10). However, recent research has reported that the brain of mature zebrafish can be a very useful model for the study of neurogenesis in the adult (1). Furthermore, in the early 1960s, new neurons were suggested to arise in the adult mammalian brain, in the hippocampus and olfactory bulb through labeling newly synthesized DNA by *in-situ* [3H]-thymidine (11). The production of new neurons is observed mainly in the subventricular zone and the subgranular zone of the telencephalon in rodents and primates (12). Unlike mammals, teleosts such as zebrafish present a higher potential of reproduction because nearly 16 regions of proliferation were found in different areas of adult zebrafish brains (13,14). Approximately six thousand cells are produced in the adult zebrafish brain every 30 minutes which is the main reason for the popularity of zebrafish to study neurogenesis of the adult (15).

Embryogenesis in Zebrafish

In zebrafish, seven developmental stages are defined as the zygote, cleavage, blastula, gastrula, segmentation, pharyngeal, and hatching (exit from chorion) in the embryonic period (16). The time between the first cleavage (split) of the newly fertilized egg, approximately 40 minutes after fertilization, is called the zygote stage. The zygote is approximately 0.7-0.78 mm in diameter at fertilization. At the first cleavage 45 minutes after fertilization, two cells of equal size are formed. The cells or blastomeres then divide at intervals of about 15 minutes; 2-cell structure (0.75 h), 4-cell structure (1 h), 8-cell structure (1.25 h), 16-cell structure (1.5 h), 32-cell structure (1.75 h), and the 64-cell structure (2 h) is formed (16,17).

Blastula refers to the period from the 128-cell structure, in which the blastodisc is ball-like, to the beginning of the gastrulation period. Structures formed during the blastula period are; 128-cell structure (2.25 h), 256-cell structure (2.5 h), 512-cell structure (2.75 h), 1 k-cell structure, high stage (3.3 h), oblong phase (3.7 h), sphere phase (4 h), dome phase (4.3 h), and 30% epiboly phase structures (4.7 h). Stages of the gastrula stage include the formations of 50% epiboly (5.3 h), germ ring (5.7 h), shield stage (6 h), 75% epiboly (8 h), 90% epiboly (9 h), and bud stage (10 h). The gastrula period is considered to be finished when the epiboly is complete and the tailbud is produced (16,18).

The identification as an embryo until the end of the third day continues as the larval stage after hatching or not. The pectoral fin, gills, and jaw continue to develop rapidly. Monitoring the development of endodermal structures such as the digestive tract is difficult at this stage (48 h) due to their deep location. The larval stage includes individuals that are no longer embryo but are not yet juvenile. The swim bladder is swollen, foraging and avoidance behaviors have started (72 h). The juvenile stage is the stage in which sexual maturity is not achieved but most of the adult characteristics are acquired. In the laboratory, this period starts after about 4 weeks and lasts up to 6-12 weeks, depending on the breeding and rearing conditions (up to 89 days, according to www.zfin.org). The adult stage in fish is defined as the production of healthy gametes and secondary sexual characteristics that reach reproductive capability (16-18). Zebrafish's developmental timeline is summarized in Figure 1 (19).

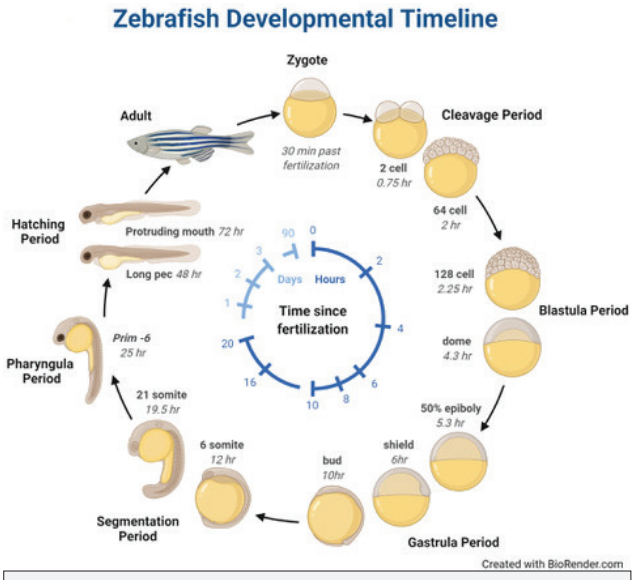

Figure 1. Zebrafish developmental timeline (19).

Neurogenesis in Zebrafish Embryos

Neuroectoderm is the first structure to be specified during the vertebrate nervous system development and this is named "neural induction" that occurs at the beginning of embryogenic development (7,8). The mesodermal layer formed at the beginning of gastrulation folds in and interacts with the above ectoderm (20,21). This possible layer of mesodermal secretes some local factors that activate or inhibit neural activation in

the ectodermal layer. Cells in the ectodermal layer are thought to differentiate into neural tissue (22).

In recent years, vertebrate neural induction has been demonstrated by extrinsic signaling factors. The bone morphogenetic protein (BMP) is one of these factors to inhibit neural activity through epidermal regulation (23). Another factor is the wingless-integrated (Wnt) proteins that are among the earliest signals to regulate the formation of the neural plate primordium (24). The expression of Wnt8 has been shown in non-axial mesendoderm required for the recovery of hindbrain fate as well as the expression of *gbx1* in the hindbrain (25). The anterior neural plate is organized through the complex interaction of the Wnt signals and the Wnt antagonists, including TLC (26).

Signaling pathways, as well as molecules that regulate the substantial processes during embryogenesis, are substantial for developmental biology. The Wnt pathway is often related to different diseases, especially with endocrine diseases as well as cancer, showing that these diseases are due to some impaired developmental processes (27). In our previous studies, we have shown that different endocrine-disrupting chemicals such as bisphenol A and DEHP activated the Wnt/β-catenin pathway in zebrafish embryos as evidenced by the increased expressions of c-*myc* which is the target gene and *wnt3a* (28,29).

Another extrinsic factor is the fibroblast growth factor (Fgf). Fgf and the intrinsic transcription factors including the B1 (SoxB1) gene family are among the important cell proliferation modulators (30,31). Significant progress has been made showing that it is based on complex interactions between these molecules. These secreted proteins allow neural fate to occur in the dorsal ectoderm and permit the formation of the neural plate. In particular, it is important to note that neural ectoderm is determined by members of the SoxB1 family (27). To date, the members of the SoxB1 family have been shown in zebrafish as *sox1 (a/b)*, *sox2, sox3,* and *sox19 (a/b)* (28). S*ox2* may be observed in the neural progenitors of zebrafish embryos and also in the neural stem cells of adult zebrafish brain (23,32). Thus, Sox2 is a very important factor needed for the maintenance of neural progenitor traits and their related functions for the vertebrates (33). In summary, SoxB1 members together with the inhibitory role of BMP signaling and induction of Fgf signaling are substantial determinants to assert the neural stem cell pool during the zebrafish embryo early gastrulation stages (8).

In the neural plate, the initiation of neurogenesis is maintained through the proneural genes in the zebrafish which is observed during the late gastrulation phase. The *neurog1* (*neurogenin1)* is one of the first proneural genes to produce transcription factors together with *achaete-scute1* (asc1). These genes coding transcription factors are referred as the bHLH genes (33). On the other hand, *shh* has a key signal inducer role and is needed for the concentration-dependent activation of *neurog1* and *ascl1*, which causes the formation of thalamic nuclei in the vertebrates (34). In the midbrain-hindbrain boundary region of the neural tube of isthmus rhombocephali, regulation of the cellular fate takes place via Fgf8 signaling (35). Through the initiation of neurogenesis, progenitor pool cells induce the formation of the differentiated cells within the midbrain-hindbrain boundary region (36). The activity of the progenitor pool is evident through *her5* and *her11* expression together with the inhibition of E(Spl) factors. These determinants inhibit the expression of the proneural genes including *neurog1*, *ascl1a*, as well as cyclin-dependent kinase inhibitors (37,38).

The SoxB1 transcriptional targets are the E(Spl) family members which are the Her and Hes genes. They are named as the hairy genes, *her* 3,5,6,9 and 11. Ectopic Her and Hes gene expressions cause the downregulation of the expression of *neurog1* but loss-of-function trials reveal up-regulated *neurog1* expression (38). SoxB1 together with the hairy genes leads to neurogenesis inhibition which is an important mechanism increasing the cell pool (39). Therefore, there is a critical mechanism that modulates the neurogenetic gradients during the embryonic central nervous system and this process is maintained spatially through the inhibition of neurogenesis, regulated through the local inhibition of the Her and Hes proteins (8,40).

Zebrafish Embryo as a Model Organism in Neurodevelopmental Toxicity Studies

Neurotoxicity is characterized as a detrimental effect on the structure and/or function of the nervous system and may result from exposure to food additives and environmental toxicants, as well as drugs used during chemotherapy, radiation therapy, and organ transplantation. Neurotoxicity is the second leading cause of drug withdrawals after cardiovascular toxicity. Diamthazole and vinyl chloride aerosol can be given as examples of some drug withdrawals due to neurotoxicity (41). Although many approved drugs have been shown to cause neurotoxic side effects, they do not have well-defined neurotoxicity profiles. For instance, an antibiotic, chloramphenicol and antituberculosis drugs such as ethambutol and isoniazid lead to cause optic neuritis (42). Antiepileptic drugs and chemotherapy agents, as well as aminoglycosides may lead to some cerebellar syndromes including dysarthria (43). Other drug-related neurological complications have also been reported including cognitive impairment, headache, and neuromuscular disorders (41-43).

Different approaches are defined to determine the neurotoxicity of a molecule and they are generally divided into three groups as the behavioral, the morphological or histopathological and finally the biochemical approach that evaluates the cellular metabolism and functions that have been changed. Currently, the preclinical analysis of neurotoxicity is generally based on the evaluation of behavioral abnormalities and/or the observation of clear histopathological lesions in the nervous tissue (44).

The most efficient methods to analyze neurotoxicity are the animal behavioral studies including aggression, survival, feeding, motor function, reproduction and, maternal behavior. These parameters may be adversely affected due to exposure to vari-

ous neurotoxins. However, most effects on the central nervous system are mute and result in alterations in function, not easily identifiable in human studies, and are likely to cause minor changes in parameters including temperament, emotion, mood and, cognition that have not been sufficiently studied in animals (45). Histological methods are effective only when lesions in the nervous system are widespread and can be detected by immunohistochemical staining methods. Several specific biochemical markers (eg, alterations in the activity of enzymes and, protein phosphorylation) have been studied, but have only been shown to be beneficial for detecting specific types of neurotoxicity. There is a need to develop rapid assay methods and new animal models to predict neurotoxicity (46).

Zebrafish are very useful for neurotoxicity studies merging different approaches including genetic, cellular and, molecular methods. The main advantages of using zebrafish as a model organism in neurotoxicity research include its external development and genetic similarity to humans whereas, the main limitation may be suggested as its translational value (1). The main advantages and limitations of using zebrafish as a model organism in neurotoxicity research are summarized in Figure 2.

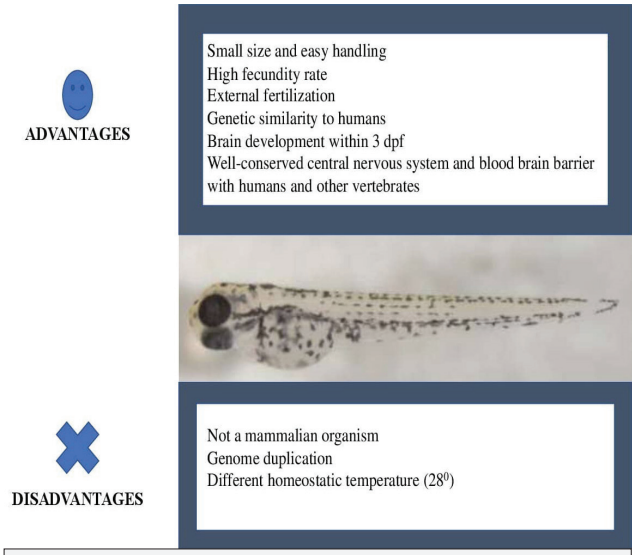

Figure 2. Advantages and disadvantages of using zebrafish as a model organism in neurotoxicity research.

Because the zebrafish embryo is transparent and develops rapidly, the formation of specific neurons and axon pathways can be screened in living embryos through differential interference contrast microscopy or by injecting live dyes (47). Special neuron types can be screened in whole mounted and fixed embryos by using immunohistochemistry or in situ hybridization (48). Motor neuron activity can be screened in vivo by using calcium imaging and patch-clamp recording (49).

The blood-brain barrier is a special type of capillary endothelial system that serves to protect the brain from substances that may be harmful in the bloodstream. It also provides the nutrients that are needed for the brain to regulate the main physiological functions. This barrier includes a complex system with special endothelial cells, macrophages, and astrocytes (50). The passage of macromolecules is prevented through tight junctions that are present between the endothelial cells (51). Lipid soluble, small molecules having molecular weight less than 400 daltons can pass the blood-brain barrier (50). The blood-brain barrier is also present in zebrafish and zebrafish is considered an excellent model organism to evaluate the molecular interactions as well as the permeability of drugs (52). It has been shown by Evans blue staining that blood-brain barrier functions are observed at 3 dpf zebrafish and the transparent feature of zebrafish embryo provides a major advantage to study the penetration of drugs during development (53).

Evaluation of Neurotoxicity in Zebrafish

Zebrafish have a population of early neurons that are named as "primary neurons". These neurons are part of a comparably basic nervous system that differentiate to regulate the movement of the larva (54). The distribution and projection properties of specific primary neurons have been explained in literature thoroughly (55). At 24 h after fertilization (24 hpf), these primary neurons of zebrafish differentiate, and in this timeline, substantially large neuronal cells may be identified by using Normarski optics *in vivo*. Brain ventricles of zebrafish are formed at 48 hpf (56). Zebrafish don't have a skull and, their body length may increase from 1 mm at 1 dpf (day post fertilization) to 5 mm at 6 dpf. Whole animal staining can be done to comprehensively evaluate the whole nervous system. Classical neurotoxins investigated in zebrafish include dopaminergic neurotoxins including rotenone, 1-methyl-4-phenyl-1,2,3,6-tetrahydropyridine (MPTP), 6-hydroxydopamine (6-OHDA), and paraquat. non-NMDA-type glutamate receptor agonists or antagonists including domoic acid, 6-cyano-7-nitroquinoxaline-2,3-dione, alpha-latrotoxin, and picrotoxin; nicotinic acetylcholine receptor antagonists such as bungarotoxins and cobratoxins or acetylcholinesterase inhibitors; and the NMDA receptor antagonist, DL-2-amino-5-phosphonovalerate (AP-5) (1).

Neurotoxicity can be evaluated in zebrafish after exposure to a neurotoxic compound in the optic nerves, motor, and dopaminergic neurons as well as the myelin sheath. Moreover, the molecular mechanisms including oxidant/antioxidant pathways, apoptosis and proliferation assays can be observed directly in transparent fish. Accordingly, zebrafish have been shown to be sensitive to different neurotoxins such as ethanol, acrylamide, retinoic acid, neomycin, and tetrachlorodibenzo-p-dioxin (57,58).

Effects of Neurotoxins on Motor Neurons and Neuronal Proliferation

In mammalian models, the effects of drug-induced neurotoxicity such as ethanol toxicity have been reported on motor neurons and also on neuronal proliferation. Ethanol has been reported to alter motor functions through the induction of motor neuron death and the inhibition of neuronal proliferation. Ethanol has also been found to affect brain and motor functions in humans (57).

Similarly, the compounds that lead to neurotoxicity in humans have been reported to induce complementary neurotoxicity in zebrafish. Ethanol caused defects in the optic nerves as well as in the motor neurons and altered neuronal proliferation. 6-OHDA led to the oxidation of neurons and loss of dopaminergic neurons and L-2-hydroxyglutaric acid caused neuronal apoptosis (58).

Effects of Neurotoxins on Dopaminergic Neurons

In the midbrain, dopaminergic neurons are the major source of dopamine (DA) in the mammalian CNS, and the loss of DA is related to Parkinson's disease which is the most important human neurological disorder (1). Dopaminergic neurons are found in the substantia nigra pars compacta, which is rich in DA and contains neuromelanin and high levels of iron. Dopaminergic neurons have a substantial role in controlling many different brain functions such as, voluntary movement and a wide range of behavioral parameters including mood, reward, addiction, and stress. To evaluate the compound effects on dopaminergic neurons, 6-OHDA was administered as a neurotoxin that destroys catecholaminergic terminals, and then immunostained using an anti-tyrosine hydroxylase antibody. Results showed that 6-OHDA led to dopaminergic neurotoxicity (1,59). Similarly, in mammals, 6-OHDA has been found to cause oxidative stress and result in neuronal death (59).

We have previously shown that as a neurotoxic pesticide that is capable of crossing the blood-brain barrier, rotenone exposure for 4 weeks led to decreased locomotor activity, dopamine, and serotonin levels and increased DOPAC and DOPAC/dopamine levels in zebrafish. Moreover, lipid peroxidation increased and antioxidant levels decreased suggesting the disrupted oxidant-antioxidant balance (60). We have also tested if exposure to rotenone disrupts the oxidant/antioxidant status in the intestine and brain of zebrafish and our results showed that lipid peroxidation increased whereas the activities of glutathione S-transferase and catalase decreased both in the intestinal tissues and brain of the rotenone exposed adult zebrafish (61).

Brain dopaminergic neurons of zebrafish embryos are sensitive to the MPTP. However, noradrenergic neurons in the medulla oblongata were not affected by MPTP exposure (62). Recently we have shown decreased locomotor activity in MPTP-exposed zebrafish embryos and morphine exerted neuroprotective effects against MPTP exposure by normalizing locomotor activity, acetylcholine esterase activity, Parkinson's Disease-related genes and oxidative stress (63). We have also shown the beneficial effects of 3-pyridineboronic in MPTP exposed zebrafish embryos by the amelioration of impaired locomotor activity and mitochondrial dysfunction (64). In zebrafish as the main dopamine-expressing neurons are located in the posterior tuberculum of the diencephalon decreased dopaminergic cells together with defects in swimming responses were also reported in zebrafish embryos (65).

Effects of Neurotoxins on Mobility

One of the biggest challenges in developing methods for assessing neurotoxicity is its association with behaviorally altered neuromorphological, neurochemical, and neurophysiological changes that are often considered abnormal movement. In zebrafish larvae, locomotor or motility patterns are stage-specific and behavioral abnormalities are easily discernible (66). Embryonic motor behavior develops sequentially; The early period consists of transient spontaneous curling contractions, followed by the appearance of twitching in response to touch, and later the ability to swim (67). At 4 dpf, the embryos are free-swimming and spontaneously change direction with characteristic ranges of speed and distance. Zebrafish also exhibit basic behaviors that include memory, non-associative learning, conditioned responses, and social behaviors such as schooling (68).

Various studies have shown that zebrafish mobility can be monitored using a computer-assisted motion detector (69). It has been shown that this assay format is useful for assessing compound-induced neurotoxicity (including seizures). Similar to results in mammals, pentylenetetrazole, a gamma-aminobutyric acid antagonist known to cause convulsions in humans, has been suggested to induce seizures in zebrafish. Moreover, electrophysiological, molecular changes, as well as the behavioral responses in zebrafish treated with pentylenetetrazole are similar to the effects reported in the rodent seizure model.

Effects of Neurotoxins on Neurodevelopment

Developmental neurotoxicity includes changes in behavior, neurohistology, neurochemistry, neurophysiology, or overall dysmorphology due to exposure during development. The developing embryonic brain is more susceptible to confusion caused by toxins due to the differentiation of specific cell types and the disruption of delicate processes that occur only during development, such as proliferation and migration of newly formed neurons (70). In addition, the developing brain is more exposed to blood-borne toxins before blood-brain barrier formation. Therefore, critical assessment of developmental neurotoxicity requires the use of an embryonic model.

In one study, well-characterized compounds were selected to validate zebrafish as a model of developmental neurotoxicity. Embryos were exposed by quasi-static immersion at stage 6 hpf to 96 or 120 hpf; The induction of brain apoptosis or necrosis seen with the compounds was confirmed as an indicator of developmental neurotoxicity, and an effect on motor neurons in the caudal third of the embryo was shown to be associated with expected defects in motility. Different environmental pollutants were screened for their effects on brain apoptosis, axon tract and motor neuron formation, and catecholaminergic neurons in developing zebrafish, and compounds that act on several neurotoxicity parameters were identified. Some compounds even showed extensive toxicity at all neuroanatomical endpoints (71, 72). Overall, these results indicate a strong correlation with mammalian data, indicating that zebrafish is a suitable animal model for developmental neurotoxicity screening.

Harmful algal blooms (HABs) are formed when the growth of algae colonies derived from simple plants in sea and freshwater

Table 1. Neurodevelopmental genes in zebrafish and their functions.

Gene name	Gene symbol	Function
neurogenin 1	*neurog1*	Basal forebrain dopaminergic neuron determinant
myelin basic protein a	*mbp*	Structural constituent of myelin sheat
α1-tubulin	*α1-tubulin*	Brain development
synapsin IIa	*syn2a*	Synaptogenesis
sonic hedgehog signaling molecule a	*shha*	Regulation of neurogenesis
ELAV like neuron-specific RNA binding protein 3	*elavl3*	Regulation of neurogenesis

are out of control. HABs have toxic effects on people and animals. Recently HABs have been also shown to cause potential neurotoxins. For instance, domoic acid (DomA) is a potent HAB neurotoxin that can accumulate in shellfish and finfish under certain environmental conditions. Exposure to the DomA resulted in long-lasting behavioral deficits in rodents and primate models (73). In humans and nonhuman primates, oral exposure to DomA induced gastrointestinal effects, neurological symptoms, seizures, memory impairment, and limbic system degeneration. Rodents are less sensitive than humans or nonhuman primates and induce behavioral abnormalities. DomA exhibits similar neurotoxic effects across species from sea lions to zebrafish (74).

The drinking water of many different geographic areas including the US, Latin America, Asia, Africa is co-contaminated by neurotoxic pollutants such as inorganic arsenic and fluoride. Inorganic arsenic and fluoride affect the neurodevelopment of children due to the exposure during the post and pre-natal periods. Although, co-contamination with inorganic arsenic and fluoride can create more risk than their exposure alone, there is a lack of information about the concurent role in the deterioration of gut microbiota that acts as an organizer in neurodevelopment (75).

In zebrafish measuring the expression levels of different biomarkers is a sensitive and fast way to find out the alterations in the gene expression sequences in case of neurotoxin treatment. Different genes of the nervous system were suggested as potential neurotoxicity markers in zebrafish embryos that were treated with ethanol using RT-PCR. Neuronal stem cell transcripts were either decreased or increased during development, and the overexpression of an astrocytes marker was significant. It has been demonstrated that evaluation of the gene expression profile of the brain is useful in analyzing the neurotoxicity of many chemicals during development (76).

The microarray hybridization method has also been used to determine the effects of environmental toxins in zebrafish embryos and organ and cell-specific alterations in the gene expressions were detected by using in situ hybridization (77). When the genome profile and in situ studies were performed in methyl mercury exposed zebrafish embryos the gene expressions were found to be altered significantly in brain different neuronal subregions (78).

To evaluate the developmental effects of neurotoxins in zebrafish embryos gene expression levels of some specific markers are determined. For instance, myelin basic proteins (MBP) was determined in propofol (anesthetic) exposed zebrafish and decreased MBP expression was evident in the central nervous system (79).

Some other neurodevelopmental genes include *syn2a* and *α1-tubulin* that were found to be down-regulated in chlorpyrifos and 1,3-dichloro-2-propyl-phosphate exposed zebrafish embryos (80). On the other hand, *neurog1* is also an important neuro-developmental gene that is shown to be affected in ibuprofen and diclofenac exposed zebrafish embryos (79,81). Ans also, *elavl3, syn2a* and*, shha* have been shown to be down regulated in triphenyl phosphate exposed zebrafish embryos (82). Zebrafish genes having specific roles in neurodevelopment are listed in Table 1.

Autism spectrum disorder (ASD) is a crucial disorder of neurodevelopment (83). Valproic acid, a pharmaceutical agent used to treat seizures, is suggested to be an ASD inducer, and defective social behavior has been shown in valproic acid exposed zebrafish embryos (84). The preliminary findings of our ongoing study show that valproic acid affects the expressions of *shank3a, adsl* and *tsc1b* that are genes related to ASD.

The utilization of gene profiling patterns can be suggested as a useful endpoint for neurotoxicity research to reveal the developmental neurotoxicity of some different and potentially toxic compounds.

CONCLUSION

Although zebrafish embryo and adult regulatory pathways are mainly different they share some similarities during the production of functional neurons. Embryonal neurons originate from the neuroectodermal epithelium whereas, adult neurons are derived from glia cells. Accordingly, it is important to reveal the specific differences between the embryo adult neurogenesis in terms of neurotoxicity research. Understanding the specific

pathways of neurodevelopment will enable the improvement of therapeutic strategies. The translational value of zebrafish will also be improved through the incorporation of knowledge into the mammalian brain in terms of neuronal circuits.

Our review provides a brief overview of the emerging potential the zebrafish embryo has in neurotoxicity research during development. Although having some limitations, using the zebrafish as a model organism in neurotoxicology provides significant advantages. Many toxicity endpoints can be combined with different assays to evaluate the impact of large numbers of potential neurotoxic compounds.

We suggest the increasing employment of zebrafish in testing chemicals will speed up this process and facilitate the understanding of neurotoxicity mechanisms. Accordingly, we believe that the use of zebrafish and zebrafish embryos in research will become widespread, as *in vivo* imaging and analysis platforms, which are developing day by day, become more accessible.

Acknowledgement: This work was supported by the research grant from Marmara University Scientific Research Projects Commission (Grant number: TYL-2021-10205).

Informed Consent: Written consent was obtained from the participants.

Peer Review: Externally peer-reviewed.

Author Contributions: Conception/Design of Study- E.E.A.; Data Acquisition- S.C.; Data Analysis/Interpretation- S.C.; Drafting Manuscript- S.C.; Critical Revision of Manuscript- E.E.A.; Final Approval and Accountability- E.E.A., S.C.

Conflict of Interest: Authors declared no conflict of interest.

Financial Disclosure: Authors declared no financial support.

REFERENCES

1. Ünal İ, Emekli-Alturfan E. Fishing for Parkinson's Disease: A review of the literature. J Clin Neurosci 2019; 62: 1-6.
2. Renier C, Faraco JH, Bourgin P, Motley T, Bonaventure P, Rosa F. Genomic and functional conservation of sedative-hypnotic targets in the zebrafish. Pharmacogenet Genomics 2007; 17: 237-53.
3. Rihel J, Prober DA, Arvanites A, Lam K, Zimmerman S, Jang S. Zebrafish behavioral profiling links drugs to biological targets and rest/wake regulation. Science 2010; 327: 348-51.
4. Howe K, Clark MD, Torroja CF, Torrance J, Berthelot C, Muffato M, et al. The zebrafish reference genome sequence and its relationship to the human genome. Nature 2013; 496: 498-503.
5. Kozol RA, Abrams AJ, James DM, Buglo E, Yan Q, Dallman JE. Function over form: modeling groups of inherited neurological conditions in zebrafish. Front Mol Neurosci 2016; 7: 9-55.
6. Engeszer RE, Patterson LB, Rao AA, Parichy DM. Zebrafish in the wild: A review of natural history and new notes from the field. Zebrafish 2007; 4: 21-40.
7. Bally-Cuif L, Vernier P. Organization and Physiology of the Zebrafish Nervous System. Fish Physiol 2010; 29: 25-80.
8. Schmidt R, Strähle U, Scholpp S. Neurogenesis in zebrafish - from embryo to adult. Neural Dev 2013; 8: 3.
9. Goulding M. Circuits controlling vertebrate locomotion: moving in a new direction. Nat Rev Neurosci 2009; 10: 507-18.
10. Brustein E, Saint-Amant L, Buss RR, Chong M, McDearmid JR, Drapeau P. Steps during the development of the zebrafish locomotor network. J Physiol Paris 2003; 97: 77-86.
11. Gould E, Gross CG. Neurogenesis in adult mammals: some progress and problems. J Neurosci 2002; 22(3): 619-23.
12. Gould E. How widespread is adult neurogenesis in mammals? Nat Rev Neurosci 2007; 8: 481-88.
13. Zupanc GKH, Hinsch K, Gage FH. Proliferation, migration, neuronal differentiation, and long-term survival of new cells in the adult zebrafish brain. J Comp Neurol 2005; 488: 290-319.
14. Grandel H, Kaslin J, Ganz J, Wenzel I, Brand M. Neural stem cells and neurogenesis in the adult zebrafish brain: origin, proliferation dynamics, migration and cell fate. Dev Biol 2006; 295: 263-77.
15. Hinsch K, Zupanc GKH. Generation and long-term persistence of new neurons in the adult zebrafish brain: a quantitative analysis. Neuroscience 2007; 146: 679-96.
16. Kimmel CB, Ballard WW, Kimmel SR, Ullmann B, Schilling TF. Stages of embryonic development of the zebrafish. Dev Dyn 1995: 203(3): 253-310.
17. Sasai Y, De Robertis EM. Ectodermal patterning in vertebrate embryos. Dev Biol 1997; 182: 5-20.
18. Spemann H, Mangold H. Induction of embryonic primordia by implantation of organizers from a different species. 1923. Int J Dev Biol 2001; 45: 13-38.
19. Zebrafish developmental timeline (Reprinted from "Zebrafish Developmental Timeline", by BioRender.com (2021). Retrieved from https://app.biorender.com/biorender-templates)
20. Doniach T, Musci TJ. Induction of anteroposterior neural pattern in Xenopus: evidence for a quantitative mechanism. Mech Dev 1995; 53: 403-13.
21. Lumsden A, Krumlauf R. Patterning the vertebrate neuraxis. Science 1996; 274: 1109-15.
22. Weinstein DC, Hemmati-Brivanlou A. Neural induction. Annu Rev Cell Dev Biol 1999; 15: 411-33.
23. Okuda Y, Ogura E, Kondoh H, Kamachi Y. B1 SOX coordinate cell specification with patterning and morphogenesis in the early zebrafish embryo. PloS Genet 2010; 6(5): e1000936.
24. Kim CH, Oda T, Itoh M, Jiang D, Artinger KB, Chandrasekharappa SC, et al. Repressor activity of Headless/Tcf3 is essential for vertebrate head formation. Nature 2000; 407: 913-16.
25. Rhinn M, Lun K, Luz M, Werner M, Brand M. Positioning of the midbrain-hindbrain boundary organizer through global posteriorization of the neuroectoderm mediated by Wnt8 signaling. Development 2005; 132: 1261-72.
26. Houart C, Westerfield M, Wilson SW. A small population of anterior cells patterns the forebrain during zebrafish gastrulation. Natur 1998; 391: 788-92.
27. Üstündağ ÜV, Emekli-Alturfan E. Wnt pathway: A mechanism worth considering in endocrine disrupting chemical action. Toxicol Ind Health 2020; 36(1): 41-53.
28. Üstündağ ÜV, Ünal İ, Ateş PS, Alturfan AA, Yiğitbaşı T, Emekli-Alturfan E. Bisphenol A and di(2-ethylhexyl) phthalate exert divergent effects on apoptosis and the Wnt/β-catenin pathway in zebrafish embryos: A possible mechanism of endocrine disrupting chemical action. Toxicol Ind Health 2017; 33(12): 901-10.
29. Bielen H, Houart C. BMP signaling protects telencephalic fate by repressing eye identity and its Cxcr4-dependent morphogenesis. Dev Cell 2012; 23: 812-22.
30. Stern CD. Neural induction: 10 years on since the "default model" Curr Opin Cell Biol 2006; 18: 692-7.

31. Penzel R, Oschwald R, Chen Y, Tacke L, Grunz H. Characterization and early embryonic expression of a neural specific transcription factor xSOX3 in Xenopus laevis. Int J Dev Biol 1997; 41: 667-77.
32. Dee CT, Hirst CS, Shih Y-H, Tripathi VB, Patient RK, Scotting PJ. Sox3 regulates both neural fate and differentiation in the zebrafish ectoderm. Dev Biol 2008; 320: 289301.
33. Kaslin J, Ganz J, Geffarth M, Grandel H, Hans S, Brand M. Stem cells in the adult zebrafish cerebellum: initiation and maintenance of a novel stem cell niche. J Neurosci 2009; 29: 6142-53.
34. Bani-Yaghoub M, Tremblay RG, Lei JX, Zhang D, Zurakowski B, Sandhu JK, et al. Role of Sox2 in the development of the mouse neocortex. Dev Biol 2006; 295: 52-66.
35. Allende ML, Weinberg ES. The expression pattern of two zebrafish achaete-scute homolog (ash) genes is altered in the embryonic brain of the cyclops mutant. Dev Biol 1994; 166: 509-30.
36. Scholpp S, Delogu A, Gilthorpe J, Peukert D, Schindler S, Lumsden A. Her6 regulates the neurogenetic gradient and neuronal identity in the thalamus. Proc Natl Acad Sci U S A 2009; 106: 19895-900.
37. Tallafuss A, Adolf B, Bally-Cuif L. Selective control of neuronal cluster size at the forebrain/midbrain boundary by signaling from the prechordal plate. Dev Dyn 2003; 227: 524-35.
38. Geling A, Itoh M, Tallafuss A, Chapouton P, Tannhäuser B, Kuwada JY, Chitnis AB, Bally-Cuif L. bHLH transcription factor Her5 links patterning to regional inhibition of neurogenesis at the midbrain-hindbrain boundary. Development 2003; 130: 1591-604.
39. Ninkovic J, Tallafuss A, Leucht C, Topczewski J, Tannhäuser B, Solnica-Krezel L, Bally-Cuif L. Inhibition of neurogenesis at the zebrafish midbrain-hindbrain boundary by the combined and dose-dependent activity of a new hairy/E(spl) gene pair. Development 2005; 132(1): 75-88.
40. Lyons DA, Guy AT, Clarke JDW. Monitoring neural progenitor fate through multiple rounds of division in an intact vertebrate brain. Development 2003; 130: 3427-36.
41. Wysowski DK, Swartz L. Adverse drug event surveillance and drug withdrawals in the United States, 1969-2002: the importance of reporting suspected reactions. Arch Intern Med 2005; 165(12): 1363-9.
42. Kulkarni HS, Keskar VS, Bavdekar SB, Gabhale Y. Bilateral optic neuritis due to isoniazid (INH). Indian Pediatr 2010; 47(6): 533-5.
43. Edson RS, Terrell CL. The aminoglycosides. Mayo Clin Proc 1999; 74(5): 519-28.
44. Moser VC. Functional assays for neurotoxicity testing. Toxicol Pathol 2011; 39(1): 36-45.
45. Kulig B, Alleva E, Bignami G, Cohn J, Cory-Slechta D, Landa V, et al. Animal behavioral methods in neurotoxicity assessment: SGOMSEC joint report. Environ Health Perspect 1996; 104(Suppl 2): 193-204.
46. Kung MP, Kostyniak PJ, Olson JR, Sansone FM, Nickerson PA, Malone MA, et al. Cell specific enzyme markers as indicators of neurotoxicity: effects of acute exposure to methylmercury. Neurotoxicology 1989; 10(1): 41-52.
47. Kuwada JY, Bernhardt RR, Nguyen N. Development of spinal neurons and tracts in the zebrafish embryo. J Comp Neurol 1990; 302(3): 617-28.
48. Moens CB, Fritz A. Techniques in neural development. Methods Cell Biol 1999; 59: 253-72.
49. Brustein E, Saint-Amant L, Buss RR, Chong M, McDearmid JR, Drapeau P. Steps during the development of the zebrafish locomotor network. J Physiol Paris 2003; 97(1): 77-86.
50. Ballabh P, Braun A, Nedergaard M. The blood-brain barrier: an overview: structure, regulation, and clinical implications. Neurobiol Dis 2004; 16(1): 1-13.
51. Engelhardt B. Development of the blood-brain barrier. Cell Tissue Res 2003; 314(1): 119-29.
52. Cserr HF, Bundgaard M. Blood-brain interfaces in vertebrates: a comparative approach. Am J Physiol 1984; 246(3): R277-88.
53. Eliceiri BP, Gonzalez AM, Baird A. Zebrafish model of the blood-brain barrier: morphological and permeability studies. Methods Mol Biol 2011; 686: 371-8.
54. Kimmel CB, Miller CT, Kruze G, Ullmann B, BreMiller RA, Larison KD, Snyder HC. The shaping of pharyngeal cartilages during early development of the zebrafish. Dev Biol 1998; 203(2): 245-63.
55. Eisen JS, Pike SH. The spt-1 mutation alters segmental arrangement and axonal development of identified neurons in the spinal cord of the embryonic zebrafish. Neuron 1991; 6(5): 767-76.
56. Schier AF, Neuhauss SC, Harvey M, Malicki J, Solnica-Krezel L, Stainier DY, et al. Mutations affecting the development of the embryonic zebrafish brain. Development 1996; 123: 165-78.
57. Biller A, Bartsch AJ, Homola G, Solymosi L, Bendszus M. The effect of ethanol on human brain metabolites longitudinally characterized by proton MR spectroscopy. J Cereb Blood Flow Metab 2009; 29(5): 891-902.
58. Parng C, Roy NM, Ton C, Lin Y, McGrath P. Neurotoxicity assessment using zebrafish. J Pharmacol Toxicol Methods 2007; 55(1): 103-12.
59. Elkon H, Melamed E, Offen D. Oxidative stress, induced by 6-hydroxydopamine, reduces proteasome activities in PC12 cells. J Mol Neurosci 2004; 24: 387-400.
60. Ünal İ, Çalışkan-Ak E, Üstündağ ÜV, Ateş PS, Alturfan AA, Altinoz MA,et al. Neuroprotective effects of mitoquinone and oleandrin on Parkinson's disease model in zebrafish. Int J Neurosci 2020; 130(6): 574-82.
61. Ünal İ, Üstündağ ÜV, Ateş PS, Eğilmezer G, Alturfan AA, Yiğitbaşı T, et al. Rotenone impairs oxidant/antioxidant balance both in brain and intestines in zebrafish. Int J Neurosci 2019; 129(4): 363-68.
62. McKinley ET, Baranowski TC, Blavo DO, Cato C, Doan TN, Rubinstein AL. Neuroprotection of MPTP-induced toxicity in zebrafish dopaminergic neurons. Brain Research. Molecular Brain Research 2005; 141(2): 128-37.
63. Cansız D, Ustundag UV, Unal I, Alturfan AA, Emekli-Alturfan E. Morphine attenuates neurotoxic effects of MPTP in zebrafish embryos by regulating oxidant/antioxidant balance and acetylcholinesterase activity. Drug Chem Toxicol 2021; 2: 1-9.
64. Üstündağ FD, Ünal İ, Cansız D, Üstündağ ÜV, Subaşat HK, Alturfan AA, et al. 3-Pyridinylboronic acid normalizes the effects of 1-Methyl-4-phenyl-1,2,3,6-tetrahydropyridine exposure in zebrafish embryos. Drug Chem Toxicol 2020; 21: 1-8.
65. Lam CS, Korzh V, Strahle U. Zebrafish embryos are susceptible to the dopaminergic neurotoxin MPTP. The European Journal of Neuroscience 2005; 21(6): 1758-62.
66. Granato M, Nüsslein-Volhard C. Fishing for genes controlling development. Curr Opin Genet Dev 1996; 6(4): 461-8.
67. Drapeau P, Saint-Amant L, Buss RR, Chong M, McDearmid JR, Brustein E. Development of the locomotor network in zebrafish. Prog Neurobiol 2002; 68(2): 85-111.
68. Best JD, Alderton WK. Zebrafish: An in vivo model for the study of neurological diseases. Neuropsychiatr Dis Treat 2008; 4(3): 567-76.
69. Winter MJ, Redfern WS, Hayfield AJ, Owen SF, Valentin JP, Hutchinson TH. Validation of a larval zebrafish locomotor assay for assessing the seizure liability of early-stage development drugs. J Pharmacol Toxicol Methods 2008; 57(3): 176-87.
70. Rice D, Barone S Jr. Critical periods of vulnerability for the developing nervous system: evidence from humans and animal models. Environ Health Perspect 2000; 108(3): 511-33.

71. Ton C, Lin Y, Willett C. Zebrafish as a model for developmental neurotoxicity testing. Birth Defects Res A Clin Mol Teratol 2006; 76: 553-67.
72. Legradi JB, Di Paolo C, Kraak MHS, van der Geest HG, Schymanski EL, Williams AJ, et al. An ecotoxicological view on neurotoxicity assessment. Environ Sci Eur 2018; 30(1): 46.
73. Panlilio JM, Aluru N, Hahn ME. Developmental Neurotoxicity of the Harmful Algal Bloom Toxin Domoic Acid: Cellular and Molecular Mechanisms Underlying Altered Behavior in the Zebrafish Model. Environ Health Perspect. 2020; 128(11): 117002.
74. Costa LG, Giordano G, Aschner M. Domoic Acid. Aminoff MJ, Daroff RB, editors. Encyclopedia of the Neurological Sciences. 2nd ed. Massachusetts: Academic Press; 2014. p. 1016-17.
75. Qiu Y, Chen X, Yan X, Wang J, Yu G, Ma W, et al. Gut microbiota perturbations and neurodevelopmental impacts in offspring rats concurrently exposure to inorganic arsenic and fluoride. Environ Int. 2020; 140: 105763.
76. Fan CY, Cowden J, Simmons SO, Padilla S, Ramabhadran R. Gene expression changes in developing zebrafish as potential markers for rapid developmental neurotoxicity screening. Neurotoxicol. Teratol 2010; 32: 91-8.
77. Yang L, Kemadjou JR, Zinsmeister C, Bauer M, Legradi J, Müller F, et al. Transcriptional profiling reveals barcode-like toxicogenomic responses in the zebrafish embryo. Genome Biol 2007; 8(10): R227.
78. Ho NY, Yang L, Legradi J, Armant O, Takamiya M, Rastegar S, et al. Gene responses in the central nervous system of zebrafish embryos exposed to the neurotoxicant methyl mercury. Environ. Sci. Technol 2013; 47: 3316-3325.
79. Xia L, Zheng L, Zhou JL. Effects of ibuprofen, diclofenac and paracetamol on hatch and motor behavior in developing zebrafish (Danio rerio). Chemosphere 2017; 182: 416-25.
80. Jeong JY, Einhorn Z, Mercurio S, Lee S, Lau B, Mione M, Wilson SW, Guo S. Neurogenin1 is a determinant of zebrafish basal forebrain dopaminergic neurons and is regulated by the conserved zinc finger protein Tof/Fezl. Proc Natl Acad Sci U S A. 2006; 28; 103(13): 5143-8.
81. Li R, Zhang L, Shi Q, Guo Y, Zhang W, Zhou B. A protective role of autophagy in TDCIPP-induced developmental neurotoxicity in zebrafish larvae. Aquat Toxicol 2018; 199: 46-54.
82. Shi Q, Wang M, Shi F, Yang L, Guo Y, Feng C, et al. Developmental neurotoxicity of triphenyl phosphate in zebrafish larvae. Aquat Toxicol 2018; 203: 80-7.
83. Lee S, Chun HS, Lee J, Park HJ, Kim KT, Kim CH, et al. Plausibility of the zebrafish embryos/larvae as an alternative animal model for autism: A comparison study of transcriptome changes. PloS one 2018; 13(9): e0203543.
84. Chen J, Lei L, Tian L, et al. Developmental and behavioral alterations in zebrafish embryonically exposed to valproic acid (VPA): An aquatic model for autism. Neurotoxicol Teratol 2018; 66: 8-16.